2012-07-11

Buckling and Crippling of Square Steel Thin-Walled Tubes Fabricated with Symmetrically-Overlapping U-Channels and Foam

David Camenish Gelder
Brigham Young University - Provo

Buckling and Crippling of Square Steel Thin-Walled Tubes Fabricated with Symmetrically-Overlapping U-Channels and Foam

David Camenish Gelder

A thesis submitted to the faculty of
Brigham Young University
in partial fulfillment of the requirements for the degree of

Master of Science

David W. Jensen, Chair
Richard J. Balling
Paul W. Richards

Department of Civil and Environmental Engineering

Brigham Young University

August 2012

ABSTRACT

Buckling and Crippling of Square Steel Thin-Walled Tubes Fabricated with Symmetrically-Overlapping U-Channels and Foam

David Camenish Gelder
Department of Civil and Environmental Engineering, BYU
Master of Science

Testing and analysis has been performed on square steel thin-walled tubes fabricated using symmetrically-overlapping U-channels and foam. This research analyzes flange-to-flange attachment, effect of foam in the columns, effect of adhesive stiffness, and influence of steel thickness, as related to the local buckling loads, global buckling loads, and crippling loads. Four 14-foot (4.27 m) foam-filled, thin-walled, galvanized steel columns were manufactured by Novatek, Inc. and tested in axial compression with pinned boundary conditions. For three of the four configurations, the two-piece 4-in. (10.2-cm) square shell surrounded prefabricated polystyrene foam inserts; the fourth column had no foam insert. The column outer shells were composed of two 16-gauge galvanized steel channels with overlapping flanges and the webs on opposite sides of the column. The two adjacent flanges on each side of the columns were adhesively bonded together in all cases. In addition to the adhesive, two columns had either periodic screws or short welds spaced evenly along the length of the columns to delay the onset of flange buckling of the outer channel, and potentially increase the compression strength. The other two columns had adhesive only bonding the flanges, one of which had no foam filler. The various configurations all exhibited similar compression strengths. Failure for all columns initiated with local buckling, followed by global buckling and local crippling, which occurred simultaneously. The method of flange attachment, the effect of the foam in the columns, and flange thicknesses were isolated and analyzed using mechanics-based analysis, parametric studies, and finite element analysis. The results show the ideal spacing of screws or short-welds, if used, is less than or equal to 5 in (12.7 cm) for the given column length. This increases the local buckling load to the Euler buckling load and preserves the original shape of the cross-section. The adhesive needs only a tensile strength of approximately 1 ksi (6.4 kPa) to prevent local buckling for any spacing of screws or short-welds, but needs to be applied uniformly (much of the adhesive in the column tests had been scraped off of the flanges during assembly). The results also show that foam core does not increase the Euler buckling load, but does increase the crippling load by delaying inward buckling of the column webs and flanges. Using foam with the given stiffness and a yield strength of 50 psi (345 kPa), uniform foam-to-steel bonding could increase the crippling strength up to 21% even without adhesive between the flanges. Using adhesive with the given stiffness between the flanges could increase the crippling strength by up to 63% without foam. The crippling strength could increase up to 72% if both adhesive between the flanges and a foam insert are used.

Keywords: foam, steel, thin-wall, column, Novatek, buckling, crippling, lightweight

ACKNOWLEDGMENTS

Thank you to Dr. David W. Jensen for the countless hours you have spent mentoring me. I appreciated your willingness to take time and explain difficult concepts to me. I've learned so much more about applying my engineering knowledge from this thesis than from any other project. Thank you also for your personal example as a role model and leader. I appreciate the time I have spent learning from you.

Thank you to Novatek, Inc. for funding a significant portion of this research. Thank you for also providing the test specimens discussed in this thesis. Thank you to David O. Anderson and Rodney V. Mayo for assisting me in testing the specimens.

Thank you to my parents, Bruce and Carolyn, for the love and guidance that you have shown me my whole life. I can't thank you enough for teaching me the importance of education from an early age. I can't thank you enough for always loving and supporting me. Thank you for being such wonderful parents.

Thank you to Bryan and Deborah Larsen, my parents-in-law. You have been so kind and loving to me. Thank you for all your support.

Finally, thank you to Laura, my dear sweet beautiful wife. Laura, you are the love of my life and my inspiration. I want to thank you for the countless hours, the late nights, and the early mornings that you have sacrificed for me. You have been there every step of the way and have spent that time with me during this long project. I can't thank you enough for all your love and support. I can't tell you enough how much I appreciate you. You are an amazing wife. Thanks for always being there for me, no matter what. I am so glad we found each other; I will love you forever.

TABLE OF CONTENTS

LIST OF TABLES ..... **xi**

LIST OF FIGURES ..... **xvi**

LIST OF NOMENCLATURE ..... **xxiv**

1 INTRODUCTION **1**

1.1 Purpose of Investigation 1

1.2 Description of Foam-Filled Steel Columns 2

1.3 Literature Review 3

1.4 Scope of Research and Ojectives 6

1.5 Limitations 7

1.6 Overview of Thesis 7

2 FOAM-FILLED COLUMN DESCRIPTION **9**

2.1 Design Concept 9

2.2 Manufacturing 10

2.3 Material Properties 11

2.3.1 Steel 11

2.3.2 Foam 12

2.3.3 Adhesive 14

2.3.4 Summary 15

2.4 Geometry 15

2.4.1 Web and Flange Nomenclature 16

2.4.2 Cross-Section 16

2.4.3 Moment of Inertia 18

2.4.4 Bending Stiffness 19

2.4.5 Axial Stiffness 19

2.4.6 Radius of Gyration and Slenderness Ratio 20
2.5 Weight 20
2.6 Design Configurations 21
2.7 Comparison with Steel Studs 24
3 COLUMN TESTING PROCEDURE 25
3.1 Preliminary Testing: Test Setup Components 25
3.1.1 Reaction Frame for 20-kip Tests 26
3.1.2 20-kip Actuator 28
3.1.3 Column Orientation 28
3.1.4 Gravity Loads 29
3.1.5 Boundary Conditions 31
3.1.6 String Potentiometers 31
3.1.7 Surface Strain Gages 33
3.2 Testing to Failure: Test Setup Components 33
3.2.1 Reaction Frame for Tests to Failure 33
3.2.2 100-kip Actuator 34
3.2.3 Column Orientation 35
3.2.4 Gravity Supports 35
3.2.5 Boundary Conditions 36
3.2.6 String Potentiometers 37
3.2.7 Surface Strain Gages 39
3.2.8 LVDT 40
3.3 Data Analysis Procedure 40
3.3.1 Load Data 40
3.3.2 Conversion of Load Data to Stress 41

3.3.3 Deflection Data 41
3.3.4 Strain Data 42
3.3.5 Euler Buckling Equation 43
3.3.6 Southwell Plot Method 44
4 RESULTS OF PRELIMINARY COLUMN TESTING 45
4.1 20-kip Test Results 45
4.1.1 Local Buckling 45
4.1.2 Load vs. Axial Deflection 47
4.1.3 Load vs. Transverse Deflection 48
4.1.4 Stress vs. Total (Local) Strain 51
4.1.5 Stress vs. Axial Strain 53
4.1.6 Stress vs. Bending Strain 55
4.1.7 Southwell Plots 56
4.2 Discussion of 20-kip Test Results 60
4.2.1 Significance of Local Buckling 60
4.2.2 Elastic Loading 61
4.2.3 Projected Buckling Load Compared to Euler Load 61
4.3 Summary 63
5 RESULTS OF COLUMN TESTING TO FAILURE 64
5.1 Column Failure Test Results 64
5.1.1 Local Buckling 64
5.1.2 Crippling and Global Buckling 66
5.1.3 Load vs. Axial Deflection 70
5.1.4 Load vs. Transverse Deflection 71
5.1.5 Stress vs. Total (Local) Strain 72

5.1.6 Stress vs. Axial Strain 75
5.1.7 Stress vs. Bending Strain 77
5.1.8 Southwell Plots 78
5.2 Discussion of Column Failure Test Results 82
5.2.1 Local Flange Buckling 82
5.2.2 Elastic Loading 83
5.2.3 Accuracy of Buckling Projections 85
5.2.4 Comparison of 20-kip and Failure Test Results 86
5.2.5 Influence of Foam Filler 87
5.2.6 Strength to Weight Ratio 88
5.3 Summary 89
6 MECHANICS ANALYSIS 91
6.1 Model Development 91
6.1.1 Assumptions 91
6.1.2 Global Boundary Conditions 93
6.1.3 Local Boundary Conditions 93
6.2 Buckling and Crippling 94
6.2.1 Global Buckling 94
6.2.2 Local Buckling 95
6.2.3 Crippling Failure 98
6.3 Parametric Studies 102
6.3.1 Effect of Foam Core Stiffness 103
6.3.2 Effect of Flange-to-Flange Attachment 105
6.3.3 Effect of Steel Thickness 109
6.4 Summary 112

7 FINITE ELEMENT ANALYSIS 113

7.1 Column Modeling 113

7.1.1 Software 113

7.1.2 Summary of Analyses 114

7.1.3 Materials 114

7.1.4 Meshing 117

7.2 Global Buckling 118

7.2.1 Description of Physical Problem 118

7.2.2 Assumptions and Modeling 119

7.2.3 Global Buckling Results 121

7.2.4 Global Buckling Discussion of Results 124

7.3 Local Buckling 125

7.3.1 Description of Physical Problem 125

7.3.2 Assumptions and Modeling 126

7.3.3 Local Buckling Results 127

7.3.4 Local Buckling Discussion of Results 133

7.4 Crippling 134

7.4.1 Description of Physical Problem 135

7.4.2 Assumptions and Modeling 135

7.4.3 Nonlinear Aspects 138

7.4.4 Crippling Convergence 138

7.4.5 Crippling Results 142

7.4.6 Crippling Discussion of Results 151

7.5 Summary 155

8 DISCUSSION OF RESULTS 157

8.1 Comparison of Analysis and Test Results 157
8.2 Local Buckling Coefficient 161
8.3 Influence of Foam on Column Compression Strength 163
8.4 Influence of Flange-to-Flange Attachment 164
8.5 Comparison of Finite Element and Mechanics-Based Plate Crippling Loads 164
9 CONCLUSION 171
9.1 Conclusions 171
9.2 Contributions 172
9.3 Recommended Future Work 173
REFERENCES 175
APPENDIX A. ADHESIVE SHEAR TEST 179
APPENDIX B. SUPPORTING CALCULATIONS 181
APPENDIX C. DETERMINATION OF GERARD CRIPPLING CONSTANT 182
APPENDIX D. FINITE ELEMENT MODEL INPUTS 184
APPENDIX E. SAMPLE FINITE ELEMENT INPUT 186
APPENDIX F. LESSONS LEARNED FOR ADINA NONLINEAR ANALYSIS 189

LIST OF TABLES

Table 2-1: Nominal Material Properties for Steel....12

Table 2-2: Specified Standard Light-Gauge Steel Thickness Values....12

Table 2-3: Material Properties for Foam-Control EPS Geofoam....13

Table 2-4: Material Properties for EPS32 Foam....13

Table 2-5: Generic Material Properties for Adhesive....15

Table 2-6: Summary and Comparison of Material Properties for Steel, Foam, and Adhesive....15

Table 2-7: Properties of Idealized Steel Cross-Section Discretized into 6 Plate Segments....18

Table 2-8: Idealized Cross-Sectional Area by Constituent Material....18

Table 2-9: Idealized Column Moments of Inertia by Constituent Material....19

Table 2-10: Idealized Column Bending Stiffness by Constituent Material....19

Table 2-11: Idealized Column Axial Stiffness by Constituent Material....20

Table 2-12: Steel Radii of Gyration and Slenderness Ratios....20

Table 2-13: Column Weight Based on Idealized Cross-Section....21

Table 2-14: Factored Axial Design Loads for Standard S-Sections Measuring 14 ft (4.27 m) Long with Yield Strength of 50 ksi (345 MPa) and Lateral Load of 5 psf (239 Pa) Based on Spacing of 16 in (40.6 cm) o.c.....24

Table 3-1: Predicted Initial Deflections Due to Self-Weight Alone....30

Table 3-2: Predicted Deflections Due to Self-Weight and 20 kips (88 kN) Axial Compression....31

Table 3-3: Critical Buckling Loads for Foam-Filled Steel Columns Based on the Euler Buckling Equation....43

Table 4-1: Axial Deflection (x-Direction) and Stiffness Values for Column Tests to 20 kips....48

Table 4-2: Transverse Deflections in the y- , z-, and Resultant Directions for Column Tests to 20 kips....51

Table 4-3: Strain at Maximum Stress (by Column Face) for Column Tests to 20 kips....53

Table 4-4: Flange and Web Axial Strain at Maximum Stress (~95 MPa or 14 ksi) for Column Tests to 20 kips 55

Table 4-5: Flange and Web Bending Strain at Maximum Stress (~95 MPa or 14 ksi) for Column Tests to 20 kips 55

Table 4-6: Slopes of Southwell Plots for Column Tests to 20 kips 59

Table 4-7: Projected Critical Buckling Loads Based on Southwell Plots for Column Tests to 20 kips 60

Table 4-8: Projected Buckling Load as a Ratio of Euler Buckling Load 62

Table 5-1: Observed Local Buckling Wavelength and Aspect Ratio 66

Table 5-2: Maximum Loads and Axial Deflections (x-Direction) for Columns Loaded to Failure (Column Stiffness Based on Deflection at 8 kips) 70

Table 5-3: Transverse Deflections in the y- , z-, and Resultant Directions for Column Tests to Failure 72

Table 5-4: Strain at Failure Stress (by Column Face) for Column Tests to Failure 75

Table 5-5: Flange and Web Axial Strain at Failure Stress (~130 MPa or 19 ksi) for Column Tests to Failure 75

Table 5-6: Flange and Web Bending Strain at Failure Stress (~130 MPa or 19 ksi) for Column Tests to Failure 78

Table 5-7: Slopes of Southwell Plots for Column Tests to Failure 81

Table 5-8: Projected Critical Buckling Loads for Column Tests to Failure 82

Table 5-9: Failure Loads Compared to Southwell Projections for Columns Based on Tests to 20 kips 85

Table 5-10: Failure Loads Compared to Southwell Projections for Columns Based on Tests to Failure 86

Table 5-11: Failure Loads Compared to Euler Buckling Loads for Columns with Pinned-Pinned Boundary Conditions (k = 1.0) 86

Table 5-12: Comparison of Southwell Projections from Tests to 20 kips and to Failure 87

Table 5-13: Comparison of Southwell Projections for Two Columns from Tests to 20 kips and to Failure 87

Table 5-14: Comparison of Mean and Standard Deviation for Columns Tested to Failure Including and Excluding “Adhesive-No-Foam” Column 88

Table 5-15: Comparison of Strength to Weight Ratios 88

Table 6-1: Dimensions of i^{th} Plate for Column Cross-Section 92

Table 6-2: Slenderness Ratio and Critical Slenderness Ratio....95

Table 6-3: Local Buckling Stress (υ = 0.3; η = 1.0) Assuming Plates are Simply-Supported on All Four Sides (k = 4.0) or Simply-Supported on Three Sides with One Edge Free (k = 0.425) 97

Table 6-4: Local Buckling Stress (υ = 0.3; η = 1.0) Assuming Plates are Clamped on All Four Sides (k = 7.0) or Clamped on Three Sides with One Edge Free (k = 1.60)....97

Table 6-5: Crippling Stress Constants 100

Table 6-6: Plate Crippling Stress for the Gerard Method (Equation 6-7) and the Boeing Method (Equation 6-8) Based on Three Sets of Boundary Condition Assumptions 101

Table 6-7: Mechanics-Based Crippling Failure Stress the Gerard Method (Equation 6-7), the Boeing Method (Equation 6-8), and the Gerard Method (Equation 6-9) Based on Three Sets of Boundary Condition Assumptions 102

Table 6-8: Column Bending Stiffness by Constituent Material....103

Table 6-9: Three Flange Attachment Model Assumptions and Implications 107

Table 6-10: Long Plate Buckling Coefficients, k, for Two Cases[3] 107

Table 6-11: Comparison of Coefficients Used to Calculate Plate Buckling Stress for Three Models....108

Table 6-12: Comparison of Plate Buckling Stress Values for Three Models....108

Table 7-1: Finite Element Analysis Summary....114

Table 7-2: Linear Elastic Material Properties for Finite Element Analysis....115

Table 7-3: Nonlinear Strain and Stress Values for Steel in Tension and Compression (υ = 0.3)....116

Table 7-4: Peak Load and Corresponding Displacement for Two 10 in (25.4 cm) Long "Adhesive Only" Models with Different Values for Adhesive Modulus of Elasticity....116

Table 7-5: Comparison of Cross-Sectional Area, Moment of Inertia, and Euler Buckling Loads from Mechanics for Two Models 119

Table 7-6: Convergence Study....122

Table 7-7: Summary of Parametric Study of Foam Elastic Modulus....123

Table 7-8: Local Buckling Stress Values to Show Mesh Convergence....130

Table 7-9: Local Buckling Stress Values to Show Mesh Convergence....133

Table 7-10: Peak Load and Corresponding Displacement for Two 10 in (25.4 cm) Long "Foam and Adhesive" Models Including a Half Model and a Full Model....138

Table 7-11: Peak Force and Stress Values for Four Model Lengths for "No Foam or Adhesive" Model with Element Edge Length of 0.50 in (1.27 cm)....139

Table 7-12: Peak Load and Stress* Values for Four Model Lengths of Four Different Configurations with Element Edge Length of 0.50 in (1.27 cm)....148

Table 7-13: Converged Peak Stress Values for Four Specimen Configurations Based on 10 in (25.4 cm) Length Model....149

Table 7-14: Plate Loads at Column Crippling Load Based on Finite Element Analysis....155

Table 8-1: Column Failure Stress from Tests to Failure Compared to Yield Stress....158

Table 8-2: Column Southwell-Based Buckling Stress Projections from Tests to Failure Compared to Yield Stress....158

Table 8-3: Column Mechanics-Based and Finite Element Global Buckling Stress Predictions Compared to Yield Stress....158

Table 8-4: Column Crippling Stress Predictions Based on Semi-Empirical Equations and SSSF Boundary Conditions for the Inner and Outer Flanges Compared to Yield Stress....159

Table 8-5: Column Finite Element Crippling Stress Predictions Compared to Yield Stress....159

Table 8-6: Summary of Failure and Buckling Stress Values Compared to Yield Stress....160

Table 8-7: Local Buckling Coefficient Comparison Between FEA and Mechanics....162

Table 8-8: Crippling Load Based on the Gerard Method (Equation 6-7) Compared to Finite Element Crippling Loads....168

Table 8-9: Crippling Load Based on the Boeing Method (Equation 6-8) Compared to Finite Element Crippling Loads....169

Table A-1: Shear Modulus and Elastic Modulus Results for Polyurethane Adhesive....179

Table B-1: Steel Moment of Inertia Calculations for Idealized Thin-Walled Model.....181

Table C-1: Plate Crippling and Buckling Boundary Condition Parameters.....182

Table D-1: Column Boundary Conditions.....184

Table D-2: Point Coordinates for Global Buckling Model (Extruded 84” (213 cm) in the x-Direction).....185

Table D-3: Point Coordinates for Global Buckling Model Based on Idealized Thin-Walled Cross-Section.....185

LIST OF FIGURES

Figure 1-1: Illustration of Foam-Filled Steel Column Cross-Section....3

Figure 1-2: Illustration of Foam-Filled Steel Column (Plan View), Modeled as Simply-Supported Compression Member....3

Figure 2-1: Photo Showing Fabrication of Columns: Application of Isogrip 4005D Adhesive....10

Figure 2-2: Photo Showing Fabrication of Columns: Insertion of EPS32 Foam into Steel Columns....11

Figure 2-3: Illustration of Thin-Walled Model Cross-Section....17

Figure 2-4: Illustration of Idealized Cross-Section Discretized into 6 Plate Segments....17

Figure 2-5: Illustration of "Adhesive-Only" Column Cross-Section: Oriented During 20-kip Test (Left); Oriented During Test to Failure (Right)....22

Figure 2-6: Illustration of "Adhesive and Welds" Column Cross-Section, as Oriented During Test to 20 kips and to Failure....22

Figure 2-7: Illustration of "Adhesive and Screws" Column Cross-Section, as Oriented During Test to 20 kips and to Failure....23

Figure 2-8: Illustration of "Adhesive-No-Foam" Column Cross-Section, as Oriented During Test to Failure....23

Figure 3-1: Photograph of "Adhesive and Welds" Column in Preliminary Testing to 20 kips Test Setup....26

Figure 3-2: Photo of Steel Reaction Frame for Test to 20 kips (Not Adequately Post-Tensioned)....27

Figure 3-3: Close-up Photo of Reaction Frame Slippage Indicated by (Reddish) Mark on Floor....27

Figure 3-4: Photo of 20-kip Actuator....28

Figure 3-5: Model of Simply-Supported Column with Gravity Load, Axial Load, Moment, Shear, and Reaction Forces....29

Figure 3-6: Photo of Vertical and Horizontal String Potentiometers Measuring Transverse Deflections for Test to 20 kips....32

Figure 3-7: Photo of String Potentiometer Attached to Reaction Frame for Test to 20 kips....32

Figure 3-8: Photo of Typical Strain Gage Attachment for Test to 20 kips.....33

Figure 3-9: Photo of Steel Reaction Frame for Tests to Failure (From Above).....34

Figure 3-10: Photo of Steel Reaction Frame for Test to Failure.....34

Figure 3-11: Photo of 100-kip Actuator for Tests to Failure.....35

Figure 3-12: Photo of Boundary Conditions (Actuator-End) During Test to Failure.....36

Figure 3-13: Close-up Photo of Boundary Conditions (Actuator-End) During Test to Failure.....37

Figure 3-14: Close-up Photo of Boundary Conditions (Reaction-End) During Test to Failure.....37

Figure 3-15: Photo of Vertical and Horizontal Transverse String Potentiometers During Test to Failure.....38

Figure 3-16: Photo of Reaction-End String Potentiometers During Test to Failure.....38

Figure 3-17: Photo of Mid-Span Strain Gages Located on Columns During Test to Failure.....39

Figure 3-18: Close-up Photo of Mid-Span Strain Gage on Column Tested to Failure.....39

Figure 3-19: Photo of LVDT used During Tests to Failure.....40

Figure 4-1: Photo of Local Buckling in “Adhesive-Only” Column During Test to 20 kips Showing Local Buckling Wavelength.....46

Figure 4-2: Photo of Local Buckling in “Adhesive and Welds” Column During Test to 20 kips.....46

Figure 4-3: Photo of Local Buckling in “Adhesive and Screws” Column During Test to 20 kips Showing Two Wavelengths Between Sets of Screws.....47

Figure 4-4: Compression Load vs. Axial Deflection (x-Direction) for Column Tests to 20 kips.....48

Figure 4-5: Compression Load vs. Transverse Deflection (y-Direction) for Column Tests to 20 kips.....49

Figure 4-6: Compression Load vs. Transverse Deflection (z-Direction) for Column Tests to 20 kips.....50

Figure 4-7: Compression Load vs. Resultant Transverse Deflection for Column Tests to 20 kips.....50

Figure 4-8: Compression Stress vs. Total Strain for “Adhesive-Only” Column Test to 20 kips 52

Figure 4-9: Compression Stress vs. Total Strain for “Adhesive and Welds” Column Test to 20 kips 52

Figure 4-10: Compression Stress vs. Total Strain for “Adhesive and Screws” Column Test to 20 kips 53

Figure 4-11: Compression Stress vs. Flange Axial Strain for Column Tests to 20 kips 54

Figure 4-12: Compression Stress vs. Web Axial Strain for Column Tests to 20 kips.....54

Figure 4-13: Compression Stress vs. Flange Bending Strain for Column Tests to 20 kips.....56

Figure 4-14: Compression Stress vs. Web Bending Strain for Column Tests to 20 kips.....56

Figure 4-15: Southwell Plots with Linear Regression Lines Based on 0.20-0.63” Transverse Deflections in the Negative z-Direction for Column Tests to 20 kips 57

Figure 4-16: Southwell Plots and Linear Regression Lines Based on 0.00-1.16” Transverse Deflections in the Negative z-Direction for Column Tests to 20 kips 58

Figure 4-17: Southwell Plots and Linear Regression Lines Based on 0.24-0.64” Transverse Resultant Deflections for Column Tests to 20 kips 58

Figure 4-18: Southwell Plots and Linear Regression Lines Based on 0.00-1.24” Transverse Resultant Deflections for Column Tests to 20 kips 59

Figure 4-19: Comparison of Southwell and Euler Projected Buckling Loads for Column Tests to 20 kips.....62

Figure 5-1: Photo of Local Buckling of “Adhesive-Only” Column During Test to Failure 65

Figure 5-2: Photo of Local Buckling of “Adhesive and Screws” Column During Test to Failure Showing Two Wavelengths Between Sets of Screws.....65

Figure 5-3: Photo of Local Buckling of “Adhesive-No-Foam” Column During Test to Failure.....66

Figure 5-4: Photo of Crippled “Adhesive-Only” Column During Test to Failure 67

Figure 5-5: Photo of Buckled “Adhesive and Welds” Column During Test to Failure 67

Figure 5-6: Photo of Rotation Produced by Crippled “Adhesive and Welds” Column at Reaction-End During Test to Failure 68

Figure 5-7: Photo of Buckled “Adhesive and Screws” Column During Test to Failure 68

Figure 5-8: Close-up Photo of Crippling of “Adhesive and Screws” Column During Test to Failure 69

Figure 5-9: Photo of Crippled “Adhesive-No-Foam” Column During Test to Failure 69

Figure 5-10: Compression Load vs. Axial Deflection for Column Tests to Failure.....70

Figure 5-11: Compression Load vs. Transverse Deflection (y-Direction) for Column Tests to Failure 71

Figure 5-12: Compression Load vs. Transverse Deflection (z-Direction) for Column Tests to Failure 71

Figure 5-13: Compression Load vs. Resultant Deflection for Column Tests to Failure 72

Figure 5-14: Compression Stress vs. Total Strain for “Adhesive-Only” Column Test to Failure.....73

Figure 5-15: Compression Stress vs. Total Strain for “Adhesive and Welds” Column Test to Failure.....73

Figure 5-16: Compression Stress vs. Total Strain for “Adhesive and Screws” Column Test to Failure.....74

Figure 5-17: Compression Stress vs. Total Strain for “Adhesive-No-Foam” Column Test to Failure 74

Figure 5-18: Compression Stress vs. Flange Axial Strain for Column Tests to Failure.....76

Figure 5-19: Compression Stress vs. Web Axial Strain for Column Tests to Failure 76

Figure 5-20: Compression Stress vs. Flange Bending Strain for Column Tests to Failure 77

Figure 5-21: Compression Stress vs. Web Bending Strain for Column Tests to Failure 78

Figure 5-22: Southwell Plots with Linear Regression Lines Based on Partial Range Transverse Deflections in the Negative y-Direction for Column Tests to Failure.....79

Figure 5-23: Southwell Plots with Linear Regression Lines Based on Full Range Transverse Deflections in the Negative y-Direction for Column Tests to Failure.....80

Figure 5-24: Southwell Plots with Linear Regression Lines Based on Partial “Linear Portion” of Resultant Transverse Deflections for Column Tests to Failure 80

Figure 5-25: Southwell Plots with Linear Regression Lines Based on Full "Linear Portion" of Resultant Transverse Deflections for Column Tests to Failure 81

Figure 5-26: Local Buckling of Flanges Observed on Column Tests to 20 kips: "Adhesive-Only" (Left) and "Adhesive and Screws" (Right) 83

Figure 5-27: Comparison of Compression Stress vs. Average Web Axial Strain for Test to 20 kips and to Failure 84

Figure 5-28: Comparison of Compression Stress vs. Average Web Bending Strain for Test to 20 kips and to Failure 84

Figure 6-1: Illustration of Column Cross-Section Used in Mechanics Analysis 92

Figure 6-2: Illustration of Cross-Section Cuts and Flanges to Determine the Gerard Constant, *g* 102

Figure 6-3: Predicted Global Buckling Load vs. Foam Elastic Modulus 104

Figure 6-4: Relative Global Buckling Load vs. Relative Foam Stiffness 105

Figure 6-5: Illustration of Three End Views of Flange Attachment Models: 1) Fully Connected Flanges; 2) Free Outer Flanges; and 3) Free Outer and Inner Flanges 106

Figure 6-6: Column Plate Segment Aspect Ratio (*b/t*) vs. Steel Thickness 110

Figure 6-7: Column Slenderness Ratio vs. Steel Thickness 111

Figure 6-8: Column Crippling Stress vs. Steel Thickness 111

Figure 6-9: Column Crippling Load vs. Steel Thickness 112

Figure 7-1: Nonlinear Stress vs. Strain for Steel in Tension 115

Figure 7-2: Axial Load vs. Applied Displacement (x-Direction) for Two "Adhesive Only" Models with Two Different Values for Adhesive Elastic Modulus 117

Figure 7-3: Elements Used in Finite Element Analysis: 20-Node Brick Element Used to Model 3-D Solid Elements (Left); and, 8-Node Quad Element Used to Model Shell Elements (Right) 117

Figure 7-4: Photo of Global Buckling of "Adhesive and Welds" Column During Test to Failure 118

Figure 7-5: End View of Column Models: 1) Shells and 3-D Solids Model; and, 2) 3-D Solids Only Model 120

Figure 7-6: Finite Element Band Plot of Buckled 3-D Solid Elements Only Model Superimposed on Original Mesh 121

Figure 7-7: Global Buckling Compression Stress vs. Number of Nodes to Show Mesh Convergence 122

Figure 7-8: Global Buckling Compression Load vs. Foam Elastic Modulus for Two Column Models 123

Figure 7-9: Relative Global Buckling Load vs. Relative Foam Elastic Modulus for Two Column Models 124

Figure 7-10: Close-up Photo of Local Buckling in "Adhesive-Only" Column During Test to 20 kips 125

Figure 7-11: Finite Element Band Plot of Local Buckling Model Measuring 8" (20.3 cm) with ½" (1.27 cm) Steel End Plate with Steel Shell (Green), Foam Core (Gray), and Adhesive (Pink) Showing Deformed Shape 126

Figure 7-12: Finite Element Band Plot of Local Buckling Model Measuring 8" (20.3 cm) with ½" (1.27 cm) Steel End Plate with Steel Shell (Green), Foam Core (Gray), Adhesive (Pink), and Springs Modeling Adhesive Between Flanges (Blue) Showing Deformed Shape 127

Figure 7-13: Local Buckling Compression Stress vs. Number of Nodes to Show Mesh Convergence for Models with No Springs Between Flanges 129

Figure 7-14: Local Buckling Compression Stress vs. Flange Aspect Ratio (Converged Values) as a Function of Modulus of Elasticity of Adhesive 131

Figure 7-15: Local Buckling Compression Load vs. Flange Aspect Ratio (Converged Values) as a Function of Modulus of Elasticity of Adhesive 131

Figure 7-16: Local Buckling Compression Stress vs. Spring Constant 132

Figure 7-17: Local Buckling Compression Stress vs. Equivalent Adhesive Stiffness 132

Figure 7-18: Close-up Photo of Crippling of "Adhesive and Screws" Column During Test to Failure 135

Figure 7-19: Finite Element Band Plot of Deformed Column Cross-Section with No Foam After Crippling Analysis Showing Effective Stress 136

Figure 7-20: Finite Element Band Plot of Deformed Crippling Analysis "No Foam or Adhesive" Model Measuring 12" (20.3 cm) with ½" (1.27 cm) Steel End Plate Showing Effective Stress 136

Figure 7-21: Axial Load vs. Applied Displacement (x-Direction) for 8 in (20.3 cm) Long "No Foam or Adhesive" Model to Compare Half Model to Full Model 137

Figure 7-22: Axial Load vs. Applied Displacement (x-Direction) for 8 in (20.3 cm) Long "No Foam or Adhesive" Model 139

Figure 7-23: Axial Load vs. Applied Displacement (x-Direction) for 10 in (25.4 cm) Long "No Foam or Adhesive" Model 140

Figure 7-24: Axial Load vs. Applied Displacement (x-Direction) for 12 in (30.5 cm) Long "No Foam or Adhesive" Model 140

Figure 7-25: Axial Load vs. Applied Displacement (x-Direction) for 14 in (35.6 cm) Long "No Foam or Adhesive" Model 141

Figure 7-26: Axial Load vs. Applied Displacement (x-Direction) for Four Specimen Lengths for "No Foam or Adhesive" Model with Converged Element Edge Length of 0.5 in (1.27 cm).....141

Figure 7-27: Finite Element Band Plot of Effective Stress for 10 in (25.4 cm) "No Foam or Adhesive" Model 142

Figure 7-28: Finite Element Band Plot of Effective Stress for 10 in (25.4 cm) "Foam Only" (No Adhesive) Model 143

Figure 7-29: Finite Element Band Plot of Effective Stress for 10 in (25.4 cm) "Adhesive Only" (No Foam) Model 143

Figure 7-30: Finite Element Band Plot of Effective Stress for 10 in (25.4 cm) "Foam and Adhesive" Model.....144

Figure 7-31: Axial Load vs. Applied Displacement (x-Direction) for 8 in (20.3 cm) Long Half-Model for Four Specimen Configurations 145

Figure 7-32: Axial Load vs. Applied Displacement (x-Direction) for 10 in (25.4 cm) Long Half-Model for Four Specimen Configurations.....145

Figure 7-33: Axial Load vs. Applied Displacement (x-Direction) for 12 in (30.5 cm) Long Half-Model for Four Specimen Configurations.....146

Figure 7-34: Axial Load vs. Applied Displacement (x-Direction) for 14 in (35.6 cm) Long Half-Model for Four Specimen Configurations.....146

Figure 7-35: Axial Load vs. Applied Displacement (x-Direction) for Four Lengths of Half-Models for Four Specimen Configurations 147

Figure 7-36: Peak Axial Load vs. Applied Displacement (x-Direction) Maximum Values for Four Model Lengths for Four Configurations 147

Figure 7-37: Finite Element Band Plot of Effective Stress in Foam for 10 in (25.4 cm) "Foam Only" (No Adhesive) Model 150

Figure 7-38: Finite Element Band Plot of z-Strain in Foam for 10 in (25.4 cm) "Foam Only" (No Adhesive) Model 150

Figure 7-39: Axial Load vs. Applied Displacement (x-Direction) for 10 in (25.4 cm) Long "No Foam or Adhesive" Model Analyzed by Flange and Webs 152

Figure 7-40: Axial Load vs. Applied Displacement (x-Direction) for 10 in (25.4 cm) Long "Foam Only" (No Adhesive) Model Analyzed by Flanges and Webs 153

Figure 7-41: Axial Load vs. Applied Displacement (x-Direction) for 10 in (25.4 cm) Long "Adhesive Only" (No Foam) Model Analyzed by Flanges and Webs 153

Figure 7-42: Axial Load vs. Applied Displacement (x-Direction) for 10 in (25.4 cm) Long "Foam and Adhesive" Model Analyzed by Flanges and Webs 154

Figure 8-1: Local Buckling Coefficient vs. Flange Aspect Ratio of Flange-Flange Attachment 163

Figure 8-2: Comparison of Results from Finite Element and Mechanics-Based Crippling Analysis for 10 in (25.4 cm) "Foam and Adhesive" Model by Flanges and Webs 165

Figure 8-3: Comparison of Results from Finite Element and Mechanics-Based Crippling Analysis for 10 in (25.4 cm) "Adhesive Only" Model by Flanges and Webs 166

Figure 8-4: Comparison of Results from Finite Element and Mechanics-Based Crippling Analysis for 10 in (25.4 cm) "Foam Only" Model by Flanges and Webs 166

Figure 8-5: Comparison of Results from Finite Element and Mechanics-Based Crippling Analysis for 10 in (25.4 cm) "No Foam or Adhesive" Model by Flanges and Webs 167

Figure A-1: Shear Load vs. Deflection for Polyurethane Adhesive Shear Test 180

Figure A-2: Average Shear Stress vs. Strain for Polyurethane Adhesive Shear Test.....180

Figure C-1: Plate Buckling Coefficient vs. Plate Crippling Boundary Condition Parameter.....183

LIST OF NOMENCLATURE

a	Local buckling plate wavelength
A	Cross-sectional area
A_f , A_s	Cross-sectional area of foam and steel respectively
E	Elastic modulus
E_f , E_s	Elastic modulus of foam (core) and steel (facings) respectively
g	Number of cuts to reduce cross-section to flanges
g_f	Local plate boundary condition parameter
G	Shear modulus
h	Depth of column cross-section or distance between strain gages
i	Index varying from 1 to n
I	Moment of inertia
I_{yy} , I_{zz}	Moment of inertia about the y-axis and the z-axis respectively
k	Effective length factor; buckling coefficient
K	Spring constant or column stiffness
L	Column length
L_e	Effective column length
m	Empirical constant
M	Moment
n	Empirical constant
$N_{x,cr}$	Compressive load intensity
P	Applied load
P_{cr}	Critical buckling load
P_n	Axial load capacity of reinforced concrete column
t	Thickness
u_1 , u_2 , u_3	Displacement in the x-, y-, and z-direction respectively
u_R	Resultant displacement
V	Shear force
w	Distributed load or unit weight
W	Total weight
z	Distance from the neutral axis
α	Empirical constant
β	Empirical constant
β_g	Empirical constant
γ	Density
δ	Deflection
δ_y	Deflection in the y-direction
δ_z	Deflection in the z-direction
ε	Total local strain
ε^o	Axial strain component
ε_u	Strain in upper face
ε_l	Strain in lower face
η	Plasticity correction value
θ	Rotational displacement
κ	Bending strain component

$\mu\varepsilon$	Microstrain
ν	Poisson's ratio
ρ	Radius of gyration
ρ_f , ρ_s	Radius of gyration of foam and steel respectively
ρ_y , ρ_z	Radius of gyration about the y-axis and z-axis respectively
σ	Average axial stress
σ_{cc}	Crippling stress
σ_{co}	Cutoff stress or column yield stress
σ_{cr}	Critical buckling stress (global or local)
σ_{cy}	Compressive yield stress
σ_f	Failure stress

1 INTRODUCTION

This thesis summarizes testing and analysis of 14-foot long lightweight columns composed of thin-walled steel, foam, and adhesive with a unique cross-sectional configuration. The columns may be used in place of traditional wood or reinforced concrete for building design. This chapter summarizes the purpose of investigation, description of foam-filled steel columns, literature review, scope of research and objectives, limitations, and overview.

1.1 Purpose of Investigation

The purpose of this investigation was to thoroughly analyze the buckling and crippling of symmetrically overlapping U-channel steel square thin-walled tubes enclosing foam in order to determine improvements which increase strength without significantly increasing overall weight. This purpose was accomplished through testing, mechanics analysis, and finite element analysis. These three tools combined provided valuable insights regarding the current design, as well as possible design improvements. Because the testing and analysis available in this thesis had not been performed previously, this thesis provides unique knowledge regarding the specific design of foam-filled steel columns described herein.

1.2 Description of Foam-Filled Steel Columns

Test columns were fabricated using two 16-gauge galvanized steel channels (one inverted relative to the other) and filled with prefabricated foam inserts. The resulting test specimens were 4" square, foam-filled, thin-walled, steel columns. The cross-section of a typical column is depicted in Figure 1-1. The figure shows that the total column cross-section measured approximately 4" x 4" (10.2 cm x 10.2 cm) and that the steel is approximately 0.06" (0.15 cm) thick. The total cross-sectional area of the steel is approximately 1.44 in^2 (9.29 cm^2). The plan view of a typical 14 feet long (4.27 m) column, modeled as a simply-supported member in compression, is depicted in Figure 1-2. The thin-walled steel shell supports the compressive loads. The thin steel also has a large moment of inertia which increases the buckling capacity. The expanded polystyrene (EPS) foam filler is intended to improve both global lateral stability, as well as local flange buckling stability. The weight of the combined light-gauge steel and foam is only approximately 70.6 lbs (32.0 kg). The thin walls help to make the structure very lightweight and easy to prefabricate; however, these thin walls also make the column susceptible to crippling failure. The adhesive needs to have sufficient tensile strength in order to fully connect the flanges. The foam core is soft relative to the steel skin. In order to adequately provide lateral stability and prevention of inward local buckling of the flanges, the foam needs to exhibit a minimum stiffness. These concepts are explored throughout the thesis.

The design and manufacturing of the columns were performed by Novatek, Inc. (2012) for building applications as part of the New Vistas project.

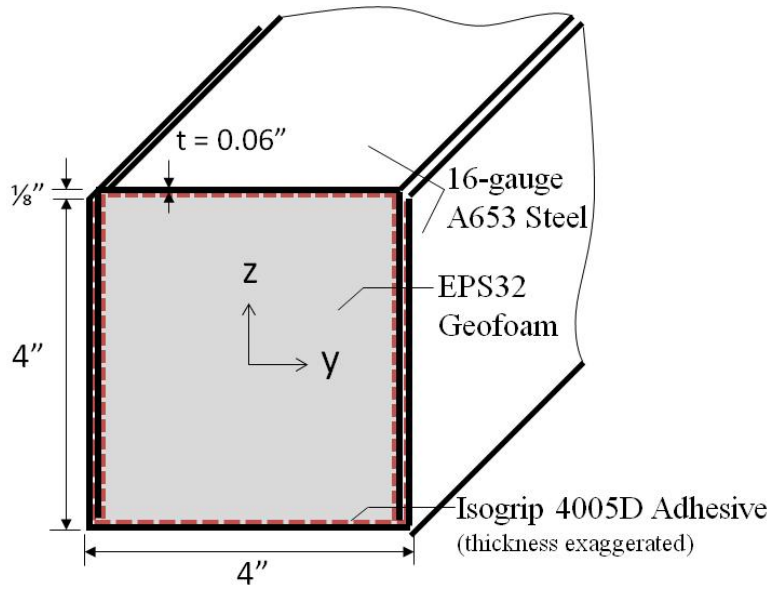

Figure 1-1: Illustration of Foam-Filled Steel Column Cross-Section

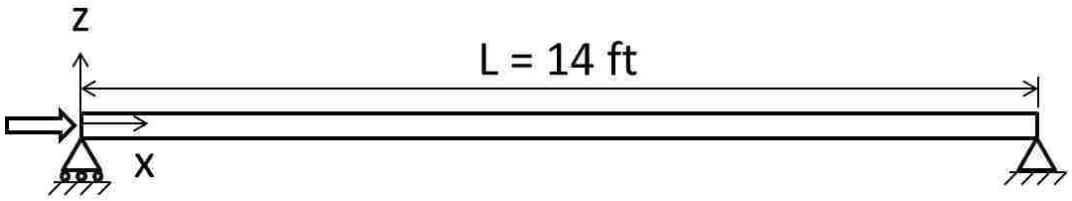

Figure 1-2: Illustration of Foam-Filled Steel Column (Plan View), Modeled as Simply-Supported Compression Member

1.3 Literature Review

Light-gauge steel combined with foam is a technology currently used by construction companies, such as Global Building Systems, Inc. (2011). The foam is used primarily as insulation and to dampen sound and the steel is the main structural element. Although lightweight structures have not traditionally been used in civil structures, there has been an increase in prevalence. Recently there has been more research for using lightweight, prefabricated structural members in building construction. For example, Hedman-Petursson (2001) stated, "The use of prefabricated building elements such as roof, wall and floor elements

[has] been increasing, [thus] improving quality and time efficiency." Additionally, lightweight structures have been vital in many industries for decades including the space, aircraft (Rivello 1969; Curtis 1997; Megson 2010), and automobile industries, mainly for fuel economy. The Steel Stud Manufacturers Association (SSMA) has standardized four structural steel stud shapes including C-Stud/Joists (S-Sections), Tracks (T-Sections), Channels (U-Sections), and Furring Channels (F-Sections) in compliance with the 2009 International Building Code (2011). These shapes are a feasible alternative for the column design discussed in this thesis, although the shapes do not incorporate foam in the design. Foam has been used in lightweight structures because of its low density. Foam may be used to define a shape, provide thermal or acoustic insulation, maintain a cross-section, and/or delay local buckling (if the foam is stiff enough). For example, many vehicles on the roads today have foam-filler, such as aluminum foam, in the steel structure (Bi, et al. 2010) for sound damping. Thus, mechanics-based analysis has been thoroughly investigated for lightweight structures. The concept of combining thin-walled shells and a soft core has been used in these industries for decades. Because many lightweight structures, including the columns analyzed in this thesis, are long, slender members susceptible to buckling, instability is a major driving design mechanism for these structures.

The study of the stability of columns dates back to Leonhard Euler (1759), who first derived the equation for global buckling. Euler's equation is widely used. The equation may be adapted for intermediate columns using the Johnson-Euler method (see, e.g., Walls 1969). Timoshenko and Gere (1961) helped to establish equations for plate buckling. These equations are useful in analyzing thin-walled columns, which may be considered to be a combination of plates. In general, the plate elements of the columns are either referred to as webs (plate

segments simply-supported on all four sides) or flanges (plate segments simply-supported on three sides and free on one unloaded side).

The Southwell method was developed for predicting the buckling load of a structure using empirical data which does not require the specimen to be loaded to failure. According to Ko (1987), "the Southwell method has been successful in the prediction of classical buckling of simple structures such as columns and plates." The method involves mathematically converting the naturally inverse-hyperbolic load versus deflection curves into straight lines; the inverse slope of the resulting straight lines is an approximation for the buckling load.

Thin-walled structures are also susceptible to crippling, a local buckling phenomenon characterized by a permanent deformation of the cross-section. Crippling can occur at a lower value than global buckling and therefore frequently drives the design of lightweight structures. Many authors helped establish semi-empirical equations for predicting crippling loads (Gerard 1958; Bruhn 1973). These equations appear in many aircraft textbooks (e.g., Curtis 1997; Megson 2010). These equations may vary slightly depending on the material. In addition to crippling, research has been conducted on the crushing of thin-walled structures (Lee, et al. 2010; Reid 1986).

In the model used in this thesis the foam is the "core" and the steel is the "skin." Using foam-filler in sandwich walls and columns is not a unique idea. Previous studies on foam-filled, thin-walled members include applications for crashworthiness designs (Bi, et al. 2010) and for static and dynamic loading (Mirfendereski, et al. 2008). Trudeau (2011) used steel facesheets with foam core. He said, "The primary use of the core is to increase the rigidity to the composite while minimizing its weight." Abundant research is available regarding sandwich walls and columns (Ji 2008). The sandwich concept is to combine facesheets, or "skin," with a lightweight

core. The facesheets carry the load and the core provides stability without adding significant weight. Many parametric analyses have taken place to study the effect of using different skins materials or configurations for such structures (Reany 2009). The effect of using different core densities, as well as the local buckling and debonding of sandwich structures and composite structural members have been analyzed (Aviles 2005; Kollár 2003). Sharaf, et al. (2010) published a work which identified various material failures (see also Gibson, et al. 1989).

In building construction, where weight is not as critical, steel columns are sometimes filled with concrete to achieve greater stability. In many building applications, concrete filler or different material columns may be suitable options; still, in some building applications the lightweight column provides a feasible alternative for quality and timely construction. As the application of such building elements increases, there will be a growing demand for more related research.

1.4 Scope of Research and Ojectives

The scope of this research is to:

- Present results for four full-scale tests.
- Compare with mechanics-based and linear and nonlinear finite element analysis to predict global buckling, local buckling, and crippling.

The objectives of this thesis are:

1. To determine whether the presence of a foam core increases compressive strength by delaying either global or local buckling or crippling;

2. To identify fundamental mechanics-based and finite element analytical procedures to predict column failure load with accuracy;

3. To validate finite element predictions with experimental test results; and,

4. To suggest design improvements including: steel thickness, foam stiffness, and flange attachment method.

1.5 Limitations

Some limitations in this study include:

- Experimental testing includes only four test samples.
- This thesis does not include constituent material testing.
- Manufacturing imperfections in the columns are not considered.
- Bending due to slight eccentricities in the loading and/or imperfections in the test specimens was ignored.
- Foam material failures are not considered.
- Tests are only performed using EPS foam.
- The finite element analysis is restricted by total memory allocated (3.5 GB).

1.6 Overview of Thesis

Chapter 2 describes the column design concept, manufacturing, material properties, geometry, weight, and design configurations in detail. Chapter 3 describes the column testing procedures. Chapter 4 describes preliminary column testing to 20 kips (88 kN). The testing described in this chapter was intended to load the columns to failure; however, the columns exceeded the strength of the 20-kip actuator. Consequently a higher capacity actuator and a larger testing fixture were used. Thus, Chapter 5 describes the column testing to failure.

Chapter 6 presents the results of mechanics-based analysis conducted using Excel 2010 and Matchcad 15.0. This chapter also includes parametric studies used to identify improved values for steel thickness, foam stiffness, and flange attachment method. These parameters are improved for strength considerations without adding significant weight to the design. Chapter 7 presents a finite element analysis which was performed to improve the performance of the columns. Chapter 8 compares the results from the full-scale testing to analysis presented in Chapters 6 and 7. Finally, Chapter 9 summarizes results identified in this thesis, contributions to the state-of-the-art, and recommendations for future work.

2 FOAM-FILLED COLUMN DESCRIPTION

This chapter describes the design concept, manufacturing, material properties, geometry, weight, and design configurations for the foam-filled, thin-walled, galvanized steel columns.

2.1 Design Concept

The foam-filled steel column design was developed by Novatek, Inc. for building applications with the New Vistas project. Two driving criteria which led to the design were that the columns needed to be: 1) lightweight; and 2) able to be assembled quickly and in mass quantity at a construction site. The first criterion was achieved by combining light-gauge steel and foam to create a column weighing approximately 70.6 lbs (32.0 kg). The second criterion was also achieved because the light-gauge (rolled) steel can be cut, folded, and adhesively bound with the foam-filler on site.

The foam in this design was inserted using expanded polystyrene, but may also be expanded within the column using polyurethane (note that the polyurethane provides self-adhesion to the columns, whereas the EPS does not). The use of screws or short welds may take place to attach the flanges in order to increase the capacity of the column. The method of attaching the column flanges is meant to be relatively simple and fast.

2.2 Manufacturing

The manufacturing of the columns was completed by Novatek, Inc. Figure 2-1 shows the adhesive being applied on the interior faces the pre-folded U-channel shapes. Figure 2-2 shows the insertion of the EPS foam being placed into the U-channels. The prefabricated foam was cut to size and inserted in the inner channel. Then the outer channel was placed so as to enclose the foam and inner channel. These channels constitute the outer shells of the columns.

Figure 2-1: Photo Showing Fabrication of Columns: Application of Isogrip 4005D Adhesive

Figure 2-2: Photo Showing Fabrication of Columns: Insertion of EPS32 Foam into Steel Columns

2.3 Material Properties

This section described the properties of the three materials composing the columns: steel, foam, and adhesive.

2.3.1 Steel

Novatek indicated that the steel used to fabricate these columns was ASTM A653, Grade 50 Class I, galvanized sheet steel with a yield strength of 50 ksi (345 MPa) and an ultimate tensile strength of 68 ksi (469 MPa). Material properties for the steel are listed in Table 2-1. The steel was 16-gauge. The standard thickness values for light-gauge steel are listed in Table 2-2 (see Rowlett 2010). Note that although the thickness of 16-gauge steel is nominally referred

to as 0.06" (1.524 mm) in the text, the actual thickness used in all calculations in this thesis was 0.0598" (1.519 mm) as listed in the table.

Table 2-1: Nominal Material Properties for Steel

Material	Density, γ [kg/m^3 (pcf)]	Yield Strength, σ_y [MPa (ksi)]	Elastic Modulus, E_s [MPa (ksi)]	Poisson's Ratio, υ [no units]
A653 Steel	7,900 (493)	345 (50)	2x10^5 (29,000)	0.3

Table 2-2: Specified Standard Light-Gauge Steel Thickness Values

Gauge	Thickness, t [mm (in)]	Gauge	Thickness, t [mm (in)]
3	6.073 (0.2391)	20	0.912 (0.0359)
4	5.695 (0.2242)	21	0.836 (0.0329)
5	5.314 (0.2092)	22	0.759 (0.0299)
6	4.935 (0.1943)	23	0.683 (0.0269)
7	4.554 (0.1793)	24	0.607 (0.0239)
8	4.176 (0.1644)	25	0.531 (0.0209)
9	3.797 (0.1495)	26	0.455 (0.0179)
10	3.416 (0.1345)	27	0.417 (0.0164)
11	3.038 (0.1196)	28	0.378 (0.0149)
12	2.657 (0.1046)	29	0.343 (0.0135)
13	2.278 (0.0897)	30	0.305 (0.0120)
14	1.897 (0.0747)	31	0.267 (0.0105)
15	1.709 (0.0673)	32	0.246 (0.0097)
16	1.519 (0.0598)	33	0.229 (0.0090)
17	1.367 (0.0538)	34	0.208 (0.0082)
18	1.214 (0.0478)	35	0.191 (0.0075)
19	1.062 (0.0418)	36	0.170 (0.0067)

2.3.2 Foam

Prefabricated expanded polystyrene geofoam (EPS32) was inserted into the columns. The foam is produced by AFM Corporation and is called Foam-Control EPS. The foam is

produced according to ASTM D6817 standards. The value 32 indicates that the foam had a density of approximately 2.0 pcf (32 kg/m^3). The properties for various foam densities are listed in Table 2-3 (see AFM Corporation 2011). The properties for EPS32 are listed in Table 2-4 (obtained from linear interpolation of Table 2-3).

Table 2-3: Material Properties for Foam-Control EPS Geofoam

Specification	Density, γ [kg/m^3 (pcf)]	Elastic Modulus, E_f [kPa (psi)]
EPS12	11.2 (0.70)	1,500 (220)
EPS15	14.4 (0.90)	2,500 (360)
EPS19	18.4 (1.15)	4,000 (580)
EPS22	21.6 (1.36)	5,000 (730)
EPS29	28.8 (1.80)	7,500 (1,090)
EPS39	38.4 (2.40)	10,300 (1,500)
EPS46	45.7 (2.85)	12,800 (1,860)

Table 2-4: Material Properties for EPS32 Foam

Material	Density, γ [kg/m^3 (pcf)]	Yield Strength, σ_y [MPa (ksi)]	Elastic Modulus, E_f [MPa (ksi)]	Poisson's Ratio, υ [no units]
EPS32 Foam	32 (2.0)	0.0836 (0.0121)	8.3 (1.2)	0.3

The foam was used for two reasons: 1) to laterally brace the columns from buckling under compression loads; and, 2) to prevent inward local buckling of the flanges. This thesis investigates the extent to which the foam accomplished these purposes.

Polyurethane-polyurea elastomer spray foam was also investigated as an alternative to EPS foam. One disadvantage of using EPS foam as opposed to the spray foam is that the EPS

foam provides no self-adhesion to the steel and thus requires additional adhesive. Also, the foam cutting must be precise in order to achieve fit in the channels with small tolerances (no gaps).

2.3.3 Adhesive

Isogrip 4005D structural adhesive (manufactured by Ashland Chemical Company) was used to bind the foam and the columns together. This adhesive is designed for use in building construction, such as wood and laminated panel applications. Figure 2-1 (shown previously) depicts how the adhesive was placed within the steel columns and how the foam was inserted in the channels during assembly. In addition to the foam being bonded, the flanges of the inner and outer channels were adhesively bonded. Notice in the figure that the adhesive was not uniformly distributed throughout the inside surfaces of the columns. Adhesive should be distributed uniformly throughout the interior surfaces in future manufacturing and testing.

Bonded flanges should increase the theoretical local buckling strength considerably. This occurs by forcing the two adjacent flanges with otherwise free side boundary conditions to act as a single unit with effectively simply-supported side boundary conditions. This thesis investigates the method of flange attachment in order to determine if adhesive alone is sufficient for providing simply-supported side boundary conditions. Specific material properties for Isogrip 4005D adhesive were not available, however generic material properties for polyurethane adhesive are listed in Table 2-5. The polyurethane elastic modulus was approximated based on results from a single shear test (see Appendix A). The epoxy elastic modulus is taken from Dean and Crocker (2001, p.3). The poisson's ratio used is a typical value for polymers (Smith and Hashemi 2010, p.995).

Table 2-5: Generic Material Properties for Adhesive

Material	Polyurethane Elastic Modulus, E_a [MPa (ksi)]	Epoxy Elastic Modulus, E_a [MPa (ksi)]	Poisson's Ratio, υ [no units]
Adhesive	2,034 (295)	2,760 (400)	0.4

2.3.4 Summary

Table 2-6 summarizes the ratio of elastic modulus of core (foam) to elastic modulus of facings (steel).

Table 2-6: Summary and Comparison of Material Properties for Steel, Foam, and Adhesive

Material	Designation	Modulus of Elasticity, E [MPa (ksi)]	Poisson's Ratio, υ
Steel	E_s	$2x10^5$ (29,000)	0.3
Foam	E_f	8.3 (1.2)	0.3
Adhesive	E_a	2.7 (0.4)	0.4
Ratio of E_f / E_s		$4.1x10^{-5}$	

2.4 Geometry

This section summarizes the column geometry. Each column measured approximately 14 feet 1/8 inch (4.29 m) in length. This thesis uses the measure column length for reducing test data, but uses a nominal value of 14 feet (4.27 m) for mechanics analysis and finite element analysis.

2.4.1 Web and Flange Nomenclature

In this thesis, “web” refers to plate segments of the cross-section which are simply-supported on all both long edges; “flange” refers to plate segments of the cross-section which are simply-supported on one long edge and free on one long edge. Both webs and flanges are assumed to be simply-supported on the ends.

2.4.2 Cross-Section

An important distinction is made in this subsection between the measured cross-section and the idealized cross-section of the columns. The total measured cross-section was approximately 4.0 inches wide by 4.125 inches deep, as illustrated previously in illustrated in Figure 1-1. The figures illustrates how the two overlapping 16-gauge galvanized steel “C” channels fit inside one other, opened towards each other. Note that because the inner and outer channels were cut and folded with identical dimensions during the manufacturing process, the flange of the inner channel sticks out up to approximately 0.25 inches, depending on the column, and the flange of the outer channel is predisposed to deflect outwards. In future assemblies, the manufacturer should considered making the inner channel slightly smaller than the outer channel in order to achieve a better fit. For consistency, the geometry of the idealized cross-section is used in all calculations in this thesis.

The thin-walled model cross-section is shown in Figure 2-3. The idealized steel cross-section areas based on six discretized plate segments is shown in Figure 2-4. The areas of each segment are listed in Table 2-7. The calculated cross-sectional area of the steel and the foam are listed in Table 2-8.

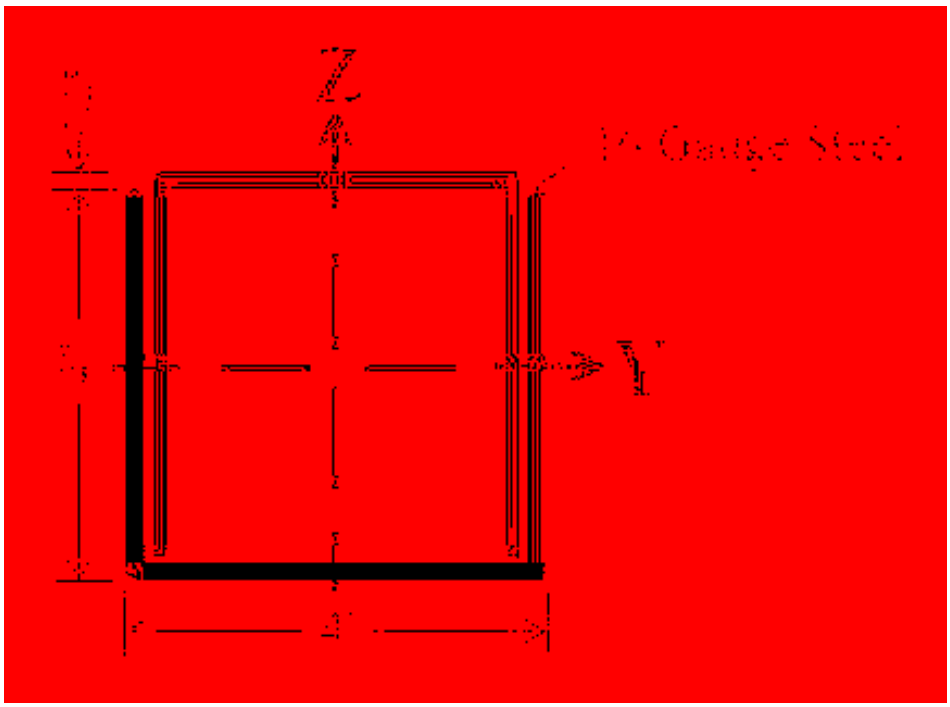

Figure 2-3: Illustration of Thin-Walled Model Cross-Section

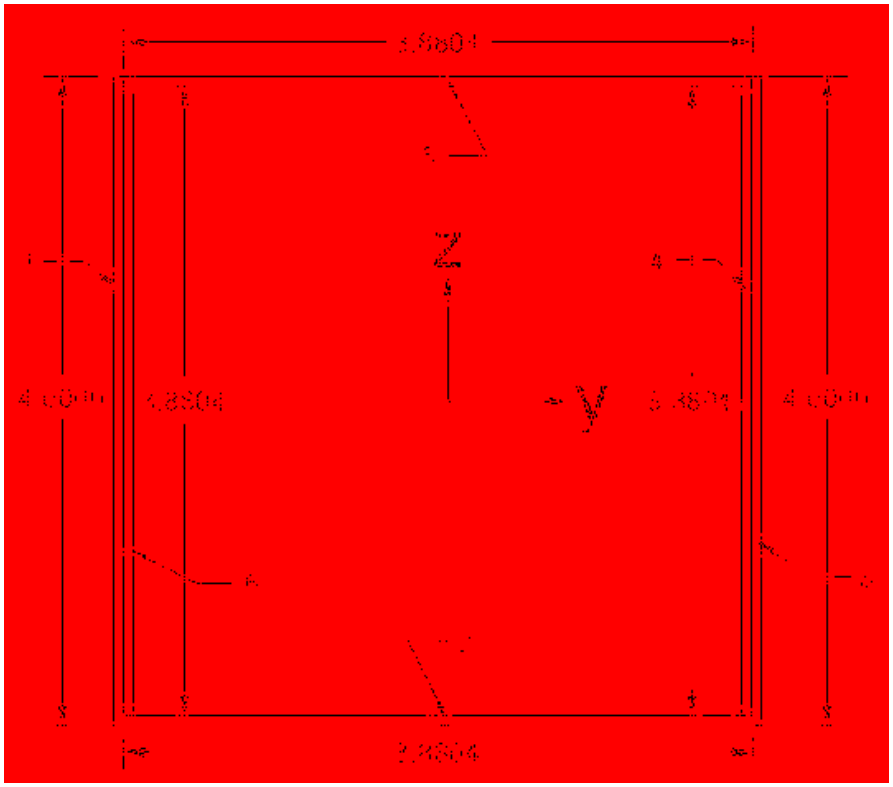

Figure 2-4: Illustration of Idealized Cross-Section Discretized into 6 Plate Segments

Table 2-7: Properties of Idealized Steel Cross-Section Discretized into 6 Plate Segments

Plate # (i)	Width, b_i [cm (in)]	Thickness, t_i [cm (in)]	Area, A_i [cm^2 (in^2)]
1	10.16 (4.0000)	0.152 (0.0598)	1.54 (0.2392)
2	9.89 (3.8804)	0.152 (0.0598)	1.50 (0.2320)
3	10.16 (4.0000)	0.152 (0.0598)	1.54 (0.2392)
4	9.89 (3.8804)	0.152 (0.0598)	1.50 (0.2320)
5	9.89 (3.8804)	0.152 (0.0598)	1.50 (0.2320)
6	9.89 (3.8804)	0.152 (0.0598)	1.50 (0.2320)
			ΣA = 9.07 (1.4066)

Table 2-8: Idealized Cross-Sectional Area by Constituent Material

Constituent Material	Cross-Sectional Area, A [cm^2 (in^2)]
Steel	9.07 (1.41)
Foam	94.2 (14.6)

2.4.3 Moment of Inertia

Moment of inertia calculations were performed separately for the steel and the foam. Supporting calculations for moments of inertia about the y- and z-axes of the column are listed in Appendix B. The results are summarized in Table 2-9. Due to the overlapping flanges, the steel moment of inertia about the y-axis is less than the moment of inertia about the z-axis. This indicates that columns will typically buckle first about the y-axis (in the z-direction, perpendicular to the webs).

Table 2-9: Idealized Column Moments of Inertia by Constituent Material

Constituent Material	Moment of Inertia	
	I_{yy} [cm^4 (in^4)]	I_{zz} [cm^4 (in^4)]
Steel	125.8 (3.02)	172.0 (4.13)
Foam	762.2 (18.3)	715.9 (17.2)
Ratio of Steel to Foam	0.166	0.240

2.4.4 Bending Stiffness

The values for column bending stiffness about the y- and z-axes are listed in Table 2-10. The bending stiffness for the steel is significantly greater than for the foam, suggesting that the foam adds little or no bending stiffness to the column as a whole, although the foam could keep the cross-section from collapsing in on itself, increasing the local and global buckling loads.

Table 2-10: Idealized Column Bending Stiffness by Constituent Material

Constituent Material	Bending Stiffness	
	EI_{yy} [kN-m^2 (kip-in^2)]	EI_{zz} [kN-m^2 (kip-in^2)]
Steel	251.5 (87,600)	344.0 (119,900)
Foam	0.064 (22.1)	0.060 (20.8)
Ratio of Steel to Foam	3,950	5,800
Combined	251.6 (87,620)	344.1 (119,920)

2.4.5 Axial Stiffness

The values for column axial stiffness about the y- and z-axes are listed by material in Table 2-11. Note that the axial stiffness of the steel is more than three magnitudes greater than the foam, indicating that the foam provides little or no additional axial stiffness to the column.

Table 2-11: Idealized Column Axial Stiffness by Constituent Material

Constituent Material	Axial Stiffness	
	EA [kN (kips)]	*K = EA/L* [kN/m (kip/ft)]
Steel	181,439 (40,791)	42,330 (2,901)
Foam	78.5 (17.6)	18.3 (1.3)
Ratio of Steel to Foam	2,311	2,311
Combined	181,518 (40,809)	42,349 (2,902)
Steel Percentage of Axial Stiffness [%]	99.96%	99.96%

2.4.6 Radius of Gyration and Slenderness Ratio

Long columns—columns with slenderness ratios greater than 100—typically buckle at low values of compressive stress. The slenderness ratio of a column is equal to L / ρ, where L is the effective length of the column and ρ is the radius of gyration of the structural member. The column length is approximately 14 ft (4.27 m). For these columns, the slenderness ratios are listed in Table 2-12. With values around 100, these are considered to be long columns, governed generally by Euler buckling.

Table 2-12: Steel Radii of Gyration and Slenderness Ratios

Radius of Gyration		Slenderness Ratio	
ρ_y [cm (in)]	ρ_z [cm (in)]	L / ρ_y [No units]	L / ρ_z [No units]
3.72 (1.47)	4.35 (1.97)	115	98

2.5 Weight

The column unit weight and total weight are summarized in Table 2-13.

Table 2-13: Column Weight Based on Idealized Cross-Section

Constituent Material	Unit Weight, *w* [kg/m (lb/ft)]	Total Weight, *W* [kg (lbs)]
Steel	7.17 (4.82)	30.7 (67.7)
Foam	0.30 (0.20)	1.3 (2.8)
Total	7.47 (5.02)	32.0 (70.6)

2.6 Design Configurations

The four columns which were tested were all different configurations. The first three columns employed different method of flange attachment. These columns are illustrated in Figure 2-5 through Figure 2-8. In this thesis the four columns are referred to based on the method of flange attachment: "Adhesive-Only," "Adhesive and Welds," "Adhesive and Screws," and "Adhesive-No-Foam." All column flanges were bonded with adhesive; however the second and third configurations also incorporated periodic spot-welds or screws, respectively. Note that the "Adhesive-Only" column was tested in the orientation shown in Figure 2-5 for testing to 20 kips, but was oriented with the outer flange opening upward for the 100-kip test. The fourth column was bonded with adhesive, but had no foam inserts. Note that the "Adhesive-No-Foam" column was tested only to failure as described in Chapter 4 (not tested with the 20-kip actuator).

It is important to note that heat from welding may degrade the adhesive bond, reduced the local flange buckling load. This merits further investigation.

The disadvantage of testing four samples with all different configurations is the confounding of variables. One single design was not isolated and tested. Therefore, there must be an understanding that the terms "average" and "standard deviation" used in the discussion of

test results have less significance than if the columns had multiple specimens of each configuration.

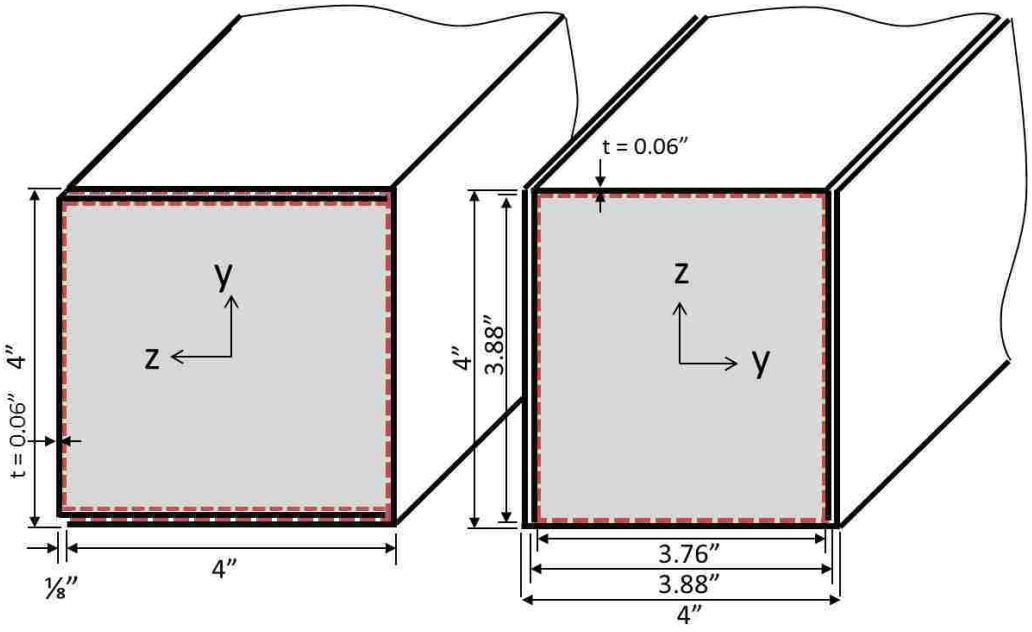

Figure 2-5: Illustration of "Adhesive-Only" Column Cross-Section: Oriented During 20-kip Test (Left); Oriented During Test to Failure (Right)

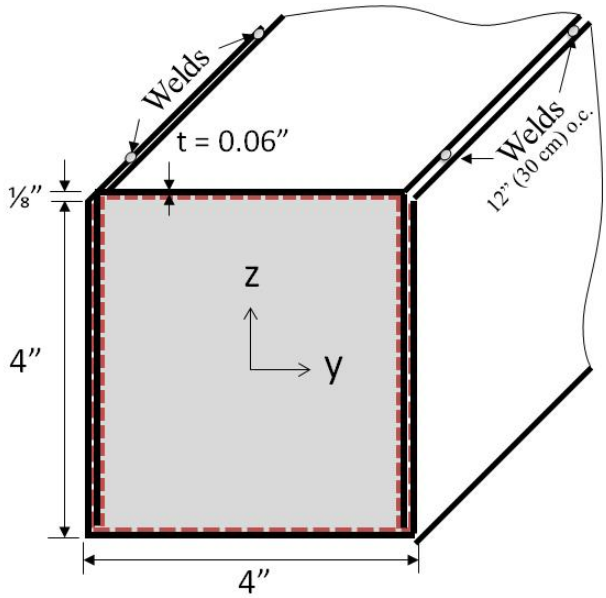

Figure 2-6: Illustration of "Adhesive and Welds" Column Cross-Section, as Oriented During Test to 20 kips and to Failure

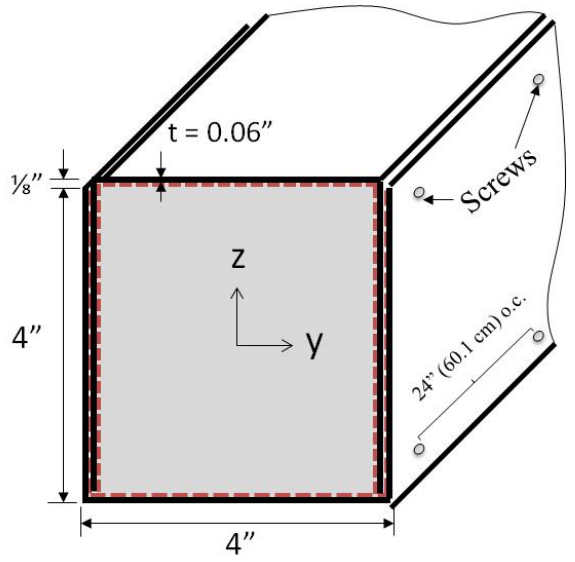

Figure 2-7: Illustration of “Adhesive and Screws” Column Cross-Section, as Oriented During Test to 20 kips and to Failure

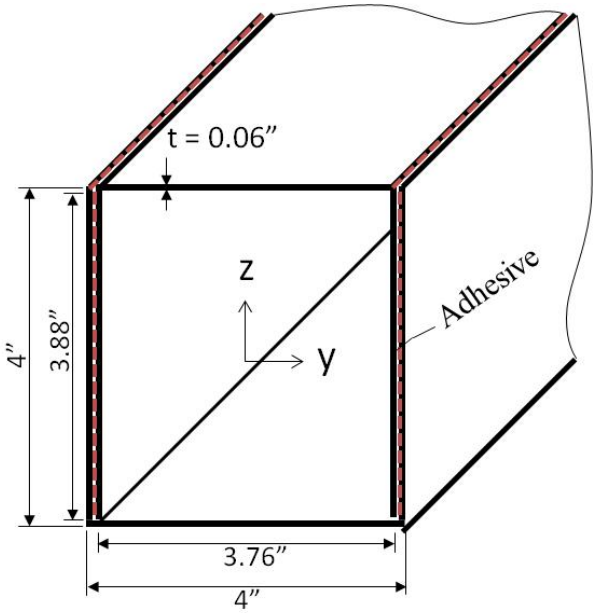

Figure 2-8: Illustration of “Adhesive-No-Foam” Column Cross-Section, as Oriented During Test to Failure

2.7 Comparison with Steel Studs

Steel studs are standardized by the Steel Stud Manufacturers Association (2011). This subsection compares the factored stress in standardized 14' (4.27 m) columns to the columns in this thesis. The standard shape that most closely resembles the columns used in this thesis is the Channel or U-Section. Due to availability of data, however, the shape that is compared in this section is the C-Stud/Joist or S-Section. Four S-Sections are listed in Table 2-14 along with the corresponding dimensions and factored design load and stress values for each section. The stress values are approximately half or less than half of the failure stress values determined experimentally for the columns in this thesis. Many factors may have influenced this outcome. First, the design loads are factored for safety. Second, the boundary conditions are not the same. For example, the design loads mentioned assume, "allowable axial loads based on lateral and torsional bracing at a maximum spacing of 4 feet on center" (SSMA 2011, p. 22). The information is useful, however, because the column design discussed in this thesis may be improved simply by using one or more standardized shapes to assemble the columns. The design strength has already been determined for these and the shapes may simply be purchased instead of cut and folded.

Table 2-14: Factored Axial Design Loads for Standard S-Sections Measuring 14 ft (4.27 m) Long with Yield Strength of 50 ksi (345 MPa) and Lateral Load of 5 psf (239 Pa) Based on Spacing of 16 in (40.6 cm) o.c.

Shape Designation	Depth [cm (in)]	Width [cm (in)]	Thickness [mm (in)]	Area, A [cm^2 (in^2)]	Load, P [kN (kips)]	Stress, σ [MPa (ksi)]
400S200-54	10.2 (4)	5.1 (2)	1.37 (0.054)	3.23 (0.500)	14.0 (3.14)	43.2 (6.3)
400S200-68	10.2 (4)	5.1 (2)	1.73 (0.068)	4.01 (0.622)	18.7 (4.21)	46.7 (6.8)
550S162-54	14.0 (5.5)	4.1 (1.62)	1.37 (0.054)	3.41 (0.528)	19.5 (4.39)	57.3 (8.3)
550S162-68	14.0 (5.5)	4.1 (1.62)	1.73 (0.068)	4.24 (0.657)	27.0 (6.07)	63.7 (9.2)

3 COLUMN TESTING PROCEDURE

Three columns were initially loaded in axial compression with a 20-kip actuator. Because the column strength exceeded the capacity of the actuator, the tests were stopped at approximately 20 kips (88 kN) and the columns were unloaded. The three original columns, in addition to a fourth column, were subsequently tested using a 100-kip actuator and a different reaction frame. The fourth column had no foam-filler and was tested to isolate the influence of the foam filling combined with the steel shell versus the steel shell only. The purpose of the tests was to measure the compressive strength of the columns and to compare the different methods of attaching the flanges of the outer channel to the inner channel. The setup, equipment, and procedure for both tests are discussed in this chapter.

3.1 Preliminary Testing: Test Setup Components

The reaction frame, loading device, column orientation, gravity loads, boundary conditions, and test instrumentation for preliminary testing to 20 kips are discussed in this section. To illustrate the entire test setup, the “Adhesive and Welds” column is shown in the test configuration for preliminary testing in Figure 3-1.

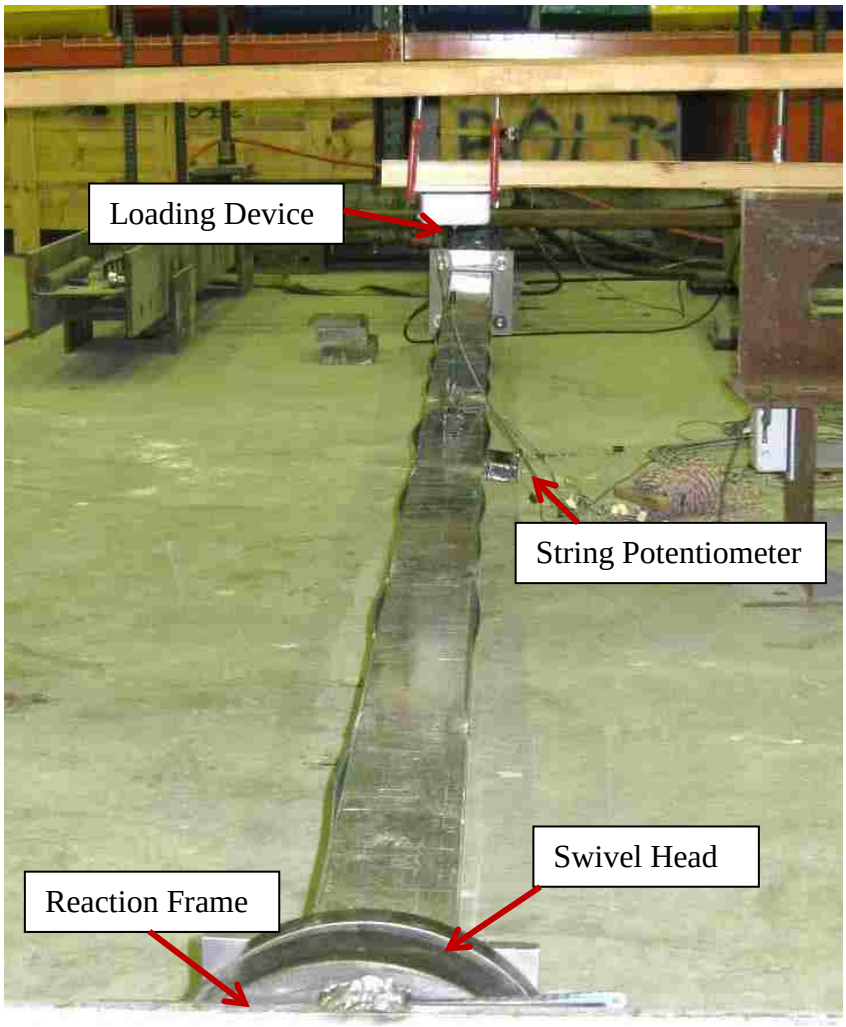

Figure 3-1: Photograph of "Adhesive and Welds" Column in Preliminary Testing to 20 kips Test Setup

3.1.1 Reaction Frame for 20-kip Tests

The steel reaction frame is shown in Figure 3-2. The frame slipped because the two threaded bars that anchored the fixture to the strong floor were not adequately post-tensioned prior to testing. This resulted in a sudden frame displacement of approximately 1 cm near loads of approximately 16-18 kips for each specimen. The load-displacement figures for these tests clearly manifest the sudden displacement which occurred (see Chapter 4). Figure 3-3 also shows indications of the slippage in the form of reddish marks on the concrete floor. The loading was not stopped during testing when the slippage occurred, but continued until the 20-kip capacity of

the machine was reached. In testing to failure, the reaction frame was more carefully constrained to ensure clean, reliable data.

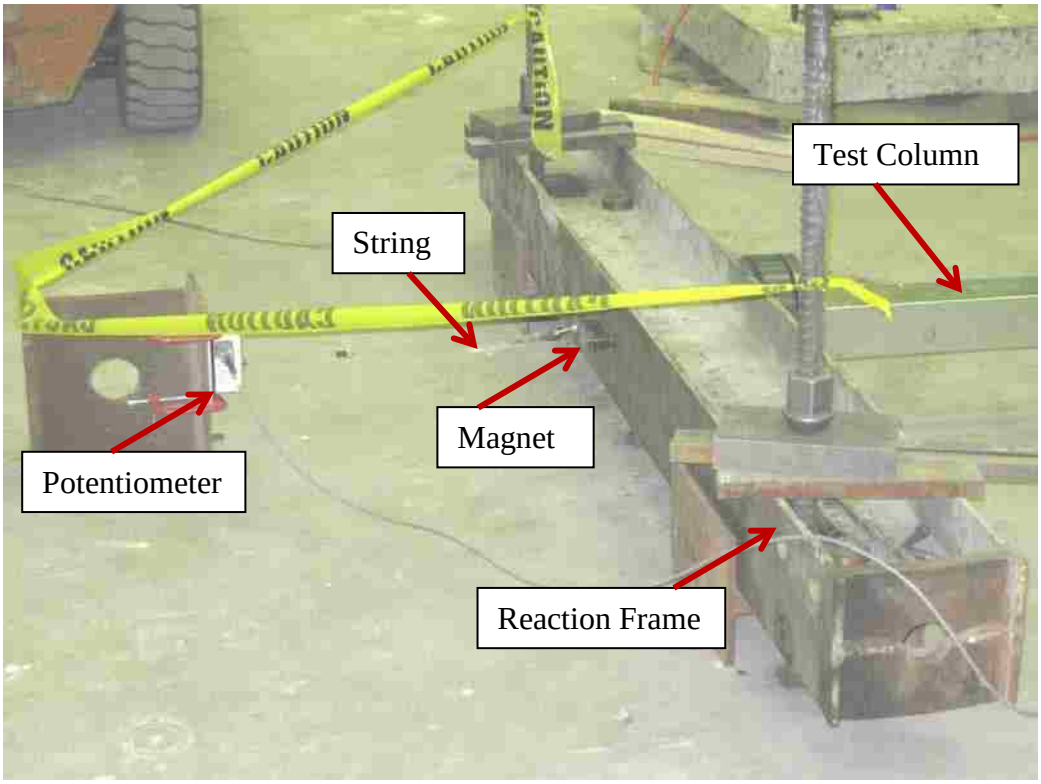

Figure 3-2: Photo of Steel Reaction Frame for Test to 20 kips (Not Adequately Post-Tensioned)

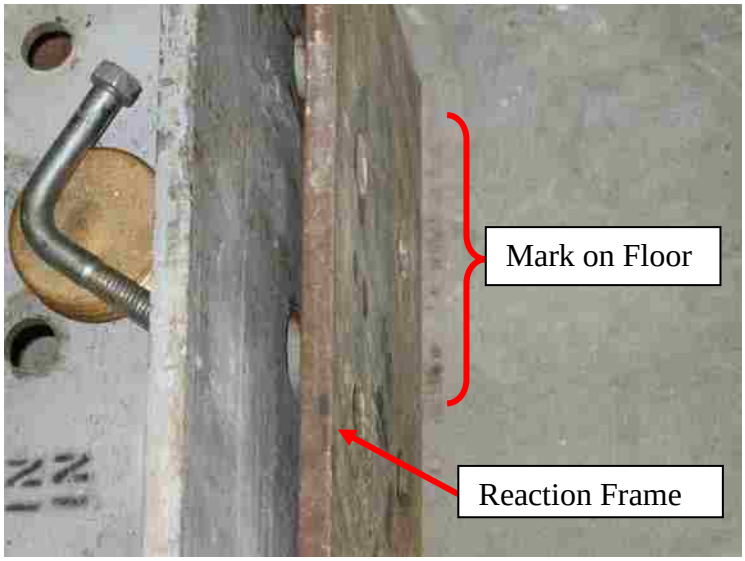

Figure 3-3: Close-up Photo of Reaction Frame Slippage Indicated by (Reddish) Mark on Floor

3.1.2 20-kip Actuator

The 20-kip actuator used in the preliminary testing is shown in Figure 3-4. The arm shown was restrained against transverse movement in both the y- and z-directions (restraint shown in both images). The head of the actuator was allowed to swivel/rotate freely during testing.

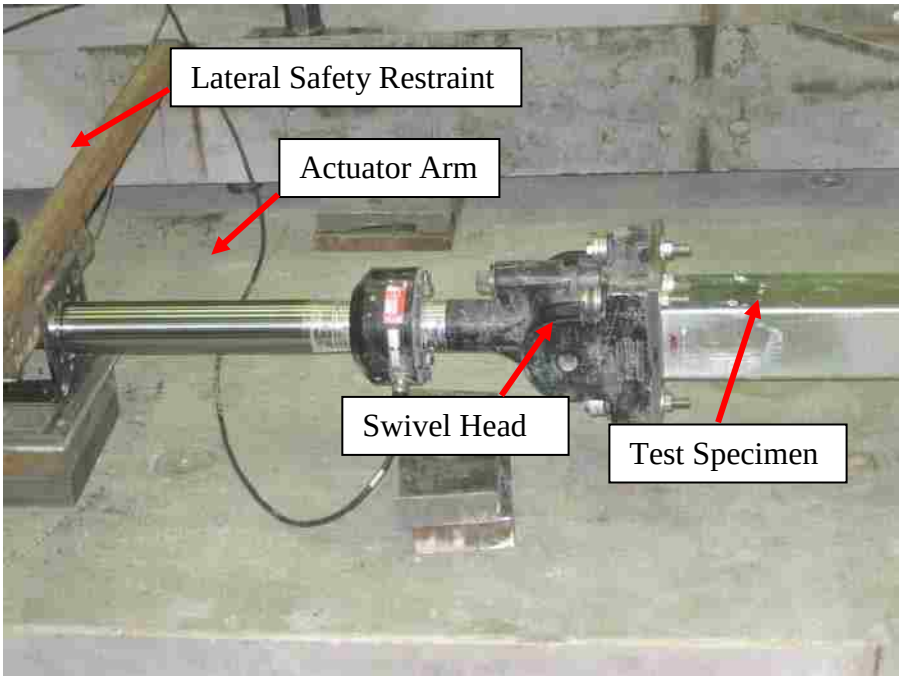

Figure 3-4: Photo of 20-kip Actuator

3.1.3 Column Orientation

Testing the columns parallel to the ground introduces a preferential buckling direction due to column weight. Additionally, column orientation influences the buckling direction. To elaborate, the outer channel may be oriented in the following ways during testing: opening upward, opening downward, or opening sideward (relative to the ground). In the testing to 20 kips, the "Adhesive-Only" column was oriented with the outer channel facing sideward (strong axis of buckling parallel to the ground). The other two columns, however, were oriented with

the outer channel facing upward during testing (strong axis of buckling perpendicular to the ground). These different orientations could slightly affect the transverse deflection behavior of the column because of gravity and because the strong and weak moments of inertia differ by only approximately 30%.

3.1.4 Gravity Loads

The columns were tested parallel to the ground, rather than in a vertical orientation. Therefore, the component of deflection due to gravity loads (self-weight) was analyzed. This is modeled in Figure 3-5.

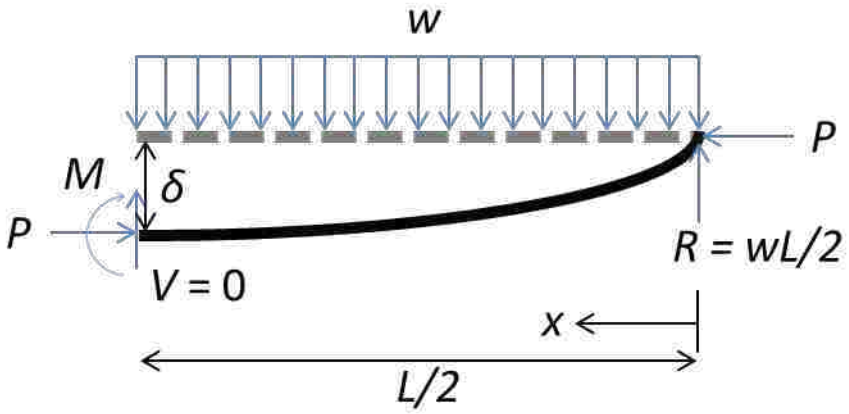

Figure 3-5: Model of Simply-Supported Column with Gravity Load, Axial Load, Moment, Shear, and Reaction Forces

The initial deflection based on gravity alone and not axial force is determined from the deflection equation of a simply-supported beam with a uniformly distributed load, *w*. The initial deflection values are shown in Table 3-1.

$$\delta_o = \frac{5wL^4}{384EI} \quad \textbf{(3-1)}$$

Table 3-1: Predicted Initial Deflections Due to Self-Weight Alone

y-Direction (strong axis)		z-Direction (weak axis)	
δ_y [cm (in)]	δ_y / L [%]	δ_z [cm (in)]	δ_z / L [%]
0.09 (0.036)	0.021%	0.13 (0.049)	0.029%

where the column unit weight, *w*, is 5.0 lb/ft (7.5 kg/m) as indicated previously in Table 2-13, the column length, *L*, is 14 ft (4.27 m), the steel elastic modulus, *E*, is 29,000 ksi (200 GPa), and the moment of inertia, *I*, is 3.02 in^4 (125.8 cm^4) about the weak axis and 4.13 in^4 (172.0 cm^4) about the strong axis as indicated previously in Table 2-9.

The moment due to self-weight and axial load was obtained by summing forces about x = *L*/2:

$$M = P\delta + \frac{wL^2}{8} \quad \textbf{(3-2)}$$

where *P* is the axial load, assumed to be 20.0 kips (88 kN), and *M* is the moment produced by both the column weight and the axial force multiplied by the deflection. The amplified deflection due to the moment was obtained by using the modified equation for deflection of a simply-supported beam with a uniformly distributed load, which takes into account the effects of the axial load multiplied by the deflected shape (TMS 2010, p. 10-29):

$$\delta = \frac{5ML^2}{48EI} \quad \textbf{(3-3)}$$

The two equations were solved iteratively and the predicted deflections are listed in Table 3-2.

Table 3-2: Predicted Deflections Due to Self-Weight and 20 kips (88 kN) Axial Compression

y-Direction (strong axis)		z-Direction (weak axis)	
δ_y [cm (in)]	δ_y / L [%]	δ_z [cm (in)]	δ_z / L [%]
0.18 (0.071)	0.042%	0.37 (0.147)	0.088%

Based on the theoretical deflection equation of a simply-supported beam carrying a distributed load, the columns will deflect laterally approximately 0.147 in (0.37 cm) about the weak axis from self-weight alone. This deflection value is approximately 29% of the average z-direction transverse deflection—0.51 in (1.31 cm)—in the tests to 20 kips. This value is also double the deflection about the strong axis due to self-weight alone. Thus, deflections due to gravity loads do induce additional deflection and the column orientation does significantly influence magnitude of transverse deflection. This should be noted while comparing the axial load versus transverse deflection results for the "Adhesive-Only" column. In future tests, columns should be tested with the same orientation.

3.1.5 Boundary Conditions

Both the actuator-end and the reaction-end of the columns were pinned; thus, the ends represented pinned-pinned boundary conditions representative of typical building construction (shown previously in Figure 1-2). The pinned-pinned boundary conditions do not change the effective length of the column used to calculate the Euler buckling load (i.e., $k = 1.0$).

3.1.6 String Potentiometers

Two string potentiometers were used to measure transverse deflections—one in the y-direction and one in the z-direction. These were attached at the center span of each column using

magnets (see Figure 3-6). One additional string potentiometer was attached to the steel reaction frame to measure axial displacement (in the x-direction) as shown in Figure 3-7.

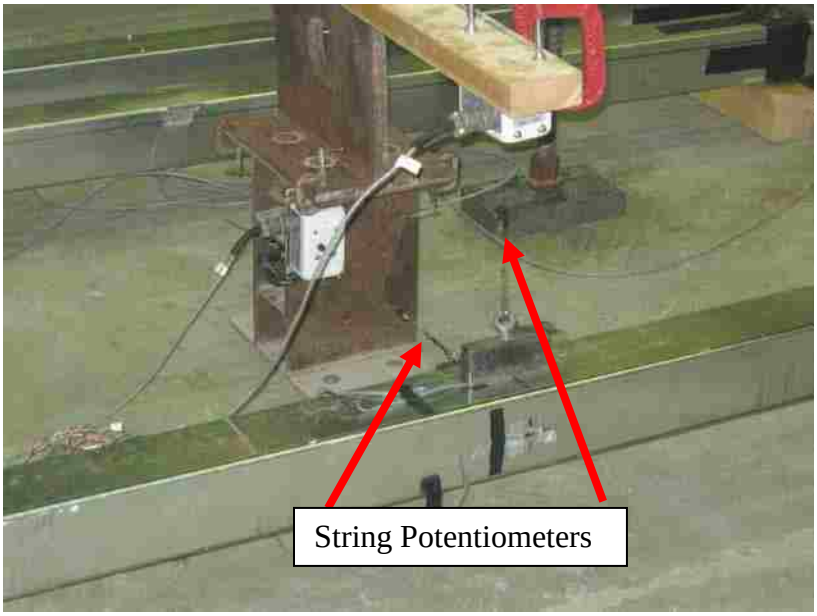

Figure 3-6: Photo of Vertical and Horizontal String Potentiometers Measuring Transverse Deflections for Test to 20 kips

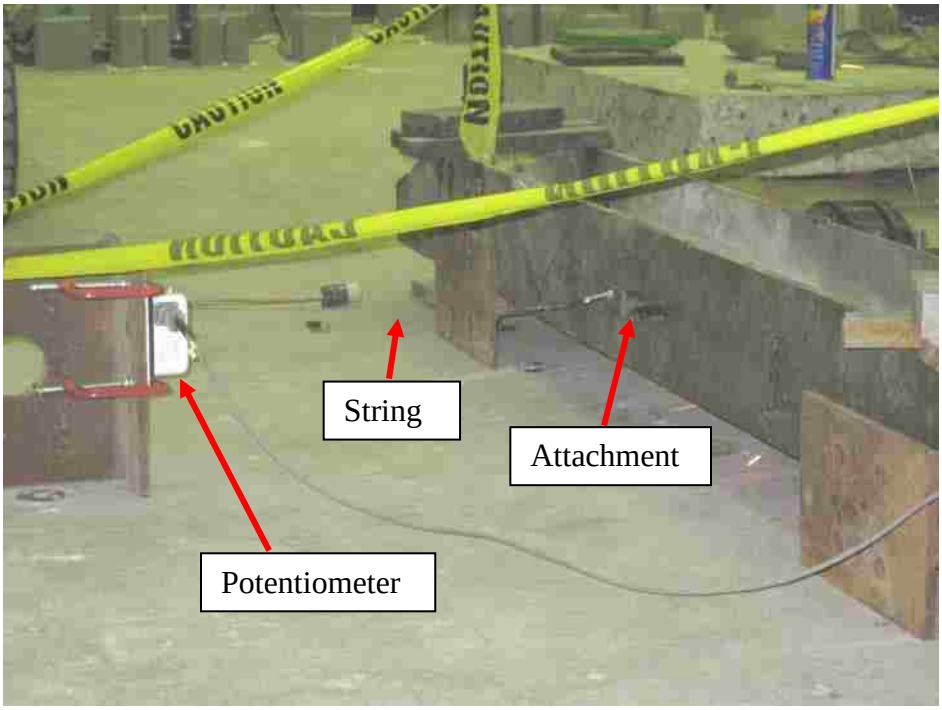

Figure 3-7: Photo of String Potentiometer Attached to Reaction Frame for Test to 20 kips

3.1.7 Surface Strain Gages

Four strain gages were used to measure elastic deformation due to axial compression—one strain gage on each of the four sides in the center span of the columns. The strain gages measured the total local strain, from which axial and bending strain components were derived. A sample strain gage attached to a column is shown in Figure 3-8.

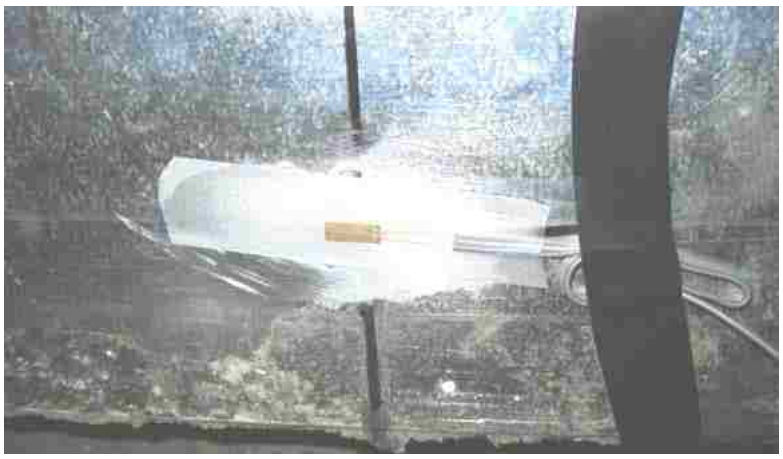

Figure 3-8: Photo of Typical Strain Gage Attachment for Test to 20 kips

3.2 Testing to Failure: Test Setup Components

The reaction frame, loading device, column orientation, gravity supports, boundary conditions, and test instrumentation for testing to failure are discussed in this section.

3.2.1 Reaction Frame for Tests to Failure

The steel reaction frame is shown in Figure 3-9. The frame was built for compression testing of wall panel and module specimens in addition to the columns. Thus, the frame appears to be over-designed for the column testing. The frame was adequately post-tensioned so that no frame slippage occurred during the tests to failure.

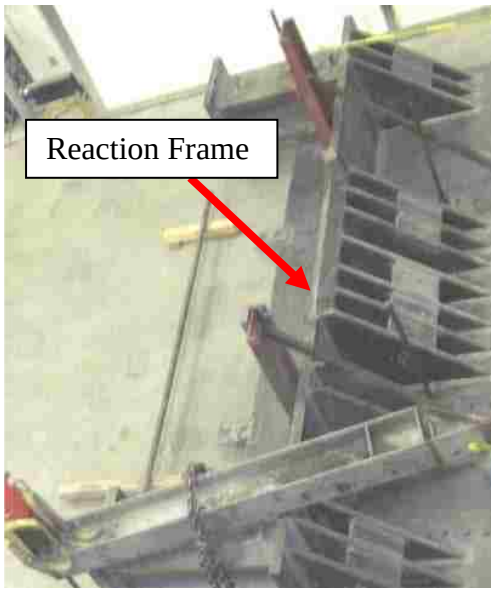

Figure 3-9: Photo of Steel Reaction Frame for Tests to Failure (From Above)

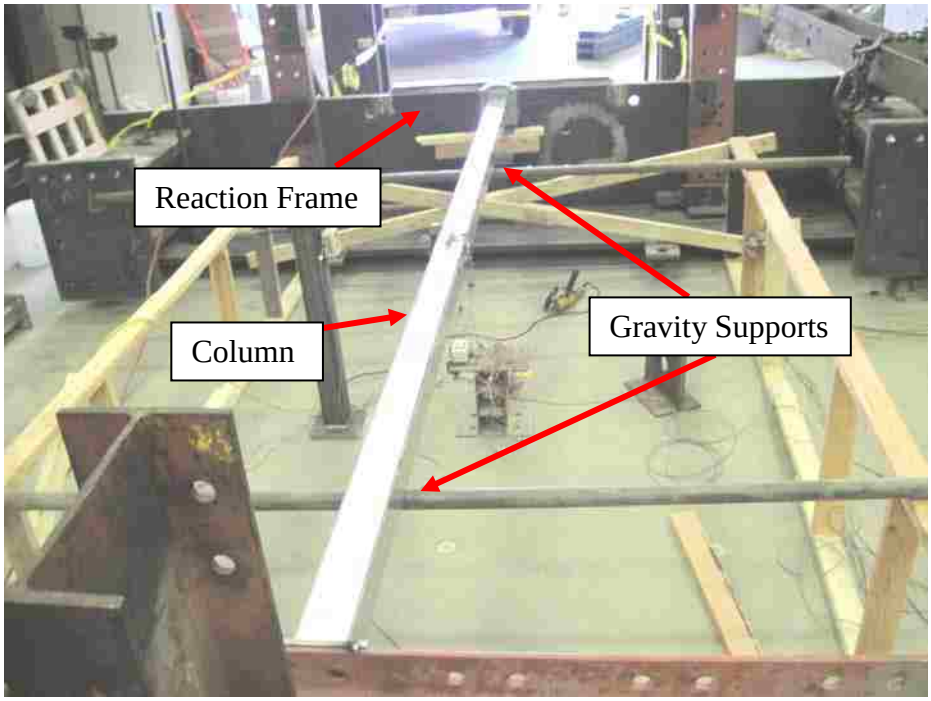

Figure 3-10: Photo of Steel Reaction Frame for Test to Failure

3.2.2 100-kip Actuator

The 100-kip actuator used to compress the columns during testing to failure is shown in Figure 3-11.

Figure 3-11: Photo of 100-kip Actuator for Tests to Failure

3.2.3 Column Orientation

All four columns were tested parallel to the floor; also, the outer channel opened upward relative to the floor. The deflections due to self-weight and column orientation were neglected in the data reduction (as discussed in Section 3.1.4).

3.2.4 Gravity Supports

During the tests to failure, the columns were partially constrained from deflecting in the negative z-direction (gravity) by two supporting bars, as shown in Figure 3-10. The bars were put in place in order to properly align the columns with the loading device and the reaction frame. These were left in place during testing. These supports may have influenced the buckling direction of the columns, since all four columns crippled about the strong axis (in the y-direction), rather than the weak axis during testing to failure (i.e., perpendicular to the flanges, rather than parallel to the flanges).

3.2.5 Boundary Conditions

As shown in Figure 3-12 and Figure 3-13, the 100-kip actuator did not have a swivel head at the loaded end and therefore provided some bending constraint. The reaction end had a swivel head, allowing rotation (see Figure 3-14). Thus, the resulting boundary conditions were in between pinned-pinned and fixed-pinned. Fixed-pinned boundary conditions decrease the effective length of the column by approximately 20% in the Euler buckling equation (i.e., k = 0.8) and increase the Euler buckling load by approximately 56%. True fixed ends, however, are rare and the actual k-value is probably somewhere between 0.8 and 1.0. The test results, however, indicate that the actual k-value was approximately 1.0. Thus, the ends are represented as pinned-pinned boundary conditions representative of typical building construction (shown previously in Figure 1-2).

Figure 3-12: Photo of Boundary Conditions (Actuator-End) During Test to Failure

Figure 3-13: Close-up Photo of Boundary Conditions (Actuator-End) During Test to Failure

Figure 3-14: Close-up Photo of Boundary Conditions (Reaction-End) During Test to Failure

3.2.6 String Potentiometers

In the tests to failure, two string potentiometers were used to measure transverse deflections—one in the y-direction and one in the z-direction. These were attached at the center span of each column using magnets (see Figure 3-15). Although six string potentiometers collected axial displacement data (x-direction), only two of these were relevant and used in the data reduction. These two were attached to the steel reaction frame end of the column (Figure 3-16).

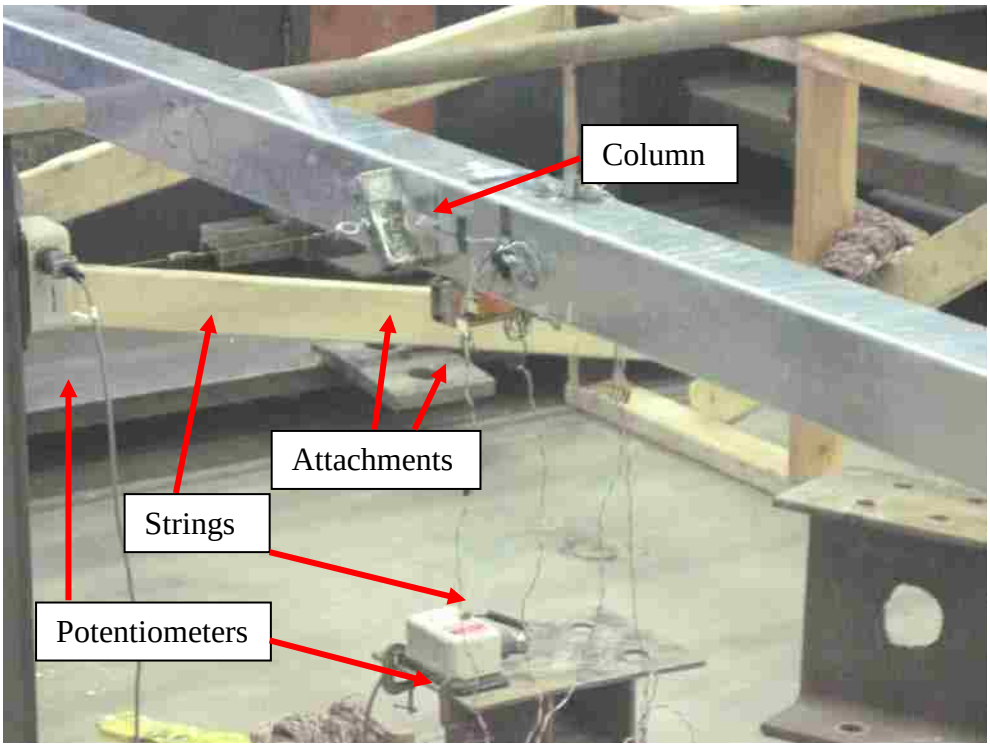

Figure 3-15: Photo of Vertical and Horizontal Transverse String Potentiometers During Test to Failure

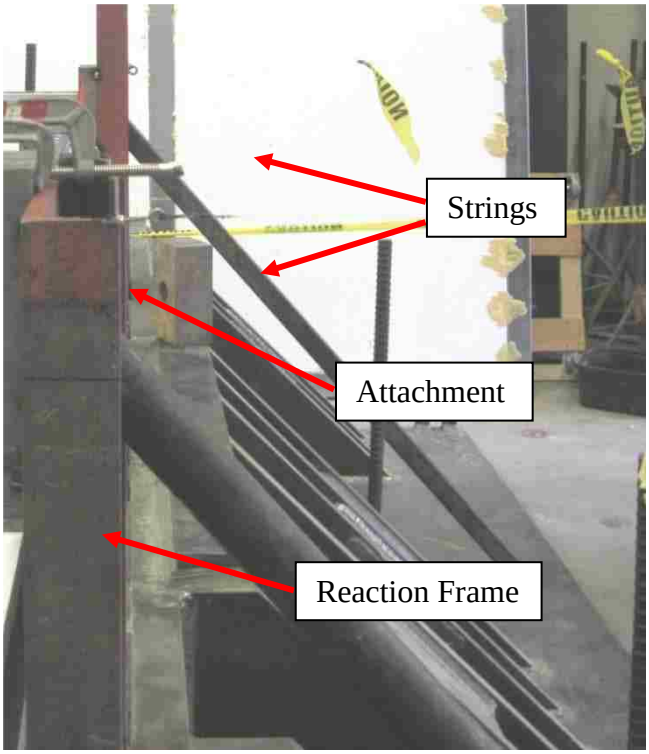

Figure 3-16: Photo of Reaction-End String Potentiometers During Test to Failure

3.2.7 Surface Strain Gages

Four strain gages were used to measure elastic deformation due to axial compression—one strain gage on each of the four sides in the center of the columns. The strain gages measured the total local strain, from which axial and bending strain components were derived. A sample strain gage attached to a column is shown in Figure 3-17 and Figure 3-18.

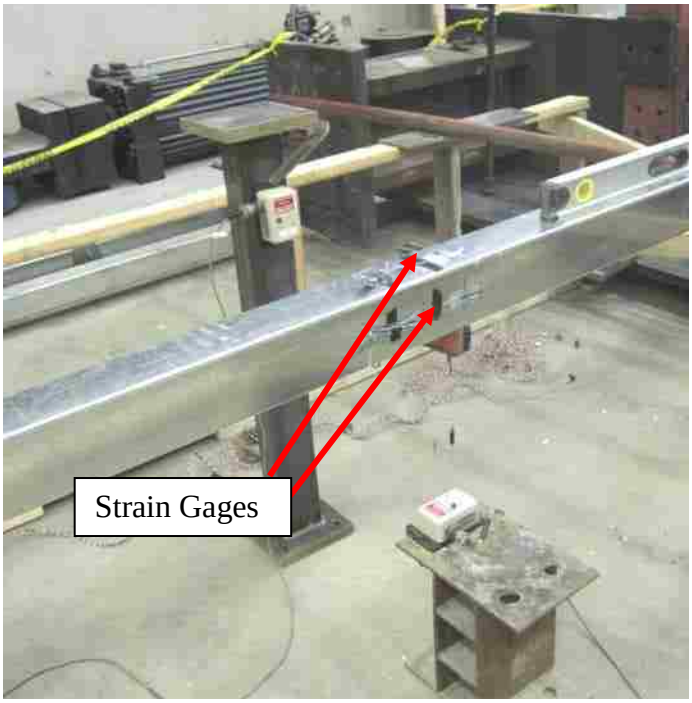

Figure 3-17: Photo of Mid-Span Strain Gages Located on Columns During Test to Failure

Figure 3-18: Close-up Photo of Mid-Span Strain Gage on Column Tested to Failure

3.2.8 LVDT

A Linear Variable Differential Transformer or LVDT was also used to measure axial deflection during the test to failure. The LVDT is shown in Figure 3-19.

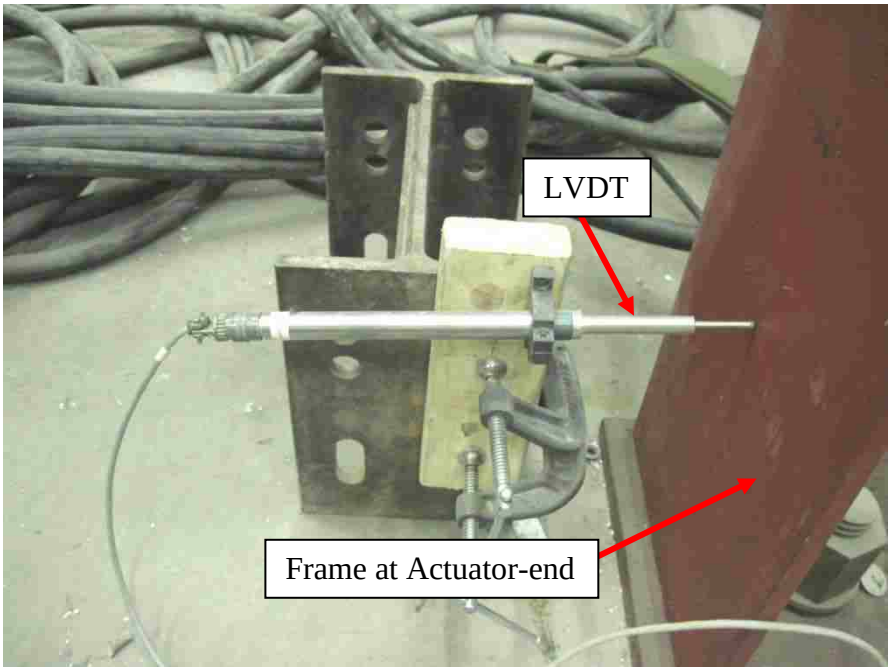

Figure 3-19: Photo of LVDT used During Tests to Failure

3.3 Data Analysis Procedure

This section outlines various methods used to reduce the data obtained during both the preliminary tests to 20 kips and the tests to failure.

3.3.1 Load Data

The load data was obtained directly from the actuator and was multiplied by a correction factor of 95%. This was to account for a calibration error in the data acquisition software. Note in the figures that compression is defined in positive notation.

3.3.2 Conversion of Load Data to Stress

The values for normal stress were obtained using the following formula:

$$\sigma = \frac{P}{A_s} \quad \textbf{(3-4)}$$

where, σ is average axial stress, P is applied axial load, and A_s is the effective cross-sectional area of the column. The foam-filled steel column is a composite of foam and steel; therefore, the term "stress" is approximated by neglecting the foam because as listed previously (Table 2-11) the stiffness of the steel is 2,300 times greater than the foam stiffness. Therefore, the column stress is calculated based on the steel only because it carries approximately 99.96% of the compressive load. For this reason, the effective cross-sectional area used to determine stress is solely the cross-sectional area of the steel—1.41 in^2 (9.07 cm^2).

3.3.3 Deflection Data

For both sets of tests, the transverse deflection data was obtained directly from the string potentiometers in the y- and z-directions attached at the center span of each of the columns. The axial deflection data was obtained by taking the difference in displacement of the actuator and the reaction frame (which was measured with a string potentiometer). Note that the axial deflection data for the tests to failure was more complex than for the tests to 20 kips because six string potentiometers, the actuator, and an LVDT measured deflection.

3.3.4 Strain Data

The total local strain was obtained directly from the strain gage readings. The total strain is plotted as a function of stress. The total strain, ε, was also used to obtain both the axial, ε^o, and bending strain, κ, components in the columns based on the following relationship:

$$\varepsilon = \varepsilon^o + z * \kappa \quad \textbf{(3-5)}$$

where z is the perpendicular distance from the neutral axis of bending to the position of interest. For strain gages mounted on opposing column faces, $z = \pm h/2$, respectively, if the overall thickness of the structure is h. The strain equation has two unknowns—axial strain and bending strain—and therefore data from upper and lower surface-mounted strain gages can be used with this equation to solve for the two strain components. Using these two sets of strain data, the equations for axial and bending strain components are (Equations 3-4 and 3-5):

$$\varepsilon^o = \frac{\varepsilon_1 + \varepsilon_2}{2} \quad \textbf{(3-6)}$$

and:

$$\kappa = \frac{\varepsilon_1 + \varepsilon_2}{h} \quad \textbf{(3-7)}$$

respectively, where ε_1 and ε_2 are the strains from the strain gages attached on opposing column faces, and h is the distance between the strain gages. For these column tests, h = 4 in (10.3 cm). Note that these calculations are not able to isolate strains caused by local flange buckling.

Average axial strain is determined using:

$$\varepsilon^o = \frac{P}{EA} \quad \textbf{(3-8)}$$

3.3.5 Euler Buckling Equation

As listed in Table 2-12 (previously), the slenderness ratio of the columns is approximately 115; therefore the columns are "long" and are susceptible to Euler buckling. The theoretical buckling load, P_{cr}, for a column can be predicted using the Euler buckling formula:

$$P_{cr} = \frac{\pi^2 EI}{(kL)^2} \quad \textbf{(3-9)}$$

where, E is the modulus of elasticity of the material, I is the moment of inertia, k is the effective column length factor, and L is the actual length of the column. The critical buckling loads are summarized in Table 3-3 for two effective length factors: k = 1.0 and k = 0.8. The actual k value was closer to 1.0 for these tests; however, the column geometry and the end fixture provided some torsional stiffness which decreases k and, thus, increases the buckling load slightly.

Table 3-3: Critical Buckling Loads for Foam-Filled Steel Columns Based on the Euler Buckling Equation

Effective Length Factor, k	Actual Column Length, L [m (ft)]	Effective Column Length, L_e [m (ft)]	Critical Buckling Load, P_{cr} [kN (kip)]
1.0	4.29 (14.1)	4.29 (14.1)	143 (32.2)
0.8	4.29 (14.1)	3.43 (11.3)	223 (50.3)

The critical Euler buckling load is predicted to be 32.2 kips (143 kN) for columns with pinned-pinned end conditions and 50.3 kips (223 kN) for columns with pinned-fixed end conditions. These values are both higher than any of the observed buckling loads. Thus, the predicted Euler buckling loads are non-conservative for these tests.

3.3.6 Southwell Plot Method

The Southwell method is a mathematical device which uses the data from an axial load vs. transverse deflection curve and projects the load at which buckling will occur (Southwell 1932). The plots convert the naturally inverse-hyperbolic load vs. deflection curves into straight lines. The transverse deflection divided by the axial load was plotted on the y-axis and the transverse deflection was plotted on the x-axis. Southwell plots were used to quantify the experimental column buckling loads based on the data from tests to 20 kips and from the tests to failure. For this research, z-direction transverse deflection and the resultant transverse deflections (based on both the y- and z-deflections) were used in the Southwell plots. Linear trend lines were added to the straightest section of each curve with corresponding equations and R-squared values for the linear portion and the entire curve. The slopes of these lines were used to determine the experimental buckling loads.

4 RESULTS OF PRELIMINARY COLUMN TESTING

This chapter summarizes the results from the three preliminary column compression tests performed to 20 kips: "Adhesive-Only," "Adhesive and Welds," and "Adhesive and Screws."

4.1 20-kip Test Results

This section summarizes the test results for three columns tested to 20 kips (88 kN).

4.1.1 Local Buckling

During testing to 20 kips, all three columns exhibited local buckling (see Figure 4-1 through Figure 4-3). The local buckling was first observed at approximately 10-12 kips (44-54 kN) compression. Based on photographs, the local buckling wavelength, *a*, ranged from approximately 8"-12" (20-30 cm) for all columns. The wavelength varied across the length of the column and also varied depending on spacing of screws and/or short-welds. The wavelengths were approximately equal for all three specimens including the "Adhesive-Only" column. The wavelength is therefore constrained by the adhesive in addition to the screws or welds. In Figure 4-2 the wavelengths were limited by the spacing of welds. In Figure 4-3 the wavelengths were shorter than the spacing of screws. The column flanges returned to their

undeformed positions when each column was unloaded, indicating that the local buckling occurred in the elastic region during the tests to 20 kips.

Figure 4-1: Photo of Local Buckling in "Adhesive-Only" Column During Test to 20 kips Showing Local Buckling Wavelength

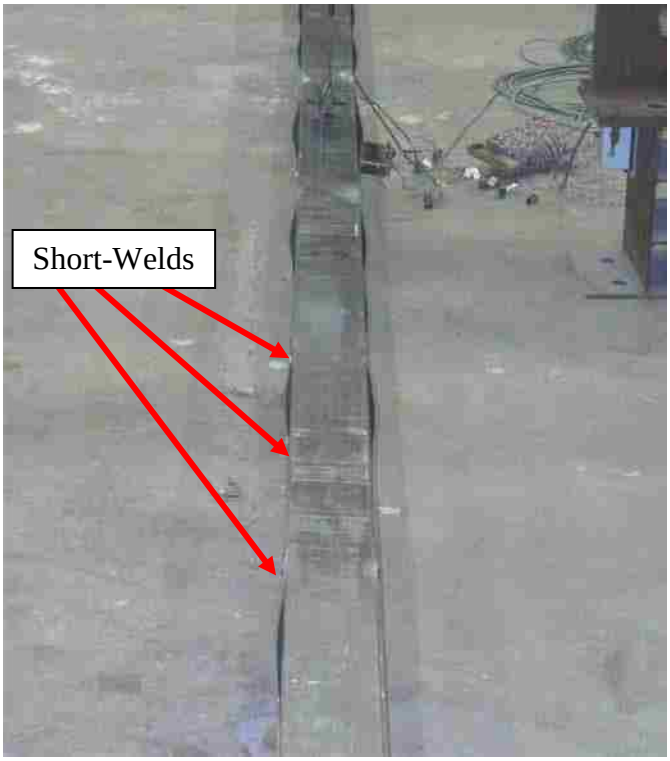

Figure 4-2: Photo of Local Buckling in "Adhesive and Welds" Column During Test to 20 kips

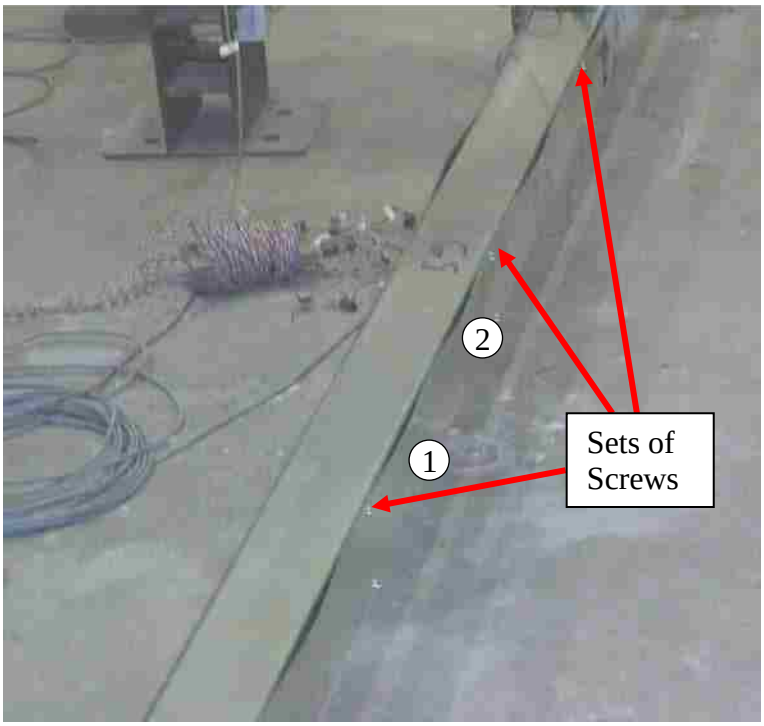

Figure 4-3: Photo of Local Buckling in "Adhesive and Screws" Column During Test to 20 kips Showing Two Wavelengths Between Sets of Screws

4.1.2 Load vs. Axial Deflection

Figure 4-4 shows the compression load versus axial deflection for the three columns tested to 20 kips. Note in the figure that each column essentially returned to zero deflection when unloaded. Thus, the axial deflection occurred in the elastic region during the tests to 20 kips. The fact that the columns unload on a different path than the loading indicates that there is an energy dissipation in the loading and unloading processes. The column axial deflection and stiffness values (at approximately 20 kips) are summarized in Table 4-1.

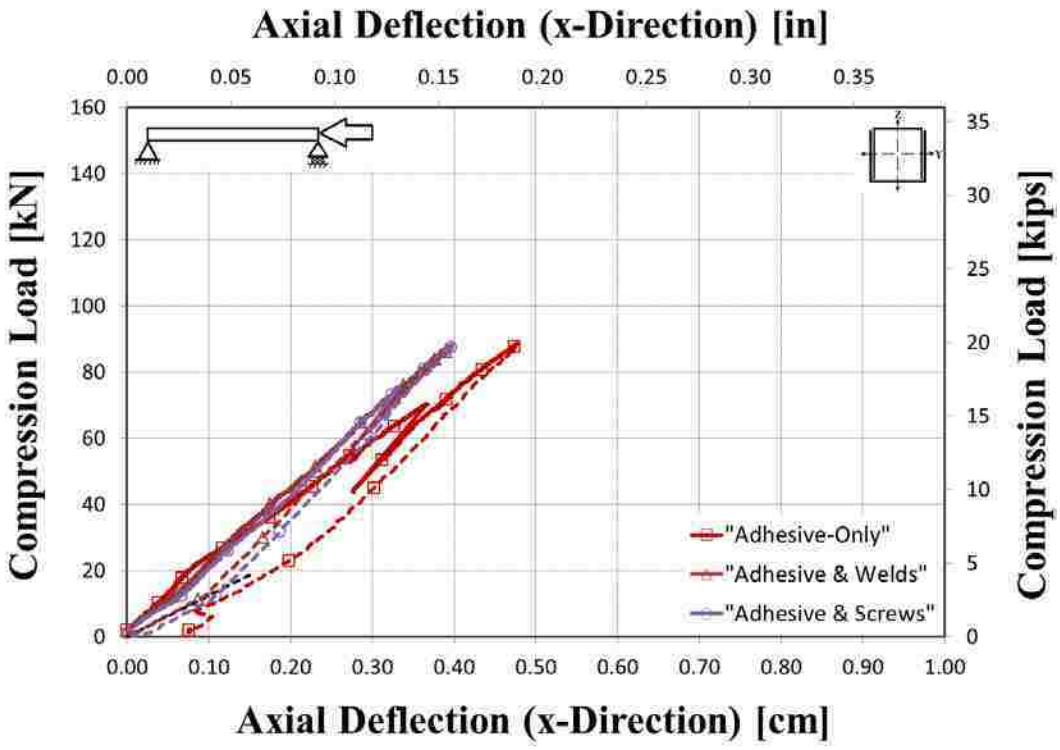

Figure 4-4: Compression Load vs. Axial Deflection (x-Direction) for Column Tests to 20 kips

Table 4-1: Axial Deflection (x-Direction) and Stiffness Values for Column Tests to 20 kips

Configuration	Maximum Load, P [kN (kip)]	Axial Deflection (x-dir.), u_1 [cm (in)]	Stiffness, K [kN/cm (kip/in)]
Adhesive-Only	88.6 (19.9)	0.48 (0.19)	186.2 (106.3)
Adhesive and Welds	88.0 (19.8)	0.40 (0.16)	222.1 (126.8)
Adhesive and Screws	88.5 (19.9)	0.40 (0.16)	221.5 (126.5)
Average	88.4 (19.9)	0.42 (0.17)	210.0 (119.9)
Standard Deviation	0.3 (0.1) 0.3%	0.04 (0.02) 10.6%	20.5 (11.7) 9.8%

4.1.3 Load vs. Transverse Deflection

The compression load versus transverse deflection in the y-, z-, and resultant directions is shown in Figure 4-5, Figure 4-6, and Figure 4-7, respectively, for the three columns loaded in axial compression to 20 kips. The deflections in the y-direction are smaller and have a larger

spread than the deflections in the z-direction, primarily due to the relative stiffness in the two directions. This is in accordance with the predictions based on relative moments of inertia in the two directions. The effects of slippage of the reaction frame are very apparent in all three figures. Note also in each figure that each column essentially returned to zero deflection when unloaded. Thus, the transverse deflections occurred in the elastic region (with little to no permanent deformation) during the tests to 20 kips. The fact that the columns unloaded along different load-deflection paths than the loading is evidence of energy dissipation in the loading and unloading processes.

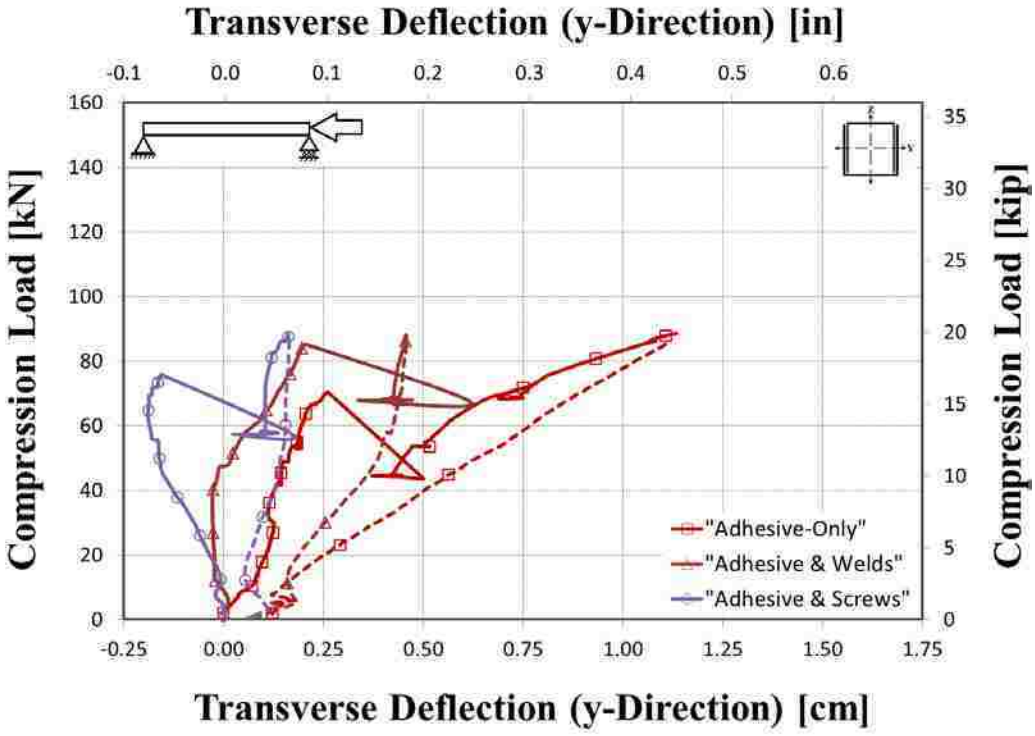

Figure 4-5: Compression Load vs. Transverse Deflection (y-Direction) for Column Tests to 20 kips

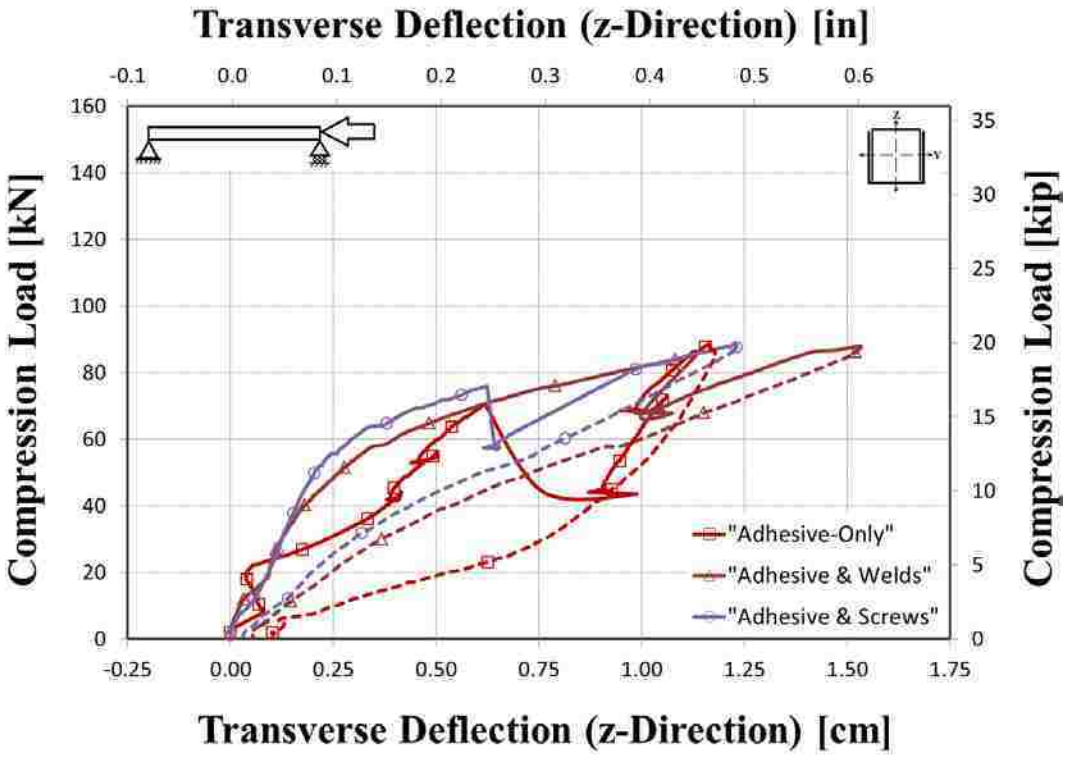

Figure 4-6: Compression Load vs. Transverse Deflection (z-Direction) for Column Tests to 20 kips

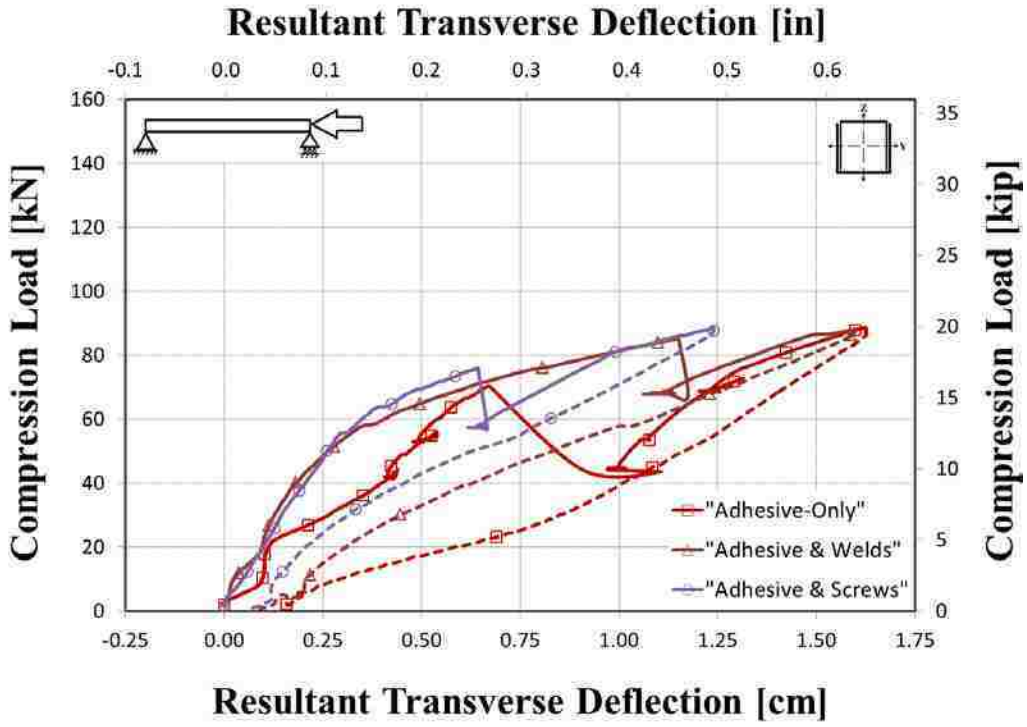

Figure 4-7: Compression Load vs. Resultant Transverse Deflection for Column Tests to 20 kips

The maximum transverse deflections of each column at 20 kips are summarized in Table 4-2. Notice the large spread in the deflections in the y-direction compared to the z-direction and the resultant direction. Although the columns are predisposed to deflect in the z-direction due to the cross-sectional geometry (the weak axis of bending is the y-y axis), other factors evidently influence transverse deflection in the y-direction. Some of these may include the effects of self-weight (gravity loads), initial imperfections in the column, or slight eccentricities in the loading.

Table 4-2: Transverse Deflections in the y- , z-, and Resultant Directions for Column Tests to 20 kips

Configuration	Deflection at approximately 20 kips		
	Transverse (y), u_2 [cm (in)]	Transverse (z), u_3 [cm (in)]	Resultant, u_R [cm (in)]
Adhesive-Only	1.13 (0.45)	1.16 (0.46)	1.62 (0.64)
Adhesive and Welds	0.46 (0.18)	1.53 (0.60)	1.60 (0.63)
Adhesive and Screws	0.16 (0.06)	1.23 (0.48)	1.24 (0.49)
Average	0.58 (0.23)	1.31 (0.51)	1.49 (0.59)
Standard Deviation	0.50 (0.20)	0.20 (0.08)	0.21 (0.08)
	85.6%	14.9%	14.5%

4.1.4 Stress vs. Total (Local) Strain

Figure 4-8 through Figure 4-10 show the compression stress versus total strain for each of three columns, individually. Note in each figure that columns returned to zero strain when unloaded (discounting effects from reaction frame slippage). Thus, the total strain occurred in the elastic region (with little to no permanent deformation) during the tests to 20 kips. The strains at maximum stress (~14 ksi or 95 MPa) are listed for each column in Table 4-3. There is a very large spread in total strain at maximum stress on all column faces (evident in all three figures and the table). This may be an indication that the total strain is highly a function of

column face. Total strain is a function of both axial strain and bending strain. These concepts are further explored in the following two subsections.

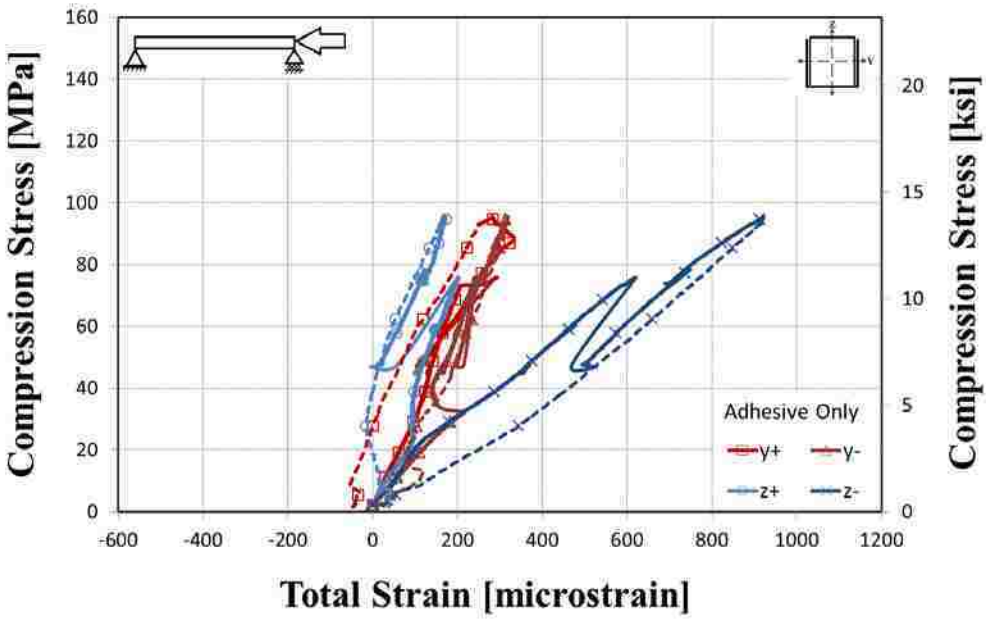

Figure 4-8: Compression Stress vs. Total Strain for "Adhesive-Only" Column Test to 20 kips

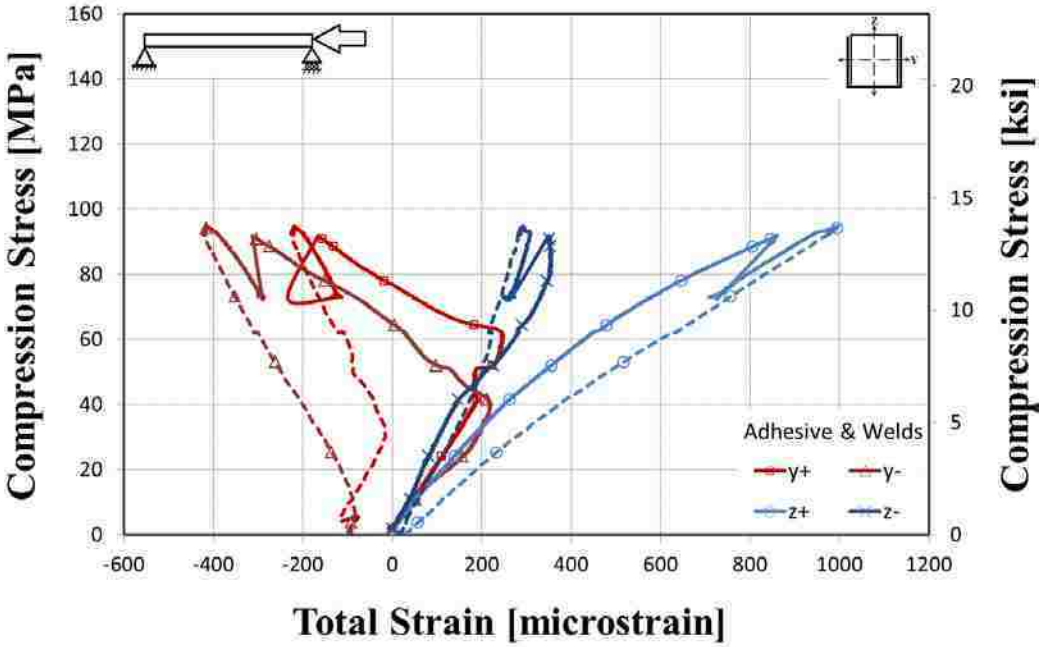

Figure 4-9: Compression Stress vs. Total Strain for "Adhesive and Welds" Column Test to 20 kips

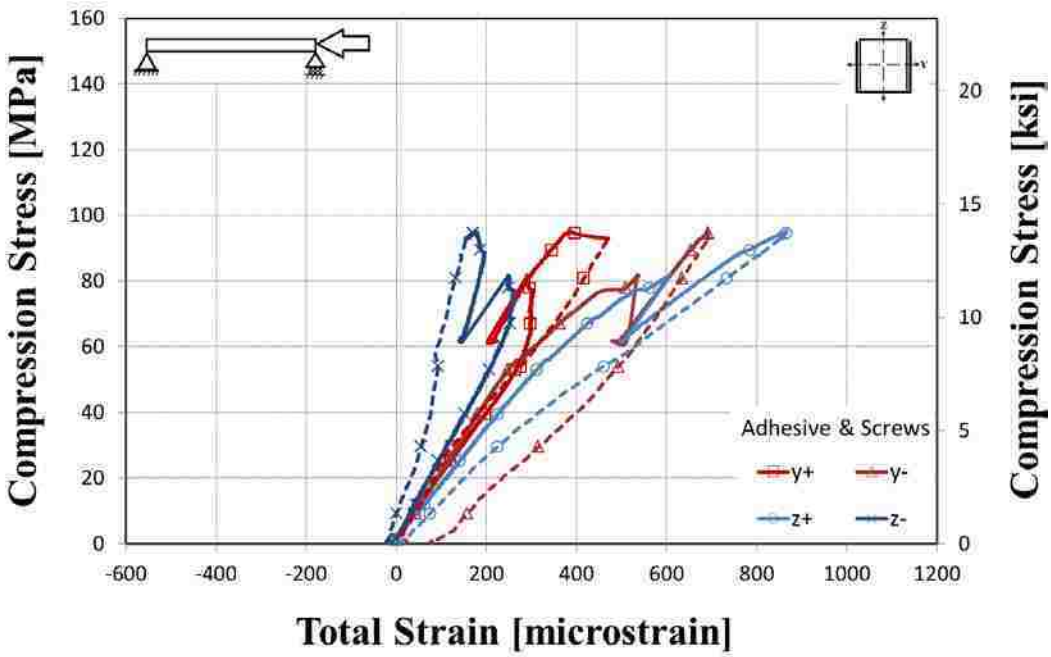

Figure 4-10: Compression Stress vs. Total Strain for "Adhesive and Screws" Column Test to 20 kips

Table 4-3: Strain at Maximum Stress (by Column Face) for Column Tests to 20 kips

Configuration	Column Face				
	Stress, σ [MPa (ksi)]	z- [με]	y+ [με]	z+ [με]	y- [με]
Adhesive-Only	95.4 (13.8)	922	282	171	318
Adhesive and Welds	94.8 (13.7)	293	-219	995	-415
Adhesive and Screws	95.3 (13.8)	175	385	866	692
Average	95.2 (13.8)	463	149	677	199
Standard Deviation	-	401	323	443	563
	-	87%	216%	65%	284%

4.1.5 Stress vs. Axial Strain

Figure 4-11 to Figure 4-12 show the compression stress versus axial strain component for the flange and web, respectively, for the columns loaded to 20 kips. The axial strain values at maximum stress are listed in Table 4-4 for all three columns. There is a significantly larger spread in compression stress versus flange axial strain than in compression stress versus web

axial strain. This is most likely due to the flanges having one free edge, which allows the flanges to buckle at a much lower load than the webs. This evidently varies the axial strain, depending on the location of the strain gage relative to the local buckling site.

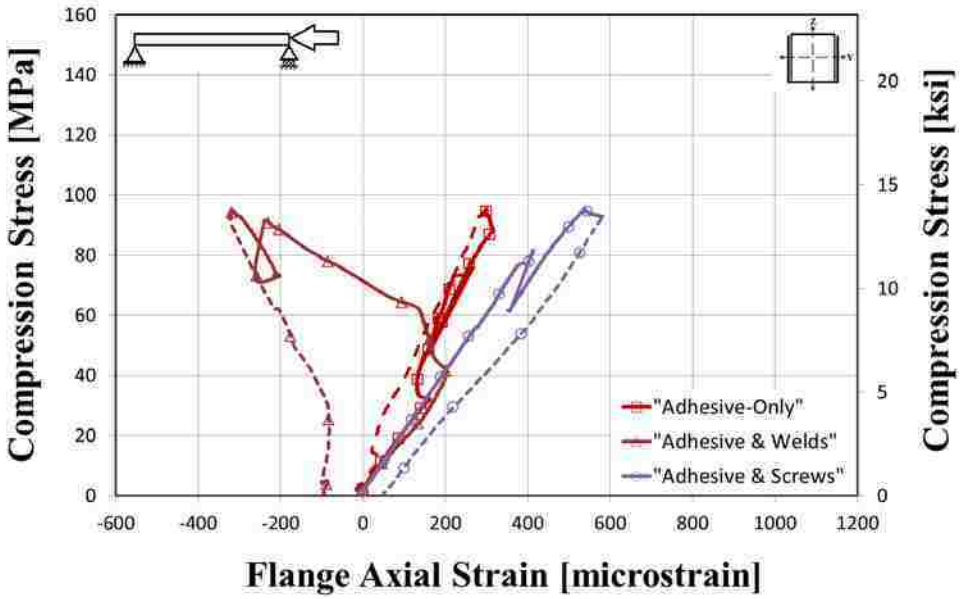

Figure 4-11: Compression Stress vs. Flange Axial Strain for Column Tests to 20 kips

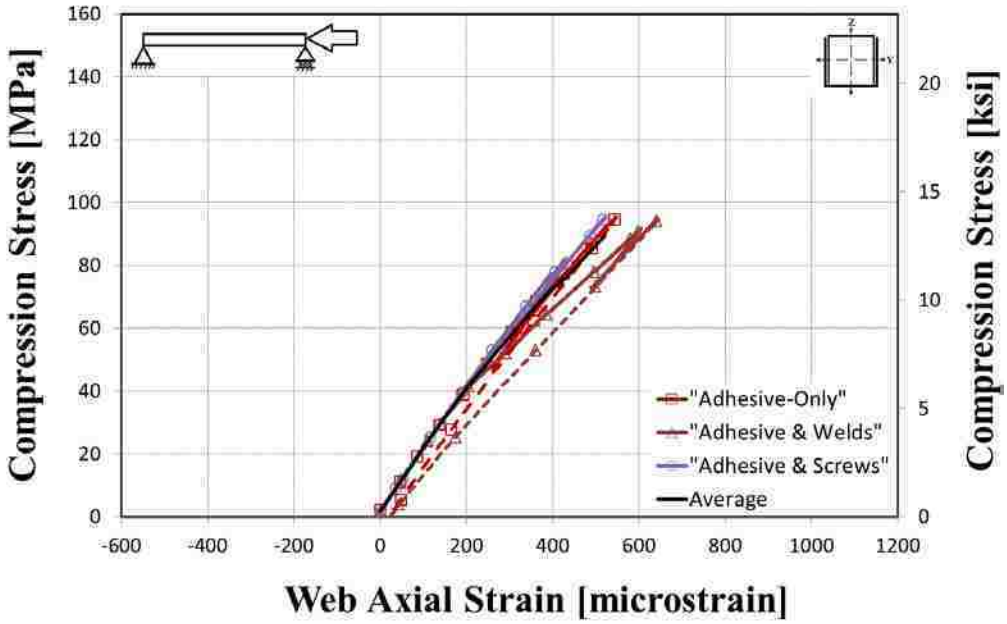

Figure 4-12: Compression Stress vs. Web Axial Strain for Column Tests to 20 kips

Table 4-4: Flange and Web Axial Strain at Maximum Stress (~95 MPa or 14 ksi) for Column Tests to 20 kips

Configuration	Flange Axial Strain [με]	Web Axial Strain [με]
Adhesive-Only	300	546
Adhesive and Welds	-317	644
Adhesive and Screws	539	521
Average	174	570
Standard Deviation	442	65
	254%	11%

4.1.6 Stress vs. Bending Strain

The bending strain values at maximum stress are listed in Table 4-5 for all three columns. Figure 4-13 to Figure 4-14 show the compression stress versus bending strain in the flange and the web for the columns loaded to 20 kips. The same scale is used for the horizontal and vertical axes in these figures as was used in the figures for stress versus axial strain to illustrate that bending strain was a small component of the total strain compared to axial strain. Notice that similarly to the stress versus axial strain that the spread of bending strain is greater for the flanges than for the webs (although on a much smaller magnitude). This is most likely due to the flanges having one free edge compared to the webs having no free edges.

Table 4-5: Flange and Web Bending Strain at Maximum Stress (~95 MPa or 14 ksi) for Column Tests to 20 kips

Configuration	Flange Bending Strain [με]	Web Bending Strain [με]
Adhesive-Only	-9	188
Adhesive and Welds	49	176
Adhesive and Screws	77	173
Average	39	179
Standard Deviation	44	8
	112%	4%

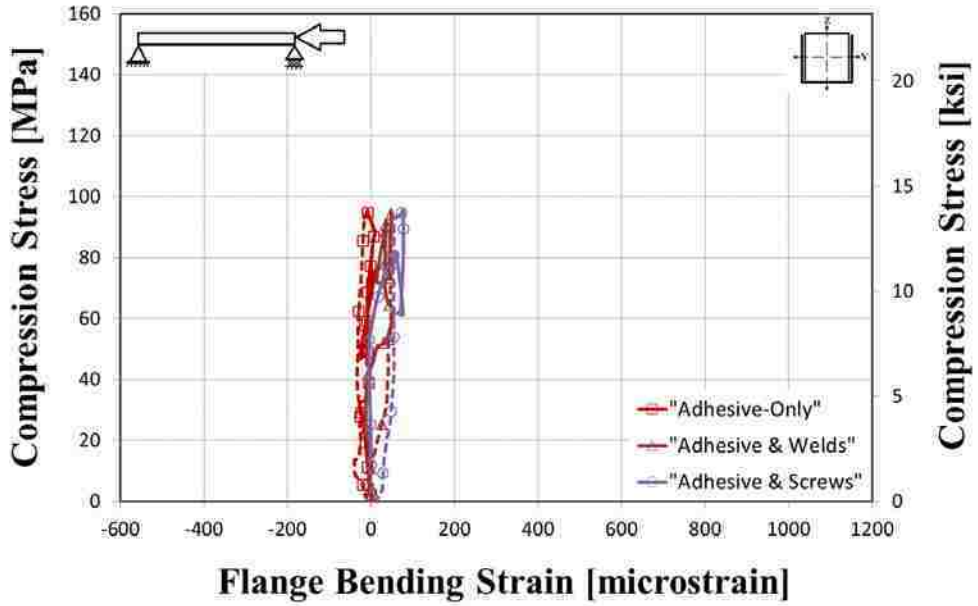

Figure 4-13: Compression Stress vs. Flange Bending Strain for Column Tests to 20 kips

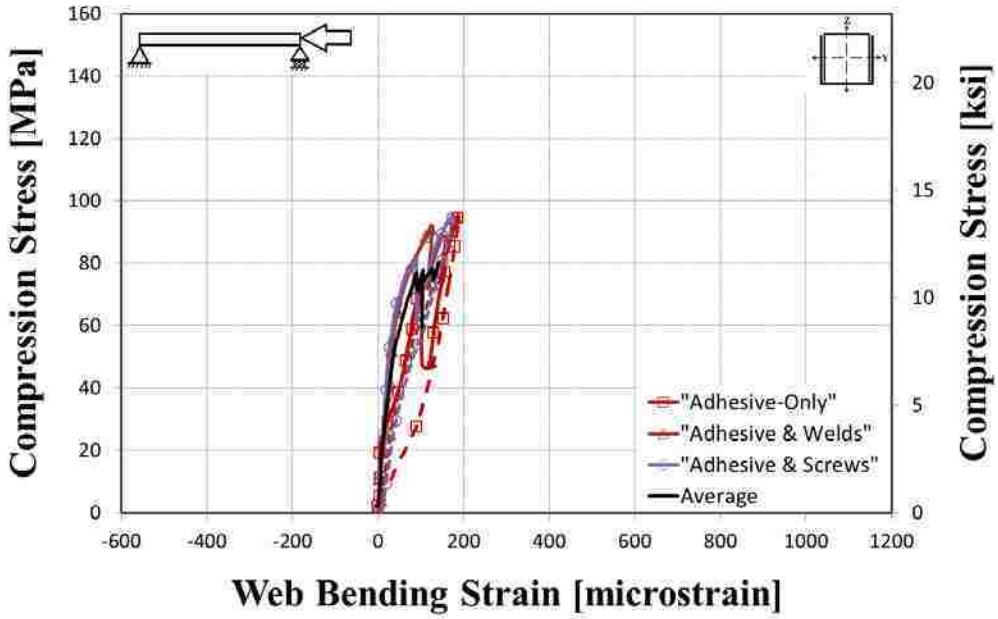

Figure 4-14: Compression Stress vs. Web Bending Strain for Column Tests to 20 kips

4.1.7 Southwell Plots

Figure 4-15 through Figure 4-18 are Southwell plots of the columns tested to 20 kips with linear regression lines over different portions of the transverse deflection curve. The different

portions consist of the region from 0.20-0.63" using transverse deflections in the negative z-direction, of the full curves using transverse deflections in the negative z-direction, of the region from 0.20-0.63" using the resultant transverse deflections, and of the full curves using the resultant transverse deflections, respectively. These portions were selected because the most linear portions of the curves were determined to be between 0.20 and 0.63 inches for the transverse deflection in the z-direction; and between 0.24 and 0.64 inches for the transverse deflection in the resultant direction. Table 4-6 summarizes the slopes obtained from the Southwell plots and Table 4-7 summarizes the predicted critical buckling loads for the different columns based on these Southwell plots.

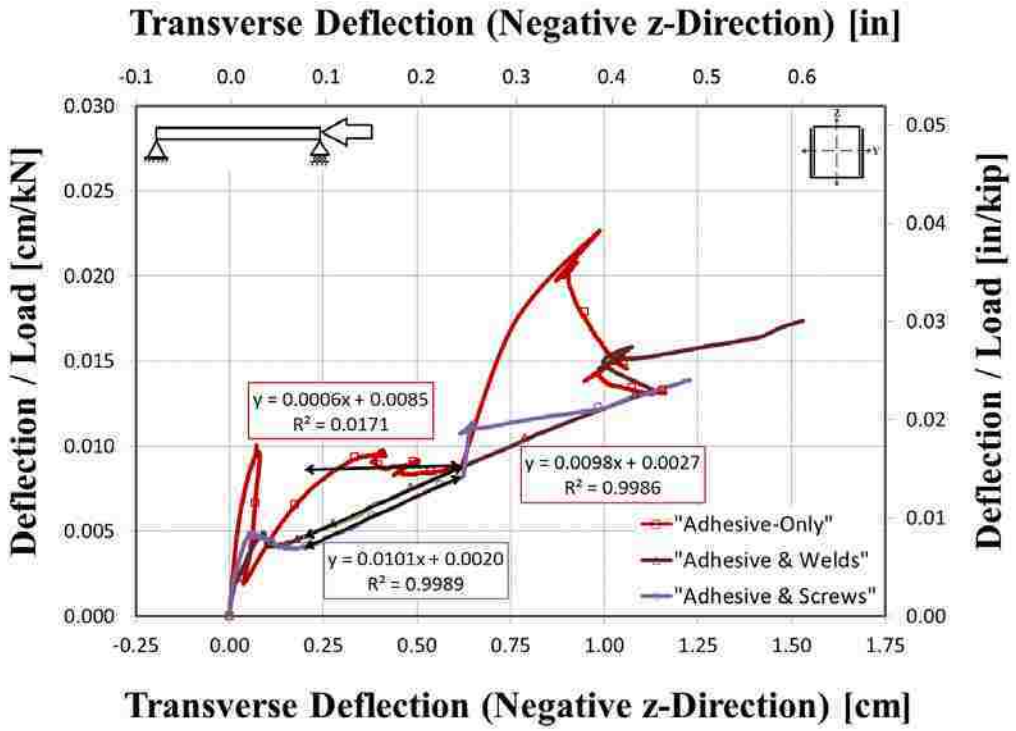

Figure 4-15: Southwell Plots with Linear Regression Lines Based on 0.20-0.63" Transverse Deflections in the Negative z-Direction for Column Tests to 20 kips

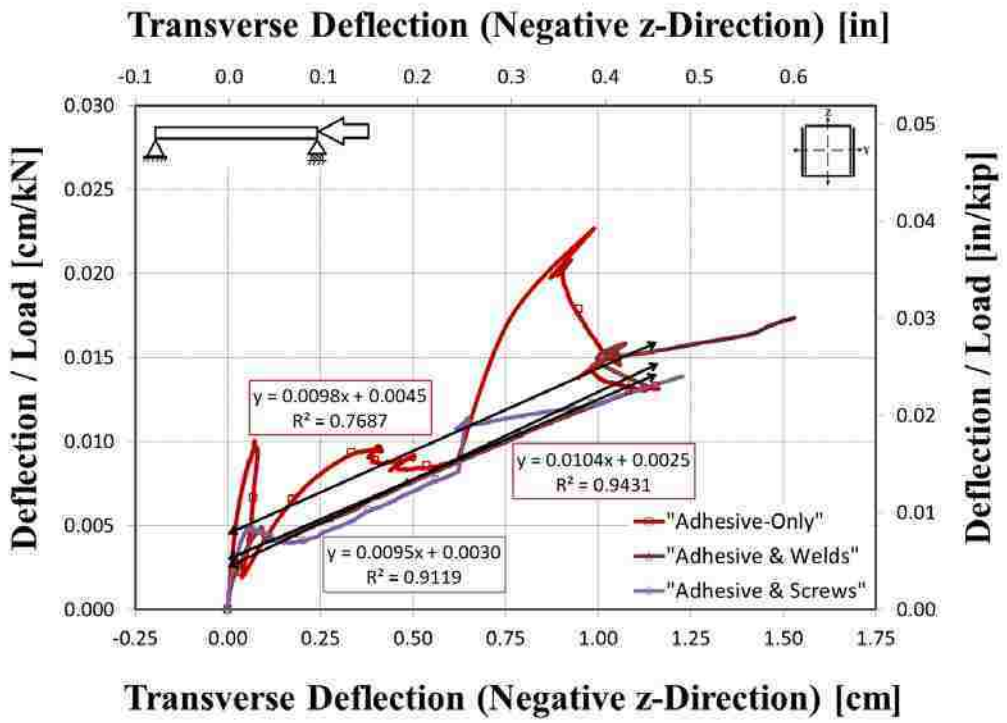

Figure 4-16: Southwell Plots and Linear Regression Lines Based on 0.00-1.16" Transverse Deflections in the Negative z-Direction for Column Tests to 20 kips

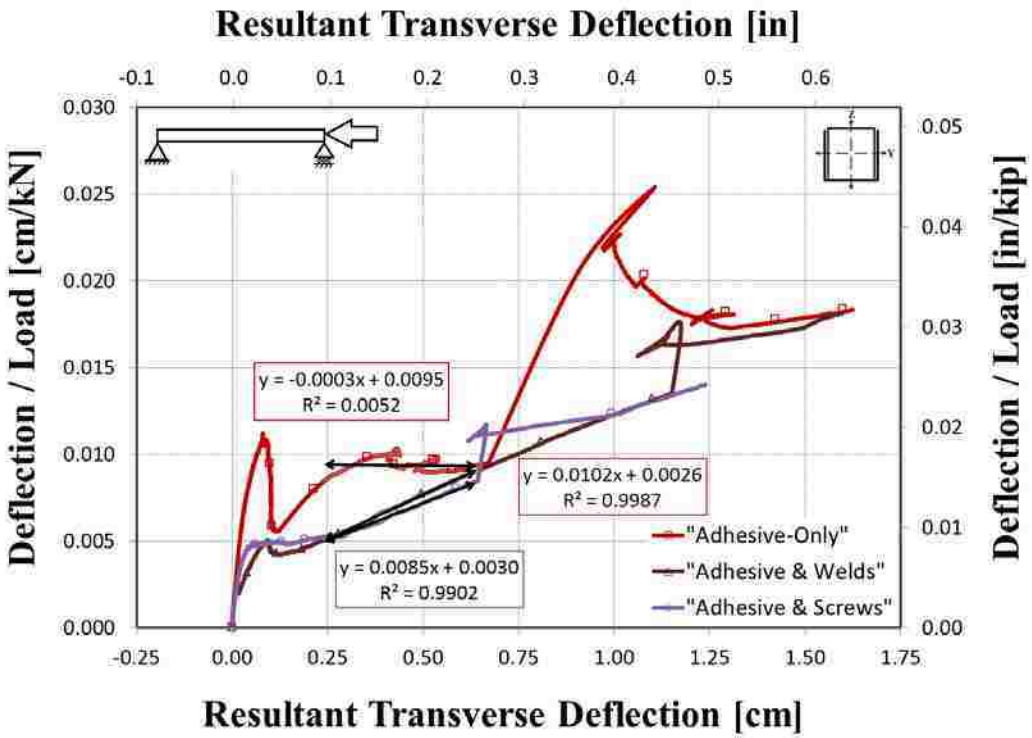

Figure 4-17: Southwell Plots and Linear Regression Lines Based on 0.24-0.64" Transverse Resultant Deflections for Column Tests to 20 kips

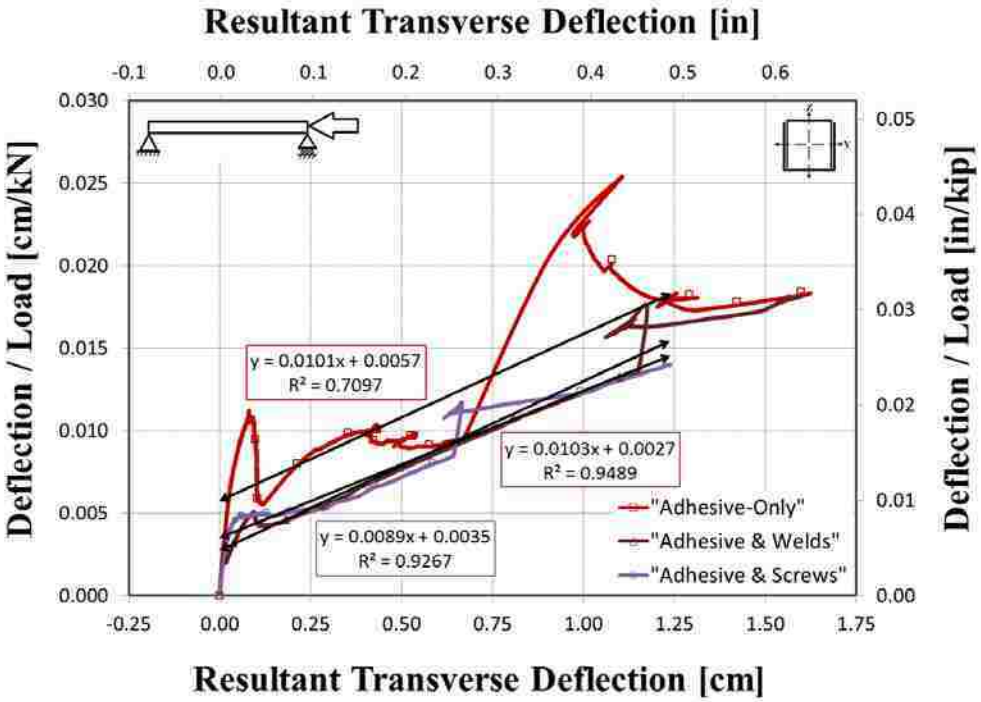

Figure 4-18: Southwell Plots and Linear Regression Lines Based on 0.00-1.24" Transverse Resultant Deflections for Column Tests to 20 kips

Table 4-6: Slopes of Southwell Plots for Column Tests to 20 kips

Configuration	Southwell Plot Slope [1/kN (1/kip)]			
Direction: Range:	z (0.20-0.63")	z (full range)	Resultant (0.24-0.64")	Resultant (full range)
Adhesive-Only	--	0.0098 (0.0436)	--	0.0101 (0.0449)
Adhesive and Welds	0.0098 (0.0436)	0.0104 (0.0463)	0.0102 (0.0454)	0.0103 (0.0458)
Adhesive and Screws	0.0101 (0.0449)	0.0095 (0.0423)	0.0085 (0.0378)	0.0089 (0.0396)
Average	0.0100 (0.0443)	0.0099 (0.0440)	0.0094 (0.0416)	0.0098 (0.0434)
Standard Deviation	0.0002 (0.0009)	0.0005 (0.0020)	0.0012 (0.0053)	0.0008 (0.0034)
	2.1%	4.6%	12.9%	7.8%

Table 4-7: Projected Critical Buckling Loads Based on Southwell Plots for Column Tests to 20 kips

Configuration	Projected Critical Buckling Load, P_{cr} [kN (kips)]				
Direction: Range:	z (0.20-0.63")	z (full range)	Resultant (0.24-0.64")	Resultant (full range)	Average
Adhesive-Only	--	102 (22.9)	--	99 (22.3)	101 (22.6)
Adhesive and Welds	102 (22.9)	96 (21.6)	98 (22.0)	97 (21.8)	98 (22.1)
Adhesive and Screws	99 (22.3)	105 (23.7)	118 (26.4)	112 (25.3)	109 (24.4)
Average	101 (22.6)	101 (22.7)	108 (24.2)	103 (23.1)	103 (23.0)
Standard Deviation	2.1 (0.5)	4.6 (1.0)	13.9 (3.1)	8.3 (1.9)	5.4 (1.2)
	2.1%	4.6%	12.9%	8.1%	5.3%

The Southwell method projections based on the three initial tests performed predicted an average critical buckling load for the foam-filled steel columns of approximately 23.2 kips (103 kN), with a standard deviation between configurations of 1.6 kips (7.2 kN). The Southwell plots for the "Adhesive and Welds" and "Adhesive and Screws" columns exhibited sections of linear data which could be used to predict a critical buckling load. The slope and corresponding critical buckling load values are omitted for the "Adhesive-Only" configuration because the R-squared value for the trend lines in both the z-direction and resultant deflection curves is approximately zero. This is unrealistic, suggesting that more columns should to be tested to find the real slope and critical buckling load, especially for the "Adhesive-Only" configuration.

4.2 Discussion of 20-kip Test Results

This section discusses the results of the three column tests to 20 kips.

4.2.1 Significance of Local Buckling

The wavelength for local buckling was approximately 12" (30.5 cm). This was equal to the spacing of periodic spot-welds; however, the screws were spaced at 24" (71.0 cm) on center

and thus two wavelengths are seen between sets of screws in Figure 4-3. In order to minimize local buckling, the spacing of spot-welds or screws must be less than the width of the column, 4 in (10.2 cm). This would not only minimize local buckling, but could strengthen the column significantly by changing the flange boundary conditions. The flange would effectively change from simply-supported on three sides and free on one side to simply-supported on all four sides. According to Gere and Timoshenko, this increases the plate buckling factor from 0.43 to 4.0 (approximately a factor of 10). Although this would not increase the total column strength by ten-fold, the stability of the cross-section would increase. The extent to which this increase may occur is analyzed more in depth in Chapters 6 and 7.

4.2.2 Elastic Loading

Based on the data presented in this chapter, the columns appear to have been loaded and unloaded in the elastic region. Thus, reloading the columns to failure should produce similar results for displacement and for strain.

4.2.3 Projected Buckling Load Compared to Euler Load

The Euler buckling stress, σ_{cr}, was 21.3 ksi (145 MPa) and the corresponding Euler buckling load, P_{cr}, based on a cross-sectional area of 1.44 in^2 (9.29 cm^2) was 30.6 kips (136 kN). The projected buckling load as a ratio of Euler buckling load results are listed in Table 4-8. Figure 4-19 shows the buckling load projections as a ratio of the Euler buckling load, as well as the averages and standard deviations between configurations for each column. Note from this figure that the empirically projected buckling loads, using Southwell plots, suggest that the

buckling load approximately 75% of the theoretical Euler buckling load. This indicates that the Euler buckling load is a non-conservative estimate of the actual buckling load for the columns.

Table 4-8: Projected Buckling Load as a Ratio of Euler Buckling Load

Configuration	Projected Critical Buckling Load, P_{cr} [kN (kips)]				
Direction: / Range:	z (0.20-0.63")	z (full range)	Resultant (0.24-0.64")	Resultant (full range)	Average
Adhesive-Only	--	0.75	--	0.73	0.74
Adhesive and Welds	0.75	0.71	0.72	0.71	0.72
Adhesive and Screws	0.73	0.77	0.86	0.83	0.80
Average	0.74	0.74	0.79	0.75	0.75
Standard Deviation	0.02	0.03	0.10	0.06	0.04
	2.1%	4.6%	12.9%	8.1%	5.3%

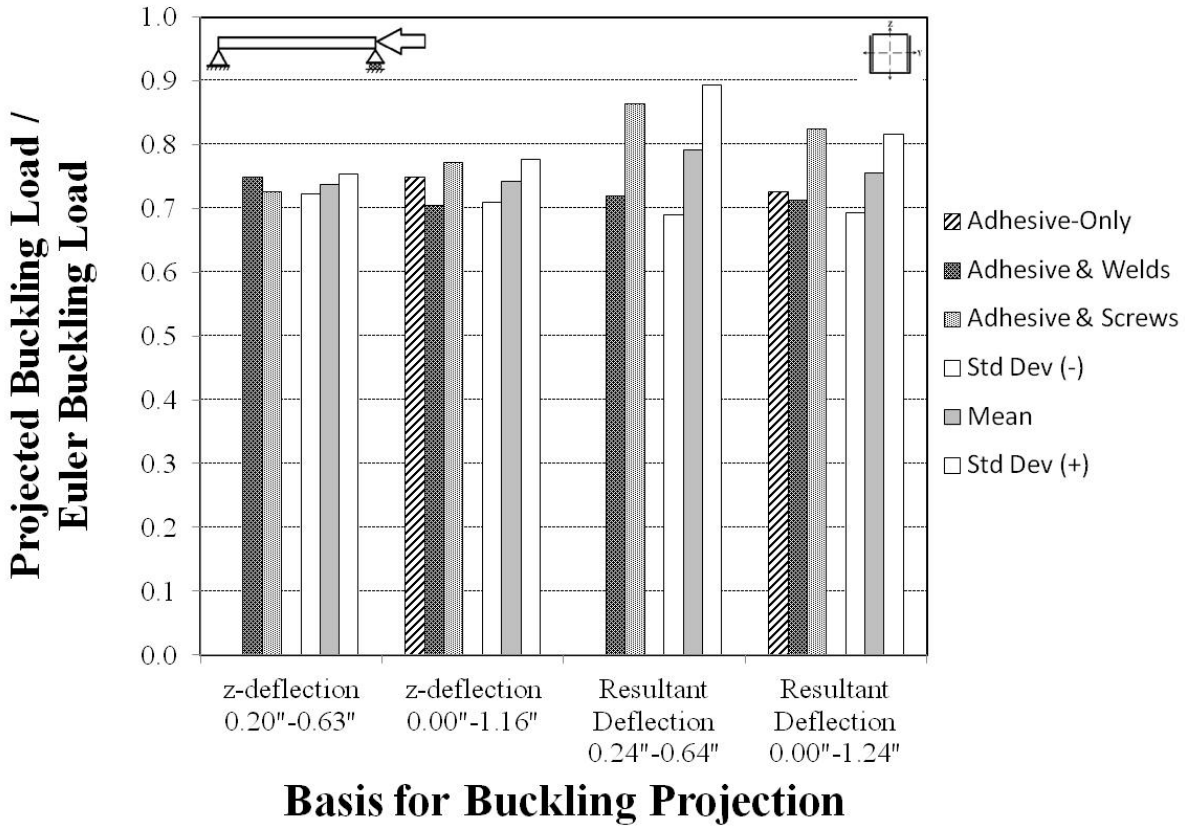

Figure 4-19: Comparison of Southwell and Euler Projected Buckling Loads for Column Tests to 20 kips

4.3 Summary

In this chapter, three different configurations of columns were tested in pure axial compression to 20 kips. Although there were not enough test samples to ensure that the data is statistically reliable, one initial indication from these tests is that the overall structural capacity of the columns appears to be similarly affected by the three different methods of flange attachment studied: "Adhesive-Only," "Adhesive and Welds," and "Adhesive and Screws." The results of the Southwell method indicate that the three columns investigated are capable of supporting approximately 23.0 kips (103 kN) with a standard deviation of 1.2 kips (5.4 kN) or 5.3% in pure axial compression. This value is 74% of the theoretical Euler buckling load for a column with pinned ends. The value that should be used for design, however, is 19.4 kips (86.3 kN) which is based on three standard deviations below the mean, ensuring that 99.7% of the population will be above this value, based on the three tests performed (however, there is no true measurable level of confidence because there was only one sample of each configuration).

5 RESULTS OF COLUMN TESTING TO FAILURE

This chapter summarizes and discusses the results from the four column compression tests performed to failure: "Adhesive-Only," "Adhesive and Welds," "Adhesive and Screws," and "Adhesive-No-Foam."

5.1 Column Failure Test Results

This section summarizes the test results for four columns tested to failure.

5.1.1 Local Buckling

All of the columns buckled locally prior to crippling failure. Figure 5-1 through Figure 5-3 show the local buckling of the columns. Note there were no photographs available for the local buckling of the "Adhesive and Welds" column. The observed local buckling wavelength and aspect ratio are listed in Table 5-1. Note that the buckling length was approximately 12 in (30.5 cm) for all columns, including the "Adhesive and Screws" column shown in Figure 5-3. This indicates that the screws were spaced too far apart to increase the local buckling load. This same phenomenon was observed in the preliminary testing to 20 kips (88 kN). The "Adhesive-No-Foam" column exhibited local buckling first near the loaded end (see Figure 5-3).

Figure 5-1: Photo of Local Buckling of "Adhesive-Only" Column During Test to Failure

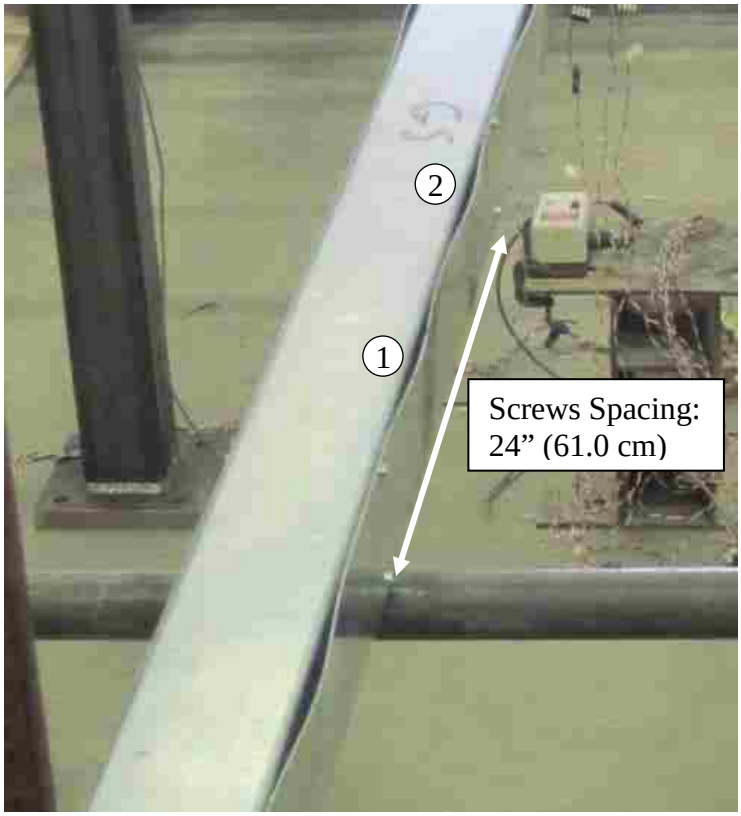

Figure 5-2: Photo of Local Buckling of "Adhesive and Screws" Column During Test to Failure Showing Two Wavelengths Between Sets of Screws

Figure 5-3: Photo of Local Buckling of "Adhesive-No-Foam" Column During Test to Failure

Table 5-1: Observed Local Buckling Wavelength and Aspect Ratio

Description	Wavelength, *a* [cm (in)]	Flange Aspect Ratio, *a* / b [no units]
Outer Flanges	30.5 (12)	~ 3.0

5.1.2 Crippling and Global Buckling

All four columns failed in the following manner: first, the cross-section crippled (i.e., exhibited permanent deformation); second, the global buckling ensued. Both of these occurred instantaneously since crippling introduced both an effective hinge and eccentricity in the geometry. Crippling and global buckling are shown in Figure 5-4 through Figure 5-9. Note that

little or no adhesive is visible in between the flanges in the photos showing crippled segments. The lack of adhesive leaves the cross-section unreinforced and less stable.

Figure 5-4: Photo of Crippled "Adhesive-Only" Column During Test to Failure

Figure 5-5: Photo of Buckled "Adhesive and Welds" Column During Test to Failure

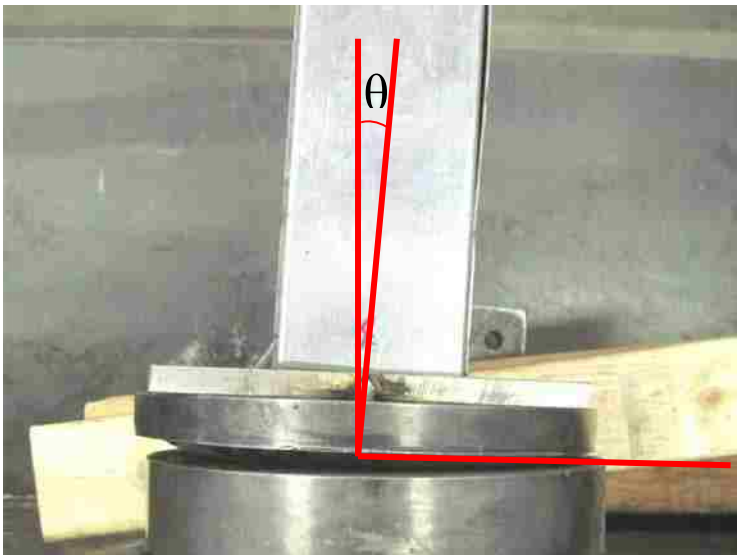

Figure 5-6: Photo of Rotation Produced by Crippled "Adhesive and Welds" Column at Reaction-End During Test to Failure

Figure 5-7: Photo of Buckled "Adhesive and Screws" Column During Test to Failure

Figure 5-8: Close-up Photo of Crippling of "Adhesive and Screws" Column During Test to Failure

Figure 5-9: Photo of Crippled "Adhesive-No-Foam" Column During Test to Failure

5.1.3 Load vs. Axial Deflection

Figure 5-10 shows the compression load versus axial deflection for all four columns loaded to failure. A summary of the maximum load values is listed in Table 5-2.

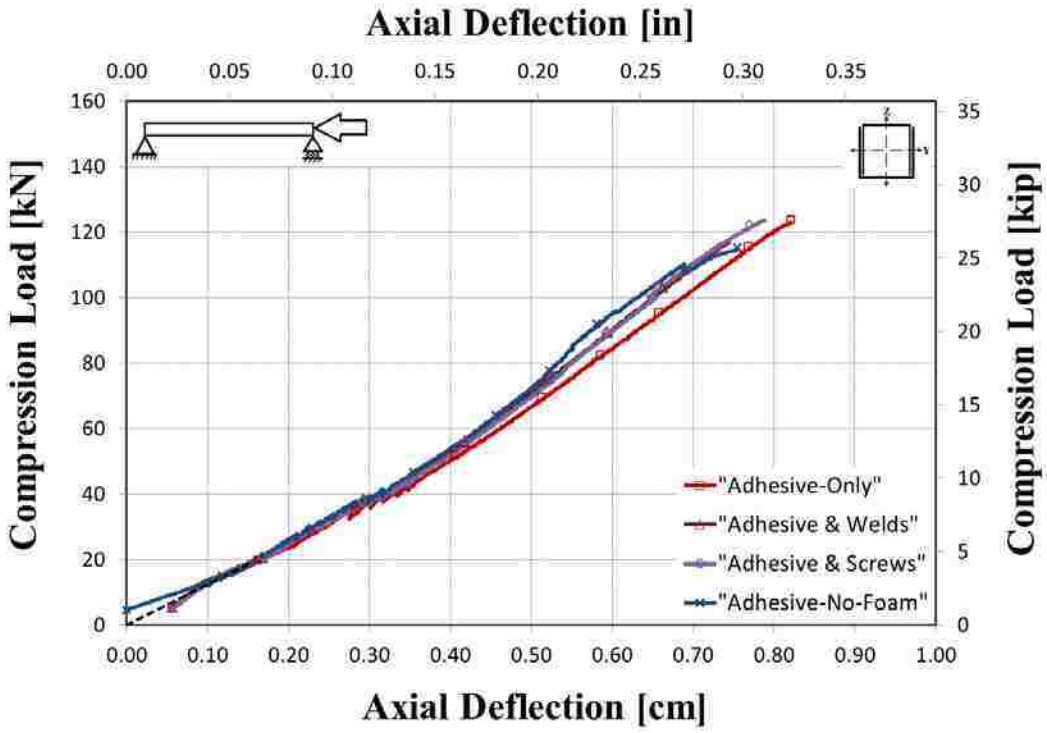

Figure 5-10: Compression Load vs. Axial Deflection for Column Tests to Failure

Table 5-2: Maximum Loads and Axial Deflections (x-Direction) for Columns Loaded to Failure (Column Stiffness Based on Deflection at 8 kips)

Configuration	Failure Load, P_{cr} [kN (kip)]	Axial Deflection (x-Dir.), $u_{1,cr}$ [cm (in)]	Column Stiffness, K [kN/cm (kip/in)]
Adhesive-Only	123.0 (27.7)	0.82 (0.32)	150 (85.6)
Adhesive and Welds	116.9 (26.3)	0.74 (0.29)	157 (89.7)
Adhesive and Screws	123.6 (27.8)	0.79 (0.31)	157 (89.7)
Adhesive-No-Foam	114.4 (25.7)	0.75 (0.30)	152 (86.6)
Average	119.5 (26.9)	0.78 (0.31)	154 (87.9)
Standard Deviation	4.5 (1.0)	0.03 (0.01)	3.6 (2.1)
	3.8%	4.4%	2.4%

5.1.4 Load vs. Transverse Deflection

Figure 5-11 through Figure 5-13 show the compression load versus transverse deflection in the y-, z-, and resultant directions for the four columns loaded in compression to failure.

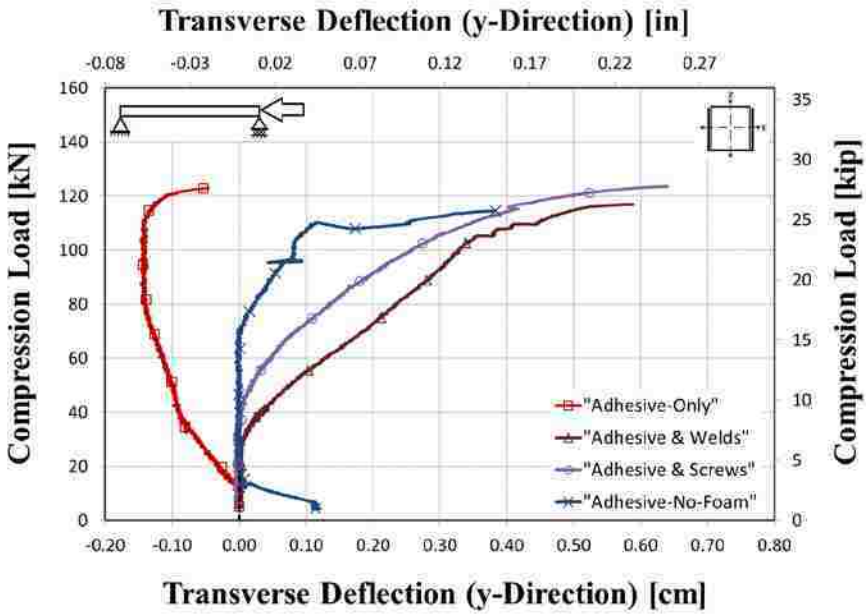

Figure 5-11: Compression Load vs. Transverse Deflection (y-Direction) for Column Tests to Failure

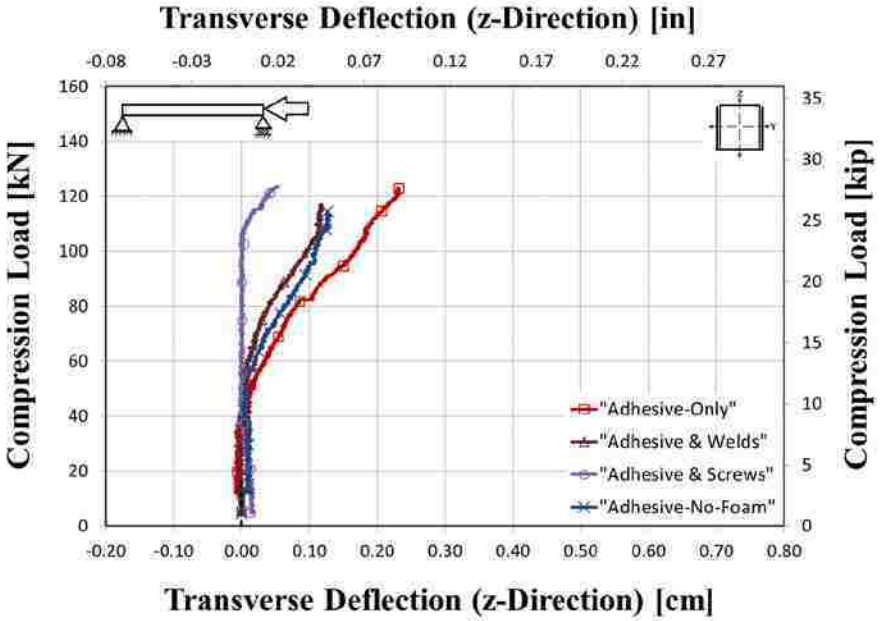

Figure 5-12: Compression Load vs. Transverse Deflection (z-Direction) for Column Tests to Failure

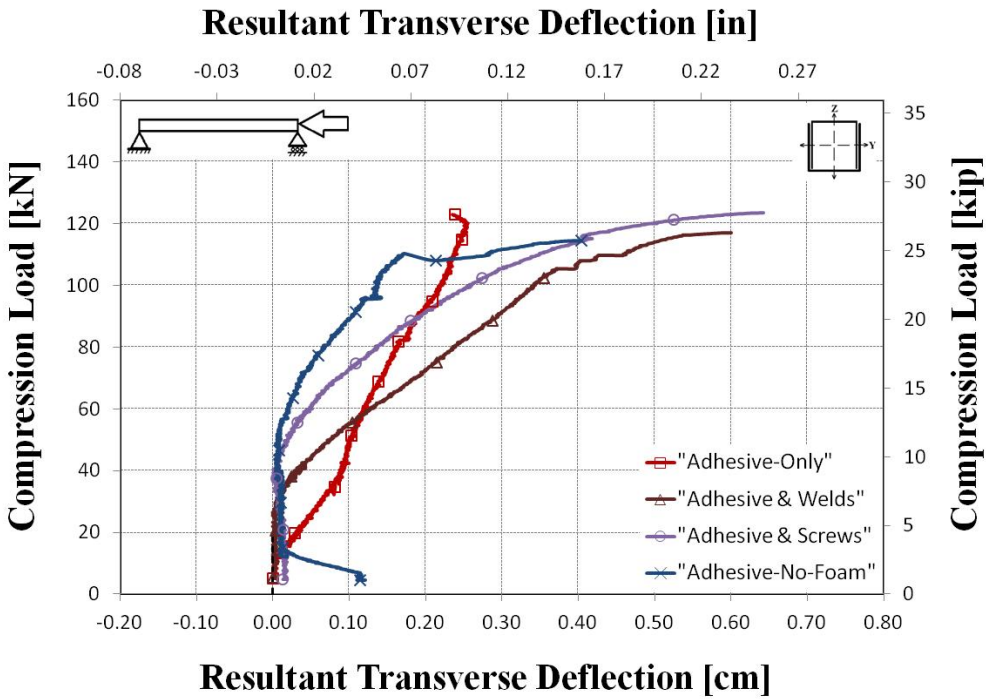

Figure 5-13: Compression Load vs. Resultant Deflection for Column Tests to Failure

Table 5-3: Transverse Deflections in the y- , z-, and Resultant Directions for Column Tests to Failure

Configuration	Deflection at Failure Load		
	Transverse (y), $u_{2,cr}$ [cm (in)]	Transverse (z), $u_{3,cr}$ [cm (in)]	Resultant, $u_{R,cr}$ [cm (in)]
Adhesive-Only	0.05 (0.02)	0.23 (0.09)	0.24 (0.09)
Adhesive and Welds	0.59 (0.23)	0.12 (0.05)	0.60 (0.24)
Adhesive and Screws	0.64 (0.25)	0.04 (0.02)	0.64 (0.25)
Adhesive-No-Foam	0.38 (0.15)	0.13 (0.05)	0.40 (0.16)
Average	0.41 (0.16)	0.13 (0.05)	0.47 (0.19)
Standard Deviation	0.27 (0.11)	0.08 (0.03)	0.19 (0.07)
	65.0%	60.4%	40.0%

5.1.5 Stress vs. Total (Local) Strain

Figure 5-14 through Figure 5-17 show the stress versus total strain for each column individually. In Figure 5-16, it is apparent that the gage measuring strain in the y-direction was

not operating correctly. The corresponding results are therefore omitted from subsequent figures. The strains at maximum stress (~130 MPa) are listed for each column in Table 5-4.

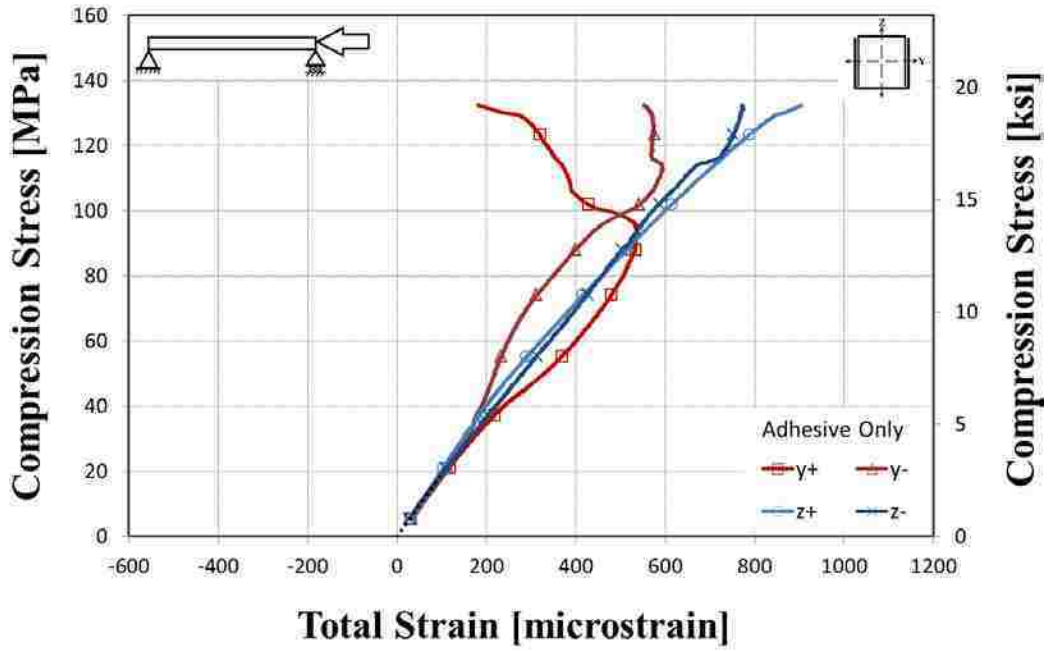

Figure 5-14: Compression Stress vs. Total Strain for "Adhesive-Only" Column Test to Failure

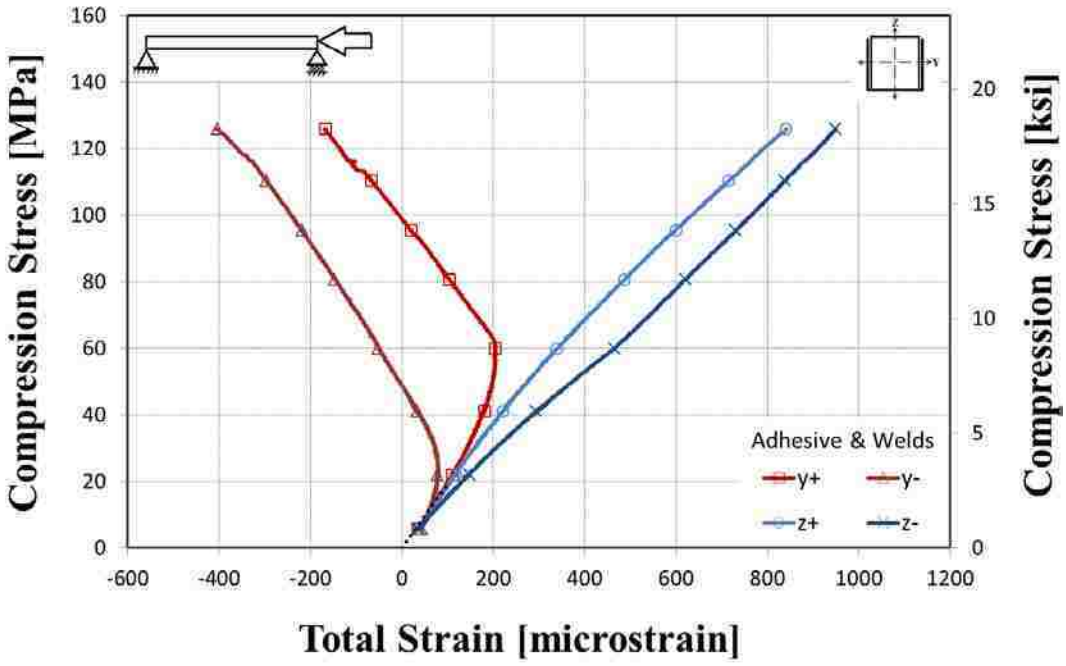

Figure 5-15: Compression Stress vs. Total Strain for "Adhesive and Welds" Column Test to Failure

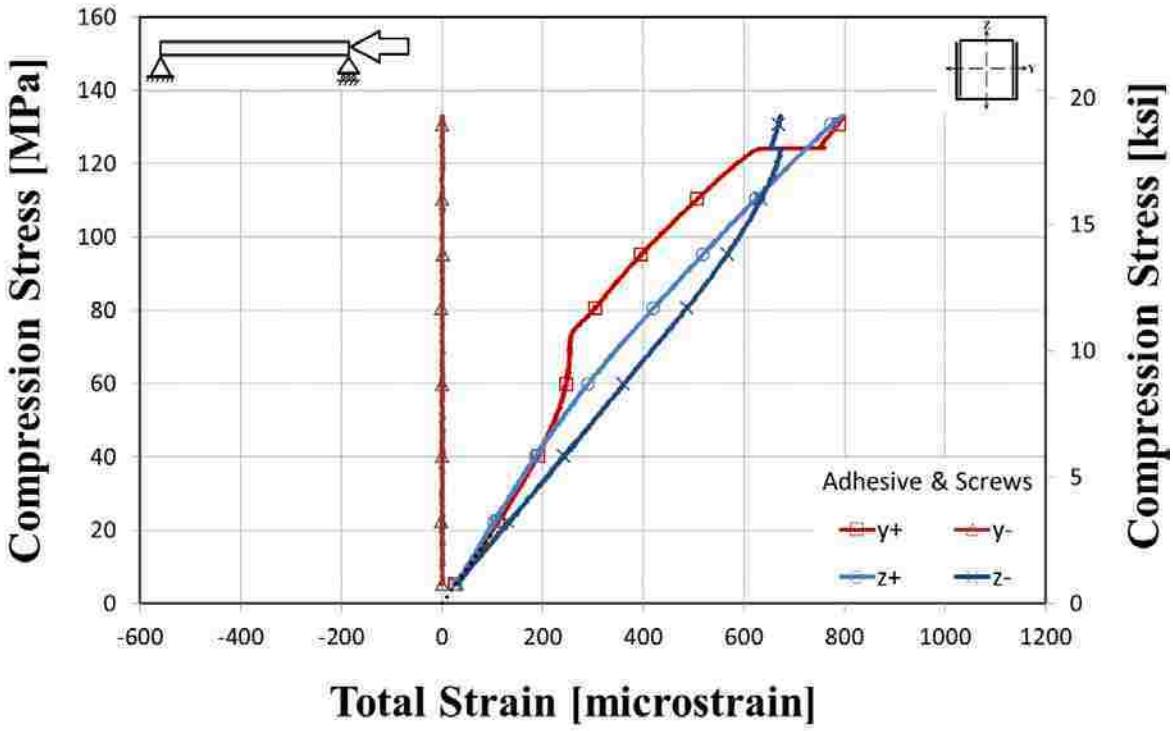

Figure 5-16: Compression Stress vs. Total Strain for "Adhesive and Screws" Column Test to Failure

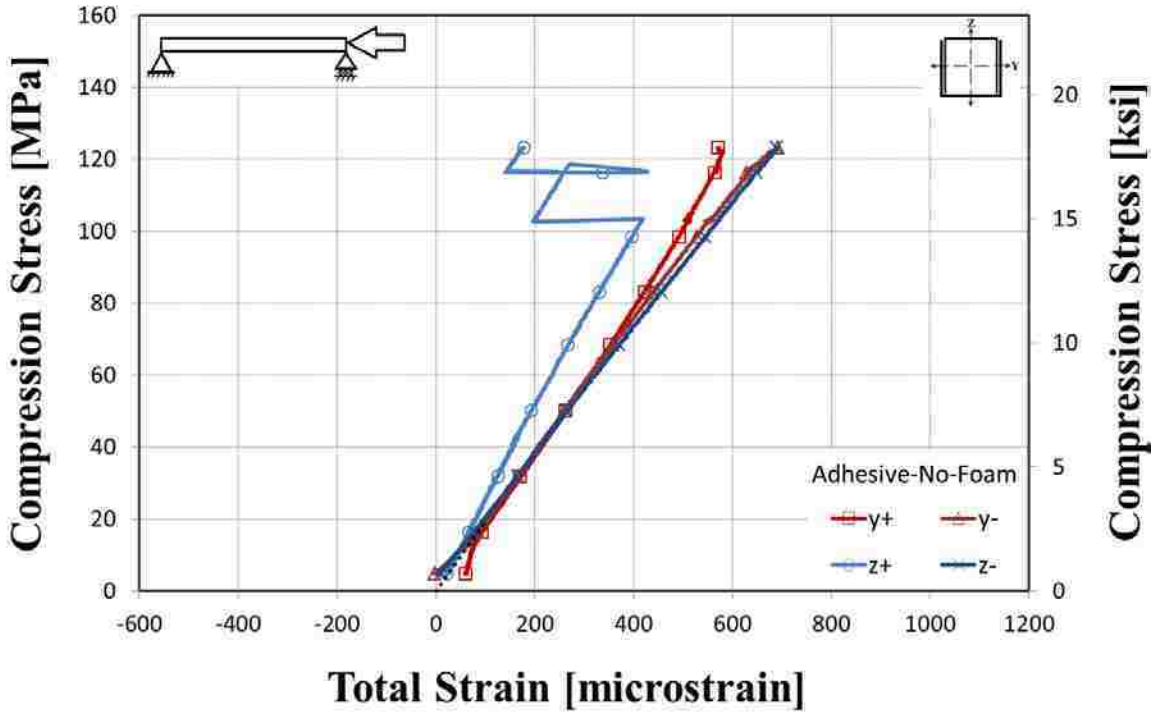

Figure 5-17: Compression Stress vs. Total Strain for "Adhesive-No-Foam" Column Test to Failure

Table 5-4: Strain at Failure Stress (by Column Face) for Column Tests to Failure

Configuration	Max Stress, σ_{cr} [MPa (ksi)]	Column Face z- [με]	y+ [με]	z+ [με]	y- [με]
Adhesive-Only	132 (19.2)	772	181	905	552
Adhesive and Welds	126 (18.3)	949	-404	841	-167
Adhesive and Screws	133 (19.3)	673	1	796	798
Adhesive-No-Foam	123 (17.9)	689	692	1/78	571
Average	129 (18.7)	771	118	680	438
Standard Deviation	4.9 (0.7)	126	454	337	419
	3.8%	16%	386%	50%	96%

5.1.6 Stress vs. Axial Strain

The axial strain values at maximum stress are listed in Table 5-5 for all four columns. Figure 5-18 through Figure 5-19 show the compression stress versus axial strain based on the flange and web strain data, respectively, for the four columns loaded to failure. There is a significantly larger spread in compression stress versus flange axial strain than in compression stress versus web axial strain. This is most likely due to the flanges having one free edge, which allows the flanges to buckle at a much lower load than the webs. This evidently varies the axial strain, depending on the location of the strain gage relative to the local buckling site.

Table 5-5: Flange and Web Axial Strain at Failure Stress (~130 MPa or 19 ksi) for Column Tests to Failure

Configuration	Flange Axial Strain [με]	Web Axial Strain [με]
Adhesive-Only	367	838
Adhesive and Welds	-286	895
Adhesive and Screws	--	735
Adhesive-No-Foam	632	434
Average	40	823
Standard Deviation	461	81
	1139%	10%

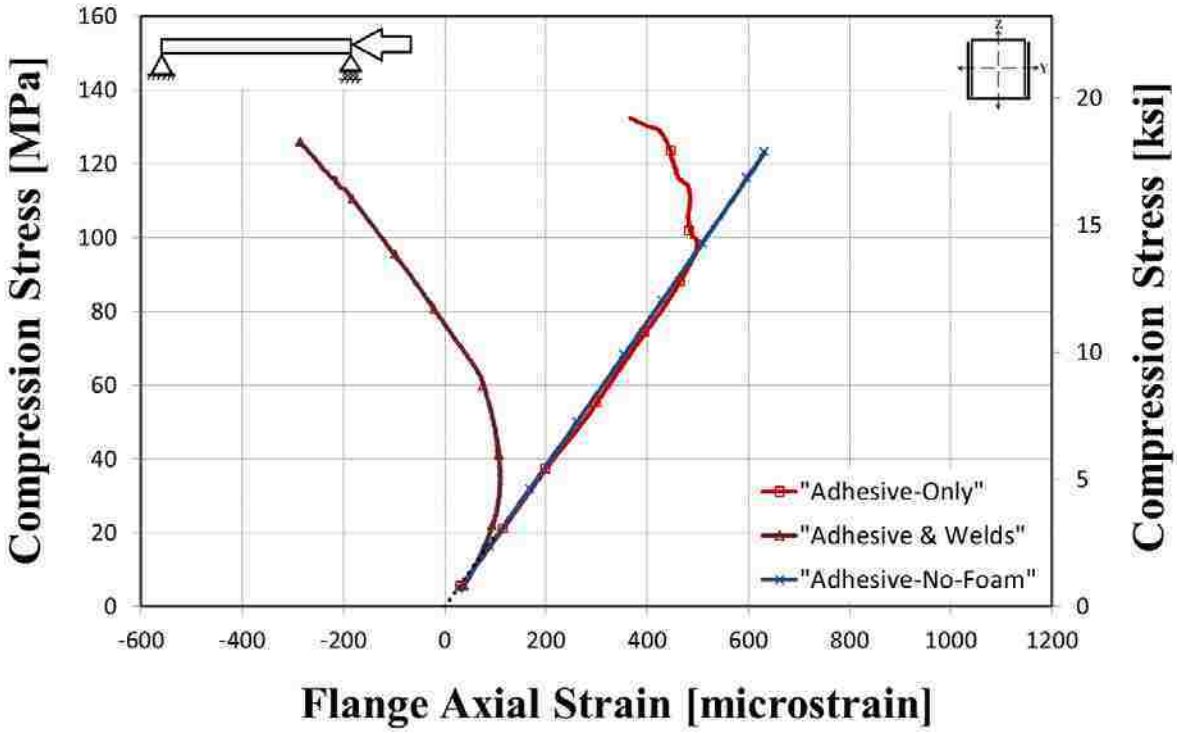

Figure 5-18: Compression Stress vs. Flange Axial Strain for Column Tests to Failure

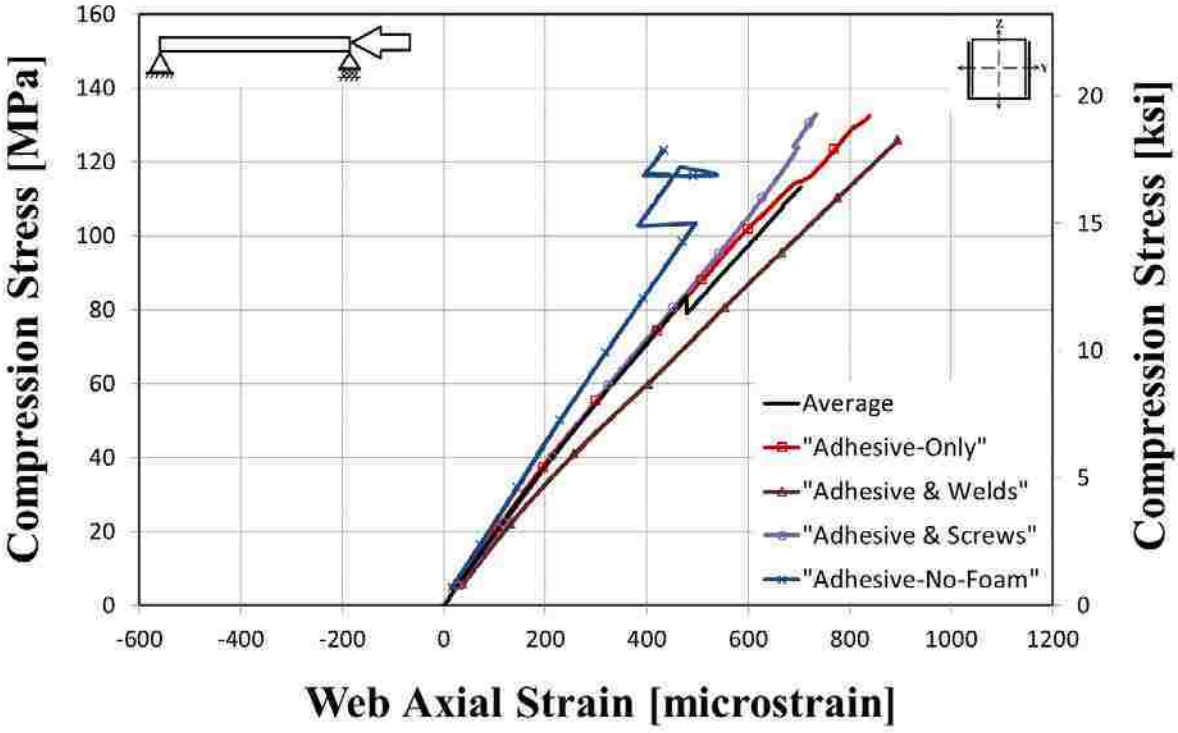

Figure 5-19: Compression Stress vs. Web Axial Strain for Column Tests to Failure

5.1.7 Stress vs. Bending Strain

Figure 4-13 through Figure 4-14 show the compression stress versus bending strain in the flange and the web, respectively, for the columns loaded to failure. The same axis scales are used as the figures for stress vs. axial strain to show that bending strain is small compared to axial strain. The bending strain values at maximum stress are listed in Table 5-6 for all four columns. Notice that contrary to the stress versus axial strain that the spread of bending strain is greater for the webs than for the flanges (although on a much smaller magnitude). This is contrary to what was expected and is either reflecting faulty readings from the strain gages or is capturing local flange bending.

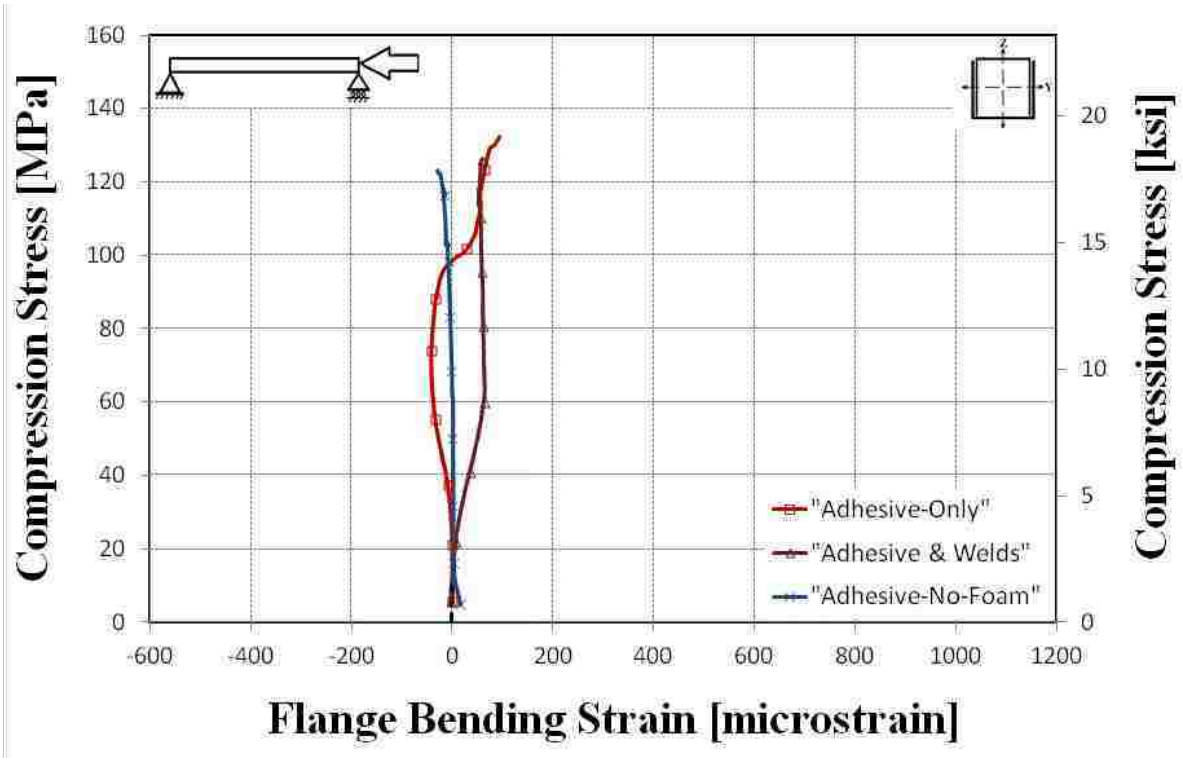

Figure 5-20: Compression Stress vs. Flange Bending Strain for Column Tests to Failure

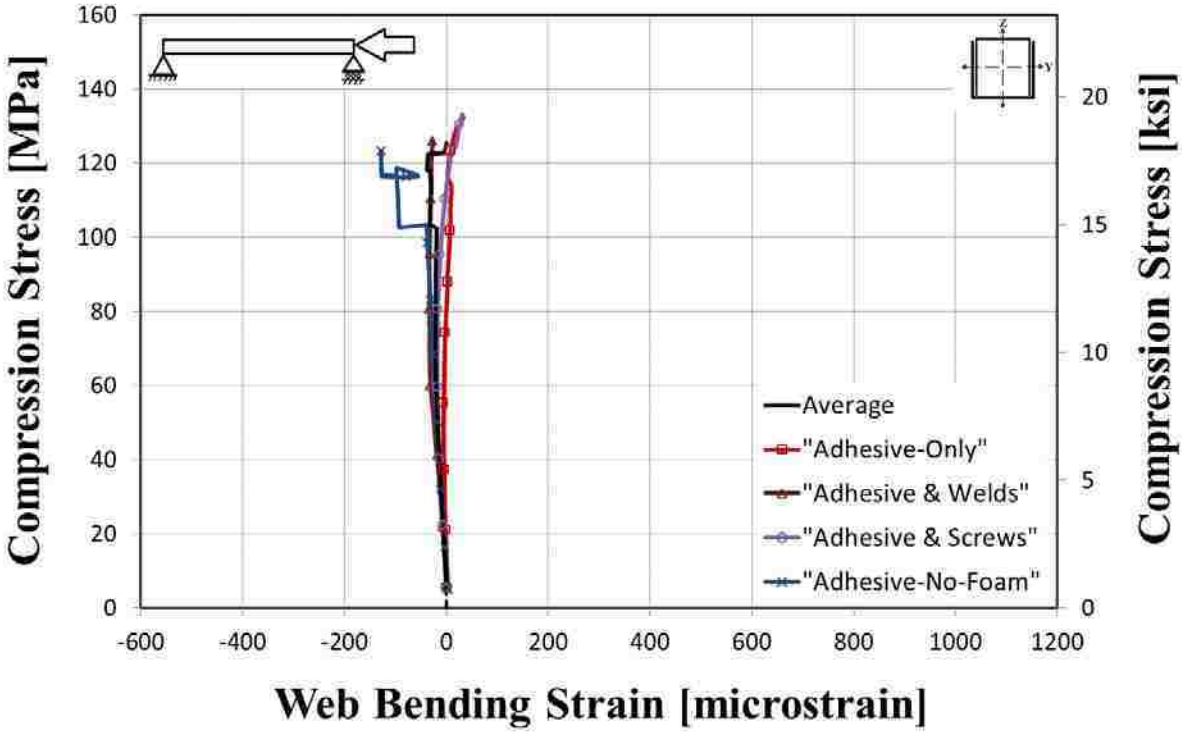

Figure 5-21: Compression Stress vs. Web Bending Strain for Column Tests to Failure

Table 5-6: Flange and Web Bending Strain at Failure Stress (~130 MPa or 19 ksi) for Column Tests to Failure

Configuration	Flange Bending Strain [με]	Web Bending Strain [με]
Adhesive-Only	93	33
Adhesive and Welds	59	-27
Adhesive and Screws	--	31
Adhesive-No-Foam	-30	-128
Average	76	12
Standard Deviation	24	34
	31%	279%

5.1.8 Southwell Plots

Figure 5-22 through Figure 5-25 are Southwell plots of the columns tested to failure with linear regression lines over different portions of the transverse deflection curve. The different

portions consist of varying partial ranges using transverse deflections in the negative z-direction, the full curves using transverse deflections in the negative z-direction, varying partial regions using the resultant transverse deflections, and the full curves using the resultant transverse deflections, respectively. These portions selected were the most linear portions of the curves. Table 5-7 summarizes the slopes obtained from the Southwell plots and Table 5-8 summarizes the predicted critical buckling loads for the different columns based on these Southwell plots. The results for the "Adhesive Only" column are omitted because the slope is significantly small compared to the other three test samples.

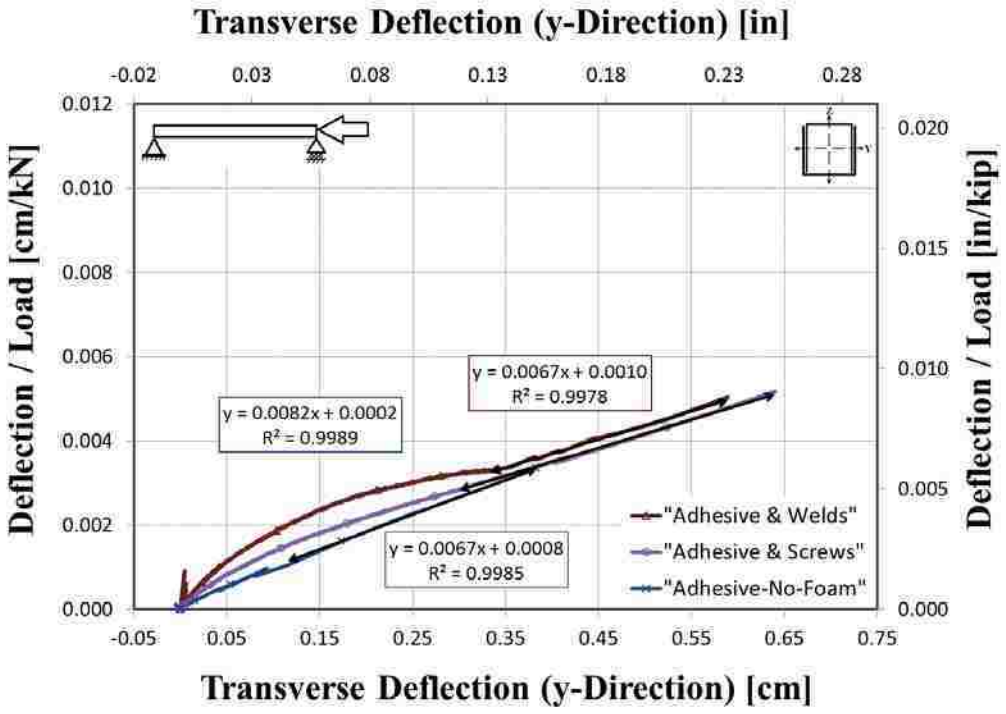

Figure 5-22: Southwell Plots with Linear Regression Lines Based on Partial Range Transverse Deflections in the Negative y-Direction for Column Tests to Failure

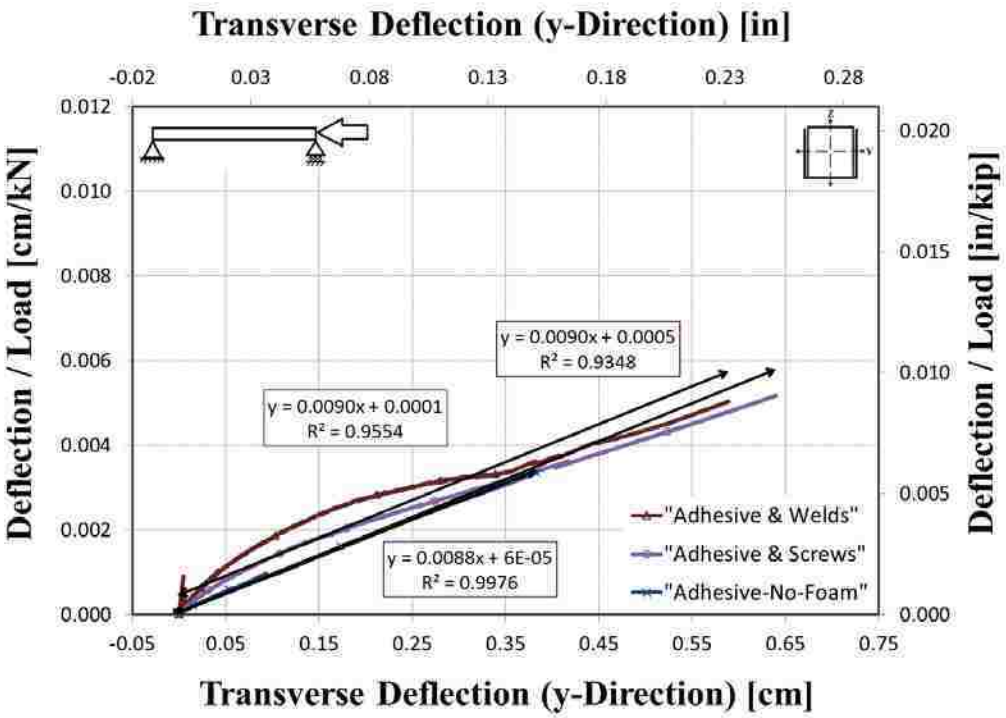

Figure 5-23: Southwell Plots with Linear Regression Lines Based on Full Range Transverse Deflections in the Negative y-Direction for Column Tests to Failure

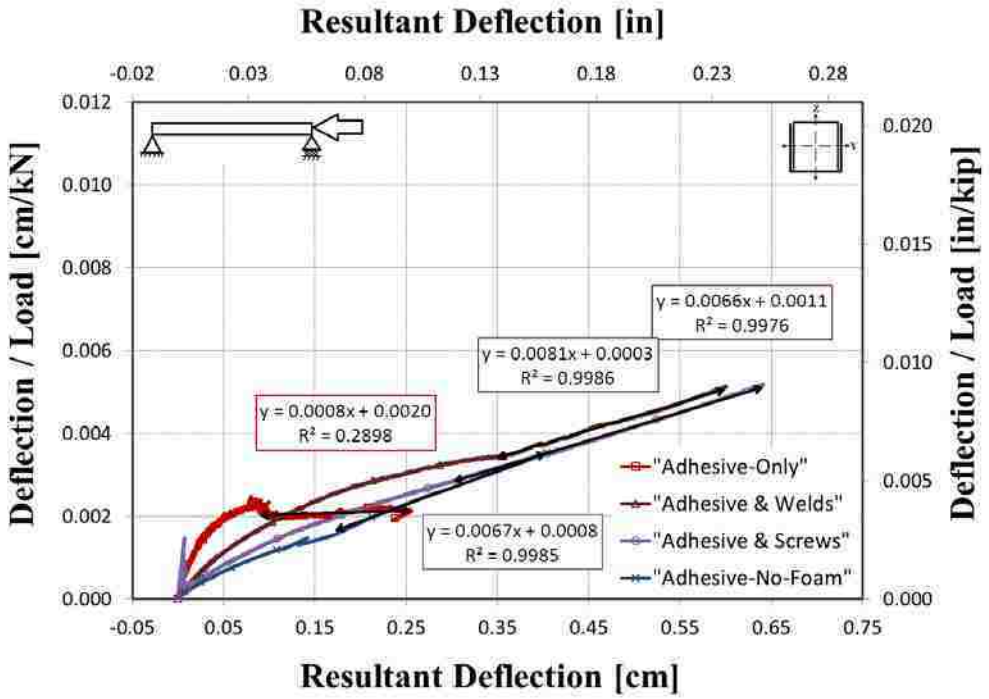

Figure 5-24: Southwell Plots with Linear Regression Lines Based on Partial "Linear Portion" of Resultant Transverse Deflections for Column Tests to Failure

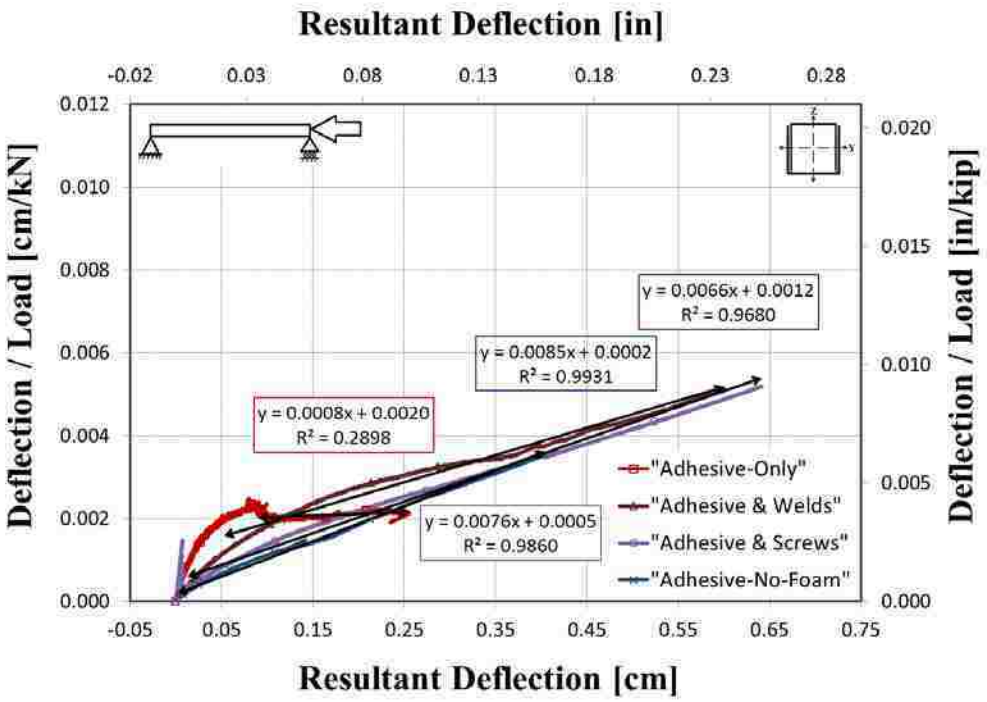

Figure 5-25: Southwell Plots with Linear Regression Lines Based on Full "Linear Portion" of Resultant Transverse Deflections for Column Tests to Failure

Table 5-7: Slopes of Southwell Plots for Column Tests to Failure

Configuration	Southwell Plot Slope [1/kN (1/kip)]			
Direction: Range:	y (partial)	y (full)	Resultant (partial)	Resultant (full)
Adhesive-Only	--	--	--	--
Adhesive and Welds	0.0067 (0.0298)	0.0065 (0.0289)	0.0066 (0.0294)	0.0066 (0.0294)
Adhesive and Screws	0.067 (0.0298)	0.0077 (0.0342)	0.0067 (0.0298)	0.0076 (0.0338)
Adhesive-No-Foam	0.0082 (0.0365)	0.0088 (0.0391)	0.0081 (0.0360)	0.0085 (0.0378)
Average	0.0072 (0.0320)	0.0077 (0.0341)	0.0071 (0.0317)	0.0076 (0.0337)
Standard Deviation	0.0009 (0.0039)	0.0012 (0.0051)	0.0008 (0.0037)	0.0010 (0.0042)
	12.0%	15.0%	11.8%	12.6%

Table 5-8: Projected Critical Buckling Loads for Column Tests to Failure

Configuration	Direction: Range:	Projected Critical Buckling Load, P_{cr} [kN (kips)] y (partial)	y (full)	Resultant (partial)	Resultant (full)	Average
Adhesive-Only		--	--	--	--	--
Adhesive and Welds		149 (33.6)	154 (34.6)	152 (34.1)	152 (34.1)	152 (34.1)
Adhesive and Screws		149 (33.6)	130 (29.2)	149 (33.6)	132 (29.6)	140 (31.5)
Adhesive-No-Foam		122 (27.4)	114 (25.5)	123 (27.8)	118 (26.4)	119 (26.8)
Average		140 (31.5)	132 (29.8)	141 (31.8)	134 (30.0)	137 (30.8)
Standard Deviation		15.8 (3.5)	20.2 (4.5)	15.6 (3.5)	17.0 (3.8)	16.4 (3.7)
		11.2%	15.3%	11.0%	12.7%	12.0%

5.2 Discussion of Column Failure Test Results

This section discusses the results of the four column tests to failure.

5.2.1 Local Flange Buckling

Many observations may be made regarding local flange buckling. The adhesive between steel flanges did not prevent buckling of the outer flanges. Local buckling and delamination of the outer flanges occurred at periodic locations throughout the entire length of each of the columns during all tests to 20 kips and tests to failure (see Figure 5-26). The local buckling is partially due to the debond failure of the adhesive (note that adhesive is predictably weak in tension) and partially due to the long aspect ratio of the column plate segments. The spacing of screws or welds to improve column strength should be further investigated. Also, in all of the images one or both of the string potentiometers appears to be resting directly on an area of peak local buckling. This implies that both the attached string potentiometer and the strain gage measurements were affected. Some of these affects are visible in the data as shown in Figure

5-14 to Figure 5-15 (previously) where the curves begin to strain in the opposite direction at about 40-60 MPa. This appears, however, to have only slightly affected the projected buckling loads based on the Southwell plots. This is because the Southwell plots are based on the dominant deflections in the y-, z- or resultant directions. Finally, note that local buckling preceded crippling in all cases. Strengthening the local buckling capacity should increase the overall column capacity.

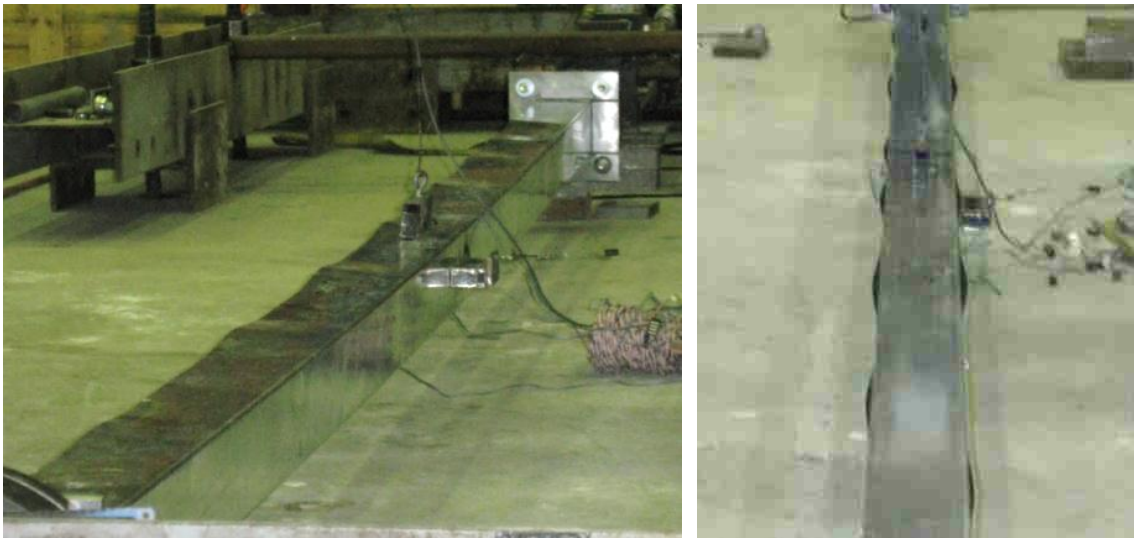

Figure 5-26: Local Buckling of Flanges Observed on Column Tests to 20 kips: "Adhesive-Only" (Left) and "Adhesive and Screws" (Right)

5.2.2 Elastic Loading

Figure 5-27 through Figure 5-28 compare the average web axial and bending strains, respectively, for all columns for both the test to 20 kips and to failure. The consistent average axial in-plane strain for the two tests confirms that the initial loading was elastic. The difference in the results for the web bending strain is because the columns tested to failure were partially constrained against bending in the direction of the webs (from the gravity supports); in contrast, during the tests to 20-kips the exhibited preferential bending in the direction of the webs.

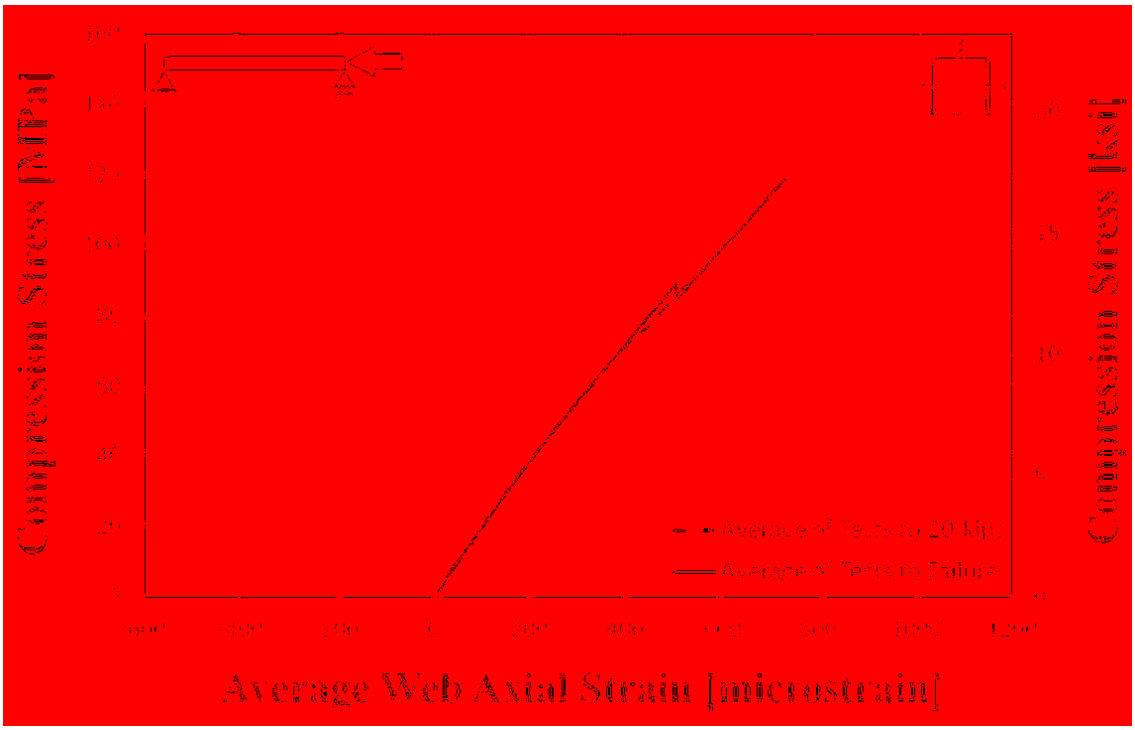

Figure 5-27: Comparison of Compression Stress vs. Average Web Axial Strain for Test to 20 kips and to Failure

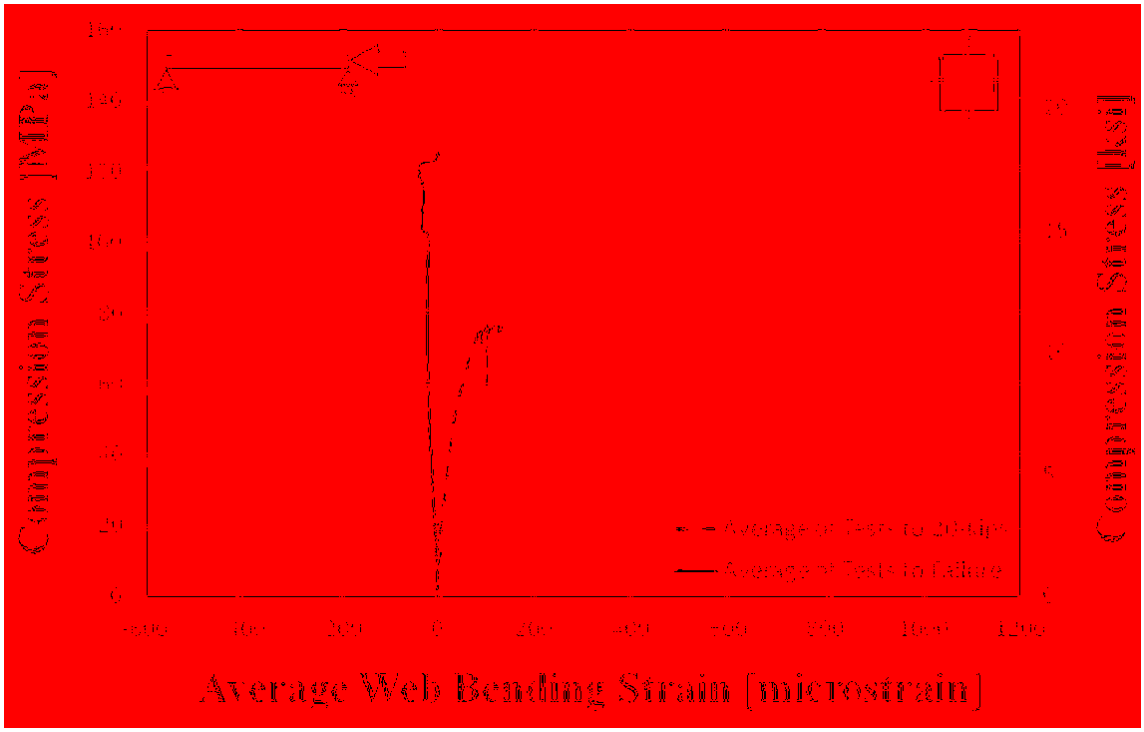

Figure 5-28: Comparison of Compression Stress vs. Average Web Bending Strain for Test to 20 kips and to Failure

5.2.3 Accuracy of Buckling Projections

Table 5-9 summarizes and compares the actual failure loads with the calculated Euler buckling loads and the projected Southwell-based buckling loads. The average crippling load from the tests to failure was 26.9 kips (120 kN). This value was 89% of the Euler buckling load based on pinned-pinned boundary conditions, 30.3 kips (135 kN); 118% of the average projected buckling load based on the Southwell plots based on tests to 20-kips, 23.0 kips (103 kN); and 88% of the average projected buckling load based on the Southwell plots based on tests to failure, 30.8 kips (137 kN). Crippling occurred at a lower stress value that global buckling would have. Thus, both the Euler buckling equation and the Southwell projections based on tests to failure over-projected the buckling capacity of the columns. The reason that the Southwell projections based on tests to 20-kips under-projected the column buckling capacity was because of the gravity supports. The gravity supports partially constrained the column from buckling in the weak direction and thus provided additional stability which was not present during the tests to 20-kips.

Table 5-9: Failure Loads Compared to Southwell Projections for Columns Based on Tests to 20 kips

Configuration	Failure Load, P_{cr} [kN (kips)]	Southwell-based Buckling Load, P_{cr} [kN (kips)]	Percent of Southwell Load [%]
Adhesive-Only	123 (27.7)	101 (22.6)	122
Adhesive and Welds	117 (26.3)	98 (22.1)	119
Adhesive and Screws	124 (27.8)	109 (24.4)	113
Adhesive No-Foam	114 (25.7)	--	--
Average	120 (26.9)	103 (23.0)	118
Standard Deviation	4.5 (1.0) 3.8%	5.4 (1.2) 5.3%	4.3 3.6%

Table 5-10: Failure Loads Compared to Southwell Projections for Columns Based on Tests to Failure

Configuration	Failure Load, P_{cr} [kN (kips)]	Southwell-based Buckling Load, P_{cr} [kN (kips)]	Percent of Southwell Load [%]
Adhesive-Only	123 (27.7)	--	--
Adhesive and Welds	117 (26.3)	152 (34.1)	87
Adhesive and Screws	124 (27.8)	140 (31.5)	92
Adhesive No-Foam	114 (25.7)	119 (26.8)	85
Average	120 (26.9)	137 (30.8)	88
Standard Deviation	4.5 (1.0)	16.4 (3.7)	4
	3.8%	12.0%	4%

Table 5-11: Failure Loads Compared to Euler Buckling Loads for Columns with Pinned-Pinned Boundary Conditions (k = 1.0)

Configuration	Failure Load, P_{cr} [kN (kips)]	Euler Buckling Load, P_{cr} [kN (kips)]	Percent of Euler Buckling [%]
Adhesive-Only	123 (27.7)	135 (30.3)	91
Adhesive and Welds	117 (26.3)	135 (30.3)	87
Adhesive and Screws	124 (27.8)	135 (30.3)	92
Adhesive No-Foam	114 (25.7)	135 (30.3)	85
Average	120 (26.9)	135 (30.3)	89
Standard Deviation	4.5 (1.0)	--	3
	3.8%	--	4%

5.2.4 Comparison of 20-kip and Failure Test Results

Table 5-12 compares the Southwell buckling projections from the tests to 20 kips and the tests to failure. Table 5-13 compares the Southwell buckling projections from the tests to 20 kips and the tests to failure for only the "Adhesive and Welds" and "Adhesive and Screws" columns. The tests to failure yielded higher load projections (~42%) than the tests to 20 kips, based on the Southwell buckling projections. The discrepancy may indicate slight differences in boundary conditions for the two test configurations. The discrepancy is likely due to the gravity supports

which were under the columns during testing and predisposed the columns to cripple about the z-z axis (strong axis). Future testing may potentially indicate that constraining the columns from buckling or crippling about the y-y axis improves the column capacity.

Table 5-12: Comparison of Southwell Projections from Tests to 20 kips and to Failure

Configuration	Southwell-based Buckling Loads, P_{cr}		Percent of
	Tests to 20 kips [kN (kips)]	Tests to Failure [kN (kips)]	Tests to 20 kips [%]
Adhesive-Only	101 (22.6)	--	--
Adhesive and Welds	98 (22.1)	152 (34.1)	155
Adhesive and Screws	109 (24.4)	140 (31.5)	128
Adhesive No-Foam	--	119 (26.8)	--
Average	103 (23.0)	137 (30.8)	142
Standard Deviation	5.4 (1.2) 5.3%	16.4 (3.7) 12.0%	19 13%

Table 5-13: Comparison of Southwell Projections for Two Columns from Tests to 20 kips and to Failure

Configuration	Southwell-based Buckling Loads, P_{cr}	
	Tests to 20 kips [kN (kips)]	Tests to Failure [kN (kips)]
Adhesive and Welds	98 (22.1)	152 (34.1)
Adhesive and Screws	109 (24.4)	140 (31.5)
Average	104 (23.3)	146 (32.8)
Standard Deviation	7.8 (1.6) 7.0%	8.5 (1.8) 5.6%

5.2.5 Influence of Foam Filler

The "Adhesive-No-Foam" column failure load was slightly more than one standard deviation below the overall average crippling load. The same column was nearly two standard deviations below the average crippling load determined using only the three remaining columns

(see Table 5-10). This could indicate that the foam is strengthening the columns. More testing and analysis will help to confirm or reject this hypothesis. The differences among the methods of flange attachment are too small to whether the screws or welds influenced the column strength.

Table 5-14: Comparison of Mean and Standard Deviation for Columns Tested to Failure Including and Excluding "Adhesive-No-Foam" Column

	Failure Load Including "Adhesive-No-Foam" Column, P_{cr} [kN (kips)]	Failure Load Excluding "Adhesive-No-Foam" Column, P_{cr} [kN (kips)]	Ratio of Including to Excluding [%]
Average	119 (26.9)	121 (27.2)	99
Standard Deviation	4.5 (1.0)	3.7 (0.8)	122
	3.8%	3.1%	124%

5.2.6 Strength to Weight Ratio

The strength to weight ratios for the columns are summarized and compared in Table 5-15. The columns carried an average of 0.380 kips of axial load per pound of column weight.

Table 5-15: Comparison of Strength to Weight Ratios

Configuration	Strength to Weight, *P/W* [kN/N (kips/lbs)]
Adhesive-Only	0.392 (0.392)
Adhesive and Welds	0.372 (0.372)
Adhesive and Screws	0.394 (0.394)
Adhesive No-Foam	0.364 (0.364)
Average	0.380 (0.380)
Standard Deviation	0.0145
	3.8%

5.3 Summary

In this chapter, four different configurations of columns were tested in pure axial compression to failure. Although there were not enough test samples to ensure that the data is statistically reliable, one initial indication from these tests is that the internal EPS32 foam may contribute to the structural strength of the columns. The overall structural capacity of the columns was not significantly affected, however, by the three different methods of flange attachment studied: adhesive-only, adhesive with welds, and adhesive with screws.

Southwell plots were used to project the critical buckling loads of the columns from the test results for both the preliminary tests and the tests to failure. This method projected buckling loads of approximately 23.0 kips (102 kN) with a standard deviation between configurations of approximately 1.6 kips (7.1 kN) or 6.9% for the preliminary tests. The Southwell plots from the tests to failure projected buckling loads of approximately 30.8 kips (137 kN) with a standard deviation of 3.7 kips (16.4 kN) or 12.0%. The columns all failed in crippling with an average strength of 26.9 kips (120 kN) and a standard deviation between configurations of approximately 1.0 kip (4.4 kN) or 3.8%. The average compressive strength was more than two standard deviations above the predicted buckling strength based on the preliminary tests and approximately one standard deviation below the projection based on the tests to failure. The discrepancy between the projections from the two methods is a result of slightly different boundary conditions in the two test setups including the slightly more rigid attachment to the 100-kip actuator than to the 20-kip actuator, as well as the gravity supports under the columns during the tests to failure. More tests are needed, however, to establish a statistically reliable value for the strength of the columns, as well as to isolate the influence of the screws, short-welds, adhesive, and foam inserts.

The columns investigated were capable of supporting approximately 26.9 kips (120 kN) in pure axial compression with a standard deviation of 1.0 kips (4.5 kN). This value is 89% of the theoretical Euler buckling load for a column with pinned ends and 88% of the Southwell buckling projection based on the tests to failure.

6 MECHANICS ANALYSIS

The mechanics analysis presented in this chapter has the following objectives: 1) calculate predicted values for buckling and crippling; and, 2) explore the effectiveness of foam stiffness, steel thickness, and flange attachment through parametric studies.

6.1 Model Development

This section describes assumptions, global boundary conditions, and local boundary conditions used in the mechanics analysis.

6.1.1 Assumptions

The following assumptions are made: loading eccentricities are ignored; imperfections in the column (e.g., material or manufacturing flaws) are ignored; axial compression is carried by the steel only; material properties provided by Novatek are assumed to be accurate (these values were not confirmed in the laboratory); strain is small and uniform at the steel-foam interface.

The nominal dimensions of the column cross-section are shown in Figure 6-1 and are listed in Table 6-1.

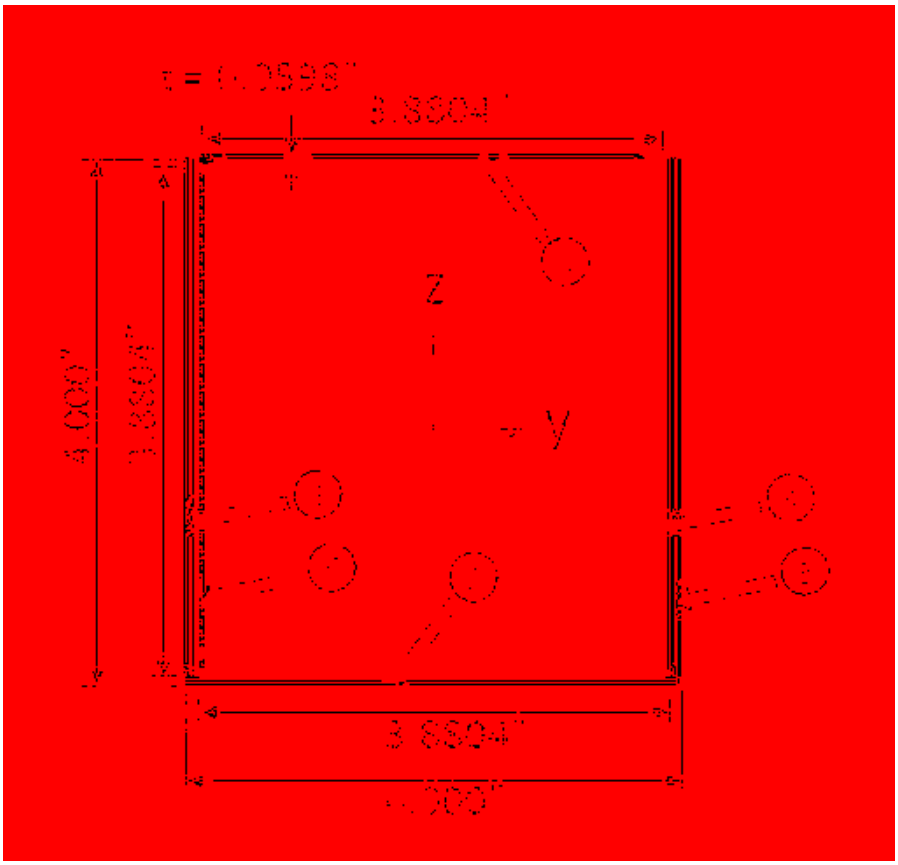

Figure 6-1: Illustration of Column Cross-Section Used in Mechanics Analysis

Table 6-1: Dimensions of ith Plate for Column Cross-Section

Plate # (i)	Description	Width, b_i [cm (in)]	Thickness, t_i [cm (in)]	Area, A_i [cm^2 (in^2)]	Ratios	
					b_i / t_i	t_i / b_i
1	Outer Flange	10.2 (4.0000)	0.152 (0.0598)	1.54 (0.239)	66.9	0.0150
2	Outer Web	9.9 (3.8804)	0.152 (0.0598)	1.50 (0.232)	64.9	0.0154
3	Outer Flange	10.2 (4.0000)	0.152 (0.0598)	1.54 (0.239)	66.9	0.0150
4	Inner Flange	9.9 (3.8804)	0.152 (0.0598)	1.50 (0.232)	64.9	0.0154
5	Inner Web	9.9 (3.8804)	0.152 (0.0598)	1.50 (0.232)	64.9	0.0154
6	Inner Flange	9.9 (3.8804)	0.152 (0.0598)	1.50 (0.232)	64.9	0.0154
				ΣA = 9.07 (1.406)		

6.1.2 Global Boundary Conditions

The global boundary conditions are assumed to be simply-supported in order to compare results from the mechanics analysis to experimental data (which was based on a simply-supported configuration). Because simply-supported global boundary conditions are used, the effective column length is equal to the actual column length and this value is used in the Euler buckling and slenderness calculations. The column length is assumed to be 14 ft (4.29 m). This chapter investigates the contribution of foam to the global buckling capacity and investigates, through a parametric study, the effect of increasing the foam stiffness on global buckling.

6.1.3 Local Boundary Conditions

Local boundary conditions greatly impact local buckling stress and overall column failure stress. Improving local boundary conditions will result in higher local buckling stress and higher column failure stress. As presented in Chapters 4 and 5, the flanges of the tested columns were highly susceptible to local buckling. In order to increase the local buckling capacity, simply-supported boundary conditions should be imposed on both sides of each flange. According to Timoshenko and Gere (1961), the buckling capacity of a long plate simply-supported on both sides is approximately ten times more stable than a long plate simply-supported on one side and free on one long edge (given the same dimensions and material properties). Achieving simply-supported boundary conditions was minimally explored during experimental testing via different methods of flange attachment (i.e., “Adhesive-Only,” “Adhesive and Screws,” “Adhesive and Welds,” and “Adhesive-No-Foam”). This chapter investigates the improvement of local boundary conditions with parametric studies: the steel thickness and the flange attachment.

6.2 Buckling and Crippling

Various mechanisms exist by which the foam-filled column may lose strength and/or fail under compressive loads. The columns tested to failure exhibited local buckling, followed by crippling and global buckling, which occurred simultaneously. This section analyzes mechanics-based predictions for stress values for these failure modes. Distinction is made in this section between buckling and crippling because a buckled element in the elastic range may continue to sustain loads, while a failed element in the inelastic range will not continue to sustain loads.

Note that global buckling due to eccentricities is ignored in this analysis; also, the presence of the foam is generally omitted from the calculations presented in this section. This is because the foam is not assumed to increase the global or local stability of the columns. The foam-steel interaction is explored, however, in Section 6.3, as well as in Chapter 7.

6.2.1 Global Buckling

The critical stress associated with global buckling, σ_{cr}, is approximated with Euler's equation:

$$\sigma_{cr} = \frac{\pi^2 E_S}{(L_e/\rho_S)^2} \qquad \textbf{(6-1)}$$

where E_s is the steel elastic modulus, L_e is the effective column length, and ρ_s is the steel radius of gyration. The calculated buckling stress value is 21.7 ksi (150 MPa), based on the elastic modulus listed in Table 2-1 and the radius of gyration listed in Table 2-12.

The ratio L_e / ρ is called the slenderness ratio and a column is considered "intermediate" if this ratio is below a critical value and "long" if this ratio is above the critical value. Curtis (1997, p. 763) explained, "If the slenderness ratio exceeds the [critical slenderness ratio] value,

then the critical stress is found by means of the Euler column formula." The formula for determining the critical value is:

$$\left(\frac{L_e}{\rho_s}\right)_{cr} = \pi\sqrt{\frac{2}{\sigma_{co}/E_s}} \qquad \textbf{(6-2)}$$

where σ_{co} is the *column* yield stress or *cutoff* stress. The column yield stress is approximately 1.1 times the compressive yield stress for low alloy steels; however, this value may range from 1.0 to 1.2 or higher depending on the material and alloy (Curtis 1997). In this analysis the cutoff stress is set equal to the steel yield strength, 50 ksi (345 MPa). The actual slenderness ratio (from Table 2-12) and critical slenderness ratio are listed in Table 6-2. The columns exceed the critical slenderness ratio and thus no intermediate column buckling equations are required in the analysis.

Table 6-2: Slenderness Ratio and Critical Slenderness Ratio

Slenderness Ratio, L_e / ρ_s [no units]	Critical Slenderness Ratio, $(L_e / \rho_s)_{cr}$ [no units]
115	107

6.2.2 Local Buckling

Local buckling occurs in the elastic region under compressive loads and is characterized by periodic waves over the length of the plate. According to Megson (2010, p. 299), "It must be appreciated that the calculation of local buckling stresses is generally complicated with no particular method gaining universal acceptance, much of the information available being experimental." This analysis adopts the general plate buckling stress equation referenced by

Megson (2010, p. 296), and the compressive buckling load intensity equation, $N_{x,cr}$, which are, respectively:

$$\sigma_{cr} = \frac{\eta k \pi^2 E_s}{12(1-\nu^2)} \left(\frac{t}{b}\right)^2 \quad \textbf{(6-3)}$$

$$N_{x,cr} = \sigma_{cr} \mathrm{t} \quad \textbf{(6-4)}$$

where η is the plasticity correction value (equal to 1.0 for the linear elastic range), k is the buckling coefficient which is determined by the plate aspect ratio and the plate boundary conditions, υ is Poisson's ratio (equal to 0.3 for steel), t is the plate thickness, and b is the plate width. The local buckling stress values are summarized in Table 6-3 with the assumption that plates 2 and 5 are simply-supported on all four sides (i.e., k = 4.0) and that plates 1, 3-4, and 6 are simply-supported on three sides with one edge free (k = 0.425). The local buckling stress values are summarized in Table 6-3 with the assumption that plates 2 and 5 are clamped on all four sides (i.e., k = 7.0) and that plates 1, 3-4, and 6 are clamped on three sides with one edge free (k = 1.60) (see Megson 2010, p. 299). The parameter k is nearly constant for $a / b > 3$ (Megson 2010, p.296). Note that the parameter b is always the smaller in-plane dimension of the plate.

The observed local buckling stress value for the flanges (plates 1, 3-4, and 6) is approximately 65 MPa (9.4 ksi). This is approximately half of the average column failure stress value discussed in Chapter 5, 129 MPa (18.7 ksi). The flanges were observed to buckle at approximately half of the failure load during testing. Also, the local buckled shape of the flanges most closely resembles clamped boundary conditions on three sides and one edge free. Thus, the

buckling coefficient, k = 1.60, is the closest approximation for the observed local buckling behavior.

Table 6-3: Local Buckling Stress (υ = 0.3; η = 1.0) Assuming Plates are Simply-Supported on All Four Sides (k = 4.0) or Simply-Supported on Three Sides with One Edge Free (k = 0.425)

Plate # (i)	Buckling Coefficient, k_i [no units]	Ratio, t_i / b_i [no units]	Buckling Stress, $\sigma_{cr,i}$ [MPa (ksi)]	Buckling Load Intensity, $N_{x,cr,i}$ [kN/cm (kip/in)]
1	0.425	0.0150	17 (2.5)	0.26 (0.15)
2	4.0	0.0154	172 (24.9)	2.61 (1.5)
3	0.425	0.0150	17 (2.5)	0.26 (0.15)
4	0.425	0.0154	18 (2.6)	0.28 (0.16)
5	4.0	0.0154	172 (24.9)	2.61 (1.5)
6	0.425	0.0154	18 (2.6)	0.28 (0.16)

Table 6-4: Local Buckling Stress (υ = 0.3; η = 1.0) Assuming Plates are Clamped on All Four Sides (k = 7.0) or Clamped on Three Sides with One Edge Free (k = 1.60)

Plate # (i)	Buckling Coefficient, k_i [no units]	Ratio, t_i / b_i [no units]	Buckling Stress, $\sigma_{cr,i}$ [MPa (ksi)]	Buckling Load Intensity, $N_{x,cr,i}$ [kN/cm (kip/in)]
1	1.60	0.0150	65 (9.4)	0.98 (0.56)
2	7.0	0.0154	300 (43.6)	4.56 (2.6)
3	1.60	0.0150	65 (9.4)	0.98 (0.56)
4	1.60	0.0154	68 (9.9)	1.04 (0.59)
5	7.0	0.0154	300 (43.6)	4.56 (2.6)
6	1.60	0.0154	68 (9.9)	1.04 (0.59)

Although local buckling does not constitute column failure, local instabilities greatly reduce the column stiffness and, consequently, the column load-carrying capacity. The moment due to eccentric load and the deformed cross-sectional geometry created by local buckling do, however, lead to crippling and failure.

6.2.3 Crippling Failure

Crippling is an inelastic failure mechanism which is initiated by local buckling. In reference to crippling Megson (2010, p. 302) wrote that, "plates retain some of their capacity to carry load even though a portion of the plate has buckled. In fact, the ultimate load is not reached until the stress in the majority of the plate exceeds the elastic limit. The theoretical calculation of the ultimate stress is difficult, since nonlinearity results from both large deflections and the inelastic stress-strain relationship."

In a discussion of local buckling of plate elements of columns, Bleich (1952) stated, "As a rule…the compression members of metal structures consist of plate elements. It is therefore conceivable that, even before the inception of instability of the kind which we have hitherto discussed and which involves integral failure of the column (primary failure), the plates of which the columns are built up will reach a state of unstable equilibrium and buckle locally, so that premature failure of the entire column characterized by a distortion of the cross section will occur. Hence, considerations concerning the stability of the plate elements enter into column design. However, it is not necessary in each individual case to undertake a tedious investigation of the condition for the occurrence of local buckling." Furthermore, Bleich instructs that there are "reliable rules for the required thickness of plates for practical purposes."

The terms crippling stress and failure stress are used interchangeably in the related literature; however, in this thesis both are referred to as crippling stress. Column crippling stress, σ_{cc}, is generally determined using the area-weighted average of the individual crippling stress values of the thin walls (or plates) which compose the column:

$$\sigma_{cc} = \frac{\sum_{i=1}^{n} \sigma_{cc_i} A_{s_i}}{\sum_{i=1}^{n} A_{s_i}} \qquad \textbf{(6-5)}$$

$$A_{s\,i} = b_i t_i \tag{6-6}$$

where i is the plate number, n is the number of plates, A_s is the steel area, b is the plate width, t is the plate thickness, and σ_{cci} is the plate crippling stress (determined using semi-empirical formulas) for the i^{th} section. In this subsection, results for three semi-empirical crippling formulas are summarized. Note that the third formula determines the column crippling stress without using Equation 6-5. Although these formulas for crippling appear to be different, upon further inspection they are quite similar—they all simplify to some percentage of the material yield strength. All crippling stress values must naturally be less than or equal to the cutoff stress, σ_{co}, which in this case is the material yield strength. All corresponding empirical constants and boundary condition parameters are summarized in Table 6-5.

The first plate crippling formula comes from Gerard (1962), as referenced in Megson (2010, p. 302):

$$\sigma_{cc\,i} = \sigma_{cy}\beta_i \left[\frac{t_i}{b_i}\sqrt{\frac{E_s}{\sigma_{cy}}}\right]^m \leq \sigma_{co} \tag{6-7}$$

where m is an empirical constant and β is a plate boundary condition parameter. The second plate crippling formula is a variation on Equation 6-7, modified by Boeing (CE523 2011):

$$\sigma_{cc\,i} = \sigma_{cy} B_{10} \left[\frac{t_i}{b_i} 10 g_{f\,i}\right]^m \sqrt{\frac{E_s}{\sigma_{cy}}} \leq \sigma_{co} \tag{6-8}$$

where B_{10} and m are empirical constants and g_f is a plate boundary condition parameter. The third crippling formula also comes from Gerard (1962), as referenced in Megson (2010, p. 303). The equation is used to predict the average crippling stress of the entire thin-walled column:

$$\sigma_{cc} = \sigma_{cy}\beta_g \left[\left(\frac{gt^2}{A_s}\right)\sqrt{\frac{E_s}{\sigma_{cy}}}\right]^m \leq \sigma_{co} \quad \textbf{(6-9)}$$

where β_g and m are empirically determined constants and the boundary condition parameter, g, is "the number of cuts required to reduce the cross section to a series of flanged sections plus the number of flanges that would exist after the cuts are made" (Megson 2010, p. 303). The determination of g is shown in Figure 6-2. The corresponding plate crippling stress values are listed in Table 6-6 and the column crippling stress values are summarized in Table 6-7. The values of t_i, b_i, and A_i were listed previously in Table 6-1. Three crippling stress values are shown for each equation in the tables, corresponding to three sets of possible boundary conditions, indicating whether the inner and/or outer flanges have one free end or no free ends, depending on the effects of the adhesive and foam. These include: 1) both of these are simply supported on all four sides (SSSS); 2) the inner flanges are simply-supported on all four sides and the outer flanges are simply-supported on three sides and free on one side (SSSF); and, 3) both the inner and outer flanges may be considered simply-supported on three sides and free on one side.

Table 6-5: Crippling Stress Constants

Parameter	Gerard (Equation 6-7)	Boeing (Equation 6-8)	Gerard (Equation 6-9)
Empirical Variables	m	m	m
	0.85	0.75	0.40
		B_{10}	β_g
		0.061	0.67
Boundary Condition	β	g_f	g
No free edges	1.42	2.3	10
One free edge	0.6*	1.0	10

*Determined using correlation (see Appendix C)

Table 6-6: Plate Crippling Stress for the Gerard Method (Equation 6-7) and the Boeing Method (Equation 6-8) Based on Three Sets of Boundary Condition Assumptions

Plate # (i)	Ratio, t_i / b_i	Gerard (Equation 6-7)			Boeing (Equation 6-8)		
		β	Cripping Stress, $\sigma_{cc,i}$ [MPa (ksi)]	$\sigma_{cc,i} A_i$ [kN (kips)]	g_f	Crippling Stress, $\sigma_{cc,i}$ [MPa (ksi)]	$\sigma_{cc,i} A_i$ [kN (kips)]
Webs, Inner Flanges, and Outer Flanges Simply-Supported							
1	0.0150	1.42	206 (29.8)	31.7 (7.1)	2.3	228 (33.0)	35.1 (7.9)
2	0.0154	1.42	211 (30.6)	31.6 (7.1)	2.3	233 (33.8)	34.8 (7.8)
3	0.0150	1.42	206 (29.8)	31.7 (7.1)	2.3	228 (33.0)	35.1 (7.9)
4	0.0154	1.42	211 (30.6)	31.6 (7.1)	2.3	233 (33.8)	34.8 (7.8)
5	0.0154	1.42	211 (30.6)	31.6 (7.1)	2.3	233 (33.8)	34.8 (7.8)
6	0.0154	1.42	211 (30.6)	31.6 (7.1)	2.3	233 (33.8)	34.8 (7.8)
				Σ = 190 (42.6)			Σ = 210 (47.1)
Webs and Inner Flanges Simply-Supported; Outer Flanges Simply-Supported on Three Sides, Free on One Side							
1	0.0150	0.60	87 (12.6)	13.4 (3.0)	1.0	122 (17.7)	18.8 (4.2)
2	0.0154	1.42	211 (30.6)	31.6 (7.1)	2.3	233 (33.8)	34.8 (7.8)
3	0.0150	0.60	87 (12.6)	13.4 (3.0)	1.0	122 (17.7)	18.8 (4.2)
4	0.0154	1.42	211 (30.6)	31.6 (7.1)	2.3	233 (33.8)	34.8 (7.8)
5	0.0154	1.42	211 (30.6)	31.6 (7.1)	2.3	233 (33.8)	34.8 (7.8)
6	0.0154	1.42	211 (30.6)	31.6 (7.1)	2.3	233 (33.8)	34.8 (7.8)
				Σ = 153 (34.4)			Σ = 177 (39.8)
Webs Simply-Supported; Inner and Outer Flanges Simply-Supported on Three Sides, Free on One Side							
1	0.0150	0.60	87 (12.6)	13.4 (3.0)	1.0	122 (17.7)	18.8 (4.2)
2	0.0154	1.42	211 (30.6)	31.6 (7.1)	2.3	233 (33.8)	34.8 (7.8)
3	0.0150	0.60	87 (12.6)	13.4 (3.0)	1.0	122 (17.7)	18.8 (4.2)
4	0.0154	0.60	89 (12.9)	13.3 (3.0)	1.0	125 (18.1)	18.7 (4.2)
5	0.0154	1.42	211 (30.6)	31.6 (7.1)	2.3	233 (33.8)	34.8 (7.8)
6	0.0154	0.60	89 (12.9)	13.3 (3.0)	1.0	125 (18.1)	18.7 (4.2)
				Σ = 117 (26.2)			Σ = 145 (32.5)

Table 6-7: Mechanics-Based Crippling Failure Stress the Gerard Method (Equation 6-7), the Boeing Method (Equation 6-8), and the Gerard Method (Equation 6-9) Based on Three Sets of Boundary Condition Assumptions

Boundary Conditions: Outer Flanges, Inner Flanges	Crippling Stress, σ_{cc} [MPa (ksi)]		
	Gerard (Equation 6-7)	Boeing (Equation 6-8)	Gerard (Equation 6-9)
SSSS, SSSS*	209 (30.3)	231 (33.5)	--
SSSF, SSSS	169 (24.5)	195 (28.3)	--
SSSF, SSSF	128 (18.6)	159 (23.1)	149 (21.6)

*SSSS is simply-supported on all four sides; SSSF is simply-supported on three sides, free on one side

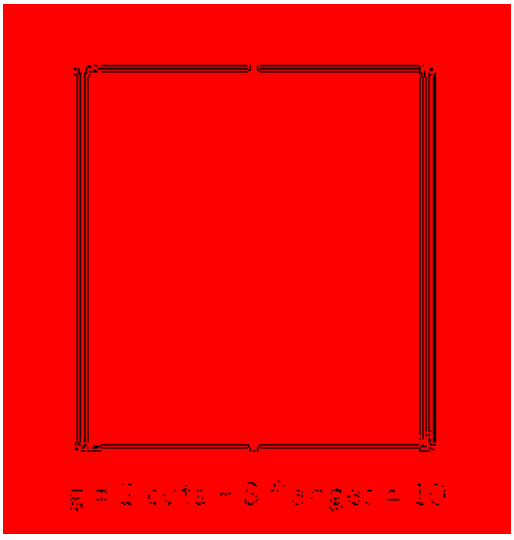

Figure 6-2: Illustration of Cross-Section Cuts and Flanges to Determine the Gerard Constant, *g*

6.3 Parametric Studies

Three parametric studies are presented in this section to assess the effects of the foam core stiffness, the skin thickness, and the flange attachment method.

6.3.1 Effect of Foam Core Stiffness

A relatively stiff core will have the effect of delaying global and/or local buckling. In order to assess this relative stiffness, the bending stiffness values previously listed in Table 2-10 are repeated in Table 6-8 for convenience. As listed in the table, the bending stiffness about the y-axis is nearly 4,000 times greater for the steel than for the foam. Thus, in the current configuration the foam is providing negligible bending capacity against global buckling compared to the steel.

Table 6-8: Column Bending Stiffness by Constituent Material

Constituent Material	Bending Stiffness	
	EI_{yy} [kN-m^2 (kip-in^2)]	EI_{zz} [kN-m^2 (kip-in^2)]
Steel	251.5 (87,600)	344.0 (119,900)
Foam	0.064 (22.1)	0.060 (20.8)
Combined	251.6 (87,620)	344.1 (119,920)
Ratio of Steel to Foam	3,950	5,800

By assuming that the column bending stiffness is the sum of the foam and steel bending stiffness values (Gere 2006), and that all variables but foam elastic modulus are held constant, then global buckling may be evaluated for a range of foam elastic modulus values as follows:

$$P_{cr} = \frac{\pi^2 (E_s I_s + E_f I_f)}{{L_e}^2} \quad \textbf{(6-10)}$$

which, for this configuration reduces to:

$$P_{cr} = P_{cr,o}\left(1 + 0.0003\frac{E_f}{E_{f,o}}\right) \quad \textbf{(6-11)}$$

The predicted global buckling load as a function of foam elastic modulus is shown in Figure 6-3. The relative buckling load versus relative foam stiffness is shown in Figure 6-4. This value indicates that by increasing the foam elastic modulus by a factor of 3,000, the predicted global buckling load will only double. Thus, increasing the foam elastic modulus is a very inefficient means of increasing the column global buckling capacity. Additionally, according to this plot, the foam is contributing negligible increase in global buckling load because the foam elastic modulus is only approximately 1.2 ksi (8.3 MPa). The foam still provides support, however, for local flange buckling. This is explored in the finite element analysis presented in Chapter 7.

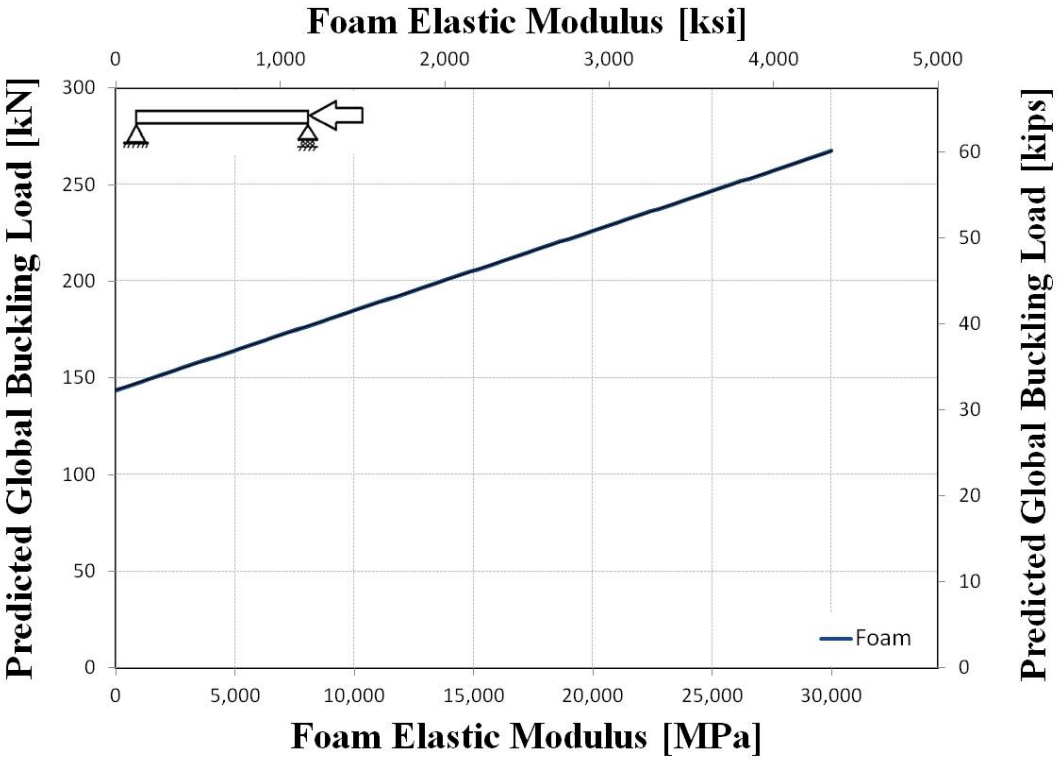

Figure 6-3: Predicted Global Buckling Load vs. Foam Elastic Modulus

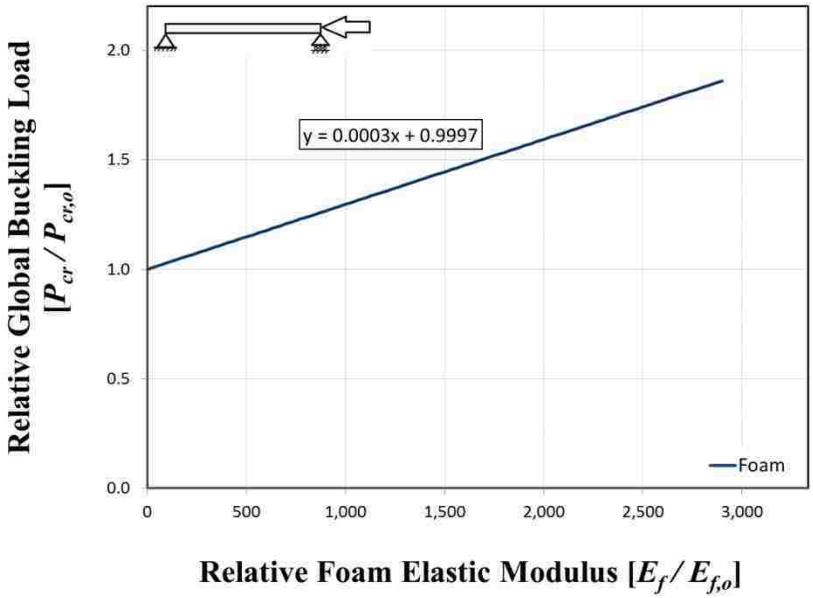

Figure 6-4: Relative Global Buckling Load vs. Relative Foam Stiffness

6.3.2 Effect of Flange-to-Flange Attachment

The flange attachment affects the local boundary conditions. Three cross-sectional flange attachment models are illustrated in Figure 6-5. There are many possible ways of achieving these configurations in the laboratory. For example, the Model 1 is a cross-section with the flanges attached rigidly. This configuration may be achieved by either applying a sufficiently strong, uniformly-distributed adhesive or by using periodic welds or screws at a close enough spacing which pin the free ends of the flanges. The Model 2 allows the outer flanges to deflect freely outward, with the inner flanges attached to the foam. This model assumes that the foam is stiff enough to prevent the inner flanges from deflecting, with the adhesive binding the flanges to the foam. The Model 3 assumes that the outer and inner flanges can both deflect freely, although they are still attached on one edge. This assumes that the foam is either not present or that the foam is not stiff enough to prevent deflection of the inner flanges. The assumptions and implications of the three models are summarized in Table 6-9.

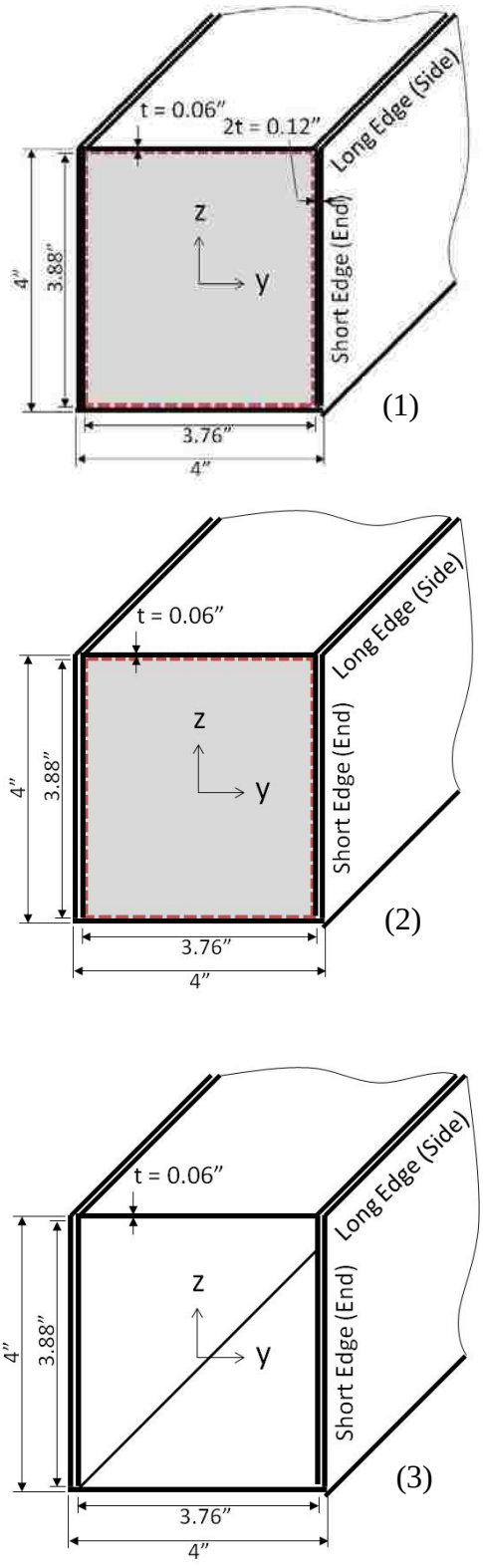

Figure 6-5: Illustration of Three End Views of Flange Attachment Models: 1) Fully Connected Flanges; 2) Free Outer Flanges; and 3) Free Outer and Inner Flanges

Table 6-9: Three Flange Attachment Model Assumptions and Implications

Model #	Assumption	Flange Boundary Conditions	Implication
1	Fully connected, pinned flanges	SSSS, SSSS	Adhesive is stiff (or screws or welds are sufficiently placed); foam is negligible
2	Pinned-free outer flanges; fully connected inner flanges	SSSF, SSSS	Adhesive is negligible (or screws or welds are inadequately placed); foam is stiff
3	Pinned-free outer flanges and inner flanges	SSSF, SSSF	Adhesive is negligible (or screws or welds are inadequately placed); foam is negligible

Concerning stability, Model 2 is superior to Model 3; and Model 1 is superior to both Model 2 and Model 3. This is based on the relationship for plate buckling stress listed previously (Equation 6-3).

The long plate buckling coefficients for different boundary conditions are listed in Table 6-10. These are used to calculate the buckling stress values for each of the three models. Based on the assumptions listed in Table 6-9, the corresponding buckling coefficients for each model are summarized in Table 6-11. The buckling stress values for each model are summarized in Table 6-12.

Table 6-10: Long Plate Buckling Coefficients, k, for Two Cases[3]

Plate Boundary Conditions		Buckling Coefficient, *k* [no units]
Long Edges (Sides)	Short Edges (Ends)	
Pinned-Free	Pinned-Pinned	0.425
Pinned-Pinned	Pinned-Pinned	4.0

[3]Gere (2004).

Table 6-11: Comparison of Coefficients Used to Calculate Plate Buckling Stress for Three Models

Plate # (i)	Model 1 [no units]		Model 2 [no units]		Model 3 [no units]	
	Buckling Coefficient, k_i	Ratio, t_i / b_i	Buckling Coefficient, k_i	Ratio, t_i / b_i	Buckling Coefficient, k_i	Ratio, t_i / b_i
1	4.0	0.0304	0.425	0.0150	0.425	0.0150
2	4.0	0.0159	4.0	0.0159	4.0	0.0159
3	4.0	0.0304	0.425	0.0150	0.425	0.0150
4	n/a	n/a	4.0	0.0154	0.425	0.0150
5	4.0	0.0159	4.0	0.0159	4.0	0.0159
6	n/a	n/a	4.0	0.0154	0.425	0.0150

Table 6-12: Comparison of Plate Buckling Stress Values for Three Models

Plate # (i)	Plate Buckling Stress, $\sigma_{cr,i}$ [MPa (ksi)]		
	Model 1	Model 2	Model 3
1	666 (96.6)	17 (2.5)	17 (2.5)
2	183 (26.5)	183 (26.5)	183 (26.5)
3	666 (96.6)	17 (2.5)	17 (2.5)
4	n/a	172 (24.9)	18 (2.6)
5	183 (26.5)	183 (26.5)	183 (26.5)
6	n/a	172 (24.9)	18 (2.6)
Area-Weighted Average	510 (74.0)	122 (17.7)	71.0 (10.3)

The method of attaching the flanges is very important because local flange buckling strength can be increased by an order of magnitude (discussed previously). As mentioned in Chapter 2, the method of attaching the flange is meant to be non-labor intensive; however, the strength gains appear to be significant if the flanges can be firmly attached. Fully connecting the flanges in order to provide simply-supported boundary conditions on all four sides can provide more strength gains than using foam with very high stiffness. The strength gains increase

progressively from Model 3 to Model 1 because the column will fail at an increasingly higher stress because the local buckling load will be increased.

6.3.3 Effect of Steel Thickness

In this study of the effect of steel thickness, the equations for buckling (Equation 6-1) and crippling (Equations 6-5 and 6-8) were expressed as functions in terms of steel thickness, t. These functions assume that the outer cross-sectional dimensions remain constant as 4" (10.2 cm) square. The range of thickness values over which the buckling and crippling stress is evaluated is from 0-0.20 in (0-5 mm). This range corresponds with standard steel gauges 6 through 36. The presence of the foam is ignored in the analysis. The three models defined in the previous section are used here.

First, a crippling check was completed. Figure 6-6 shows the column plate segment aspect ratio (*b/t*) versus steel thickness. The figure reveals that the column is susceptible to crippling for the full range because the aspect ratio (*b/t*) is greater than the critical aspect ratio, 10, even for relatively thick values of steel. Next, a slenderness check was completed to determine if the column becomes an intermediate column within the given range of steel thickness values. If the column is intermediate, Equation 6-8 is modified using the Johnson-Euler formula. Figure 6-7 shows the column slenderness ratio versus steel thickness. This figure reveals that the column is 'long' or exceeds the critical slenderness ratio for the full range of evaluated steel thickness. This indicates that Euler buckling is applicable and Johnson-Euler buckling does not need to be calculated (used for 'intermediate' columns only).

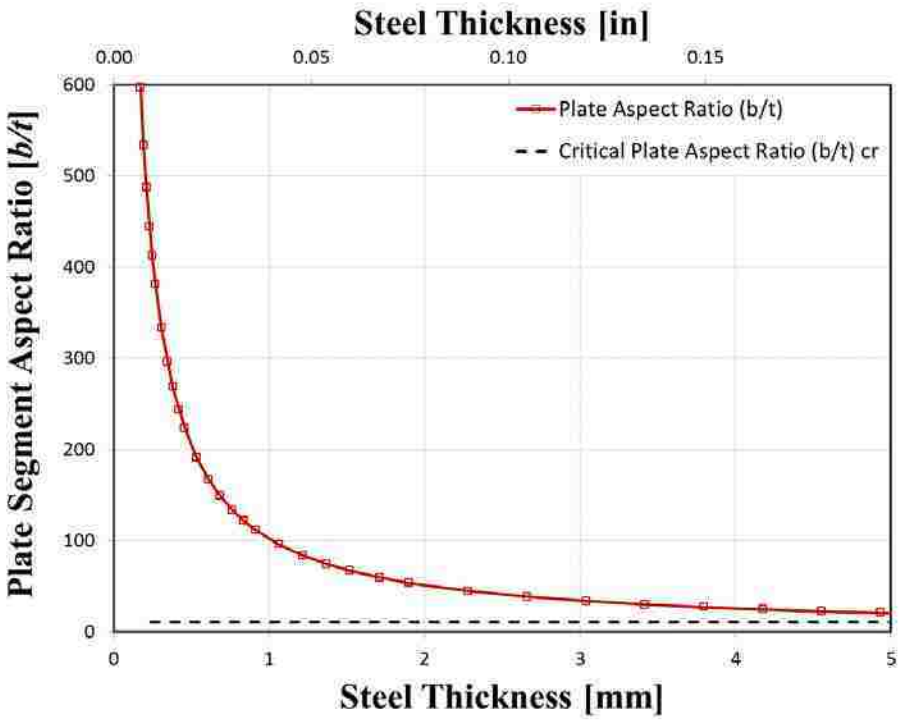

Figure 6-6: Column Plate Segment Aspect Ratio (*b/t*) vs. Steel Thickness

Figure 6-8 shows the column crippling stress versus steel thickness. This figure shows that the crippling stress increases progressively from Model 3 to Model 1 for any value of steel thickness. Thus, the strength gains which can be achieved by strengthening the flange attachment are significant. In fact, the figure shows that the same strength achieved during testing may occur with a much thinner steel if the flanges were attached more rigidly. The figure also shows that Euler buckling introduces a ceiling for stress values that is less than half the yield stress. This is expected because long columns generally lose stability prior to failure due to yielding. Finally, the figure shows that the test data points approach, but do not exceed the predicted crippling stress values. This reflects imperfections in the materials, the manufacturing, and the testing. Figure 6-9 shows the column crippling load versus steel thickness.

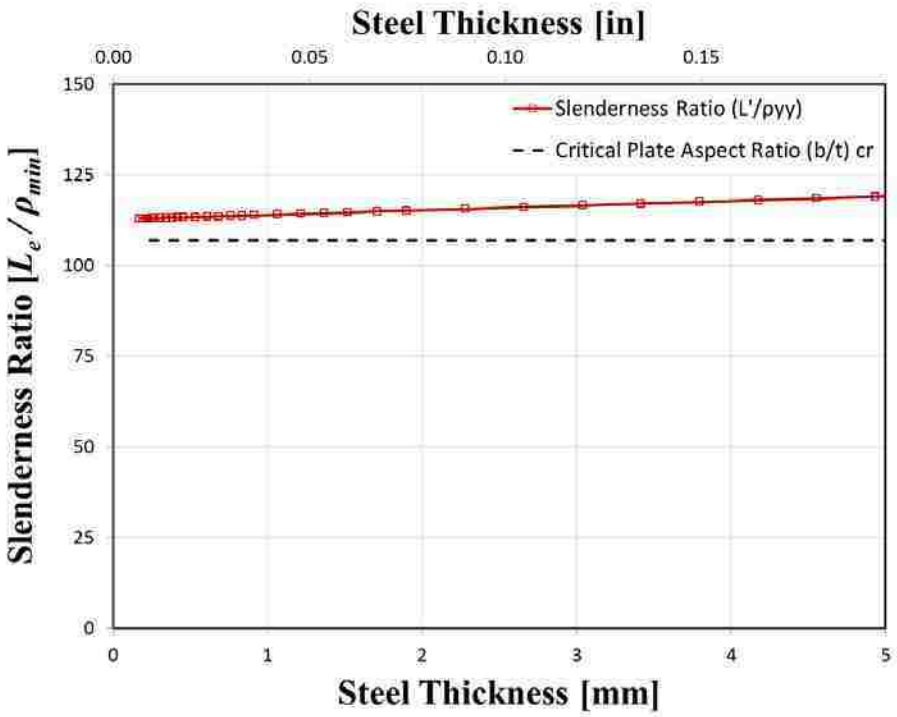

Figure 6-7: Column Slenderness Ratio vs. Steel Thickness

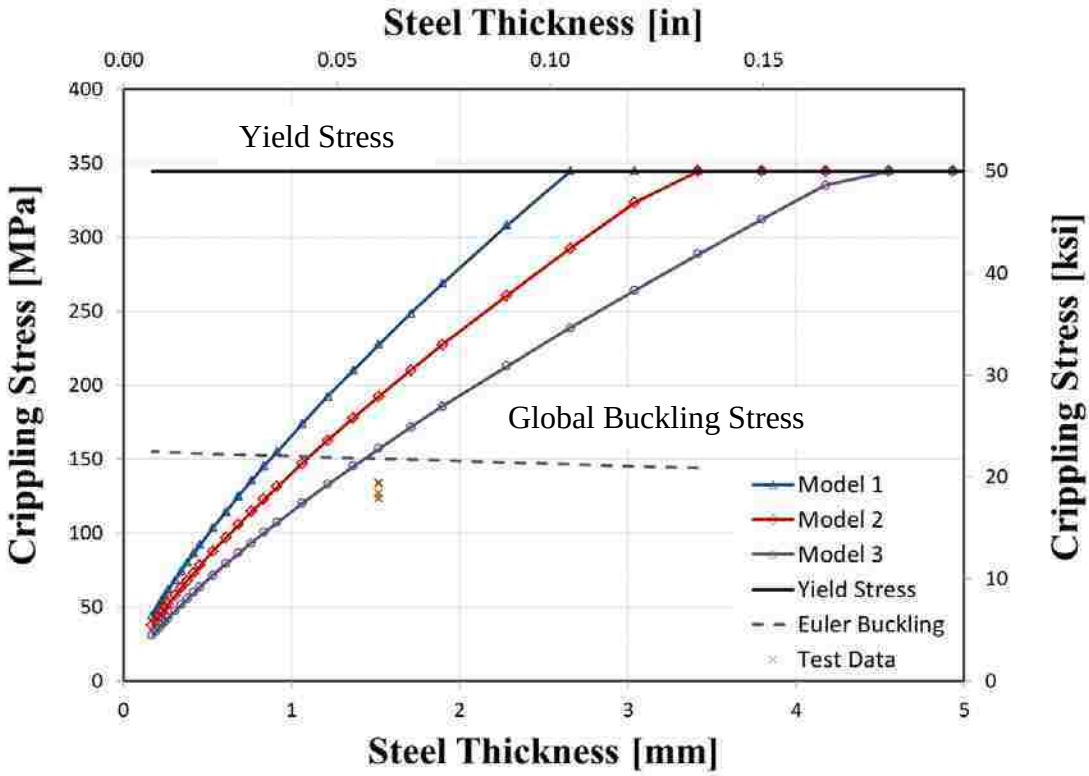

Figure 6-8: Column Crippling Stress vs. Steel Thickness

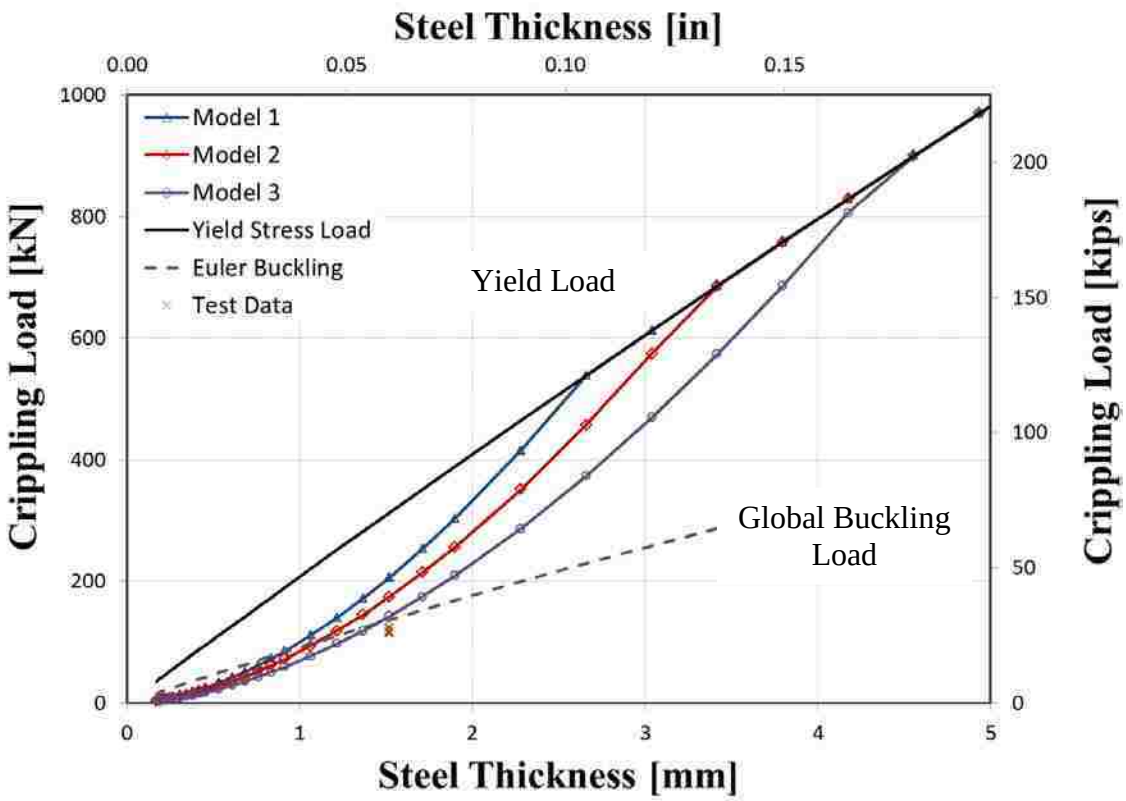

Figure 6-9: Column Crippling Load vs. Steel Thickness

6.4 Summary

Based on the mechanics analysis in this chapter, the design improvement with greatest potential impact is to attach the column flanges more securely. This has the effect of increasing the strength of the column without significantly increasing the weight. If a fully-connected flange attachment can be achieved, the column cross-section will be greatly strengthened against local buckling and crippling, with an upper strength bound equal to the Euler buckling load. This chapter also shows that increasing the foam stiffness will not significantly improve the global buckling capacity of the columns; although, increasing the foam stiffness may delay local buckling of the cross-section, as well as provide additional stability for the cross-section. This concept is further explored in Chapter 7.

7 FINITE ELEMENT ANALYSIS

This chapter summarizes a finite element analysis performed on 14’ (4.27 m) thin-walled steel columns with foam inserts and adhesive, as well as finite element analysis performed on shorter column segments measuring 6-14” (15.2-35.6 cm). The purpose of the finite element analysis was to capture local deformation phenomenon of the columns under axial compression. By looking at the local stresses and deformations, future iterations of the column design can be improved. The chapter discusses the column modeling, global buckling, local buckling, and crippling.

7.1 Column Modeling

This section describes the column modeling, including a description of the analysis software, a summary of the analyses performed, the material models, and the finite element meshing.

7.1.1 Software

All computer-based finite element analysis was performed using ADINA (Automatic Dynamic Incremental Nonlinear Analysis) version 8.6.4 (build 3.15.2010). All screen shots in

this chapter are taken directly from ADINA. The node numbering and element numbering were performed automatically by the ADINA software.

7.1.2 Summary of Analyses

The finite element analyses performed for this thesis are summarized in Table 7-1.

Table 7-1: Finite Element Analysis Summary

Failure Type	Analysis Type	Elements Used	Material Linearity	Variable Studied
Global Buckling	Linearized Buckling	Shells, 3-D Solids	Linear Elastic	Foam (E_f)
Local Buckling	Linearized Buckling	3-D Solids	Linear Elastic	Adhesive (E_a) & Length (a)
Crippling	Statics	3-D Solids	Nonlinear	Foam (E_f) & Adhesive (E_a)

7.1.3 Materials

The linear material properties listed previously in Table 2-1, Table 2-4, and Table 2-5 are summarized again in Table 7-2 for convenience. The materials are numbered 1-3 for use in the finite element program. The piecewise linear representation of the nonlinear stress and strain material properties for steel are shown in Figure 7-1 and are listed in Table 7-3. These values are based on tension only, but were input was both tension and compression values. The values are typical for ASTM A653 Class I Galvanized Steel (Limited Blue Scope Steel 2005; Tons and Tons 2007).

Table 7-2: Linear Elastic Material Properties for Finite Element Analysis

Material #	Material Model	Material Description	Elastic Modulus, E [MPa (ksi)]	Poisson's Ratio, υ
1	Isotropic Linear Elastic	Steel	$200x10^3$ (29,000)	0.3
2	Isotropic Linear Elastic	Foam	8.27 (1.2)	0.3
3	Isotropic Linear Elastic	Adhesive	$2.75x10^3$ (400)	0.4

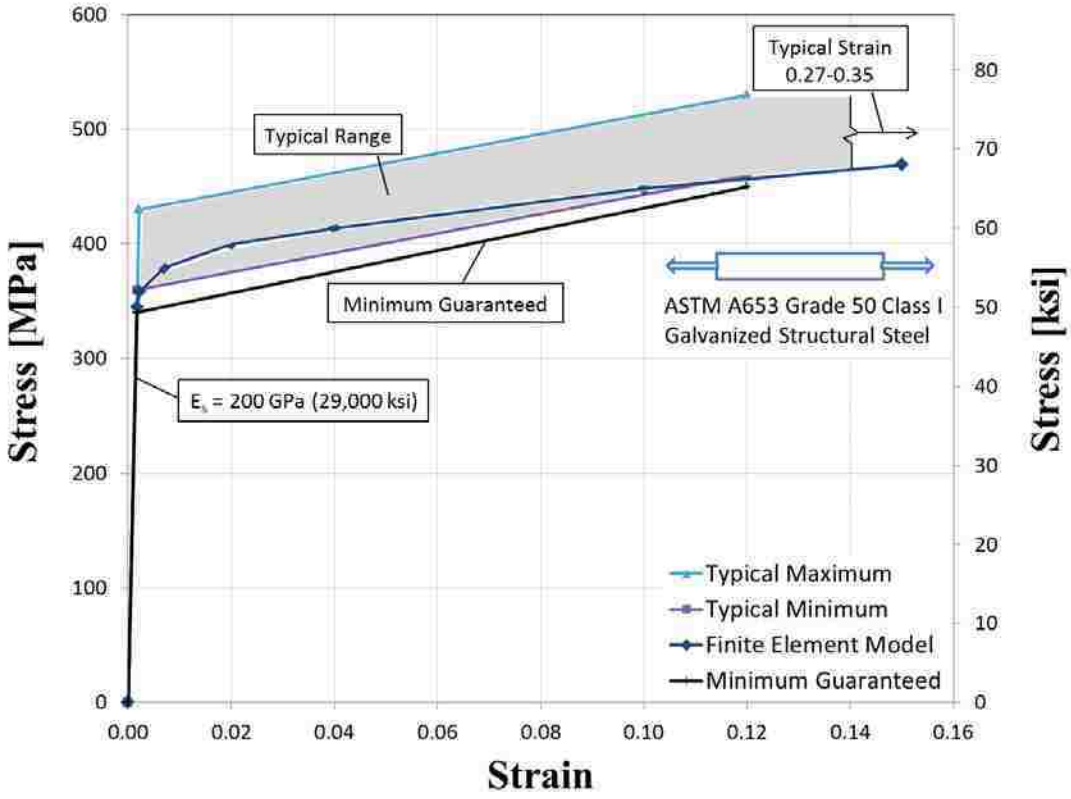

Figure 7-1: Nonlinear Stress vs. Strain for Steel in Tension

Table 7-3: Nonlinear Strain and Stress Values for Steel in Tension and Compression (υ = 0.3)

Segment #	Strain, ε [no units]	Stress, σ [MPa (ksi)]
1	0.000	0 (0.0)
2	0.00172	345 (50.0)
3	0.0023	359 (52.0)
4	0.007	379 (55.0)
5	0.02	400 (58.0)
6	0.04	414 (60.0)
7	0.1	448 (65.0)
8	0.15	469 (68.0)

Although the elastic modulus for adhesive used in the finite element analyses was 400 ksi (2,758 MPa) as indicated in Table 7-2, the actual modulus of elasticity for the adhesive was closer to 295 ksi (2,034 MPa) (see Appendix A). Therefore, in order to conform that this difference in elastic modulus did not change the results, an analysis was conducted to compare the two. The analysis consisted of two "Adhesive Only" models, one with each of the two moduli of elasticity for adhesive indicated, loaded to failure in crippling. The results of the analysis are listed in Table 7-4 and are shown in Figure 7-2. As listed in the table, the percent difference in the peak load between the two models is less than 1% and is therefore considered negligible. Thus, analyses based on either value of adhesive modulus produce essentially the same peak load.

Table 7-4: Peak Load and Corresponding Displacement for Two 10 in (25.4 cm) Long "Adhesive Only" Models with Different Values for Adhesive Modulus of Elasticity

Model Description	x-Displacement, u_1 [cm (in)]	Peak Load, P_{cr} [kN (kips)]
E_a = 2,758 MPa (400 ksi); Adhesive Only	0.0471 (0.0186)	295 (66.3)
E_a = 2,034 MPa (295 ksi); Adhesive Only	0.0470 (0.0185)	294 (66.2)
Percent Difference	0.54%	0.12%

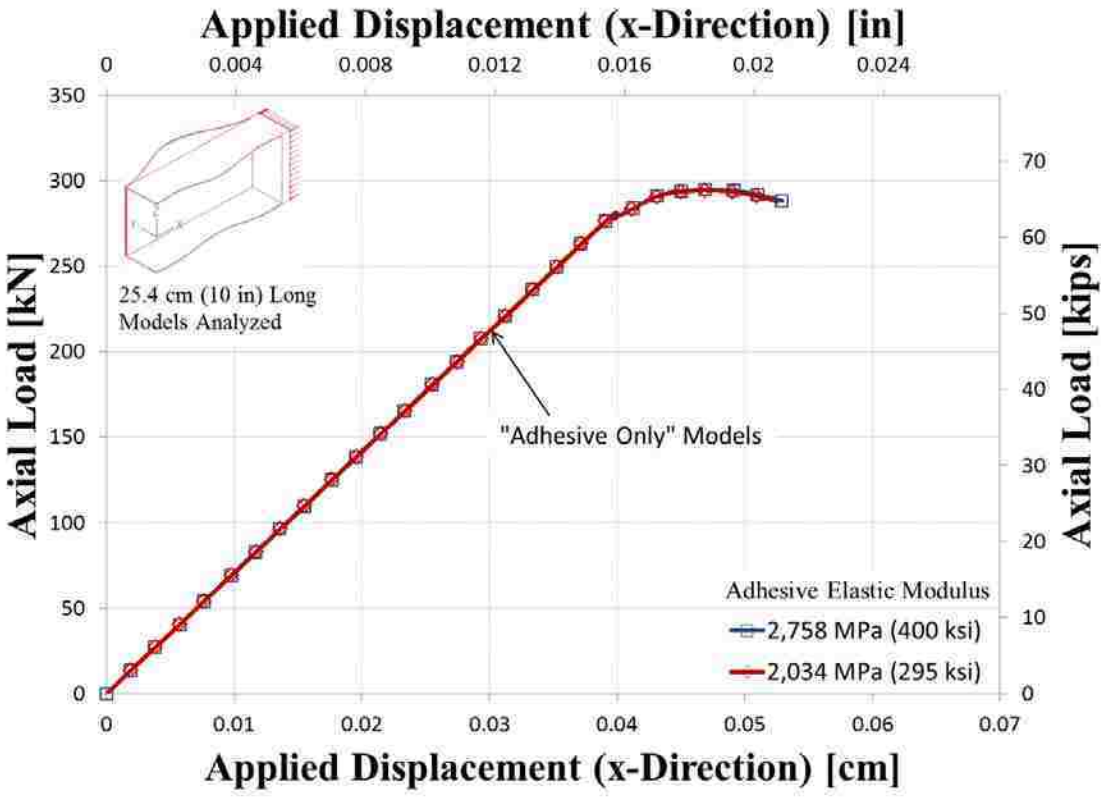

Figure 7-2: Axial Load vs. Applied Displacement (x-Direction) for Two "Adhesive Only" Models with Two Different Values for Adhesive Elastic Modulus

7.1.4 Meshing

The two element types used in the finite element analysis are shown in Figure 7-3. The 20-node brick element was used to model 3-D solid elements and the 8-node quad element was used to model shell elements.

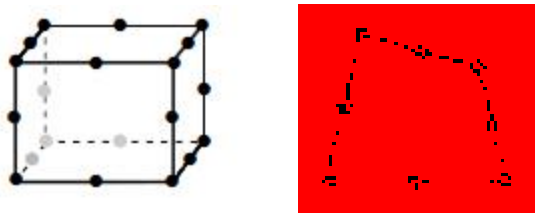

Figure 7-3: Elements Used in Finite Element Analysis: 20-Node Brick Element Used to Model 3-D Solid Elements (Left); and, 8-Node Quad Element Used to Model Shell Elements (Right)

7.2 Global Buckling

This section summarizes the column global buckling analysis. Two model types were compared: a model with shells and 3-D solid elements and a model with only 3-D solid elements. This section includes the problem description, the assumptions and modeling, the results, and the discussion of results.

7.2.1 Description of Physical Problem

The columns discussed in this thesis buckled inelastically due to crippling failure, followed by inelastic global buckling (see Figure 7-4). Global buckling analysis was performed using finite element analysis for comparison. Elastic global buckling was also used to compare element types and also to determine how the foam influences the global buckling capacity.

Figure 7-4: Photo of Global Buckling of "Adhesive and Welds" Column During Test to Failure

7.2.2 Assumptions and Modeling

The analysis type was linearized buckling and large displacements were used to induce buckling. No body forces were considered because the columns are relatively lightweight. Symmetry was used in modeling in order to improve processing speed—only half of the full column length was modeled. Mesh convergence was employed in order to improve solution accuracy. The center of the column span was constrained from translation in the x-, y-, and z-directions; the end of the column was free to translate in these three directions and to rotate about the x-, y-, and z-axes. These boundary conditions were employed to ensure symmetric behavior. The first five buckling modes were solved (only the results for the first mode are presented here).

Two models were created which are referred to as "Shells and 3-D Solid Elements" and "3-D Solid Elements Only". The cross-sectional area and moment of inertia values are compared for the two models in Table 7-5; illustrations are shown in Figure 7-5. The outer flanges were assumed to be fully connected to the column. Point coordinates and surface connectivity are summarized in Appendix D. Because shells have rotational degrees of freedom and solids do not, ADINA transitions from shells to solids using transition nodes (Bathe 2009, p.127). The shell mid-surface nodes and solid face nodes are shared between elements because the shells lie on top of the solid elements in this model (not perpendicular).

Table 7-5: Comparison of Cross-Sectional Area, Moment of Inertia, and Euler Buckling Loads from Mechanics for Two Models

Model Description	Area, A [cm^2 (in^2)]	Moment of Inertia, I_{yy} [in^4 (cm^4)]	Euler Buckling, P_{cr} [kN (kips)]
Shells and 3-D Solids Model	1.44 (9.29)	3.19 (133)	144 (32.3)
3-D Solids Only Model	1.41 (9.10)	3.02 (126)	136 (30.6)
Ratio of Shells and 3-D Solids to 3-D Solids Only	1.02	1.06	1.06

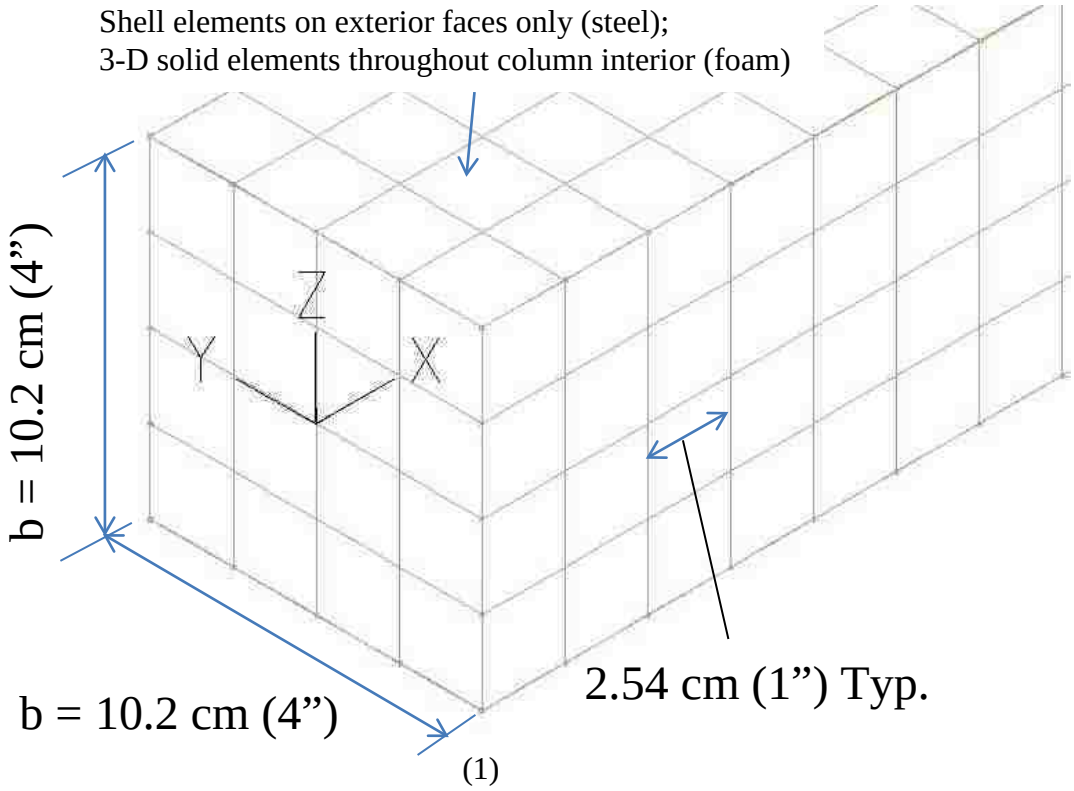

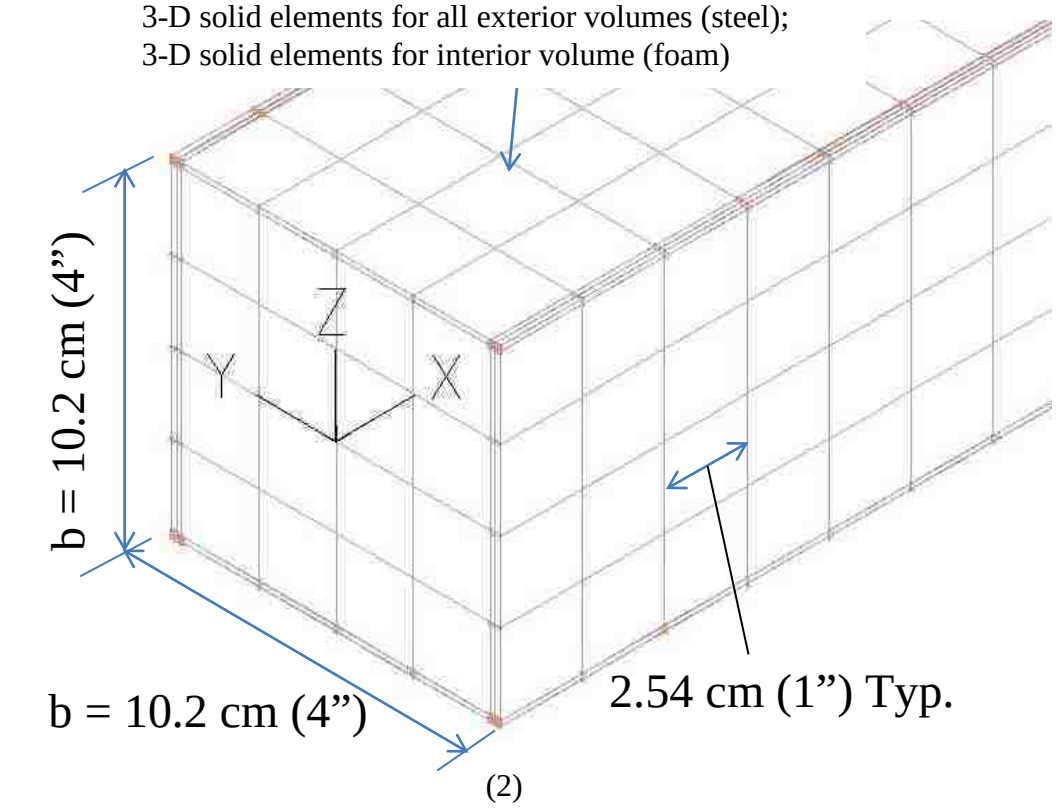

Figure 7-5: End View of Column Models: 1) Shells and 3-D Solids Model; and, 2) 3-D Solids Only Model

7.2.3 Global Buckling Results

Figure 7-6 shows a buckled column superimposed on the original mesh. The mesh convergence results are listed in Table 7-6 and are shown in Figure 7-7. Note that the mesh converged immediately with elements of 1.0 in (2.54 cm) edge lengths. Therefore, this was the elements size used for modeling the effect of foam stiffness in global buckling.

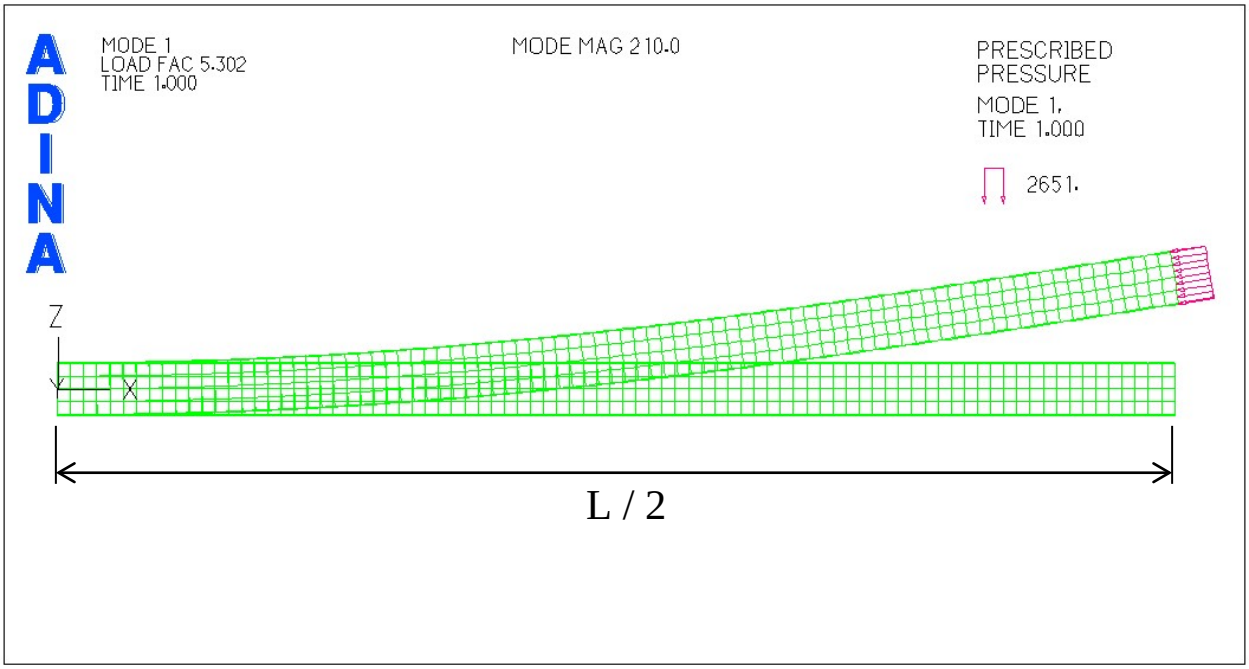

Figure 7-6: Finite Element Band Plot of Buckled 3-D Solid Elements Only Model Superimposed on Original Mesh

The buckling loads associated with several foam stiffness values are listed in Table 7-7 and are shown in Figure 7-8. These values are normalized and are shown in Figure 7-9. Note that the difference in buckling values for the two models is primarily due to the slightly different geometry of the two models (see Figure 7-5). The shells and 3-D solid elements model has a slightly higher moment of inertia because the thickness of the shells is defined at the faces of the columns.

Table 7-6: Convergence Study

Model Description	Element Edge Length [cm (in)]	Elements*			Nodes	Global Buckling Load, P_{cr} [kN (kips)]	Global Buckling Stress, σ_{cr} [MPa (ksi)]
		Steel	Foam	Total			
Shells and 3-D Solid Elements	2.54 (1.0)	1,360	1,344	2,704	2,704	143 (32.2)	158 (22.9)
	1.69 (0.66)	3,060	4,536	7,596	7,596	143 (32.2)	158 (22.9)
	1.27 (0.5)	5,440	10,752	16,192	16,192	143 (32.2)	158 (22.9)
3-D Solid Elements Only	2.54 (1.0)	2,736	1,344	4,080	20,233	133 (29.9)	146 (21.2)
	1.69 (0.66)	5,704	4,536	10,240	48,405	133 (29.9)	146 (21.2)

*No 'Adhesive' elements were used in these models

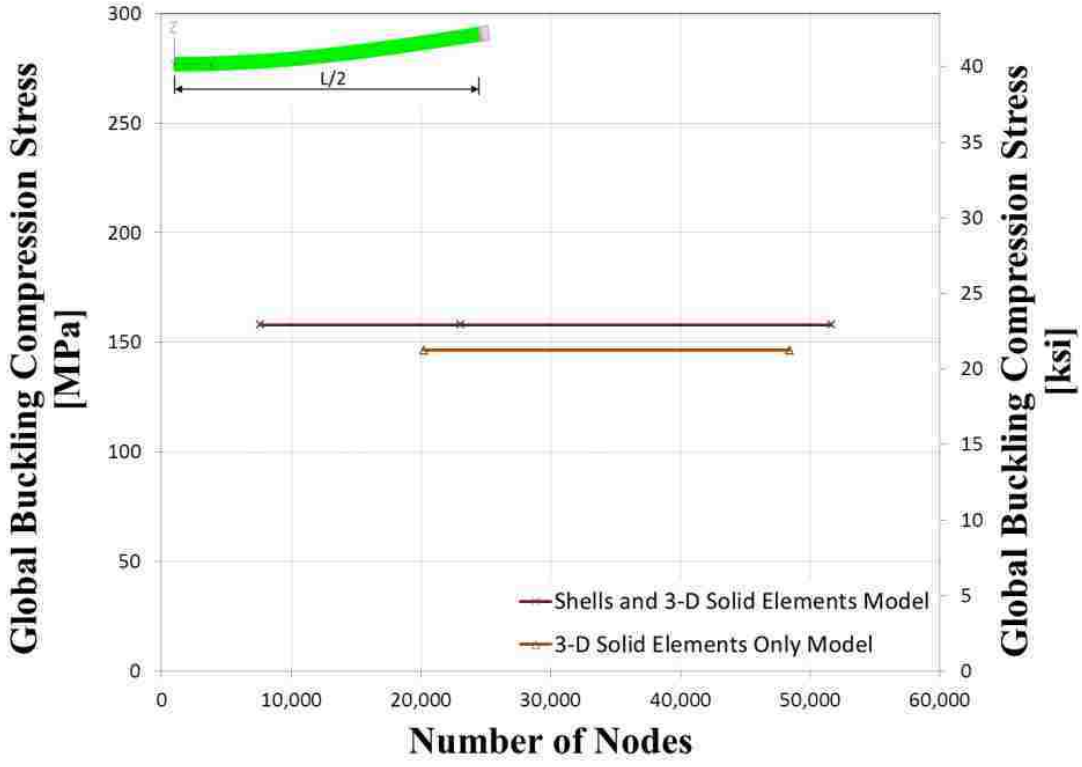

Figure 7-7: Global Buckling Compression Stress vs. Number of Nodes to Show Mesh Convergence

Table 7-7: Summary of Parametric Study of Foam Elastic Modulus

Foam Elastic Modulus, E_f [MPa (ksi)]	Stiffness Increase [%]	Shells and 3-D Solids		3-D Solids Only	
		Global Buckling Load, P_{cr} [kN (kips)]	Strength Increase [%]	Global Buckling Load, P_{cr} [kN (kips)]	Strength Increase [%]
8 (1.2)	1	143 (32.2)	0	133 (29.9)	0
6,895 (1,000)	833	177 (39.7)	21	161 (36.1)	23
13,790 (2,000)	1,667	210 (47.2)	42	189 (42.4)	46
20,685 (3,000)	2,500	243 (54.7)	63	217 (48.7)	70
27,580 (4,000)	3,333	276 (62.1)	84	244 (54.9)	93
34,475 (5,000)	4,167	310 (69.6)	105	272 (61.2)	116

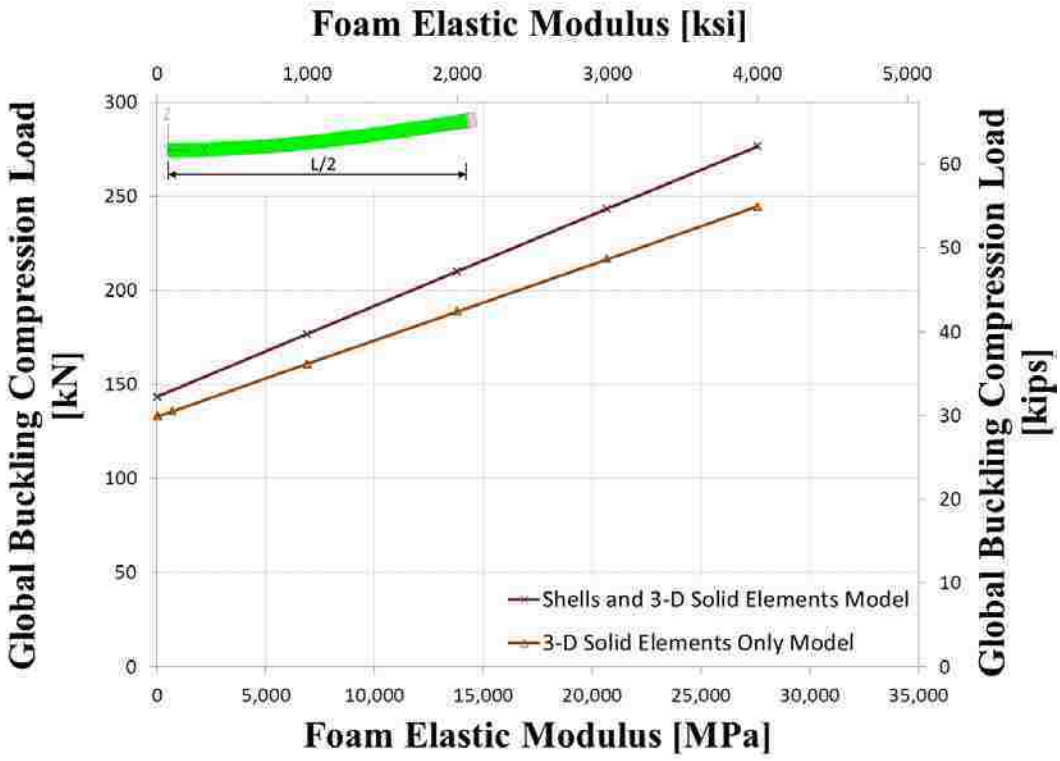

Figure 7-8: Global Buckling Compression Load vs. Foam Elastic Modulus for Two Column Models

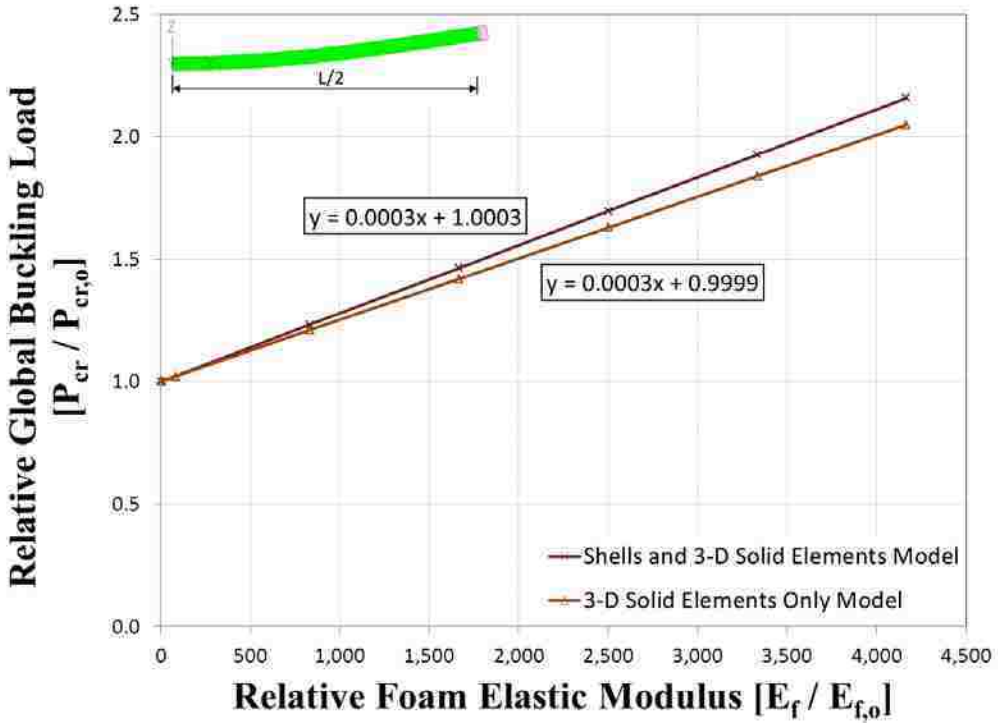

Figure 7-9: Relative Global Buckling Load vs. Relative Foam Elastic Modulus for Two Column Models

7.2.4 Global Buckling Discussion of Results

The global buckling finite element results are approximately the same as the results for global buckling based on mechanics presented in Chapter 6. Thus, the Euler buckling equation is sufficient to calculate the global elastic buckling load. Also, the foam will only increase the global buckling capacity by 50% if the foam is approximately 2,000 times stiffer than the current stiffness. Thus, increasing the foam stiffness is not an effective means of increasing the global buckling capacity (although the foam may increase the local buckling capacity and/or the crippling capacity). Finally, the global buckling capacity is 6% greater using the thin-walled assumptions ("Shells and 3-D Solid Elements" model) than for the nominal model ("3-D Solid Elements" model).

7.3 Local Buckling

This section summarizes the column local buckling analysis. Nine different models were analyzed, each with different length increments. Once mesh convergence was established, the nine models were analyzed again with varying spring stiffness values in order to determine the required adhesive stiffness. This section includes the problem description, the assumptions and modeling, the results, and the discussion of results.

7.3.1 Description of Physical Problem

The columns are susceptible to local buckling as discussed in Chapters 4 and 5 (see Figure 7-10). The buckling wavelength, *a*, not only varied across column length, but also depended on the spacing of screws or short-welds (if any).

Figure 7-10: Close-up Photo of Local Buckling in "Adhesive-Only" Column During Test to 20 kips

7.3.2 Assumptions and Modeling

The objective of this local buckling analysis was to determine a critical local buckling length which exceeds the global buckling strength. Thus, nine different wavelengths were modeled from 4 in (10.2 cm) to 12 in (30.5 cm). The finite element model of the 8" (20.3 cm) length is shown in Figure 7-10. The applied boundary conditions restrained rotation of the short edges of the flanges (observed in Figure 7-12). The same 20-node brick element used to model global buckling was also used to model local buckling (see Figure 7-3). The elastic isotropic material properties used to model global buckling were also used to model local buckling. The analysis type was linearized buckling and large displacements were used (see Table 7-2). No body forces were considered in the analysis because the columns are relatively lightweight. The first five buckling modes were solved (only the results for the first mode are presented here).

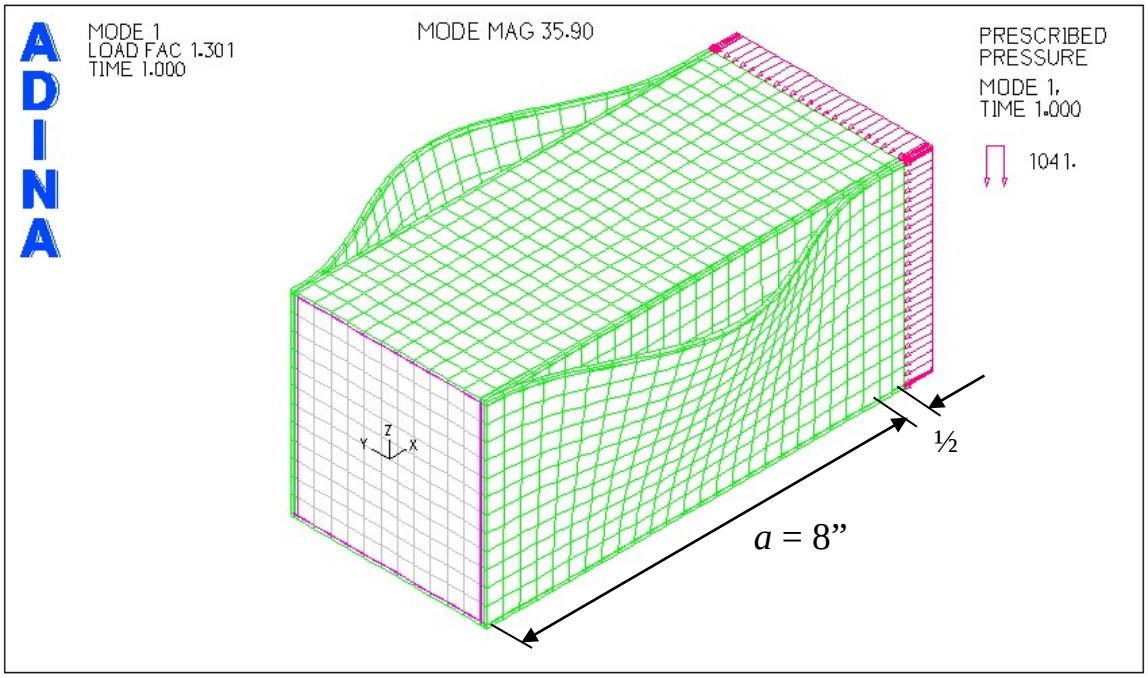

Figure 7-11: Finite Element Band Plot of Local Buckling Model Measuring 8" (20.3 cm) with ½" (1.27 cm) Steel End Plate with Steel Shell (Green), Foam Core (Gray), and Adhesive (Pink) Showing Deformed Shape

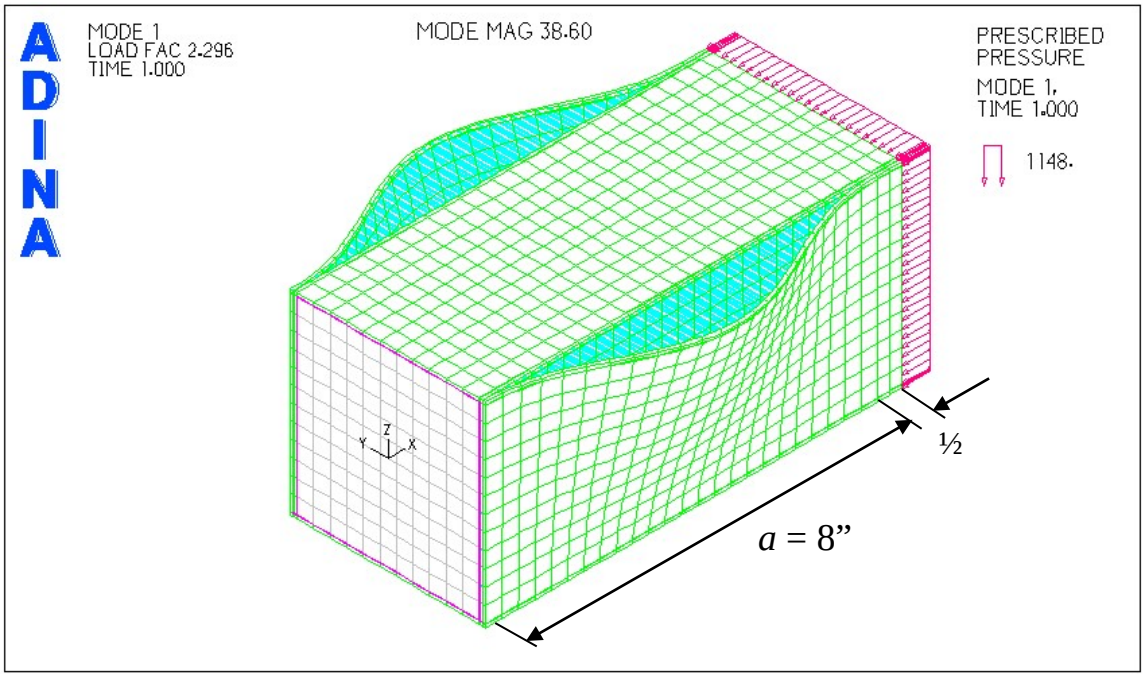

Figure 7-12: Finite Element Band Plot of Local Buckling Model Measuring 8” (20.3 cm) with ½” (1.27 cm) Steel End Plate with Steel Shell (Green), Foam Core (Gray), Adhesive (Pink), and Springs Modeling Adhesive Between Flanges (Blue) Showing Deformed Shape

7.3.3 Local Buckling Results

Mesh convergence was determined using models with no spring elements. Several mesh sizes were used to determine convergence corresponding to local buckling stress values for the different specimen lengths. The local buckling stress and load results are shown in Figure 7-13 and listed in Table 7-8. Local buckling stress values were considered to be converged when the normalized slope was less than 1 percent.

Once convergence was achieved, the influence of adhesive for local buckling stress was studied by creating spring elements between the adjacent nodes of inner and outer flanges. The spring constant, K, was increased until the local buckling stress exceeded the global buckling stress. The gap that the springs spanned measure 0.01 in (0.0254 cm) which represented the space between the flanges due to adhesive thickness. The adhesive modulus of elasticity, E_a, was determined from the formula:

$$E_a = \frac{KL}{A} \quad \textbf{(7-1)}$$

where *K* is the spring constant in units of force per length (input in ADINA as pounds per inch), *L* is the thickness of the gap between the flanges which was 0.01 in (0.0254 cm), and *A* is the average tributary area of one spring which was approximately 0.0536 in^2 (0.346 cm^2).

The results for each spring constant are plotted in Figure 7-14 and Figure 7-15 as flange aspect ratio versus local buckling stress and flange aspect ratio versus local buckling load, respectively. Euler buckling for the 14' (4.27 m) long column is also plotted on these figures as a strength upper bound. Based on the results, local buckling stress approaches a constant value as the flange aspect ratio increases to approximately 3, indicating no energy change for local buckling stress above this aspect ratio. The figures also show that increasing the adhesive stiffness increases the local buckling load of the short columns above the global buckling load. Figure 7-16 and Figure 7-17 plot the same data as the prior two figures, but in terms of spring constant instead of flange aspect ratio. These plots show a lower bound of local buckling stress for each spring constant. The modulus of elasticity for polyurethane adhesive was approximately 295 ksi (2,034 MPa)—more than two orders of magnitude greater than the required adhesive elastic modulus to prevent buckling. Thus, the polyurethane elastic modulus is not plotted.

Note that the local buckling analyses were performed with a foam elastic modulus of 1,500 psi (10.34 MPa) instead of 1,200 psi (8.27 MPa). Tests for 4 in (10.2 cm), 8 in (20.3 cm), and 10 in (25.4 cm) long specimens with an element edge length of 0.5 in (1.27 cm) were repeated using a foam elastic modulus of 1,200 psi (8.27 MPa). The results differed less than 1% from the results using a foam elastic modulus of 1,500 psi (10.34 MPa). Thus, the difference in the final results was considered to be negligible. The foam elastic modulus of 1,200 psi (8.27 MPa) was used for the local buckling analyses with springs.

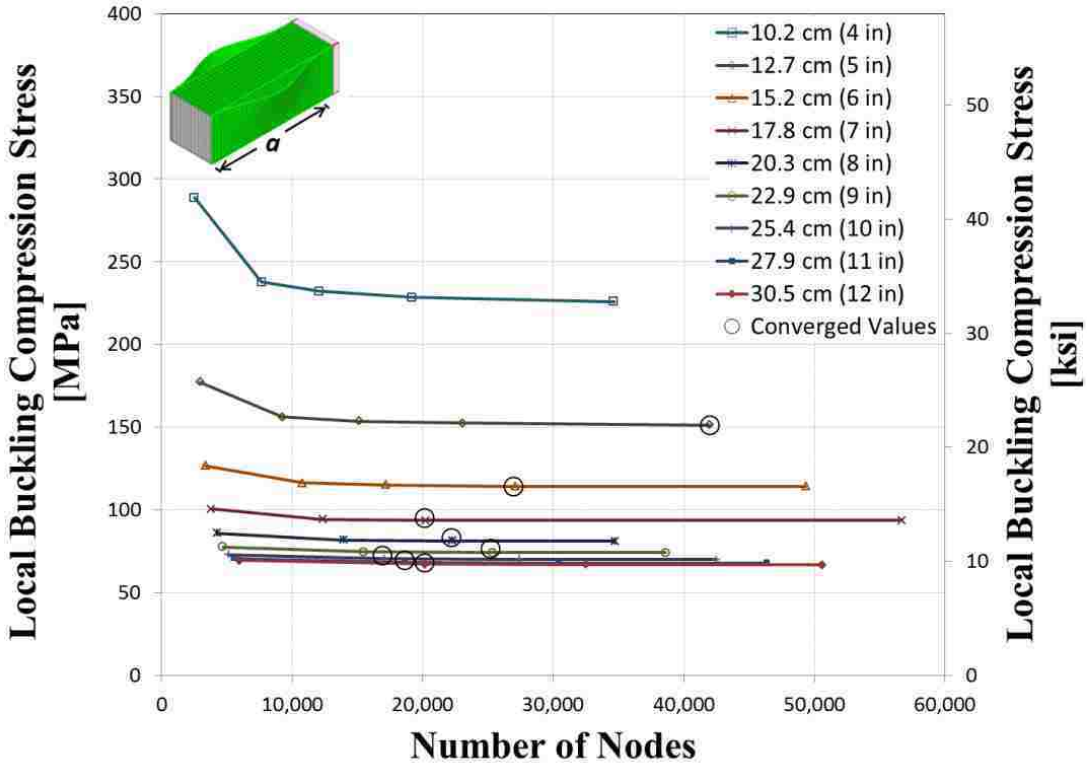

Figure 7-13: Local Buckling Compression Stress vs. Number of Nodes to Show Mesh Convergence for Models with No Springs Between Flanges

Table 7-8: Local Buckling Stress Values to Show Mesh Convergence

Buckling Length, a [cm (in)]	Element Length [cm (in)]	Elements	Nodes	Pressure at Buckling [MPa (psi)]	Slope %	Buckling Load, P_{cr} [kN (kips)]	Buckling Stress, σ_{cr} [MPa (ksi)]
10.2 (4.0)	2.54 (1.0)	432	2,511	25.3 (3,675)		262 (58.8)	288 (41.7)
	1.27 (0.5)	1,460	7,662	20.9 (3,026)	-8.6	215 (48.4)	237 (34.3)
	1.02 (0.4)	2,378	12,054	20.4 (2,956)	-4.0	210 (47.3)	231 (33.0)
	0.85 (0.33)	3,920	19,169	20.1 (2,910)	-2.6	207 (46.6)	228 (33.0)
	0.64 (0.25)	7,322	34,620	19.8 (2,876)	-1.4	205 (46.0)	225 (32.6)
12.7 (5.0)	2.54 (1.0)	516	2,945	15.6 (2,256)		161 (36.1)	177 (25.6)
	1.27 (0.5)	1,780	9,228	13.7 (1,990)	-5.5	142 (31.8)	156 (22.6)
	1.02 (0.4)	3,020	15,123	13.5 (1,957)	-2.6	139 (31.3)	153 (22.2)
	0.85 (0.33)	4,748	23,054	13.4 (1,941)	-1.6	138 (31.1)	152 (22.0)
	0.64 (0.25)	8,934	41,988	13.3 (1,927)	-0.9	137 (30.8)	151 (21.9)
15.2 (6.0)	2.54 (1.0)	600	3,379	11.1 (1,615)		115 (25.8)	126 (18.3)
	1.27 (0.5)	2,100	10,794	10.2 (1,480)	-3.8	105 (23.7)	116 (16.8)
	1.02 (0.4)	3,448	17,169	10.1 (1,466)	-1.6	104 (23.5)	115 (16.6)
	0.85 (0.33)	5,774	27,109	10.0 (1,455)	-1.3	108 (24.4)	119 (17.3)
	0.64 (0.25)	10,546	49,356	10.0 (1,454)	-0.1	103 (23.3)	114 (16.5)
17.8 (7.0)	2.54 (1.0)	684	3,813	8.8 (1,282)		91 (20.5)	100 (14.5)
	1.27 (0.5)	2,420	12,360	8.3 (1,202)	-2.8	86 (19.2)	94 (13.6)
	1.02 (0.4)	4,090	20,238	8.2 (1,193)	-1.0	85 (19.1)	93 (13.5)
	0.85 (0.33)	12,158	56,724	8.2 (1,191)	-0.7	85 (19.1)	93 (13.5)
20.3 (8.0)	2.54 (1.0)	768	4,247	7.6 (1,096)		78 (17.5)	86 (12.4)
	1.27 (0.5)	2,740	13,926	7.2 (1,043)	-2.1	74 (16.7)	82 (11.8)
	1.02 (0.4)	4,518	22,284	7.2 (1,037)	-1.2	74 (16.6)	81 (11.8)
	0.85 (0.33)	7,232	34,709	7.1 (1,041)	-0.1	74 (16.7)	81 (11.8)
22.9 (9.0)	2.54 (1.0)	852	4,681	6.8 (990)		70 (15.8)	77 (11.2)
	1.27 (0.5)	3,060	15,492	6.5 (950)	-1.8	68 (15.2)	74 (10.8)
	1.02 (0.4)	5,160	25,353	6.5 (945)	-0.8	67 (15.1)	74 (10.7)
	0.85 (0.33)	8,060	38,594	6.5 (945)	0.1	67 (15.1)	74 (10.7)
25.4 (10.0)	2.54 (1.0)	936	5,115	6.4 (930)		66 (14.9)	73 (10.6)
	1.27 (0.5)	3,380	17,058	6.2 (897)	-1.5	64 (14.4)	70 (10.2)
	1.02 (0.4)	5,588	27,399	6.2 (893)	-0.7	64 (14.3)	70 (10.1)
	0.85 (0.33)	8,888	42,479	6.1 (892)	-0.3	63 (14.3)	70 (10.1)
27.9 (11.0)	2.54 (1.0)	1,020	5,549	6.2 (899)		64 (14.4)	70 (10.2)
	1.27 (0.5)	3,700	18,624	6.0 (870)	-1.4	62 (13.9)	68 (9.9)
	1.02 (0.4)	6,230	30,468	6.0 (865)	-0.8	66 (14.7)	72 (10.4)
	0.85 (0.33)	9,716	46,364	6.0 (865)	0.0	62 (13.8)	68 (9.8)
30.5 (12.0)	2.54 (1.0)	1,104	5,983	6.1 (865)		63 (14.2)	69 (10.0)
	1.27 (0.5)	4,020	20,190	5.9 (856)	-1.4	31 (13.7)	67 (9.7)
	1.02 (0.4)	6,658	32,514	5.9 (853)	-0.7	61 (13.6)	67 (9.7)
	0.85 (0.33)	10,940	50,599	5.9 (850)	-0.7	64 (14.3)	70 (10.1)

*Pressure applied over end plate area of 103 cm^2 (16 in^2)

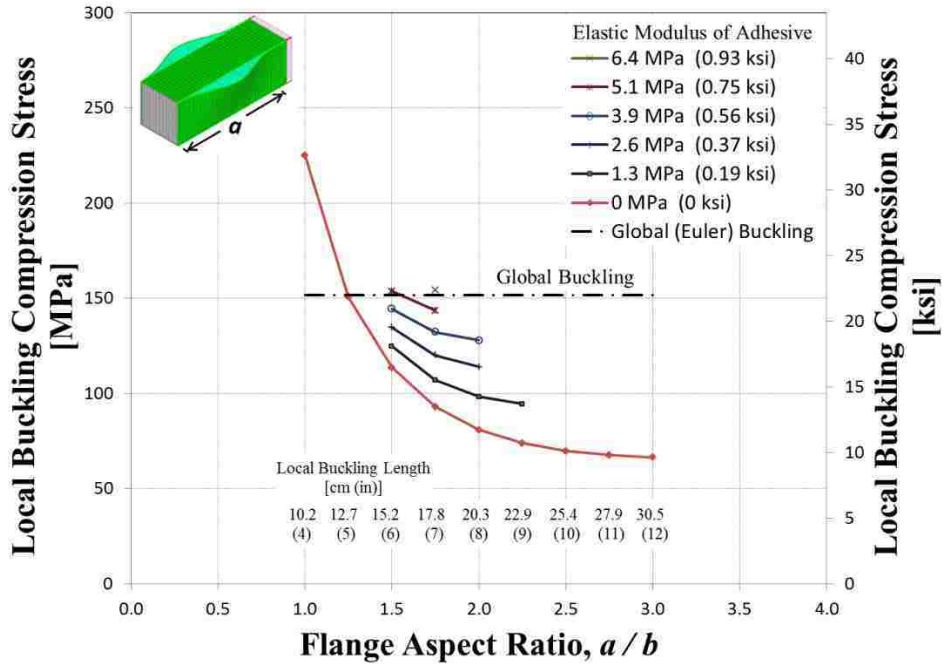

Figure 7-14: Local Buckling Compression Stress vs. Flange Aspect Ratio (Converged Values) as a Function of Modulus of Elasticity of Adhesive

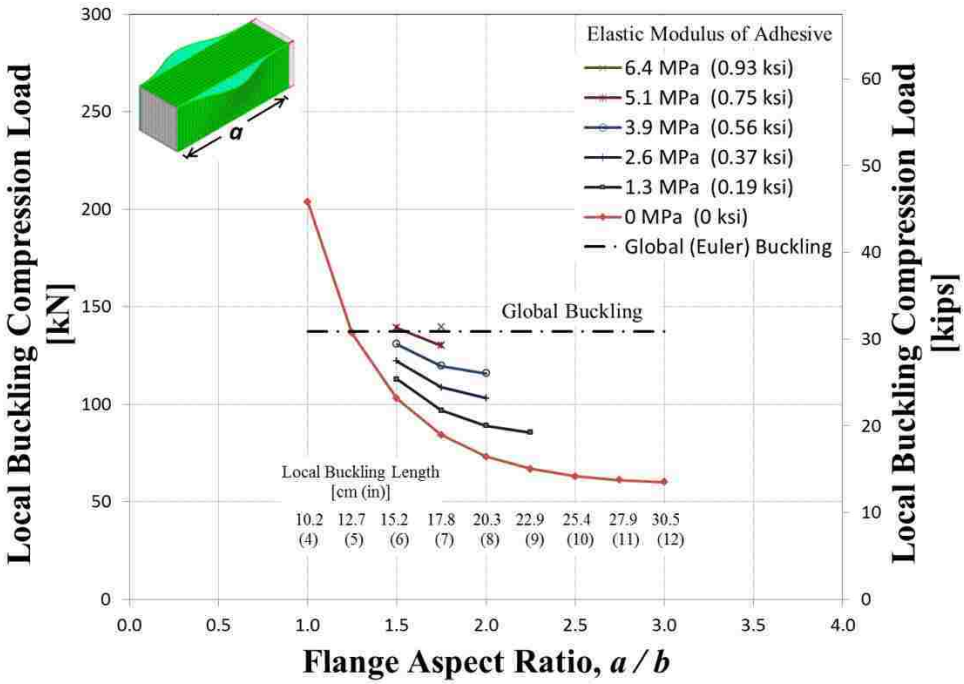

Figure 7-15: Local Buckling Compression Load vs. Flange Aspect Ratio (Converged Values) as a Function of Modulus of Elasticity of Adhesive

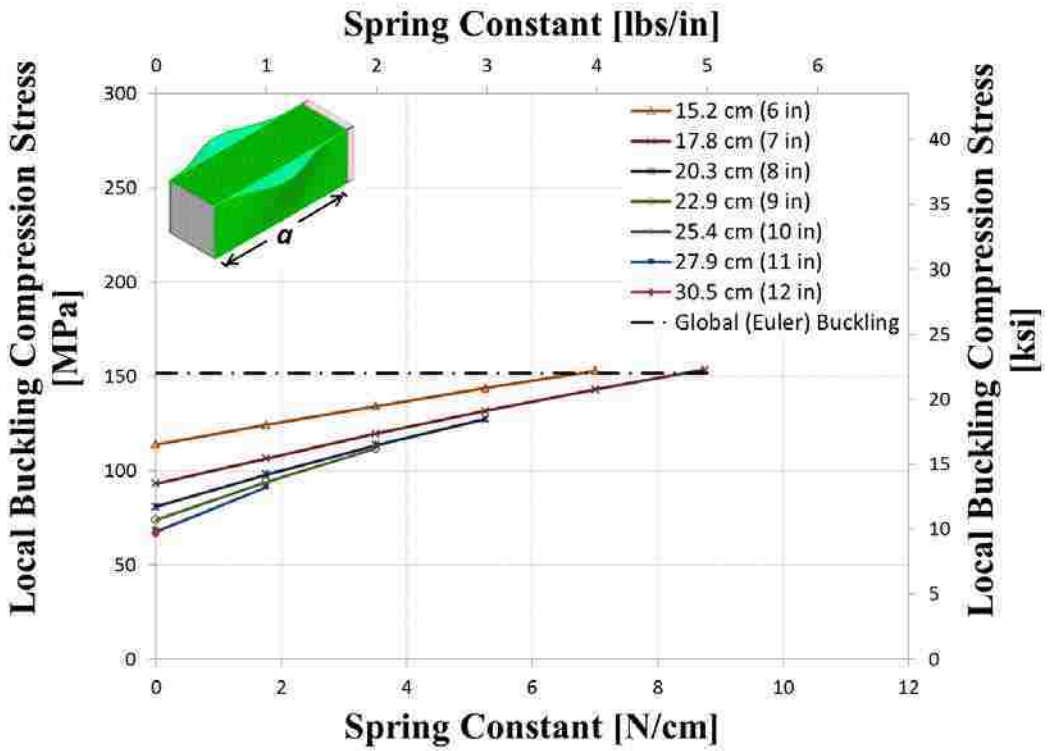

Figure 7-16: Local Buckling Compression Stress vs. Spring Constant

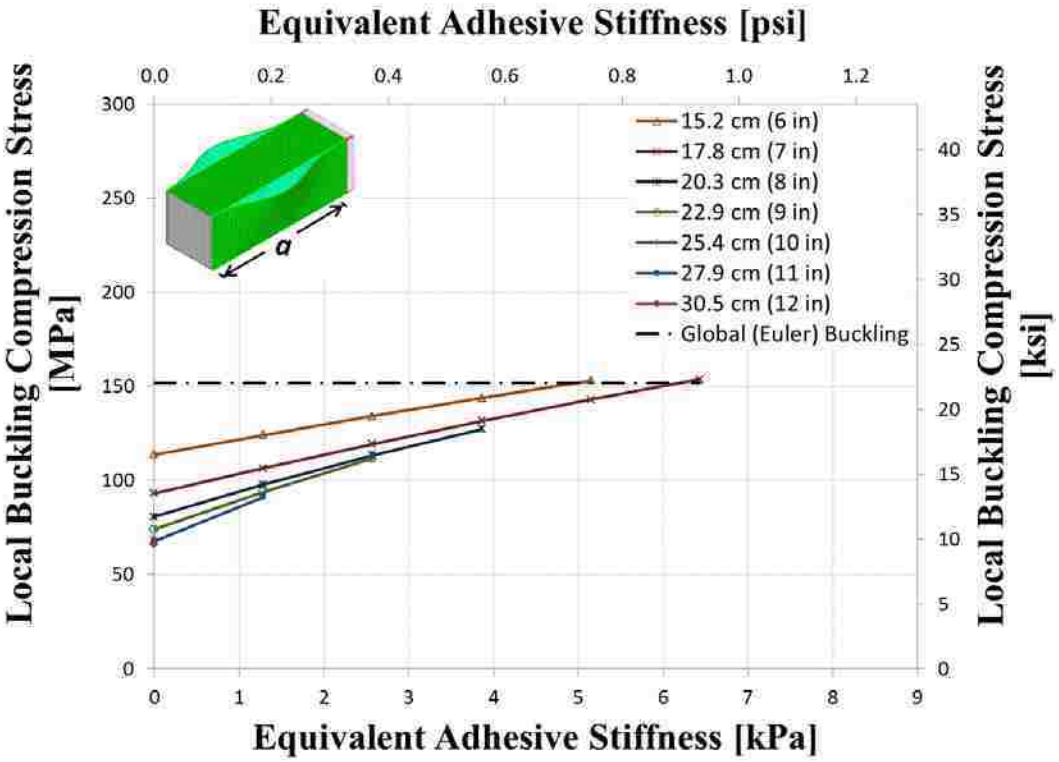

Figure 7-17: Local Buckling Compression Stress vs. Equivalent Adhesive Stiffness

Table 7-9: Local Buckling Stress Values to Show Mesh Convergence

Buckling Length, a [cm (in)]	Spring Constant, K [N/cm (lbs/in)]	Pressure at Buckling* [MPa (psi)]	Equivalent Adhesive Stiffness [MPa (ksi)]	Local Buckling Load, P_{cr} [kN (kips)]	Local Buckling Stress, σ_{cr} [MPa (ksi)]
15.2 (6.0)	0 (0.0)	10.0 (1,454)	0 (0.0)	103 (23.3)	114 (16.6)
	1.8 (1.0)	10.9 (1,587)	1.3 (0.19)	113 (25.4)	125 (18.1)
	3.5 (2.0)	11.8 (1,715)	2.6 (0.37)	122 (27.4)	135 (19.5)
	5.3 (3.0)	12.7 (1,838)	3.9 (0.56)	131 (29.4)	144 (20.9)
	7.0 (4.0)	13.5 (1,956)	5.1 (0.75)	139 (31.3)	154 (22.3)
17.8 (7.0)	0 (0.0)	8.2 (1,191)	0 (0.0)	85 (19.1)	94 (13.6)
	1.8 (1.0)	9.4 (1,361)	1.3 (0.19)	97 (21.8)	107 (15.5)
	3.5 (2.0)	10.5 (1,527)	2.6 (0.37)	109 (24.4)	120 (17.4)
	5.3 (3.0)	11.6 (1,682)	3.9 (0.56)	120 (26.9)	132 (19.2)
	7.0 (4.0)	12.6 (1,828)	5.1 (0.75)	130 (29.2)	144 (20.8)
	8.8 (5.0)	13.5 (1,963)	6.4 (0.93)	140 (31.4)	154 (22.4)
20.3 (8.0)	0 (0.0)	7.1 (1,033)	0 (0.0)	74 (16.5)	81 (11.8)
	1.8 (1.0)	8.6 (1,250)	1.3 (0.19)	89 (20.0)	98 (14.2)
	3.5 (2.0)	10.0 (1,450)	2.6 (0.37)	103 (23.2)	114 (16.5)
	5.3 (3.0)	11.2 (1,627)	3.9 (0.56)	116 (26.0)	128 (18.5)
22.9 (9.0)	0 (0.0)	6.5 (945)	0 (0.0)	67 (15.1)	74 (10.8)
	1.8 (1.0)	8.3 (1,201)	1.3 (0.19)	85 (19.2)	94 (13.7)
25.4 (10.0)	0 (0.0)	6.1 (892)	0 (0.0)	63 (14.3)	70 (10.2)
27.9 (11.0)	0 (0.0)	6.0 (865)	0 (0.0)	62 (13.8)	68 (9.9)
30.5 (12.0)	0 (0.0)	5.9 (850)	0 (0.0)	60 (13.6)	67 (9.7)

*Pressure applied over end plate area of 103 cm^2 (16 in^2)

7.3.4 Local Buckling Discussion of Results

Based on the results shown in Figure 7-14 and Figure 7-15, the critical flange aspect ratio at which the local buckling stress and the global buckling stress are equal is approximately 1.25. This corresponds to a local buckling wavelength of 5 in (12.7 cm). Thus, constraining the flanges at this distance (or less) should result in the columns buckling globally prior to buckling locally. Also, there is a lower bound for the local buckling stress for any adhesive stiffness value which is approximately 9.6 ksi (66 MPa). The aspect ratio where buckling is minimum is approximately 3.0. This minimum value indicates that the flanges will buckle in the first mode

or in smaller wavelengths—on the order of 12 in (30.5 cm)—with approximately the same applied stress. The value of adhesive modulus at which the local buckling stress is approximately equal to the global buckling stress for any local buckling length is approximately 1.0 ksi (6.9 MPa). Thus, a small amount of tension from adhesive will prevent the flanges from buckling in the first mode. This explains why the "Adhesive-Only," "Adhesive and Welds," and "Adhesive and Screws" columns all buckled locally at approximately 12 in (30.5 cm) wavelengths. In fact, the test results showed that two local buckling wavelengths occurred in between the screw spacing of 24 in (71 cm) for the "Adhesive and Screws" column. This confirms a statement made by Ji (2008, p. 190), "In local instability, the flanges and webs buckle like plates, with a resulting change in the cross section of the column. The wavelength of the buckle is of the order of the widths of the plate elements, and the corresponding critical stress is generally independent of the length of the column when the length is equal to or greater than three times the width of the largest plate element in the column cross-section.

7.4 Crippling

This section summarizes the column crippling analysis. Using nonlinear finite element analysis, the peak load was determined for four different model lengths. Mesh convergence is shown. The four models were analyzed with and without foam for comparison. The models were analyzed to slightly beyond the peak load. Crippling becomes apparent when running the analysis far beyond the peak load. This section includes the problem description, nonlinear aspects, results, and discussion of results.

7.4.1 Description of Physical Problem

Crippling is the critical failure mechanism of the columns. Crippling is shown in Figure 7-18. The cross-section permanently deforms due to yielding of the material. Crippling is initiated by local buckling. The deformed cross-section creates an effective hinge in the column, which simultaneously buckles globally.

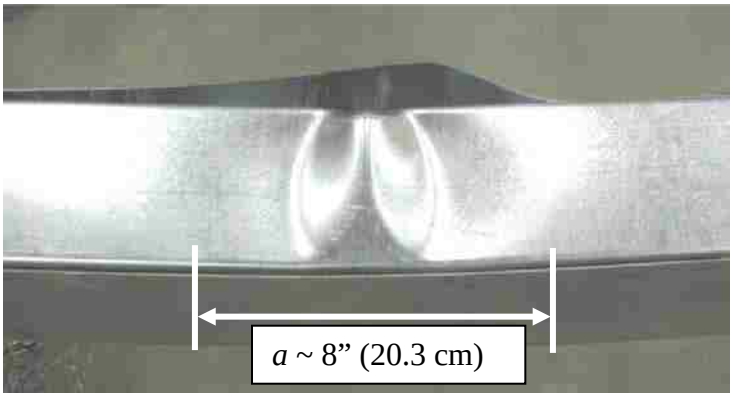

Figure 7-18: Close-up Photo of Crippling of "Adhesive and Screws" Column During Test to Failure

7.4.2 Assumptions and Modeling

Four models were analyzed and are referred to as, "No Foam or Adhesive" (no foam core and no adhesive between flanges), "Foam Only" (no adhesive between flanges), "Adhesive Only" (No foam core), and "Foam and Adhesive" (both a foam core and adhesive between flanges). For the "No Foam or Adhesive" model, the inner flanges were modeled as pinned using a small amount of adhesive at points A and B (Figure 7-19). This was to prevent the inner U-channel flanges from deflecting through the outer U-channel flanges in the finite element analysis. The crippled shape and the effective stress for a 12 in (20.3 cm) long "No Foam or Adhesive" model from two different isometric views are shown in Figure 7-20.

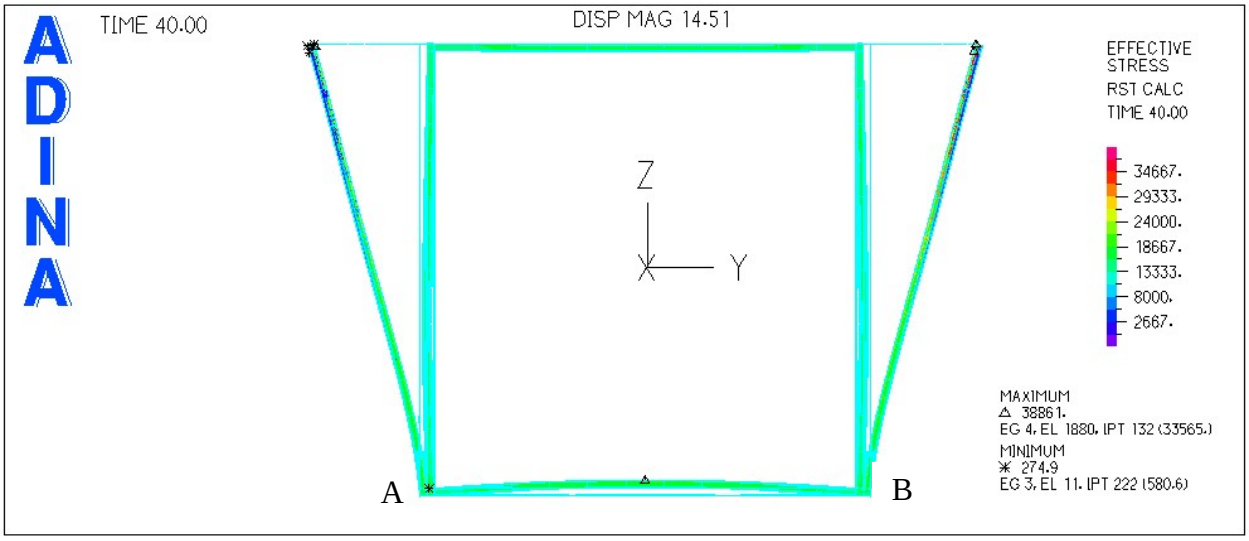

Figure 7-19: Finite Element Band Plot of Deformed Column Cross-Section with No Foam After Crippling Analysis Showing Effective Stress

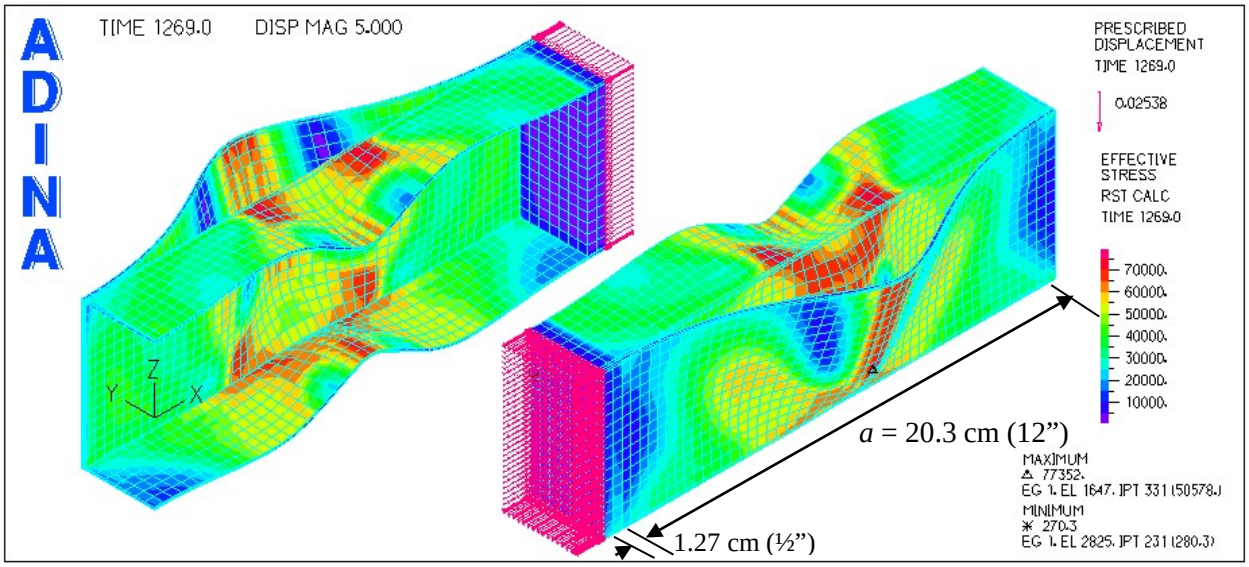

Figure 7-20: Finite Element Band Plot of Deformed Crippling Analysis "No Foam or Adhesive" Model Measuring 12" (20.3 cm) with ½" (1.27 cm) Steel End Plate Showing Effective Stress

Symmetry was used in the analysis. Half models (see Figure 7-20) were analyzed in order to save on computational time and the reaction forces were doubled in order to determine the corresponding axial load for a full model. The surface that was cut to exploit symmetry was constrained from translation in the y- and z- directions. The surface was only allowed translation in the x-direction. Two models were analyzed and results were compared. The results are shown in Figure 7-21 and are listed in Table 7-10. As listed in the table, the percent difference in the peak load between the two models is less than 1% and is therefore considered negligible. Thus, the half models (exploiting symmetry) produce essentially the same results as the full models.

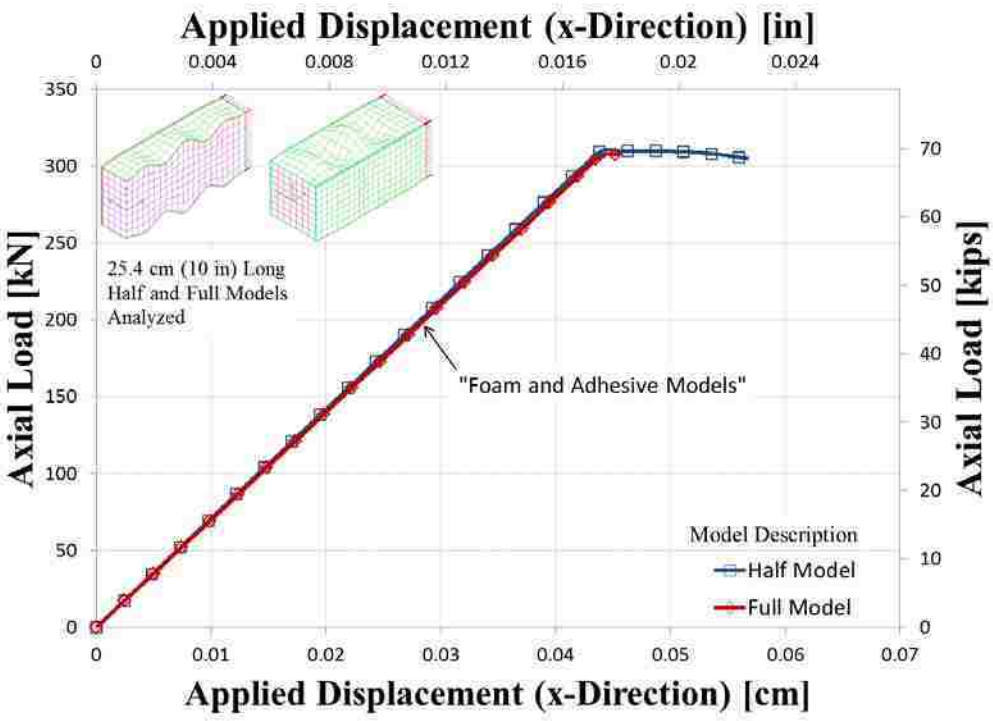

Figure 7-21: Axial Load vs. Applied Displacement (x-Direction) for 8 in (20.3 cm) Long "No Foam or Adhesive" Model to Compare Half Model to Full Model

Table 7-10: Peak Load and Corresponding Displacement for Two 10 in (25.4 cm) Long "Foam and Adhesive" Models Including a Half Model and a Full Model

Model Description	x-Displacement, u_1 [cm (in)]	Peak Load, P_{cr} [kN (kips)]
Half Model; Foam and Adhesive	0.0446 (0.0176)	311 (69.9)
Full Model; Foam and Adhesive	0.0447 (0.0176)	308 (69.3)
Percent Difference of Half Compared to Full	0%	0.86%

7.4.3 Nonlinear Aspects

Large displacements were used to induce local buckling. Numerical time stepping was used with the static analysis. The displacement stepping value employed was 0.0001" (0.00025 cm) and the maximum displacement was 0.0180" (0.046 cm). The Full Newton method was used with a maximum of 15 iterations to execute the nonlinear analysis. The nonlinear stress and strain material properties for steel were shown previously in Figure 7-1 and listed in Table 7-3.

7.4.4 Crippling Convergence

Mesh convergence for crippling analysis was determined using the "No Foam or Adhesive" models. The axial load versus applied displacement in the x-direction for models measuring 8 in (20.3 cm), 10 in (25.4 cm), 12 in (30.5 cm), and 14 in (35.6 cm) is shown in Figure 7-22 through Figure 7-25, respectively. The axial load was determined from the reaction force of the half model multiplied by two to represent the full model reaction force. The results for all mesh sizes are essentially identical up to the peak load, at which the mesh evidently converges with an element edge length of 0.50 in (1.27 cm). Beyond the peak load, finer meshes produce more accurate load-displacement results. Because the primary objective of the crippling analysis was to determine the peak load for different configurations, an element edge length of

0.50 in (1.27 cm) was determined to give sufficiently accurate results and thus was used in subsequent crippling analyses. The converged results using an element edge length of 0.5 in (1.27 cm) for four specimen lengths are shown together in Figure 7-26. With this edge length, the peak load for the four models with no foam is approximately 39.6 kips (176 kN) or 28.1 ksi (194 MPa) (see Table 7-11).

Table 7-11: Peak Force and Stress Values for Four Model Lengths for "No Foam or Adhesive" Model with Element Edge Length of 0.50 in (1.27 cm)

Specimen Length, a [cm (in)]	x-Displacement, u_1 [cm (in)]	Peak Stress, σ_{cr} [MPa (ksi)]	Peak Force, P_{cr} [kN (kips)]
20.3 (8.0)	0.031 (0.012)	208 (30.2)	189 (42.5)
25.4 (10.0)	0.037 (0.015)	198 (28.7)	180 (40.4)
30.5 (12.0)	0.045 (0.018)	194 (28.1)	176 (39.7)
35.6 (14.0)	0.051 (0.020)	194 (28.1)	176 (39.6)

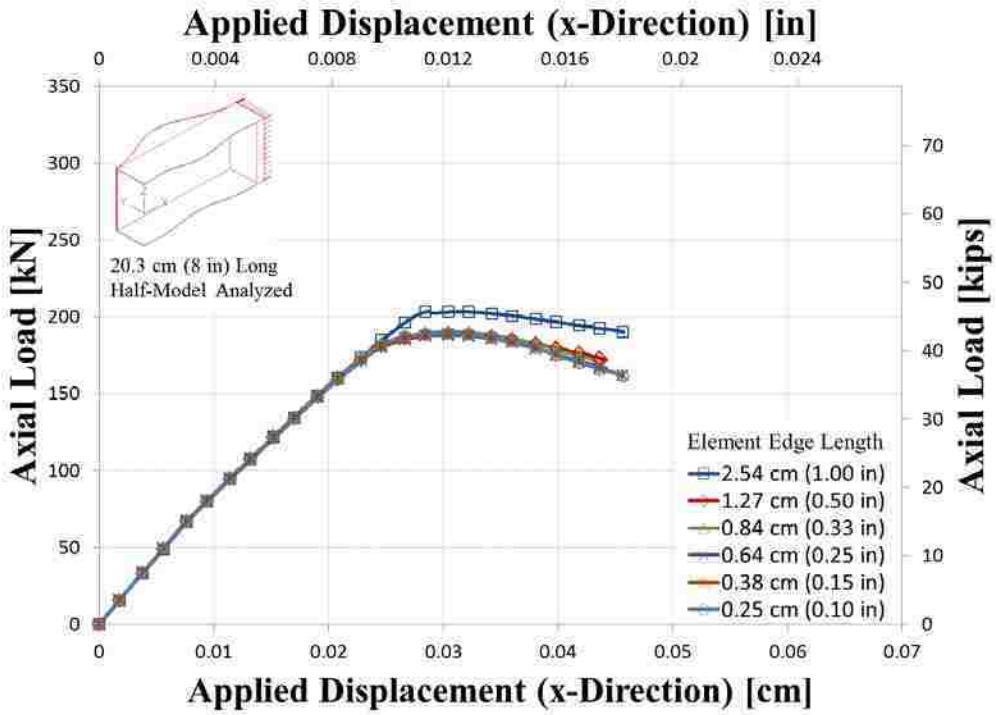

Figure 7-22: Axial Load vs. Applied Displacement (x-Direction) for 8 in (20.3 cm) Long "No Foam or Adhesive" Model

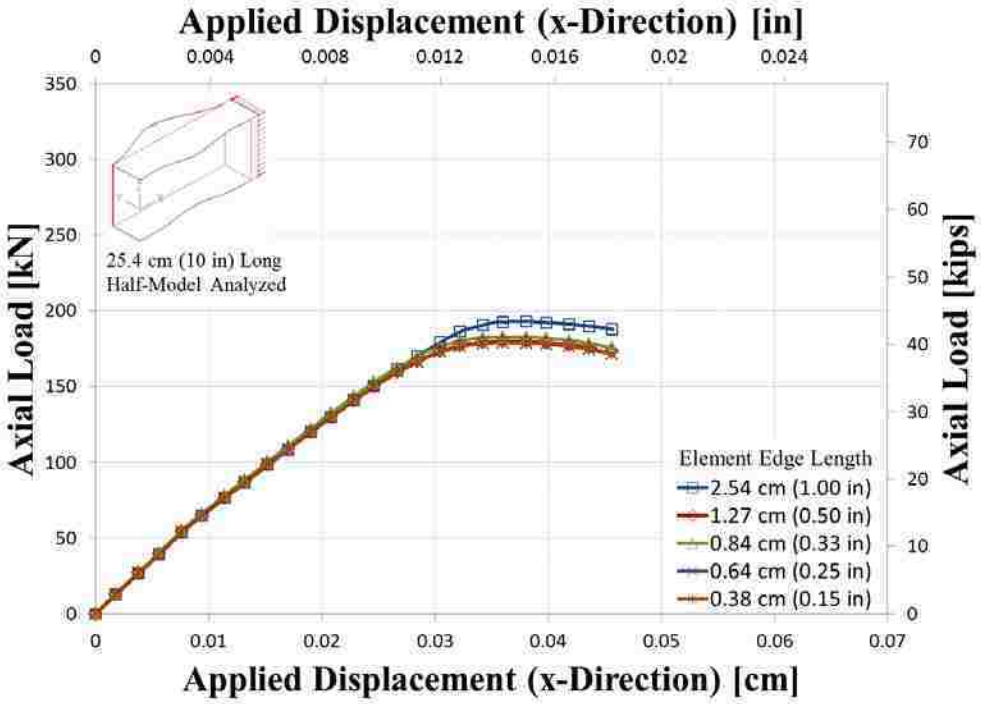

Figure 7-23: Axial Load vs. Applied Displacement (x-Direction) for 10 in (25.4 cm) Long "No Foam or Adhesive" Model

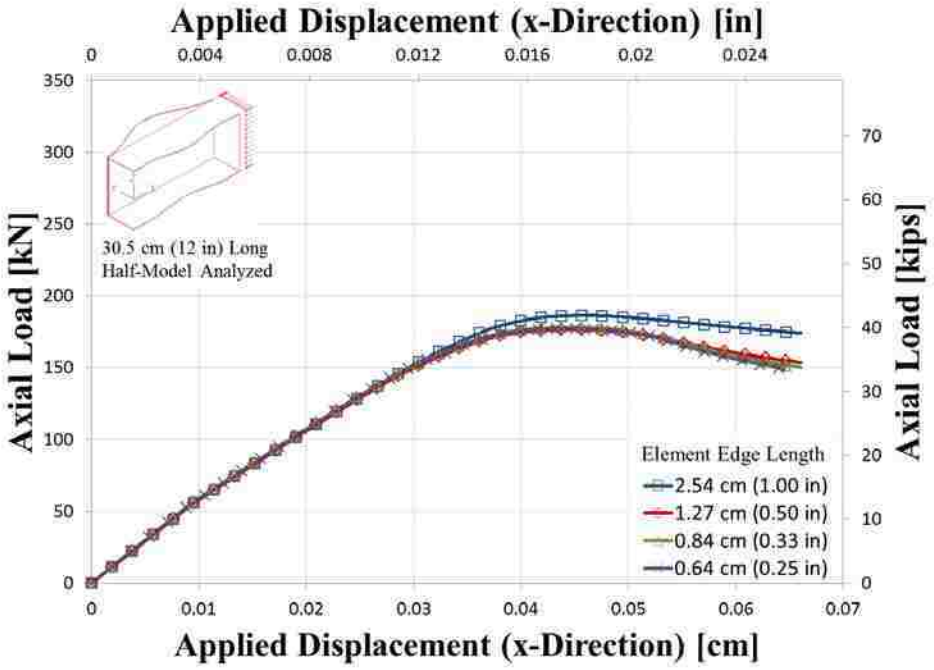

Figure 7-24: Axial Load vs. Applied Displacement (x-Direction) for 12 in (30.5 cm) Long "No Foam or Adhesive" Model

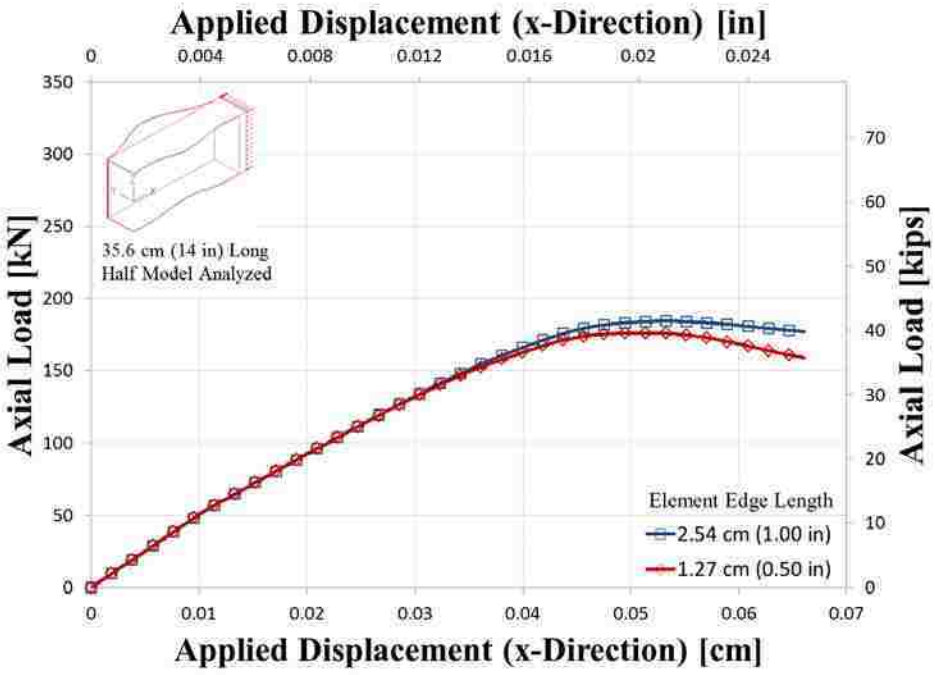

Figure 7-25: Axial Load vs. Applied Displacement (x-Direction) for 14 in (35.6 cm) Long "No Foam or Adhesive" Model

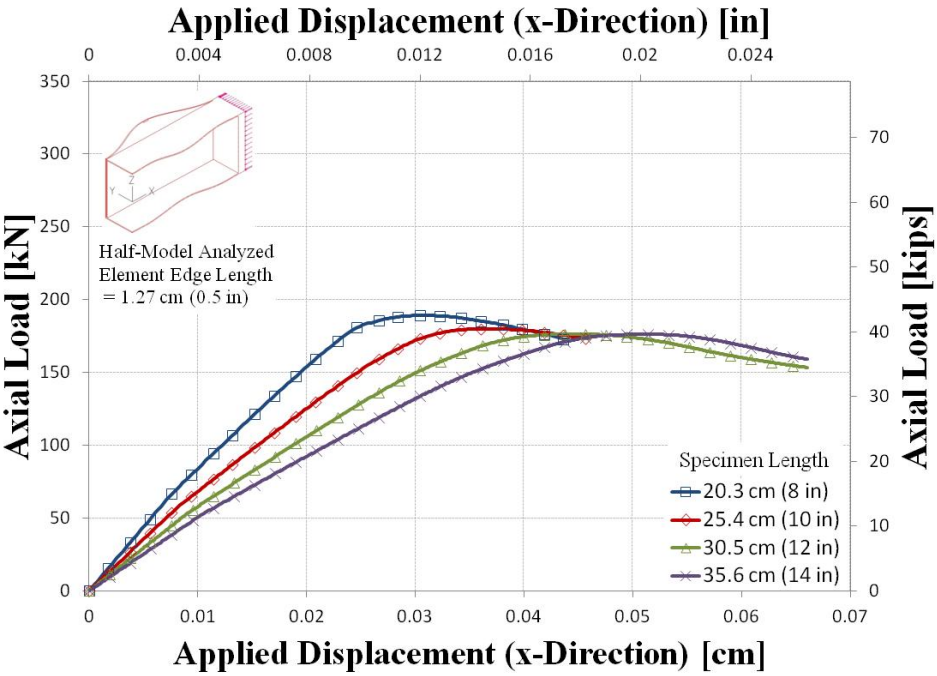

Figure 7-26: Axial Load vs. Applied Displacement (x-Direction) for Four Specimen Lengths for "No Foam or Adhesive" Model with Converged Element Edge Length of 0.5 in (1.27 cm)

7.4.5 Crippling Results

In the previous subsection mesh convergence was determined. This subsection discusses how the results for four different models compare using the converged mesh. Figure 7-27 to Figure 7-30 show finite element band plots of effective stress for 10 in (25.4 cm) specimens including "No Foam or Adhesive," "Foam Only," "Adhesive Only," and "No Foam or Adhesive" models, respectively. These models all have element edge lengths of 0.5 in (1.27 cm). Based on these figures the webs crippled in approximately the same mode shape for the "No Foam or Adhesive" and "Foam Only" models; the webs also crippled in approximately the same mode shape for the "Adhesive Only" and "Foam and Adhesive" models. Thus, the adhesive increased the peak load by forcing the specimen to cripple in a higher local buckling mode shape; the linear elastic foam elements did not. The foam elements were sufficiently stiff, however, to increase the buckling load by delaying the flanges and webs from local buckling. The foam used in the models had the elastic material properties listed previously in Table 7-2.

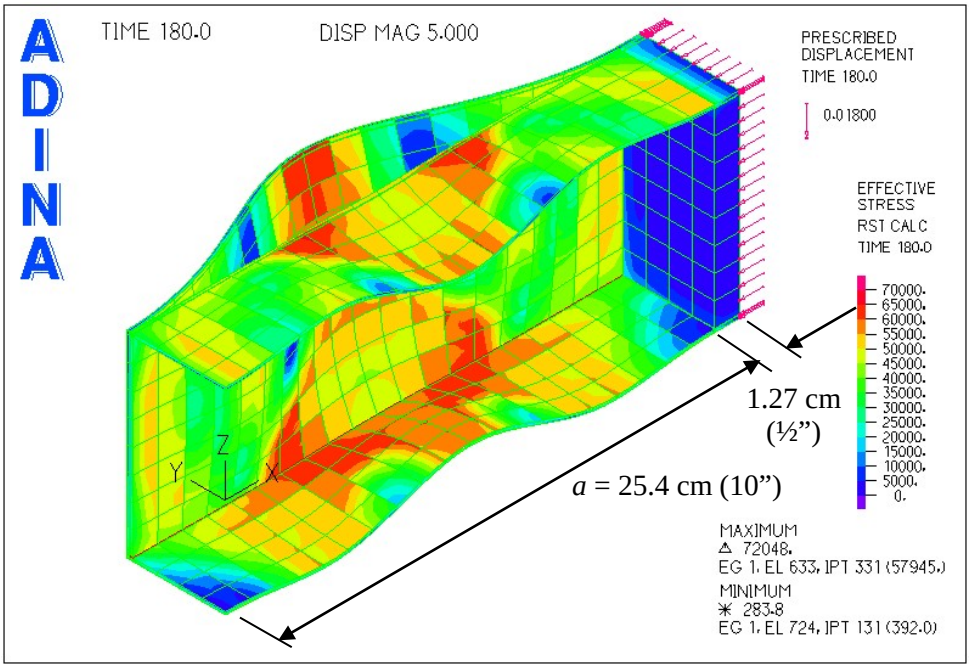

Figure 7-27: Finite Element Band Plot of Effective Stress for 10 in (25.4 cm) "No Foam or Adhesive" Model

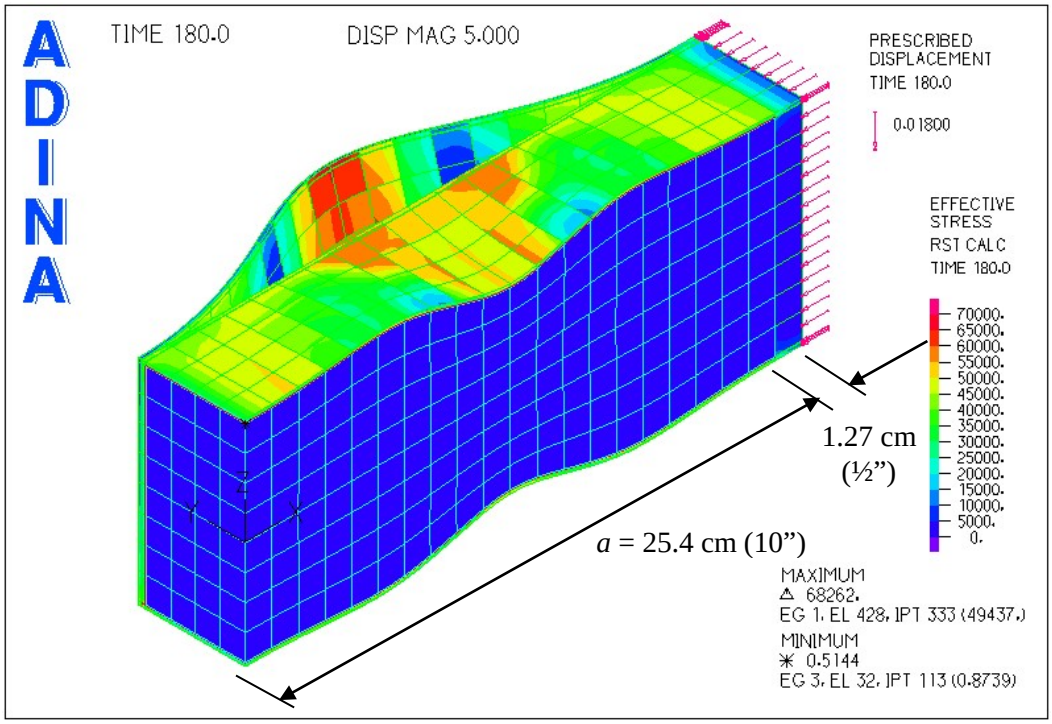

Figure 7-28: Finite Element Band Plot of Effective Stress for 10 in (25.4 cm) "Foam Only" (No Adhesive) Model

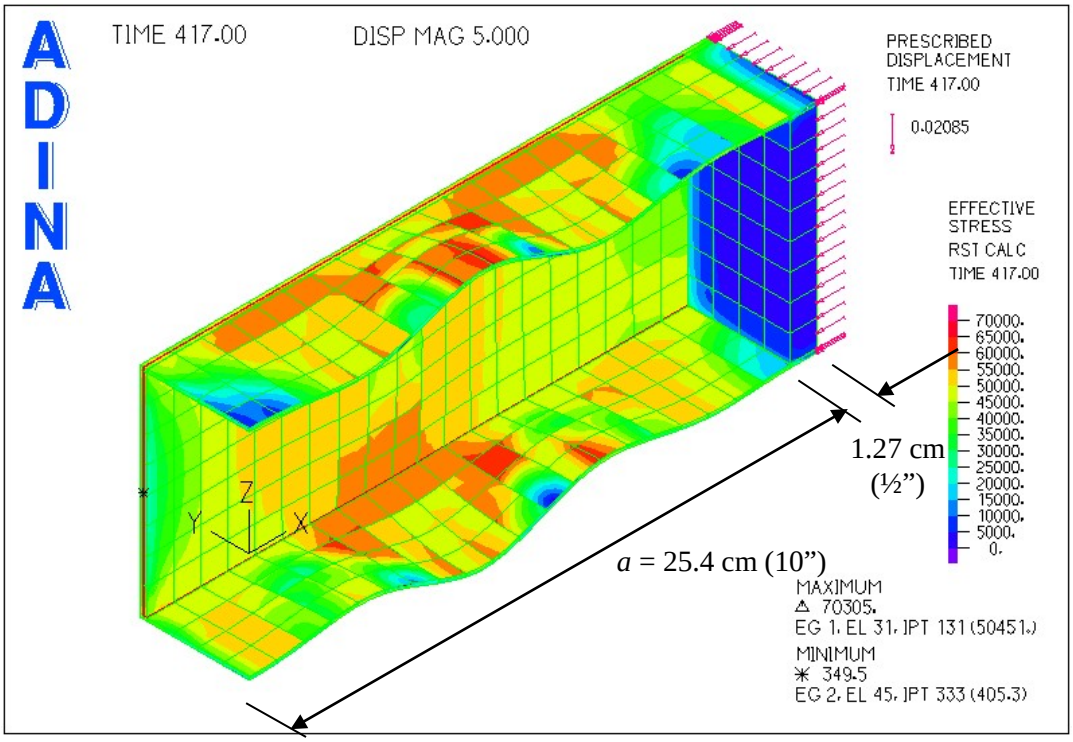

Figure 7-29: Finite Element Band Plot of Effective Stress for 10 in (25.4 cm) "Adhesive Only" (No Foam) Model

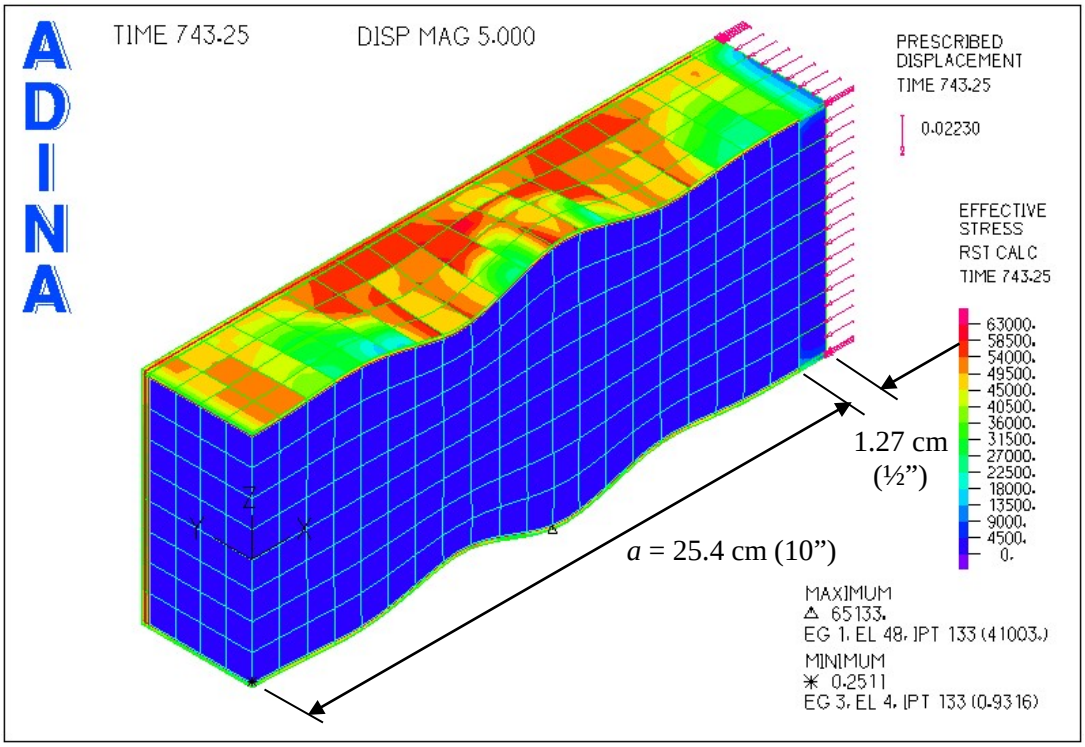

Figure 7-30: Finite Element Band Plot of Effective Stress for 10 in (25.4 cm) "Foam and Adhesive" Model

The axial load versus applied displacement in the x-direction is shown in Figure 7-31 to Figure 7-34 for models measuring 8 in (20.3 cm), 10 in (25.4 cm), 12 in (30.5 cm), and 14 in (35.6 cm), respectively. Each figure shows four curves indicating results for one of each of the four model configurations described in Section 7.4.2. In these figures note the differences in the sharpness of the peaks for each model configuration. This is discussed in more detail in Section 7.4.5. The results from all four of these figures are combined in Figure 7-35. Notice that the four models had consistent results for the different specimen lengths analyzed. For example, the "Foam and Adhesive" models consistently sustained the highest axial load prior to collapse, followed by the "Adhesive Only" models, the "Foam Only" models, and lastly the "No Foam or Adhesive" models. The peak values are shown in Figure 7-36 and are listed in Table 7-12.

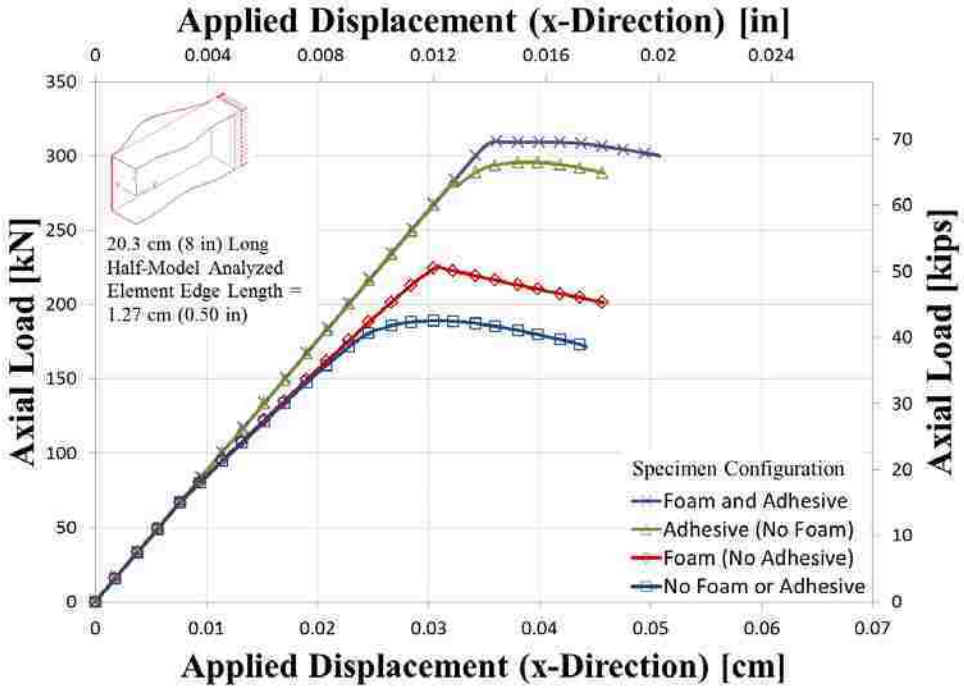

Figure 7-31: Axial Load vs. Applied Displacement (x-Direction) for 8 in (20.3 cm) Long Half-Model for Four Specimen Configurations

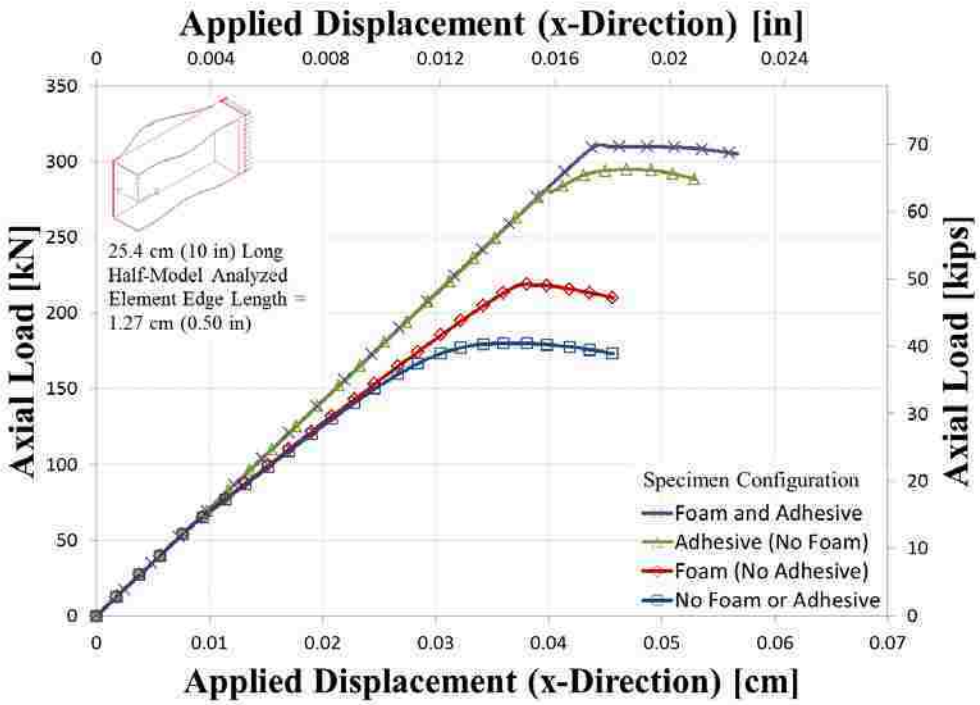

Figure 7-32: Axial Load vs. Applied Displacement (x-Direction) for 10 in (25.4 cm) Long Half-Model for Four Specimen Configurations

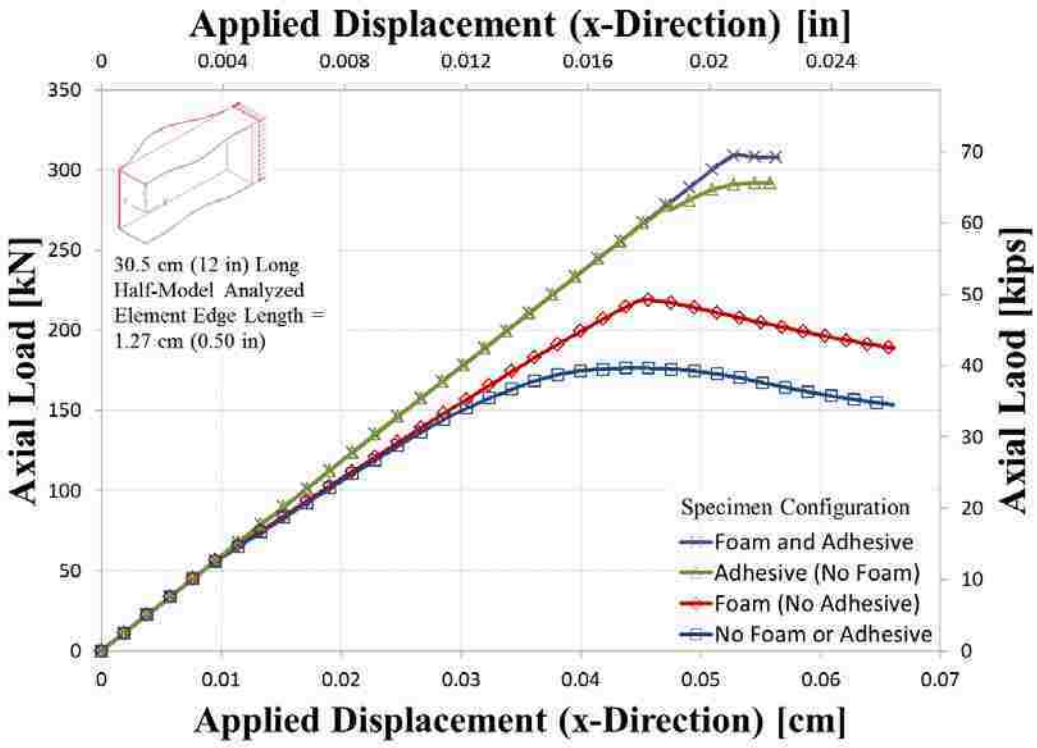

Figure 7-33: Axial Load vs. Applied Displacement (x-Direction) for 12 in (30.5 cm) Long Half-Model for Four Specimen Configurations

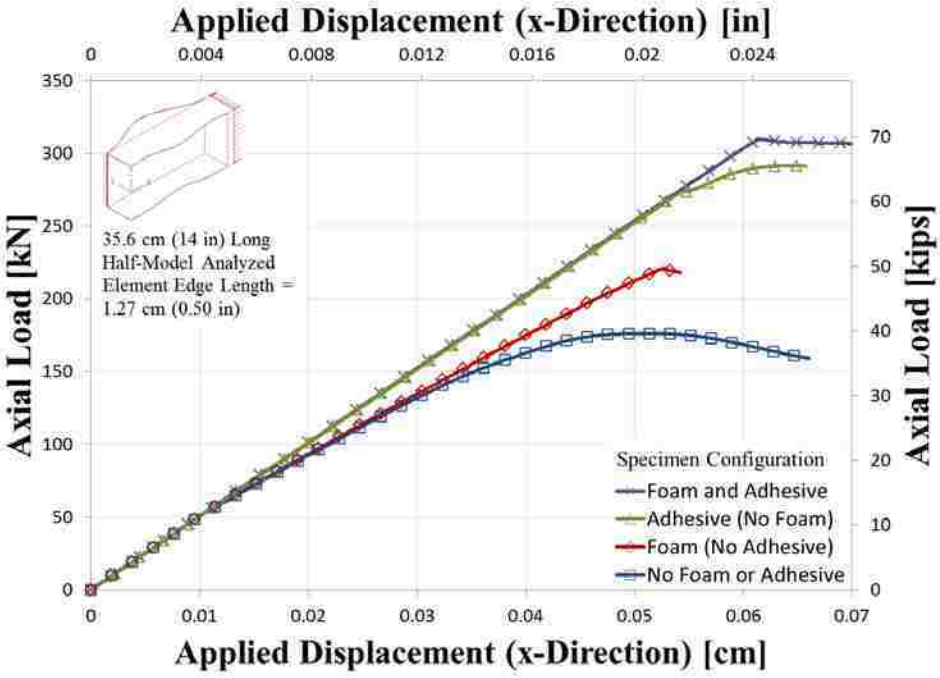

Figure 7-34: Axial Load vs. Applied Displacement (x-Direction) for 14 in (35.6 cm) Long Half-Model for Four Specimen Configurations

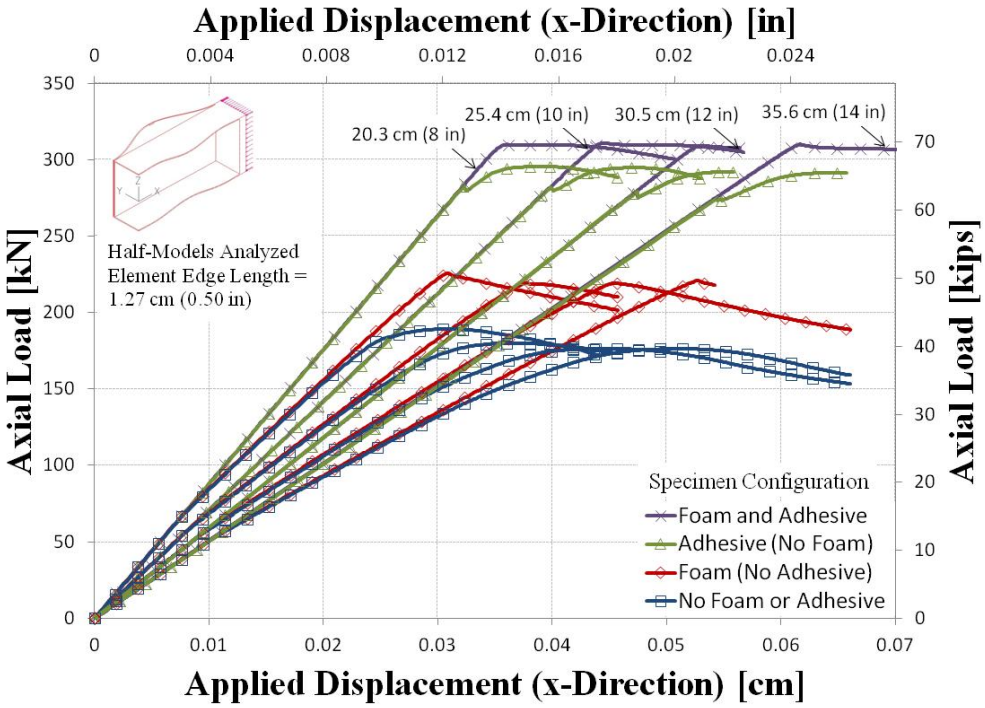

Figure 7-35: Axial Load vs. Applied Displacement (x-Direction) for Four Lengths of Half-Models for Four Specimen Configurations

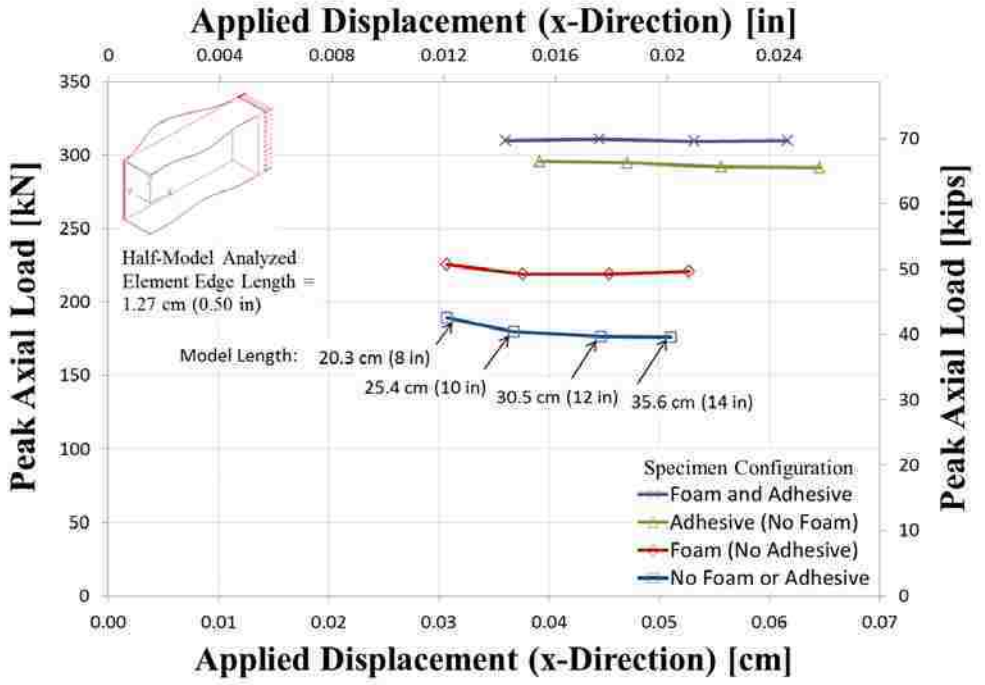

Figure 7-36: Peak Axial Load vs. Applied Displacement (x-Direction) Maximum Values for Four Model Lengths for Four Configurations

Table 7-12: Peak Load and Stress* Values for Four Model Lengths of Four Different Configurations with Element Edge Length of 0.50 in (1.27 cm)

Model	Specimen Length, a [cm (in)]	Displacement, u_1 [cm (in)]	Peak Load, P_{cr} [kN (kips)]	Peak Stress, σ_{cr} [MPa (ksi)]	Peak Stress / Yield Stress, σ_{cr}/σ_y	Percent Change
Foam and Adhesive	20.3 (8.0)	0.036 (0.014)	310 (69.7)	341 (49.4)	98.8%	--
	25.4 (10.0)	0.045 (0.018)	311 (69.9)	342 (49.6)	99.1%	0.3%
	30.5 (12.0)	0.053 (0.021)	309 (69.5)	340 (49.3)	98.6%	-0.5%
	35.6 (14.0)	0.062 (0.024)	310 (69.7)	341 (49.4)	98.9%	0.3%
Adhesive Only	20.3 (8.0)	0.039 (0.015)	296 (66.5)	325 (47.1)	94.3%	--
	25.4 (10.0)	0.047 (0.019)	295 (66.3)	324 (47.0)	94.0%	-0.3%
	30.5 (12.0)	0.056 (0.022)	292 (65.7)	319 (46.3)	92.5%	-1.5%
	35.6 (14.0)	0.065 (0.025)	291 (65.5)	320 (46.5)	92.9%	0.4%
Foam Only	20.3 (8.0)	0.031 (0.012)	226 (50.7)	248 (36.0)	72.0%	--
	25.4 (10.0)	0.038 (0.015)	219 (49.2)	241 (34.9)	69.8%	-3.0%
	30.5 (12.0)	0.045 (0.018)	219 (49.3)	241 (34.9)	69.9%	0.1%
	35.6 (14.0)	0.053 (0.021)	221 (49.7)	243 (35.2)	70.5%	0.8%
No Foam or Adhesive	20.3 (8.0)	0.031 (0.012)	189 (42.5)	208 (30.2)	60.3%	--
	25.4 (10.0)	0.038 (0.015)	180 (40.4)	198 (28.7)	57.4%	-4.9%
	30.5 (12.0)	0.045 (0.018)	176 (39.7)	194 (28.1)	56.3%	-2.0%
	35.6 (14.0)	0.053 (0.021)	176 (39.6)	194 (28.1)	56.2%	-0.1%

*Stress values based on a cross-sectional area of 1.41 in^2 (9.10 cm^2)

Based on the results in Table 7-12, the peak load and stress values generally converged with increasing specimen length for all four different model configurations. The 10 in (25.4 cm) models were determined to be converged for the different models because the percent change in peak force was less than 5% for all models and only 0.3% for both the "Foam and Adhesive" and "Adhesive Only" models. Thus, the peak load and stress values for this specimen length are summarized in Table 7-13 using a model length of 10 in (25.4 cm). The percent increase from the "No Foam or Adhesive" model is also listed in this table. The results indicate the foam and the adhesive both increase the crippling strength of the models. The "Adhesive Only" model has three times the strength increase as the "Foam Only" model. Thus, establishing a more fully connected flange-to-flange attachment has nearly three times the strength gains than using foam

alone. The foam also added more significant strength gains to the columns with no adhesive between the flanges than to the columns with adhesive connecting the flanges. The material model used for foam, however, was linear elastic. Thus, further analysis is required using nonlinear material properties for foam.

Table 7-13: Converged Peak Stress Values for Four Specimen Configurations Based on 10 in (25.4 cm) Length Model

Model Configuration	Converged Peak Load, P_{cr} [kN (kips)]	Converged Peak Stress, σ_{cr} [MPa (ksi)]	Peak Stress / Yield Stress, σ_{cr}/σ_y	Increase from "No Foam or Adhesive" Model
Foam and Adhesive	311 (69.9)	342 (49.6)	99.1%	72.7%
Adhesive Only (No Foam)	295 (66.3)	324 (47.0)	94.0%	63.8%
Foam Only (No Adhesive)	219 (49.2)	241 (34.9)	69.8%	21.7%
No Foam or Adhesive	180 (40.4)	198 (28.7)	57.4%	0.0%

In order to determine the needed strength of the foam for the "Foam Only" model, a band plot of the effective stress of the foam is shown in Figure 7-37 and a band plot of the z-strain is plotted in Figure 7-38. Based on Figure 7-37, the maximum effective stress in the foam was approximately 50 psi (345 kPa). This exceeded the yield strength of the foam which was approximately 12.1 psi (83.6 kPa). Thus, the polystyrene foam used in the experiment would yield under the maximum stress determined from this analysis, limiting its ability to strengthen the columns. Note that the ideal foam used in this configuration would be polyurethane foam in order to achieve optimum bonding with the polyurethane adhesive.

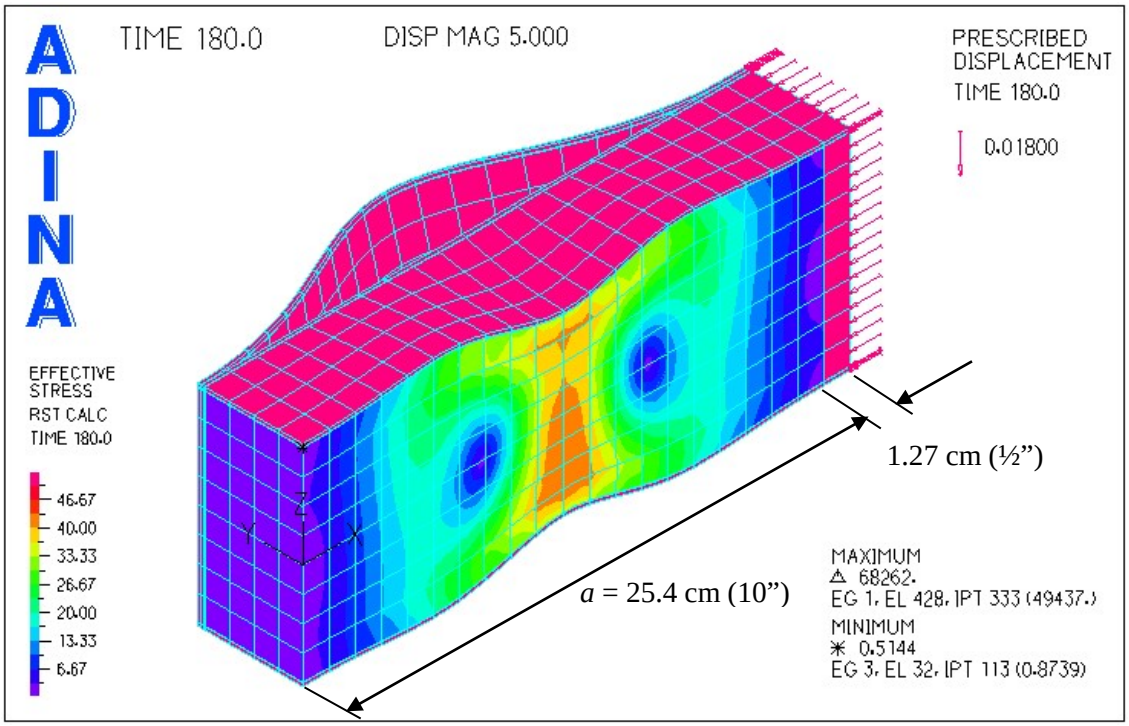

Figure 7-37: Finite Element Band Plot of Effective Stress in Foam for 10 in (25.4 cm) "Foam Only" (No Adhesive) Model

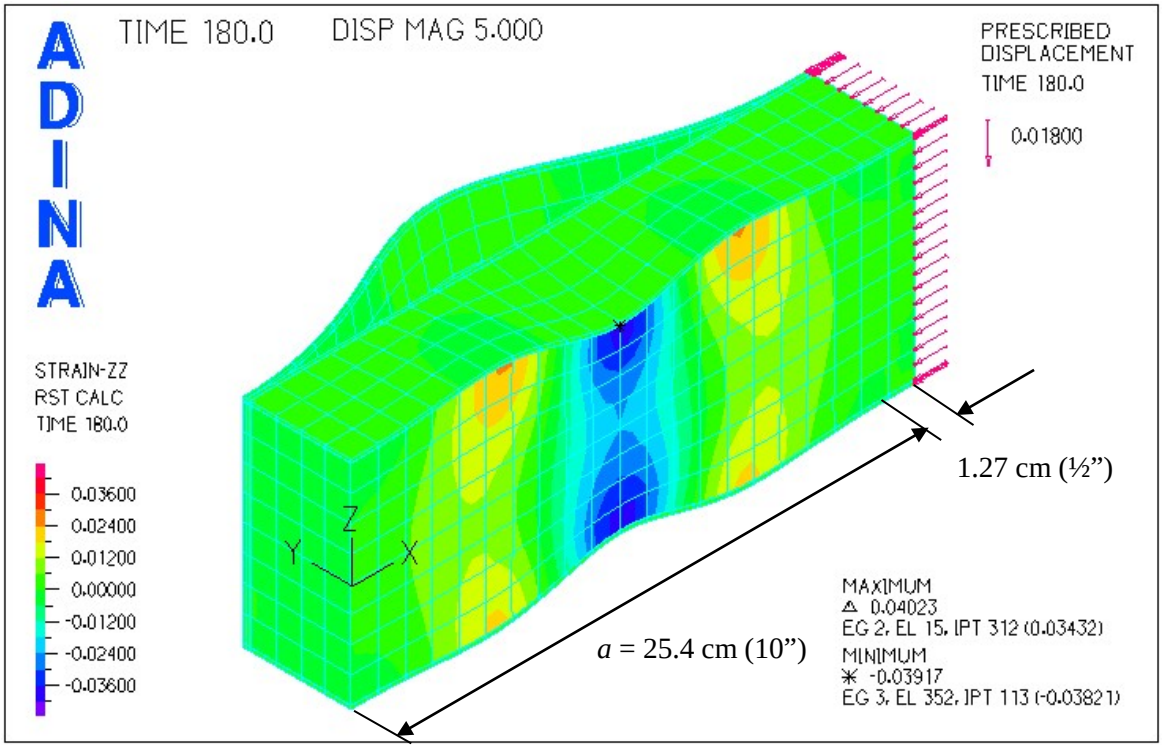

Figure 7-38: Finite Element Band Plot of z-Strain in Foam for 10 in (25.4 cm) "Foam Only" (No Adhesive) Model

7.4.6 Crippling Discussion of Results

The previous subsection showed the different peaks associated with the four models analyzed. This subsection discusses the column behavior on the plate level in order to understand more clearly what is happening at the column level. Figure 7-39 to Figure 7-42 show axial load versus applied displacement for 10 in (25.4 cm) long specimens by flange and web components for "No Foam or Adhesive," "Foam Only," "Adhesive Only," and "No Foam or Adhesive" models, respectively. As indicated previously, the 10 in models were assumed have converged peak loads because the models all had less than a 5% change in results. The peak loads for each configuration are summarized in Table 7-14.

The figures give insight as to why the models had smooth or sharp slopes at the peak loads. For example, compare Figure 7-39 and Figure 7-40. The peak load for the "Foam Only" model was approximately 50 kips (222 kN) or 35.4 ksi (244 MPa). This was approximately 26% higher than the "No Foam or Adhesive" model. This was because the foam delays buckling of the inner flanges and webs. Also, the peak load for the "Foam Only" model is much sharper than the "No Foam or Adhesive" model. By observing the load carried by each plate, it becomes clear that the plates do not all peak with the same applied displacement for the "No Foam or Adhesive" model and the peaks on the plate level are relatively smooth; thus, the sum of the flanges and webs is a smooth load-displacement curve. In contrast, however, all the plates do peak at approximately the same displacement for the "Foam Only" column and the inner U-channel flanges have a sharp peak; thus, the sum of the flanges and webs produces a sharp peak in the load-displacement curve. Note also that the "Foam Only" model has a more defined slope beyond the peak load than the "No Foam or Adhesive" model. This was primarily due to the inner U-channel flanges of the "Foam Only" model exhibiting a definite downward slope beyond

the peak load. The inner flange was delayed against local buckling by the foam until the inner flange buckled (or crippled) suddenly, as opposed to gradually as in the case with the "No Foam or Adhesive" model.

In summary, the results show that the cross-section cripples once the individual plates begin to cripple. The way to prevent crippling of the cross-section is to stabilize against plate crippling. This was accomplished with the foam and/or adhesive in the finite element models as shown in the figures. Additional nonlinear finite element modeling is needed with stress-strain data from material testing, primarily for foam and adhesive, in order to improve the finite element results. The results still indicate, however, that foam and adhesive with the given stiffness values have the potential to stabilize the cross-section, delay local buckling, and thus increase strength against crippling.

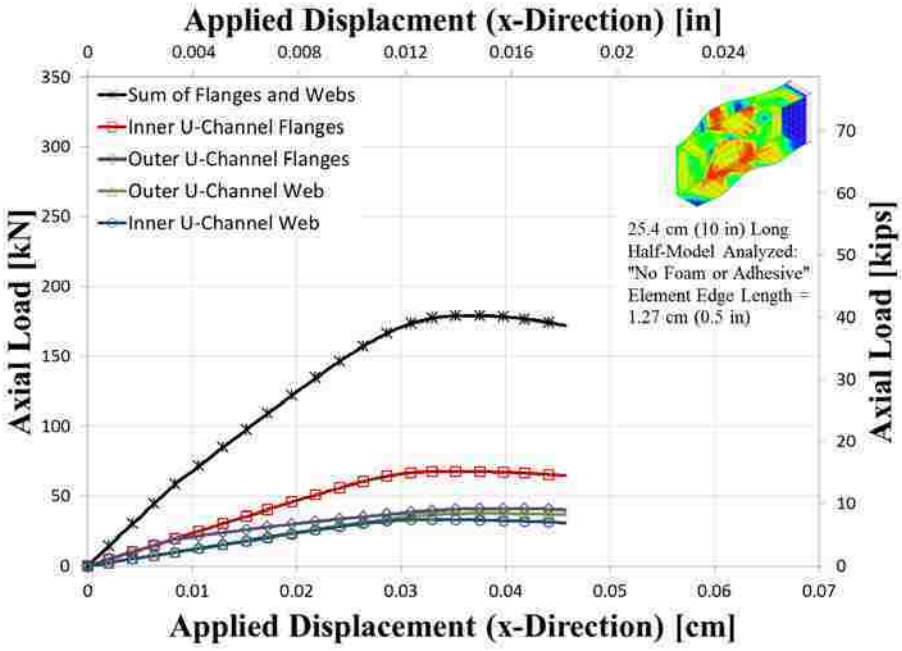

Figure 7-39: Axial Load vs. Applied Displacement (x-Direction) for 10 in (25.4 cm) Long "No Foam or Adhesive" Model Analyzed by Flange and Webs

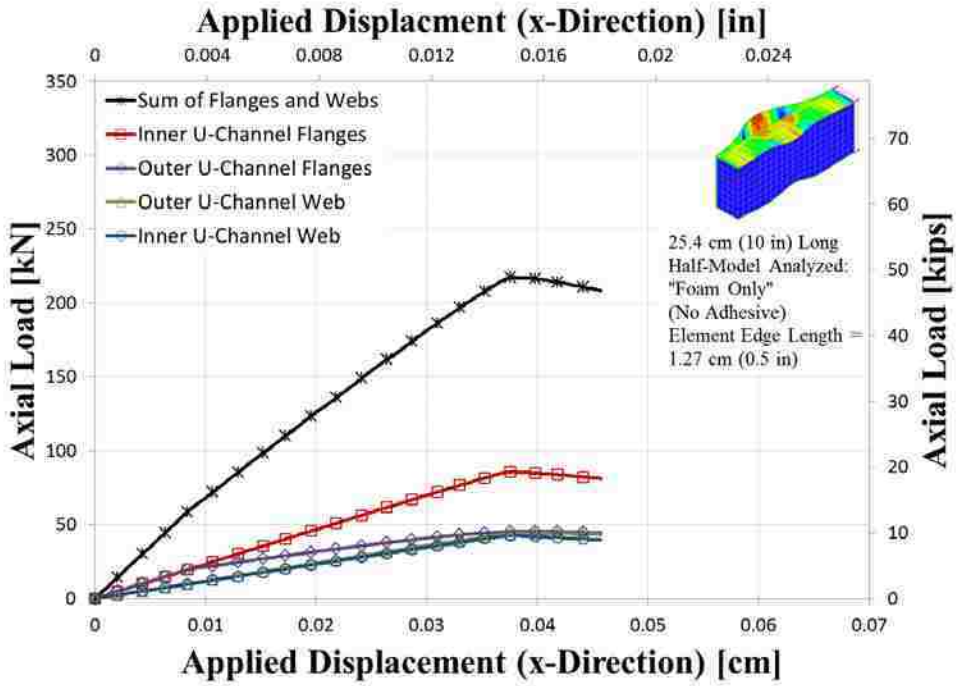

Figure 7-40: Axial Load vs. Applied Displacement (x-Direction) for 10 in (25.4 cm) Long "Foam Only" (No Adhesive) Model Analyzed by Flanges and Webs

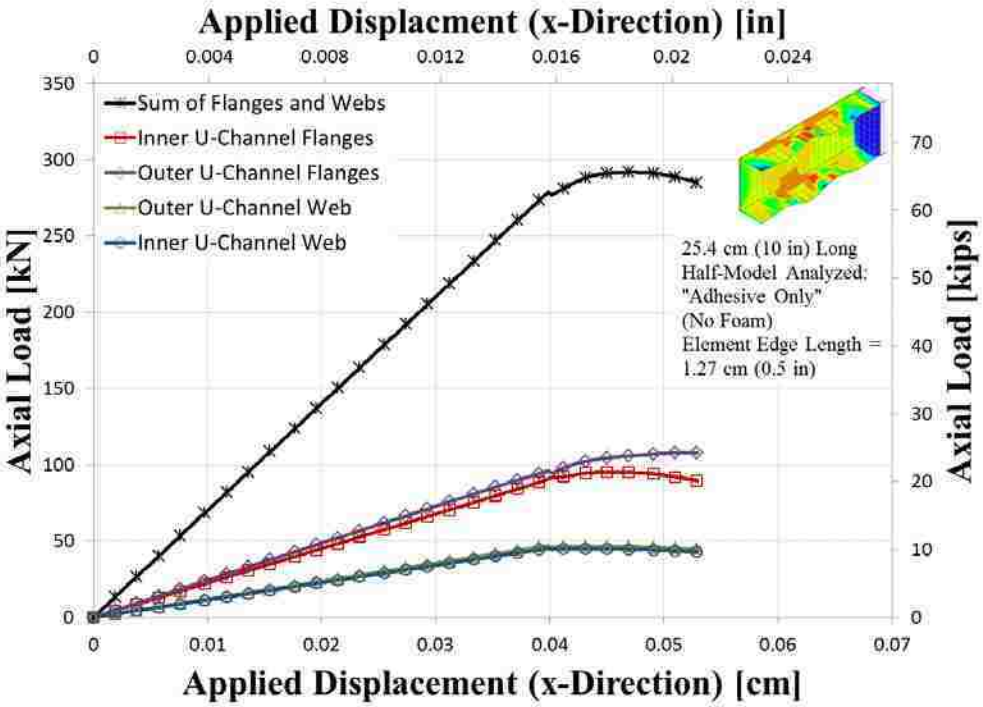

Figure 7-41: Axial Load vs. Applied Displacement (x-Direction) for 10 in (25.4 cm) Long "Adhesive Only" (No Foam) Model Analyzed by Flanges and Webs

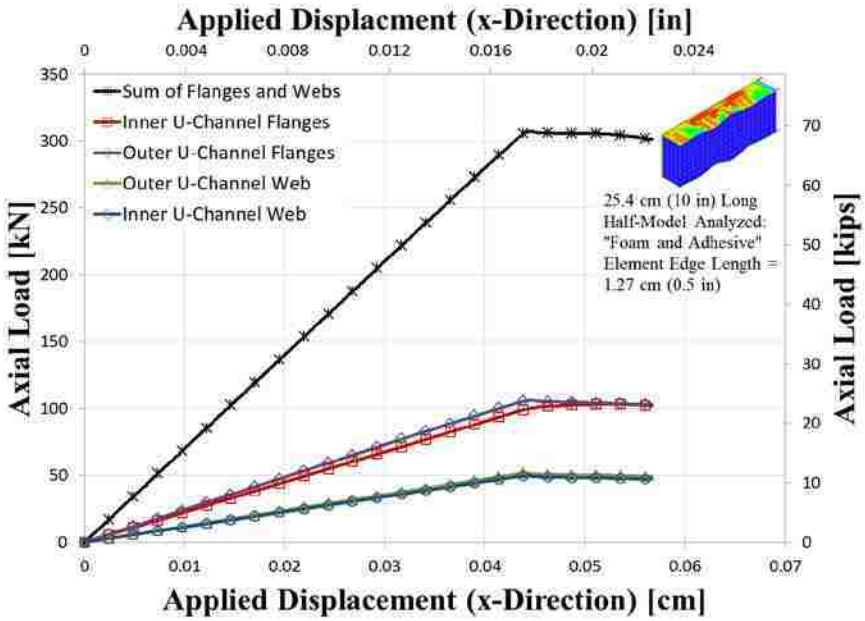

Figure 7-42: Axial Load vs. Applied Displacement (x-Direction) for 10 in (25.4 cm) Long "Foam and Adhesive" Model Analyzed by Flanges and Webs

Table 7-14: Plate Loads at Column Crippling Load Based on Finite Element Analysis

Model Description	Plate Description	Plate Load at Peak Column Load [kN (kips)]	Percent of Peak Column Load
Foam and Adhesive	Inner U-Channel Flanges	100 (22.5)	33.2%
	Outer U-Channel Flanges	106 (23.9)	34.2%
	Outer U-Channel Web	51 (11.5)	16.6%
	Inner U-Channel Web	49 (11.1)	16.0%
	Peak Column Load	Σ = 310 (69.8)	100%
Adhesive Only	Inner U-Channel Flanges	95 (21.4)	32.2%
	Outer U-Channel Flanges	106 (23.8)	36.5%
	Outer U-Channel Web	46 (10.4)	15.9%
	Inner U-Channel Web	45 (10.0)	15.4%
	Peak Column Load	Σ = 295 (66.4)	100%
Foam Only	Inner U-Channel Flanges	86 (19.3)	39.3%
	Outer U-Channel Flanges	45 (10.2)	20.9%
	Outer U-Channel Web	44 (9.8)	20.2%
	Inner U-Channel Web	43 (9.6)	19.6%
	Peak Column Load	Σ = 218 (49.0)	100%
No Foam or Adhesive	Inner U-Channel Flanges	68 (15.2)	37.7%
	Outer U-Channel Flanges	41 (9.1)	22.8%
	Outer U-Channel Web	38 (8.5)	21.0%
	Inner U-Channel Web	33 (7.4)	18.6%
	Peak Column Load	Σ = 180 (40.4)	100%

7.5 Summary

This chapter described the finite element analyses performed to study global buckling, local buckling, and crippling. The findings of the finite element analyses are: (1) increasing the foam stiffness by a factor of approximately 2,000 increases the global buckling capacity by 50%, thus the foam does little to improve global buckling capacity; (2) constraining the local buckling length to 5” (12.7 cm) or less will increase the local buckling stress to be approximately equal to the global buckling stress; (3) a tensile stiffness for the adhesive of approximately 1.0 ksi (6.9 MPa) should be sufficient to delay local buckling up to the global buckling stress for 14’ (4.27

m) long columns, assuming the adhesive is applied uniformly on all contact surfaces; (4) the crippling stress is essentially independent of local buckling length in the range of 10-14" (25.4-35.6 cm) and was predicted to be approximately 57% of the material yield stress for the "No Foam or Adhesive" model, 70% of yield stress for the "Foam Only" model, 94% of yield stress for the "Adhesive Only" model, and 99% of yield stress for the "Foam and Adhesive" model (further testing should be conducted to validate these results; correction factors for material, manufacturing, or testing imperfections may apply); and, finally, (5) the foam inserts with the given stiffness at a yield strength of at least 50 psi (345 kPa) delay buckling of the webs and inner flanges and significantly improve the column crippling stress.

8 DISCUSSION OF RESULTS

This chapter compares the results from the mechanics analysis (Chapter 6) and the finite element analysis (Chapter 7) to the experimental test results (Chapters 4 and 5). Additionally, the mechanics-based local buckling coefficient, the influence of the foam in strengthening the column against global buckling and crippling, and the effect of the flange-to-flange attachment method in strengthening the column against global buckling and crippling are discussed.

8.1 Comparison of Analysis and Test Results

The experimental results and analytical predictions of failure are listed in terms of stress and also as a ratio of material yield stress, 50 ksi (345 MPa), for A653 steel. The experimental results are summarized in Table 8-1; the Southwell-based buckling projections are summarized in Table 8-2; and, the buckling predictions based on the Euler equation and finite element analyses are summarized in Table 8-3. The crippling predictions based on semi-empirical equations analyses are summarized in Table 8-4; and the crippling predictions based on nonlinear finite element analyses are summarized in Table 8-5.

Table 8-3 clarifies that the results for the Euler buckling equation and the finite element analysis are approximately equal. Thus, the Euler buckling equation is sufficient for predicting the global buckling stress of these columns.

Table 8-1: Column Failure Stress from Tests to Failure Compared to Yield Stress

Configuration	Foam	Failure Stress, σ_{cr} [MPa (ksi)]	Ratio of Yield Stress, σ_{cr} / σ_y
Adhesive-Only	Yes	132 (19.2)	38.4%
Adhesive and Welds	Yes	126 (18.3)	36.6%
Adhesive and Screws	Yes	133 (19.3)	38.6%
Adhesive-No-Foam	No	123 (17.9)	35.8%
Average		129 (18.7)	37.4%
Standard Deviation		4.9 (0.7) 3.7%	1.4%

Table 8-2: Column Southwell-Based Buckling Stress Projections from Tests to Failure Compared to Yield Stress

Configuration	Foam	Tests to Failure	
		Projected Buckling Stress, σ_{cr} [MPa (ksi)]	Ratio of Yield Stress, σ_{cr} / σ_y
Adhesive-Only	Yes	--	--
Adhesive and Welds	Yes	163 (23.7)	47.4%
Adhesive and Screws	Yes	151 (21.9)	43.8%
Adhesive No-Foam	No	128 (18.6)	37.2%
Average		147 (21.4)	42.8%
Standard Deviation		17.7 (2.6) 12.0%	5.1%

Table 8-3: Column Mechanics-Based and Finite Element Global Buckling Stress Predictions Compared to Yield Stress

Method	Global Buckling Stress, σ_{cr} [MPa (ksi)]	Ratio of Yield Stress, σ_{cr} / σ_y
Euler Buckling (Thin-Walled)	150 (21.7)	43.4%
Euler Buckling (Normal)	147 (21.3)	42.6%
Finite Element Analysis (Thin-Walled)	158 (22.9)	45.8%
Finite Element Analysis (Normal)	146 (21.2)	42.4%
Average	150 (21.8)	43.6%
Standard Deviation	5.4 (0.8) 3.6%	1.6%

Table 8-4: Column Crippling Stress Predictions Based on Semi-Empirical Equations and SSSF Boundary Conditions for the Inner and Outer Flanges Compared to Yield Stress

Method	Crippling Stress, σ_{cc} [MPa (ksi)]	Ratio of Yield Stress, σ_{cc} / σ_y
Gerard (Equation 6-7)	129 (18.6)	37.2%
Boeing (Equation 6-8)	168 (24.3)	48.6%
Gerard (Equation 6-9)	149 (21.6)	43.2%
Average	148 (21.5)	43.0%
Standard Deviation	19.7 (2.9) 13.3%	5.7%

Table 8-5: Column Finite Element Crippling Stress Predictions Compared to Yield Stress

Model Description	Crippling Stress, σ_{cc} [MPa (ksi)]	Ratio of Yield Stress, σ_{cc} / σ_y
Foam and Adhesive	342 (49.6)	99.1%
Adhesive Only	324 (47.0)	94.0%
Foam Only	241 (34.9)	69.8%
No Foam or Adhesive	198 (28.7)	57.4%

Table 8-5 shows that the crippling predictions based on finite element analysis are significantly higher than the predictions based on the semi-empirical equations discussed in Chapter 6. This indicates that the semi-empirical equations have built-in adjustment factors which correct for the inherent material imperfections and loading eccentricities in any experiment. Given perfect 10-14" (25.4-35.6 cm) long test specimens and perfectly concentric loading, the samples should fail under the stress provided in this table. More testing would help indicate which crippling constants most closely predict actual crippling stress.

The averaged failure and buckling stress values are summarized in Table 8-6. The tables show that the averaged failure stress value for four column configurations was 37.4% of yield stress. The averaged Southwell projection values from the tests to 20 kips and from tests to

failure predicted a buckling stress were 32.0% of yield stress and 42.8% of yield stress, respectively. The Euler buckling equation and finite element global buckling analysis predicted an average buckling stress of 43.6% of yield stress. The semi-empirical equations for crippling discussed in Chapter 6 predicted an average crippling stress of 46.0% of yield stress. The finite element crippling analysis predicted a converged stress value of 56.2% of yield stress and 70.4% of yield stress for models with no foam and models with foam, respectively.

Table 8-6: Summary of Failure and Buckling Stress Values Compared to Yield Stress

Averaged Values	Critical Stress, σ_{cr} [MPa (ksi)]	Ratio of Yield Stress, σ_{cr} / σ_y	Ratio of Experiment
Experiment (4 Samples)	129 (18.7)	37.4%	100
Southwell Projections – Tests to Failure	147 (21.4)	42.8%	115
Semi-Empirical Crippling Predictions	148 (21.5)	43.0%	115
Global Buckling Predictions	150 (21.8)	43.6%	117
Finite Element Crippling with No Foam	194 (28.1)	56.2%	150
Finite Element Crippling with Foam	243 (35.2)	70.4%	188

To summarize, the column global buckling strength is approximately 43.6% of yield stress. The columns failed at approximately 86% of this stress value. Because the columns failed inelastically due to crippling of the cross-section prior to global buckling, the conclusion can be drawn that imperfections in the structure and/or eccentricities in the loading may have caused the columns to fail prematurely. Thus, by improving the column manufacturing and by assuring the eccentricities in the loading are minimized, the column strength could improve by up to 16%.

In order to achieve the crippling results predicted by the model with foam, the foam must have uniform adhesion with all inner column surfaces. The foam must also have a minimum tensile and compression strength of approximately 50 psi (345 kPa), assuming that the foam

stiffness is 1,200 psi (8,274 kPa). These results need to be validated by testing 10-14" (25.4-35.6 cm) long specimens.

8.2 Local Buckling Coefficient

The local buckling coefficient values, *k*, based on finite element analyses as a function of the aspect ratios of the flange-flange attachment is compared to the predicted local buckling coefficient from mechanics-based analysis results are listed in Table 8-7 and are shown in Figure 8-1. The local buckling coefficient is approximately 40% higher based on the finite element analysis than the local buckling coefficient from mechanics analysis based on simply-supported boundary conditions on three sides and free on one side (SSSF). The local buckling coefficient (Megson 2010, p.2 97) based on clamped boundary conditions on three sides and free on one side (CCCF) is approximately equal to the prediction based on the finite element analysis. That is because the buckled outer flanges of the column have the same boundary conditions as fixed on the ends and one side and free on one side. Thus, the plate buckling equation from mechanics analysis (Equation 6-3) may be used for estimating the local buckling value of the outer column flanges. The SSSF-based buckling coefficient will predict a conservative value for the buckling capacity. The CCCF-based buckling coefficient will predict a higher value for the buckling capacity, which agrees more closely with the numerical predictions.

Table 8-7: Local Buckling Coefficient Comparison Between FEA and Mechanics

Flange Aspect Ratio, a / b [no units]	Local Buckling Coefficient, k [no units]				
	Finite Element Analysis (FEA)	Clamped Three Sides, Free One (CCCF)	FEA as a Percent of CCCF	Simply-Supported Three Sides, Free One (SSSF)	FEA as a Percent of SSSF
1.00	5.56	4.40	26.5%	3.80	46.4%
1.25	3.73	3.40	9.7%	2.60	38.1%
1.50	2.81	2.80	0.5%	2.00	34.0%
1.75	2.30	2.25	2.4%	1.65	35.6%
2.00	2.00	2.00	-0.1%	1.50	37.8%
2.25	1.83	1.80	1.6%	1.40	40.7%
2.50	1.73	1.70	1.5%	1.35	38.0%
2.75	1.67	1.65	1.4%	1.30	39.4%
3.00	1.64	1.60	2.8%	1.28	43.0%

The local buckling coefficient, *k*, was back-calculated for the results from the finite element analysis using the formula:

$$k = \frac{\sigma_{cr} 12(1-\nu^2)}{\eta \pi^2 E_s} \left(\frac{b}{t}\right)^2 \quad \textbf{(8-1)}$$

where σ_{cr} is the local buckling stress which is determined using finite element analysis, υ is Poisson's ratio (equal to 0.3 for steel), b is the plate width, t is the plate thickness, η is the plasticity correction value (equal to 1.0 for the linear elastic range), and E_s is the steel modulus of elasticity. This equation is normally expressed in terms of buckling stress, σ_{cr}, (see Equation 6-3). Performing additional local buckling analysis on a model with no foam would useful for comparison.

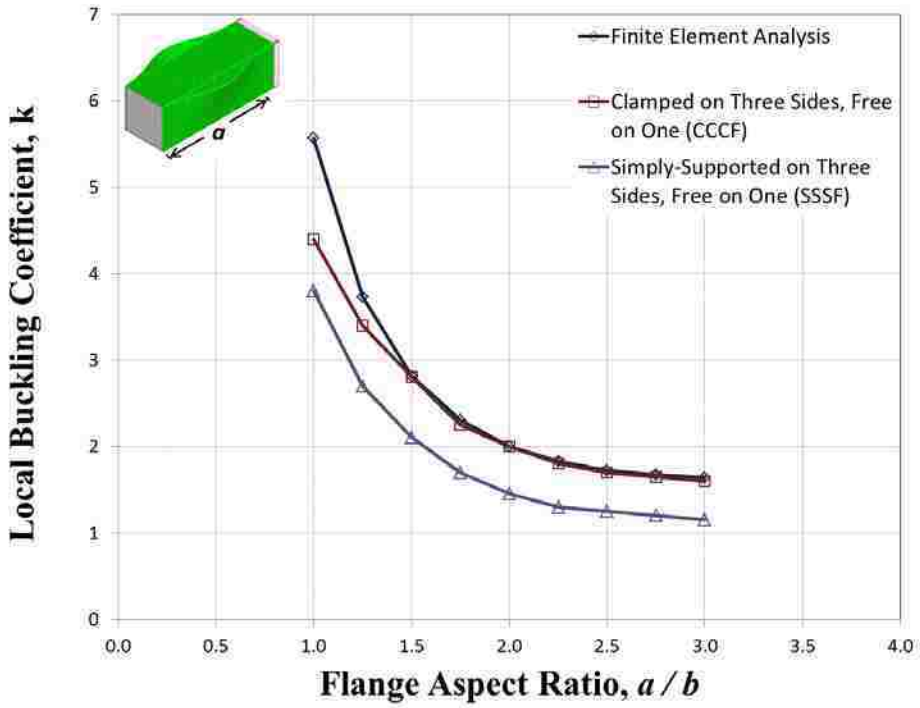

Figure 8-1: Local Buckling Coefficient vs. Flange Aspect Ratio of Flange-Flange Attachment

8.3 Influence of Foam on Column Compression Strength

Experimental results showed that the "Adhesive-No-Foam" column failed nearly two standard deviations below the average failure stress for the three other columns (see Table 5-14). This indicates that the foam may have provided additional stability against local buckling and crippling, as predicted by the finite element analysis. More test samples of each configuration are needed to provide statistical reliability for this claim.

Nonlinear finite element analysis indicates that the foam will, however, improve crippling stress with the given material stiffness, 1,200 psi (8,270 kPa). Using a linear elastic foam material model, the crippling strength improved by 26%. The analysis indicated, however, that the required yield strength for crippling strength improvement was approximately 50 psi (345 kPa).

Both the Euler equation and finite element analysis confirm that the foam increases the global buckling strength at a rate of 0.003% for every doubling of foam stiffness (see Figure 6-4 and Figure 7-9). Thus, increasing the foam stiffness is not an efficient means of increasing the buckling strength. Also, the Euler buckling equation is sufficient for predicting the effect of global buckling for the foam.

8.4 Influence of Flange-to-Flange Attachment

The purpose of attaching the flanges is to delay local buckling and thus delay the onset of crippling. The mechanics-based analysis shows that a fully-connected flange-to-flange attachment will increase the crippling stress above the global buckling stress for 14’ (4.27 m) long columns. Finite element analysis shows that a fully-connected flange attachment will increase the local buckling stress above the global buckling stress for 14’ (4.27 m) long columns for any local buckling length by uniformly applying adhesive with a stiffness of 0.93 ksi (6.4 MPa). In addition to fully-connected flange-to-flange attachment, the flanges may be pinned together using periodic short-welds or screws. Finite element analysis shows that pinning the flanges together at a spacing of 5” (12.7 cm) or less will increase the local buckling stress to exceed the global buckling stress for 14’ (4.27 m) long columns.

8.5 Comparison of Finite Element and Mechanics-Based Plate Crippling Loads

The results from finite element and mechanics-based crippling analysis for flange and web crippling loads are shown in Figure 8-2 to Figure 8-5 for 10 in (25.4 cm) models of “Foam and Adhesive,” “Adhesive Only,” “Foam Only,” and “No Foam or Adhesive,” respectively. The flange and web crippling loads are compared to the finite element crippling loads in Table 8-8 to

Table 8-9 based on the Gerard method (Equation 6-7) and the Boeing method (Equation 6-8), respectively (see also Table 7-14). Note that the mechanics-based crippling results were the same for both the "Foam and Adhesive" and "Adhesive Only" finite element models because the boundary conditions parameters were identical for these in the mechanics analysis. Note also that the mechanics-based crippling results were the same for the two finite element models without adhesive between the flanges ("Foam Only" and "No Foam or Adhesive") because the boundary conditions parameters were identical for these in the mechanics analysis.

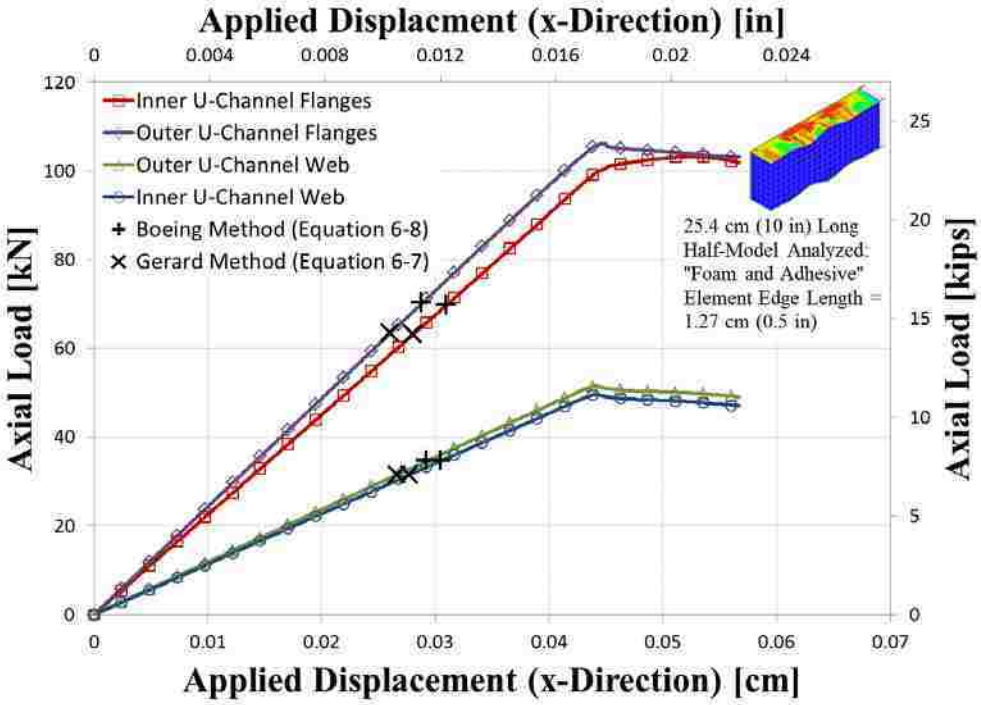

Figure 8-2: Comparison of Results from Finite Element and Mechanics-Based Crippling Analysis for 10 in (25.4 cm) "Foam and Adhesive" Model by Flanges and Webs

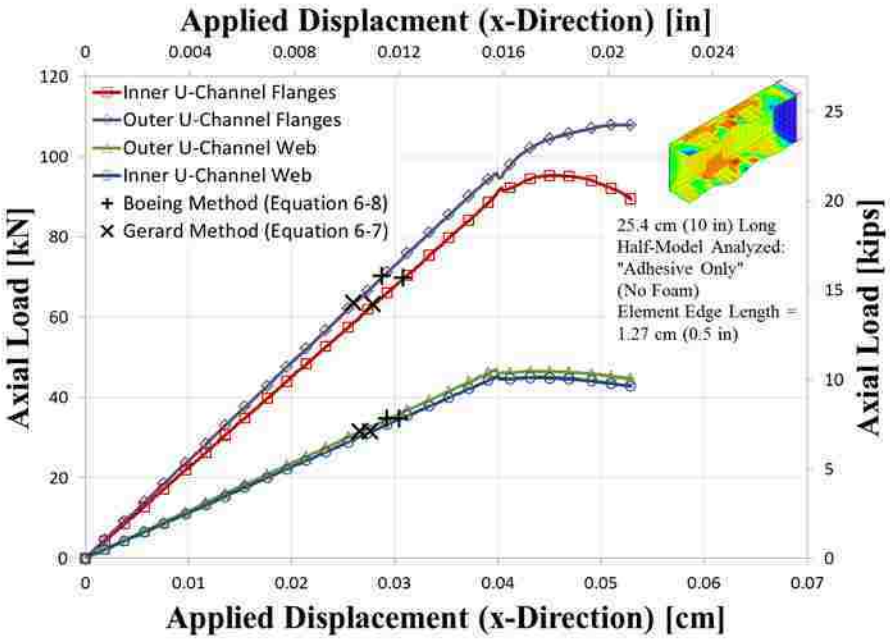

Figure 8-3: Comparison of Results from Finite Element and Mechanics-Based Crippling Analysis for 10 in (25.4 cm) "Adhesive Only" Model by Flanges and Webs

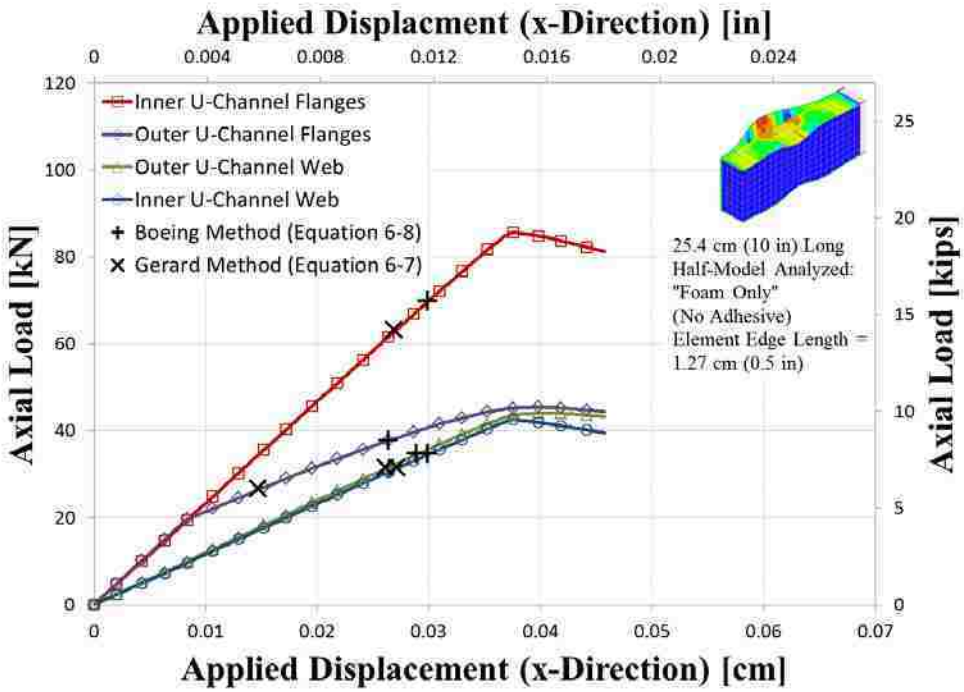

Figure 8-4: Comparison of Results from Finite Element and Mechanics-Based Crippling Analysis for 10 in (25.4 cm) "Foam Only" Model by Flanges and Webs

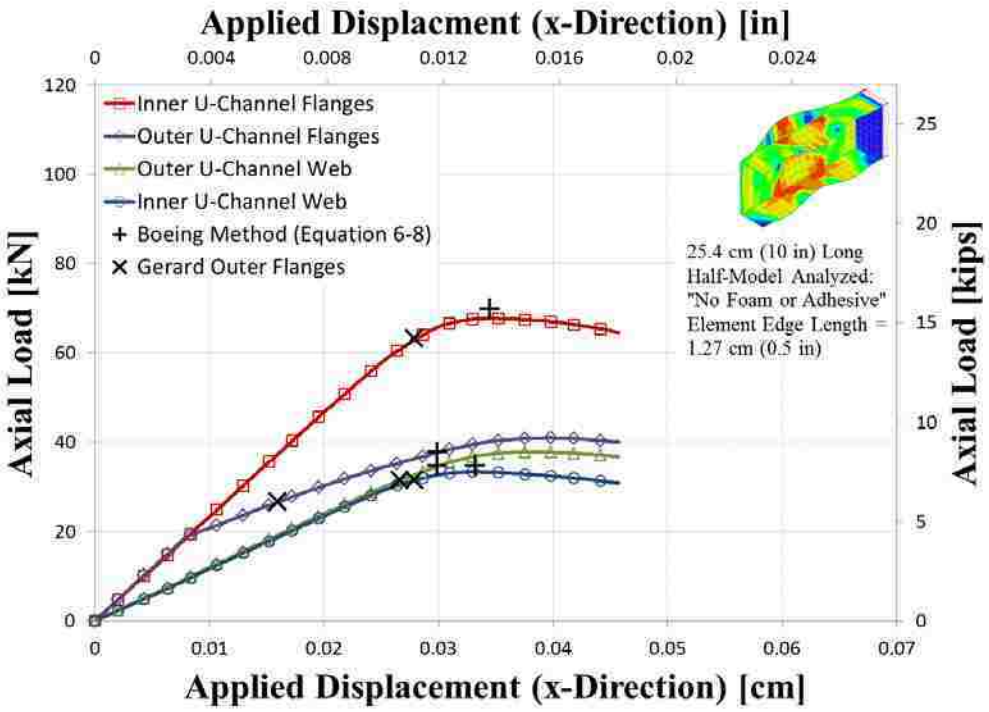

Figure 8-5: Comparison of Results from Finite Element and Mechanics-Based Crippling Analysis for 10 in (25.4 cm) "No Foam or Adhesive" Model by Flanges and Webs

Table 8-8: Crippling Load Based on the Gerard Method (Equation 6-7) Compared to Finite Element Crippling Loads

Outer Flange, Inner Flange Attachment	Corresponding FEA Model	Plate Description	Plate Crippling Load [kN (kips)]	Percent of FEA Crippling Load
SSSS, SSSS	Foam and Adhesive	Inner U-Channel Flanges	63.1 (14.2)	63%
		Outer U-Channel Flanges	63.4 (14.3)	60%
		Outer U-Channel Web	31.6 (7.1)	62%
		Inner U-Channel Web	31.6 (7.1)	64%
			Σ = 190 (42.6)	Ave = 62%
SSSS, SSSS	Adhesive Only	Inner U-Channel Flanges	63.1 (14.2)	66%
		Outer U-Channel Flanges	63.4 (14.3)	60%
		Outer U-Channel Web	31.6 (7.1)	68%
		Inner U-Channel Web	31.6 (7.1)	71%
			Σ = 190 (42.6)	Ave = 66%
SSSF, SSSS	Foam Only	Inner U-Channel Flanges	63.1 (14.2)	74%
		Outer U-Channel Flanges	26.8 (6.0)	59%
		Outer U-Channel Web	31.6 (7.1)	72%
		Inner U-Channel Web	31.6 (7.1)	74%
			Σ = 153 (34.4)	Ave = 70%
SSSF, SSSS	No Foam or Adhesive	Inner U-Channel Flanges	63.1 (14.2)	93%
		Outer U-Channel Flanges	26.8 (6.0)	66%
		Outer U-Channel Web	31.6 (7.1)	84%
		Inner U-Channel Web	31.6 (7.1)	96%
			Σ = 153 (34.4)	Ave = 85%
SSSF, SSSF	n/a	Inner U-Channel Flanges	26.7 (6.0)	n/a
		Outer U-Channel Flanges	26.8 (6.0)	
		Outer U-Channel Web	31.6 (7.1)	
		Inner U-Channel Web	31.6 (7.1)	
			Σ = 117 (26.2)	

Table 8-9: Crippling Load Based on the Boeing Method (Equation 6-8) Compared to Finite Element Crippling Loads

Outer Flange, Inner Flange Attachment	Corresponding FEA Model	Plate Description	Plate Crippling Load [kN (kips)]	Percent of FEA Crippling Load
SSSS, SSSS	Foam and Adhesive	Inner U-Channel Flanges	69.7 (15.7)	70%
		Outer U-Channel Flanges	70.2 (15.8)	66%
		Outer U-Channel Web	34.8 (7.8)	68%
		Inner U-Channel Web	34.8 (7.8)	70%
			Σ = 210 (47.1)	Ave = 68%
SSSS, SSSS	Adhesive Only	Inner U-Channel Flanges	69.7 (15.7)	73%
		Outer U-Channel Flanges	70.2 (15.8)	66%
		Outer U-Channel Web	34.8 (7.8)	75%
		Inner U-Channel Web	34.8 (7.8)	78%
			Σ = 210 (47.1)	Ave = 73%
SSSF, SSSS	Foam Only	Inner U-Channel Flanges	69.7 (15.7)	81%
		Outer U-Channel Flanges	37.6 (8.5)	83%
		Outer U-Channel Web	34.8 (7.8)	80%
		Inner U-Channel Web	34.8 (7.8)	81%
			Σ = 177 (39.8)	Ave = 81%
SSSF, SSSS	No Foam or Adhesive	Inner U-Channel Flanges	69.7 (15.7)	103%
		Outer U-Channel Flanges	37.6 (8.5)	93%
		Outer U-Channel Web	34.8 (7.8)	92%
		Inner U-Channel Web	34.8 (7.8)	105%
			Σ = 177 (39.8)	Ave = 98%
SSSF, SSSF	n/a	Inner U-Channel Flanges	37.3 (8.4)	n/a
		Outer U-Channel Flanges	37.6 (8.5)	
		Outer U-Channel Web	34.8 (7.8)	
		Inner U-Channel Web	34.8 (7.8)	
			Σ = 145 (32.5)	

For the "Foam and Adhesive" model, the Gerard and Boeing methods predicted approximately 62% and 68%, respectively, of the finite element results. For the "Adhesive Only" model, the Gerard and Boeing methods predicted approximately 66% and 73%, respectively, of the finite element results. For the "Foam Only" model, the Gerard and Boeing methods predicted approximately 70% and 81%, respectively, of the finite element results. For the "No Foam or Adhesive" model, the Gerard and Boeing methods predicted approximately

85% and 98%, respectively, of the finite element results. Based on these results, both the Gerard and Boeing equations have built-in parameters to account for material imperfections, as well as eccentricities in the loading. That is why the mechanics-based semi-empirical results were lower than the finite element results in every case. The Gerard method predicted slightly lower values than the Boeing method in every case. Thus, the Gerard method used slightly more conservative parameters than the Boeing method. Finally, the difference between the mechanics-based predictions and the finite element analysis for crippling predictions was much larger for models with adhesive (fully attached flanges) than for models without (flanges with one free end). This may be an indication that in the laboratory the adhesive does not perform as well as in numerical analysis. More testing will help to clarify this point, as well as additional finite element analysis utilizing nonlinear material stress-strain curves for the adhesive.

9 CONCLUSION

The testing and analysis of 14-foot long foam-filled steel columns has been presented and discussed in this thesis. This chapter summarizes conclusions, contributions to the state-of-the-art, and recommended future work.

9.1 Conclusions

The average value for column failure for the four configurations was approximately 14% below the Euler buckling stress prediction; 19% below the crippling stress prediction based on an average of three semi-empirical equations; and 33% below the crippling stress prediction based on finite element analysis. Although the predictions for crippling stress exceed the global buckling stress prediction, the tests showed that the columns crippled prior to buckling globally. Thus, improvements in manufacturing and in loading must be made in order to ensure that global buckling controls failure.

The most beneficial modification to the design is to fully-connect the inner and outer flanges. Based on the crippling analysis, establishing a more fully connected flange-to-flange attachment has nearly three times the strength gains than using foam alone. This will improve the local buckling stress to above the global buckling stress for 14’ (4.27 m) long columns. This may be achieved by either uniformly applying adhesive with an elastic modulus of at least 0.93 ksi (6.4 MPa) or by spacing short-welds or screws at no more than 5” (12.7 cm) apart.

The results show that a yield strength of at least 50 psi (345 kPa) for the foam is required in order to obtain the predicted results. Using foam alone with no adhesive between the flanges will improve the crippling capacity by as much as 21% if the tensile and compressive yield strengths meet this specification. The foam used in the experiment did not exceed this strength and would therefore yield prior to the peak load. The crippling results still indicate, however, that foam and adhesive with the given stiffness values have the potential to stabilize the cross-section, delay local buckling, and thus increase strength against crippling.

The mechanics-based results were much lower than the finite element results. Both the Gerard method (Equation 6-7) and Boeing method (Equation 6-8) use parameters which reduced the numerically predicted crippling stress to match experimental results. In this analysis, the Gerard method used slightly more conservative parameters than the Boeing method. More testing and additional finite element analysis utilizing nonlinear material stress-strain curves for the adhesive are needed.

Finally, simple hand-calculations give results for crippling and buckling which are as accurate or almost as accurate as complex finite element analysis when compared to the test results. The finite element analysis is useful, however, for isolating and studying a wide range of variables such as foam stiffness, adhesive stiffness, or local buckling length. A greater quantity of test results will help to validate these results in the future.

9.2 Contributions

The original features and contributions to the State-of-the-Art of this thesis include:

- The study of thin-walled steel columns with foam inserts.
- Experimental test results of foam-filled, two-piece steel columns.

- Mechanics-based parametric study showing how steel thickness affects column crippling stress.
- Finite-element-based parametric study showing effect of adhesive stiffness values in flange-to-flange attachment on local buckling stress.
- Linear and nonlinear finite element analysis for buckling and crippling of foam-filled steel columns.

9.3 Recommended Future Work

It is recommended that several additional full-scale tests of each configuration be performed in order to establish statistical reliability. Some manufacturing improvements should be made including properly sizing the inner channel to fit inside the outer channel with a tolerance of approximately 0.01” (0.025 cm), cutting the foam inserts to fit with a similar tolerance, applying adhesive uniformly throughout all interior contact surfaces, and spacing screws or short-welds uniformly along the length of the column, preferably not much further apart than the width of the column. Using standardized shapes as part of the design should also be investigated. It is also recommended to use polyurethane foam to bond well with the polyurethane adhesive. The manufacturing improvements consist of precision in dimensioning, cutting and aligning the inner and outer U-channels, uniform application of adhesive, precision in cutting the foam, and precision in uniformly bonding the foam to the inner column surfaces. The loading improvements consist of minimizing loading eccentricities by carefully aligning the actuator, test specimen, and reaction frame; removing gravity supports; and testing columns with the same orientation with respect to the floor (if tested parallel with the floor).

Based on the finite element analyses, it is recommended that several samples of 5” (12.3 cm) to 12” (30.5 cm) length be tested in order to further study local buckling and crippling. Testing should be performed on 10-14” (25.4-35.6 cm) long specimens in order to validate the finite element crippling predictions. Nonlinear finite element modeling is needed with component material stress-strain data based on material testing in order to improve the results. Finally, additional finite element analysis is recommended to understand how changing the steel thickness affects the column crippling strength.

REFERENCES

AFM Corporation (2011). "Physical Properties of Foam-Control EPS Geofoam." EPS Geofoam Technical Properties, <http://www.geofoam.com/technical.asp>. (June 28, 2012).

Aviles, F. (2005). "Local buckling and debond propagation in sandwich columns and panels," dissertation, presented to Florida Atlantic University at Boca Raton, FL, in partial fulfillment of the requirements for the degree of Doctor of Philosophy.

Bathe, K. J. 2009. *ADINA Theory and Modeling Guide.* ADINA R & D, Inc., U.S.A.

Bi, J., Fang, H., Wang, Q., and Ren, X. (2010). "Modeling and optimization of foam-filled thin-walled columns for crashworthiness designs." Finite Elements in Analysis and Design, 46(9), 698-709.

Bleich, F. (1952). *Buckling Strength of Metal Structures*. McGraw-Hill, New York, U.S.A.

Bruhn, E. F. (1973). *Analysis and Design of Flight Vehicle Structures*. Jacobs Publishing, Inc., U.S.A.

CE 523 (2011). "Design and Analysis of Aircraft Structures." Class NotesBrigham Young University, Provo, UT.

Curtis, H. D. (1997). *Fundamentals of Aircraft Structural Analysis*. WCB/McGraw-Hill, U.S.A.

Dean, G., and Crocker, L. (2001). "The Use of Finite Element Methods for Design with Adhesives." NPL Measurement Good Practice Guide, 48, ed., National Physical Laboratory, Middlesex, UK.

Euler, L. (1759). "E238 -- Sur la force des colonnes." Memoires de l'academie des sciences de Berlin, 13, 252-282.

Gerard, G. (1958). "The crippling strength of compression elements." J. Aeron. Sci., 25(1), 37-52.

Gerard, G. (1962). *Introduction to Structural Stability Theory.* McGraw-Hill, U.S.A.

Gere, J. M. (2006). *Mechanics of Materials.* Russell-Hibbeler, U.S.A.

Gibson, L. J. (1989). "Modelling the Mechanical Behavior of Cellular Materials." Journal of Materials Science and Engineering, 110, 1-36.

Global Building Systems Inc. (2011). "Advantages of the Step-Tech™ System." GBSI-Step, <http://www.gbsi-step.com/>. (June 13, 2012).

Hedman-Petursson, E. (2001). "Column Buckling with Restraint from Sandwich Wall Elements," thesis, presented to Luleå University of Technology at Luleå, Sweden, in partial fulfillment of the requirements for the degree of Doctor of Philosophy.

Ji, W. (2008). "Static and dynamic response of a sandwich structure under axial compression," thesis, presented to University of Michigan, at Ann Arbor, MI, in partial fulfillment of the requirements for the degree of Doctor of Philosophy.

Ko, W. L. (1987). "Accuracies of Southwell and Force/Stiffness Methods in the Prediction of Buckling Strength of Hypersonic Aircraft Wing Tubular Panels." *Technical Memorandum 88295,* NASA, U.S.A.

Kollár, L. P. (2003). "Local Buckling of FRP Composite Structural Members with Open and Closed Cross Sections." Journal of Structural Engineering, 129, 1503-1513.

Lee, L. S., Ali, A., Sanuddin, A. B., and Afshar, R. (2010). "Simulation and Experimental Work on a Thin-Walled Structure Under Crushing " Journal of Failure Analysis and Prevention, 10(2), 143-151.

Limited Blue Scope Steel (2005). "Zincform ASTM A653 Grade 50/1." Brochures, <http://www.bluescopesteel.ae/assets/literature/brochures/ZINCFORM-ASTM-A653-50-Rev-01.pdf>. (June 23, 2012).

Megson, T. H. G. (2010). *An Introduction to Aircraft Structural Analysis*. Elsevier Ltd., Burlington, MA.

Mirfendereski, L., Salimi, M., and Ziaei-Rad, S. (2008). "Parametric study and numerical analysis of empty and foam-filled thin-walled tubes under static and dynamic loadings." International Journal of Mechanical Sciences, 50(6), 1042-1057.

Novatek, Inc. (2012). "NewVistas Principles." NewVistas Lab, <https://www.novatek.com/labs-detail.php?projectID=9>. (June 13, 2012).

Reany, J. (2009). "Corrugated skin composite sandwich panels," dissertation, presented to Lehigh University, at Bethlehem, PA, in partial fulfillment of the requirements for the degree of Doctor of Philosophy.

Reid, S. R., and Reddy, T. Y. (1986). "Static and dynamic crushing of tapered sheet metal tubes of rectangular cross-section." International Journal of Mechanical Sciences, 28(9), 623-637.

Rivello, R. M. (1969). *Theory and Analysis of Flight Structures.* McGraw-Hill, U.S.A.

Rowlett, R. (2010). "Sheet Metal Thickness Gauges." How Many? A Dictionary of Units of Measurement, <http://www.unc.edu/~rowlett/units/scales/sheetmetal.html>. (June 14, 2012).

Sharaf, T., Shawkat, W., and Fam, A. (2010). "Structural Performance of Sandwich Wall Panels with Different Foam Core Densities in One-way Bending." Journal of Composite Materials, 44(19), 2249-2263.

Smith, W. F., Hashemi, J. (2010). *Foundations of Materials Science and Engineering.* McGraw-Hill, U.S.A.

Southwell, R. V. (1932). "On the Analysis of Experimental Observations in Problems of Elastic Stability." Proceedings of the Royal Society, 135(Series A), 601-616.

Steel Stud Manufacturers Association (2011). "SSMA Product Technical Information." Technical Library, <http://www.ssma.com/filebin/pdf/SSMA_Product_Technical_Info_Catalog_2011_FINAL.pdf>. (June 27, 2012).

The Masonry Society (2010). *Masonry Designers' Guide.* The Masonry Society, U.S.A.

Timoshenko, S. P., and Gere, J. M. (1961). *Theory of Elastic Stability.* McGraw-Hill, U.S.A.

Tons and Tons (2007). "Galvannealed Steel Sheet." Product Summary, <http://tonsandtons.com/PDF/Featured/Featured_Product_Galvannealed.pdf>. (June 23, 2012).

Trudeau, P. A. (2011). "Analysis and optimization of a new method for creating sandwich composites using polyurethane foam," thesis, presented to École Polytechnique de Montréal, at Montreal, Canada, in partial fulfillment of the requirements for the degree of Masters of Science.

Walls, J. C. (1969). "Interaction of Crippling and Torsional-Flexural Instability for Centrally Loaded Columns." *Report No. 61287,* NACA, U.S.A.

APPENDIX A. ADHESIVE SHEAR TEST

Figure A-1 shows the shear load versus deflection for a single test of Isogrip 4005D polyurethane adhesive in shear. Figure A-2 shows the average shear stress versus strain for the same sample of polyurethane adhesive in shear. The conversion from load to stress uses an area of 18.5 in^2 (119 cm^2). The shear modulus, *G*, was converted to elastic modulus, *E*, using the well-known conversion formula:

$$E = 2G(1 + \nu) \quad \textbf{(A-1)}$$

The results are listed in Table A-1.

Table A-1: Shear Modulus and Elastic Modulus Results for Polyurethane Adhesive

Material Description	Shear Modulus, *G* [MPa (ksi)]	Poisson's Ratio, *v* [no units]	Elastic Modulus, *E* [MPa (ksi)]
Polyurethane Adhesive	783 (113)	0.4	2,035 (295)

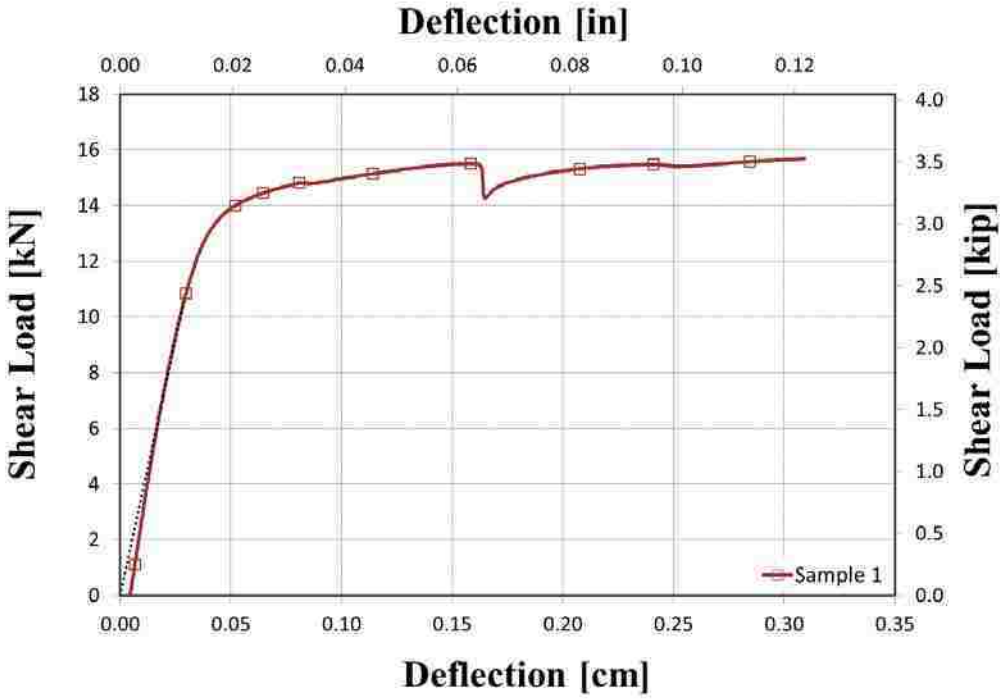

Figure A-1: Shear Load vs. Deflection for Polyurethane Adhesive Shear Test

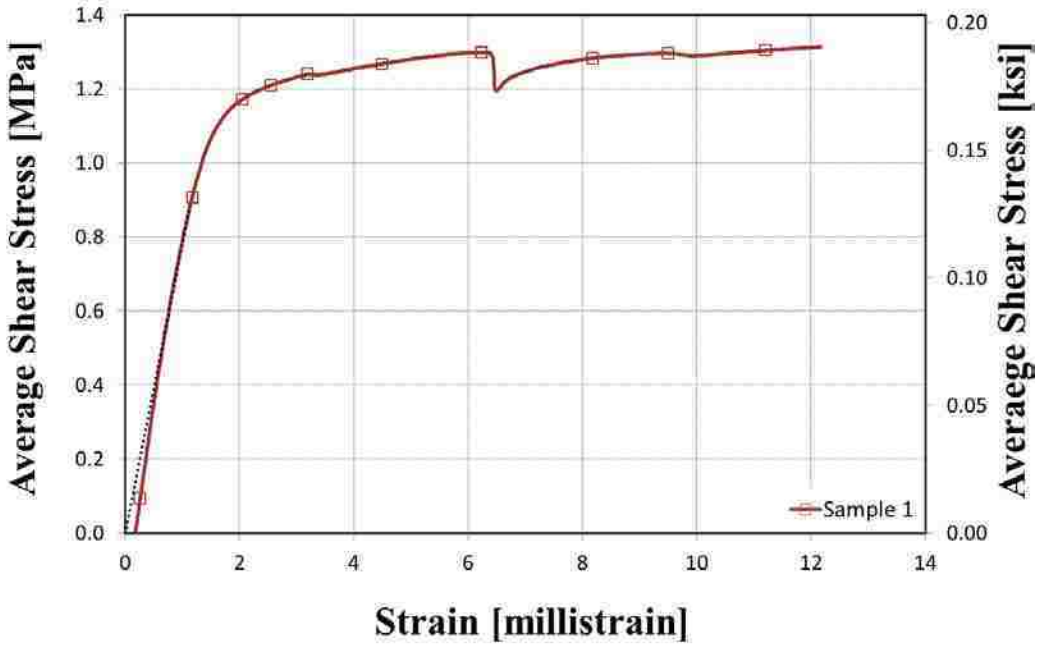

Figure A-2: Average Shear Stress vs. Strain for Polyurethane Adhesive Shear Test

APPENDIX B. SUPPORTING CALCULATIONS

Table B-1 shows the supporting calculations for the steel moment of inertia for an idealized thin-walled cross-section. The final values appear in Section 2.4.3 of the text. The moment of inertia is useful for determining buckling capacity of the columns.

Table B-1: Steel Moment of Inertia Calculations for Idealized Thin-Walled Model

Plate #	Width		Plate Centroid		Moment of Inertia		Transfer Term	
	b_y	b_z	z	y	$b_y b_z^3/12$	$b_z b_y^3/12$	$b_y b_z\, z^2$	$b_y b_z\, y^2$
	[cm (in)]		[cm (in)]		[cm^4 (in^4)]		[cm^4 (in^4)]	
1	0.152 (0.0598)	10.16 (4.0000)	0	5.00 (1.97)	0.810 (0.319)	0	0	2.358 (0.928)
2	9.89 (3.8804)	0.152 (0.0598)	5.00 (1.97)	0	0	0.740 (0.291)	2.288 (0.901)	0
3	10.16 (4.0000)	0.152 (0.0598)	0	5.00 (1.97)	0.810 (0.319)	0	0	2.358 (0.928)
4	9.89 (3.8804)	0.152 (0.0598)	0	4.85 (1.91)	0.740 (0.291)	0	0	2.151 (0.847)
5	9.89 (3.8804)	0.152 (0.0598)	4.85 (1.91)	0	0	0.740 (0.291)	2.288 (0.901)	0
6	9.89 (3.8804)	0.152 (0.0598)	0	4.85 (1.91)	0.740 (0.291)	0	0	2.151 (0.847)
				Σ	3.100 (1.220)	1.480 (0.583)	4.575 (1.801)	9.018 (3.550)

APPENDIX C. DETERMINATION OF GERARD CRIPPLING CONSTANT

The crippling constant, β, for a plate simply-supported on three sides and free on one side (SSSF) for the Gerard crippling method (Equation 6-7) was determined using interpolation. Because the parameter β was unknown for the SSSF boundary condition, known plate crippling boundary condition values were plotted against known plate buckling coefficient values. A best fit third order polynomial line which passed through the origin was used to approximate the unknown value (see Figure C-1). The known values are listed in Table C-1, along with the approximated value for β under SSSF boundary conditions. The value is an approximation and is used in the crippling analysis in Chapter 6.

Table C-1: Plate Crippling and Buckling Boundary Condition Parameters

Boundary Condition Description	Boundary Condition Symbol	Plate Crippling Parameter, β	Plate Buckling Coefficient, k
Clamped on All Four Sides	CCCC	1.8	7.6
Simply-Supported on All Four Sides	SSSS	1.42	4.0
Simply-Supported on Three Sides, Free on One Side	SSSF or SSFS	0.6	0.425

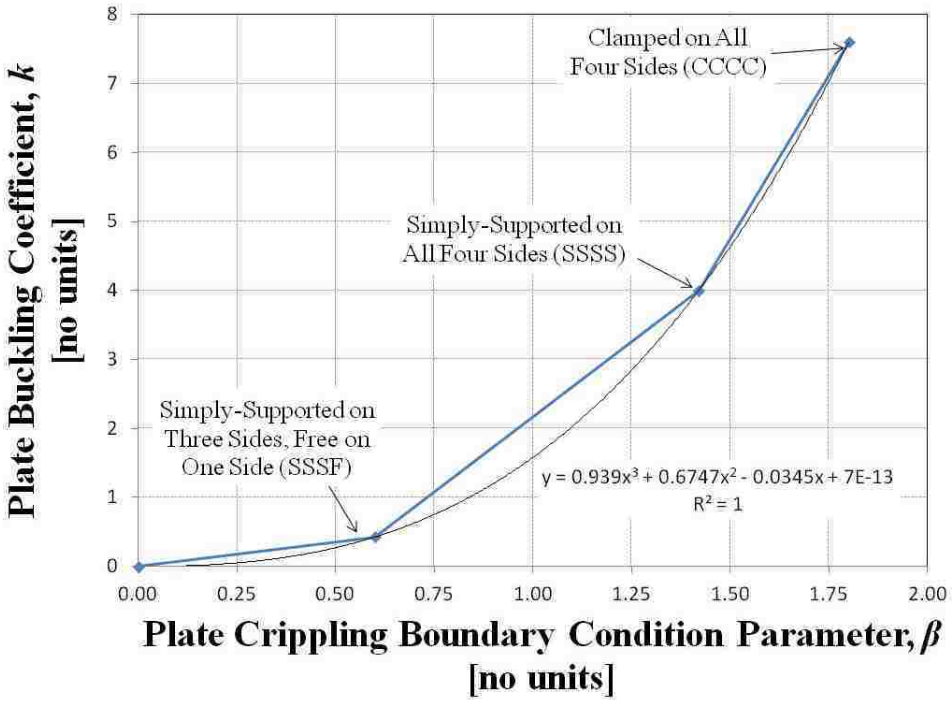

Figure C-1: Plate Buckling Coefficient vs. Plate Crippling Boundary Condition Parameter

APPENDIX D. FINITE ELEMENT MODEL INPUTS

The boundary conditions are summarized for the local buckling and crippling models in Table D-1, where *a* is the length of the short columns. Because symmetry was used for the global buckling analyses, the boundary conditions in this table were also used for global buckling, where *a* represents the half length of the column analyzed. As listed in the table, three displacement degrees of freedom and three rotational degrees of freedom were permitted for the analyses. Boundary conditions are imposed at the ends of the column to constrain displacements. Pressure loads were applied on end surface for the local and global buckling analyses. Displacements were applied on the end surface for the crippling analysis.

Table D-2 lists the point coordinates used to create the global buckling model. Table D-3 lists the point coordinates used to create the global buckling model based on an idealized thin-walled cross-section.

Table D-1: Column Boundary Conditions

Type	Identifier	Unconstrained Degrees of Freedom						Location (x,y,z) [no units]
		x	y	z	θ_1	θ_2	θ_3	
Roller	B	✓	-	-	✓	✓	✓	(*a*,0,0)
Pin	C	-	-	-	✓	✓	✓	(0,0,0)

Table D-2: Point Coordinates for Global Buckling Model (Extruded 84" (213 cm) in the x-Direction)

Point	x [in]	y [in]	y symbolic	z [in]	z symbolic
1	0	-2.0	-*b*/2	-2.0	- *b*/2
2	0	-1.9402	- *b*/2+t	-2.0	- *b*/2
3	0	1.9402	*b*/2-t	-2.0	- *b*/2
4	0	2.0	*b*/2	-2.0	- *b*/2
5	0	-1.9402	- *b*/2+t	-1.9402	- *b*/2+t
6	0	-1.8804	- *b*/2+2t	-1.9402	- *b*/2+t
7	0	1.8804	*b*/2-2t	-1.9402	- *b*/2+t
8	0	1.9402	*b*/2-t	-1.9402	- *b*/2+t
9	0	-1.8804	- *b*/2+2t	1.9402	*b*/2-t
10	0	1.8804	*b*/2-2t	1.9402	*b*/2-t
11	0	-2.0	- *b*/2	2.0	*b*/2
12	0	-1.9402	- *b*/2+t	2.0	*b*/2
13	0	-1.8804	- *b*/2+2t	2.0	*b*/2
14	0	1.8804	*b*/2-2t	2.0	*b*/2
15	0	1.9402	*b*/2-t	2.0	*b*/2
16	0	2.0	*b*/2	2.0	*b*/2

Table D-3: Point Coordinates for Global Buckling Model Based on Idealized Thin-Walled Cross-Section

Point	x_1 [in]	x_2 [in]	x_3 [in]
1	0	-2	-2
2	0	2	-2
3	0	2	2
4	0	-2	2
5	168	-2	-2
6	168	2	-2
7	168	2	2
8	168	-2	2

APPENDIX E. SAMPLE FINITE ELEMENT INPUT

The controls from two finite element analysis input files are listed in this appendix. The following input file is for a nonlinear static (crippling) analysis performed on an 8” (20.3 cm) long test model with an element edge length of 0.25” (0.64 cm).

```
*ADINA-A 8.6.E
C*!!! DO NOT EDIT THE NEXT   4 RECORDS WHICH CONTROL FILE I/O
C*FILEIO   2
C*RES   8   2
C*POR  60   2
C*FILEIO
C*ADINA
Crippling
C***  [1] MASTER CONTROL RECORD 1
    15024   0000000    0    2    1      180  1.000000000000       0     15024
  0.000000000000    010 4    0    1  0 0    0    0    2    0    0 00 0       0.0
       0        0       0.08.50000000       0.0    0    0    0   24  100    0
   0    0    0    0       0.0       0.0    0    0        0        0 0  0    0
C***  [2] MASTER CONTROL RECORD 2
       1     2178        0    0    0    2 3000 1 0 0 0 0 0 0 0 00001      01
       0    15024        0        0        0        0    15024        0
       0.100000E-9    1    0    0    0    0    0    0 0  0    0    0    0    0
C***  [3] LOAD CONTROL
       0        0        0        0        0        0        0        0
     952        0        0        0        0        0        0        0
       0        0        0        0        0        0        0        0
   0    0    0    0    2    0    0    0    0    0    0    0    0    0    0 0  0
C***  [4] MASS AND DAMPING CONTROL
   0    0    0    0       0.0       0.0        0        0.100000E-3    0
C***  [5] EIGENVALUE SOLUTION CONTROL
   0    1    0   -1    0    0    0    0    0          0.0    1   50
   0    0    0    0    1
C***  [6] TIME INTEGRATION METHOD CONTROL
   0    00.500000000.25000000    0    0    0    0    00.01000000
        10.900000000.001000008.00000000       0.0       0.01.000000000.50000000
```

```
C***  [7] INCREMENTAL SOLUTION CONTROL
 3ATS   -3  1 120 150.001000000.010000000.050000000.50000000       0.0       0.0
C***  [7A] ITERATIVE SOLUTION PARAMETERS
   0    8    1.100000E-5.100000E-3.100000E-71.00000000       0.0    0       0.0
C***  [7B] AUTOMATIC SOLUTION (ATS) PARAMETERS
      10    00.001000003.00000000    0    0.100000E-32.000000001.00000000
C***  [8] PRINT-OUT CONTROL
   1    0    0    1    1    1    0    0    1    0    0    1    0        0    0
C***  [9] PORTHOLE SAVE CONTROL
   1    1    1   60   60              1    1    1    1    1    0    0
```

The following input file is for a linearized buckling (local buckling) analysis performed on an 10” (25.4 cm) long test model with an element edge length of 0.4” (1.02 cm).

```
*ADINA-A 8.6.E
C*!!! DO NOT EDIT THE NEXT   4 RECORDS WHICH CONTROL FILE I/O
C*FILEIO   2
C*RES   8   2
C*POR  60   2
C*FILEIO
C*ADINA
LIST
Local Buckling
C***  [1] MASTER CONTROL RECORD 1
    27399   0000000    0    3    1        2  1.000000000000        0     27399
  0.000000000000    010 0    0    1  0 0    0    0    2    0    0 00 0       0.0
       0        0       0.010.5000000       0.0    0    0    0   24  100    0
   0    0    0    0       0.0       0.0    0    0         0         0 0  0    0
C***  [2] MASTER CONTROL RECORD 2
       1     5588         0    0    0    2 3000 1 0 0 0 0 0 0 0 00001      00
       0    27399         0         0         0         0    27399         0
       0.100000E-9    1    0    0    0    0    0    0 0  0    0    0    0    0
C***  [3] LOAD CONTROL
       0         0       238         0         0         0         0         0
       0         0         0         0         0         0         0         0
       0         0         0         0         0         0         0         0
   0    0    0    0    2    0    0    0    0    0    0    0    0    0    0 0  0
C***  [4] MASS AND DAMPING CONTROL
   0    0    0    0       0.0       0.0         0         0.100000E-3    0
C***  [5] EIGENVALUE SOLUTION CONTROL
   3    1    5   -1    5    0    0    0    0          0.0    6   50
   0    0    0    0    1
```

```
C***  [6] TIME INTEGRATION METHOD CONTROL
   0    00.500000000.25000000    0    0    0    0    00.01000000
        10.900000000.001000008.00000000       0.0       0.01.000000000.50000000
C***  [7] INCREMENTAL SOLUTION CONTROL
 3  0   -3  1 120 150.001000000.010000000.050000000.50000000       0.0       0.0
C***  [7A] ITERATIVE SOLUTION PARAMETERS
   0    8    1.100000E-5.100000E-3.100000E-71.00000000       0.0    0       0.0
C***  [8] PRINT-OUT CONTROL
   1    0    0    1    1    1    1    0    1    0    0    1    0         0    0
C***  [9] PORTHOLE SAVE CONTROL
   1    1    1   60   60              1    1    1    1    1    0    0
```

APPENDIX F. LESSONS LEARNED FOR ADINA NONLINEAR ANALYSIS

Nonlinear analysis is complicated and is a very time consuming process. Although there is no 'instruction manual' for any new finite element problem, many lessons can be learned from the experience of developing the models and analyses presented in this thesis. These will be useful to future students interested in using ADINA to execute nonlinear analyses. It is important for the student to understand that executing nonlinear analysis is at iterative process in multiple senses. This includes iterations in the modeling, meshing, load stepping, synthesizing results, etc. Adequate final results may only be obtained by iterating through each of these multiple times. In general, it is recommended to start with a coarser mesh in order to improve computational time and obtain 'ball park' results. When the results begin to match what was observed in the laboratory, the mesh density should be increased until results converge.

Important nonlinear settings for pre-processing include:

1) Statics analysis
    a. Turn on Automatic Time Stepping (Analysis Options>Use Automatic Time Stepping (ATS))
2) Elastic nonlinear material curve (ideally obtained from material testing) (Model>Materials>Manage Materials…)
    a. Hint: Be sure to input both the tension (positive) and compression (negative) portions of the nonlinear material curve.

3) Selecting an element with mid-side nodes in order to capture nonlinear stress variation through the element. The 20-node brick element is recommended for 3-D modeling (Meshing>Create Mesh>Volume…>Nodes per Element)
4) Large displacements to trigger local buckling and subsequently crippling (Controls>Kinematics>Large Displacements)
5) Small displacement steps: ~0.001% of specimen length (will vary depending on model)
    a. Apply a unit displacement (Model>Loading>Apply…>Displacement)
    b. Control the displacement step using time step and time function settings (Controls>Time Function; and Controls>Time Step)
6) Large strains were not used in the analyses presented in this thesis; however, they may be used in future analyses (Controls>Kinematics>Large Strains)
7) Sparse solution process (Controls>Solution Process>Sparse)
    a. Select "Continue Even When Non-Positive Stiffness Matrix Encountered"
8) Initial eccentricity in geometry or loading (not used in the analyses for this thesis, but may be useful for future work)

How to capture peak load in post-processing:

1) Capture nodes on reaction surface using the Query locator action (labeled with a question mark, "?")
2) Define a node combination (Post-processing>Definitions>Model Point (Combination)>Node…>Sum)
3) Output reaction load at each time step (List>Value List>Model Point>Variables to List>Reaction>Apply)

Using these settings, the peak load based on nonlinear analysis is able to be obtained. The crippling phenomenon is only able to be captured, however, by extending the displacement stepping significantly beyond the peak load (small displacement step must be used) and by using an adequately fine mesh (convergence study required).

Finally, exploit symmetry whenever possible. This requires using adequate boundary conditions to ensure symmetric behavior. Using symmetry reduces total computational time significantly.